# Comptes Rendus de l'Académie des sciences

1878-1535 (electronic)

# *Physique*

Volume 21, Special Issue 1, janvier 2020

**Special issue / *Numéro thématique***
A perspective of High Energy Physics from precision measurements / *La physique des Hautes Energies du point de vue des mesures de précision*

**Guest editors / *Rédacteurs en chef invités***
Stéphane Monteil, Marie-Hélène Schune

**Académie des sciences — Paris**

INSTITUT DE FRANCE
Académie des sciences

CENTRE MERSENNE

# *Comptes Rendus*
# *Physique*

**Objective of the journal**
*Comptes Rendus Physique* is a peer-reviewed electronic journal of international standing, covering all fields of physics and astrophysics. It publishes mainly thematic issues, but also original research articles, preliminary announcements, review articles, historical perspectives, pedagogical texts or conference proceedings, without length limit, in English or in French. It also publishes special issues devoted to certain recent and/or significant aspects of the discipline, whose authors are chosen from among the most active researchers on the subject and whose coordination is assured by guest editors.
*Comptes Rendus Physique* is published according to a virtuous policy of diamond open access, free for authors (no publication fees) as well as for readers (immediate and permanent open access).



**About the journal**
All journal's information, including the text of published articles, which is fully open access, is available from the journal website at https://comptes-rendus.academie-sciences.fr/physique/.

**Author enquiries**
For enquiries relating to the submission of articles, please visit this journal's homepage at https://comptes-rendus.academie-sciences.fr/physique/.

**Contact**
Académie des sciences
23, quai de Conti, 75006 Paris, France
Tel: (+33) (0)1 44 41 43 72
CR-Physique@academie-sciences.fr

*Comptes Rendus*
*Physique*
**2020**, 21, nº 1

# Contents / *Sommaire*

*Comptes Rendus*
*Physique*
**2020**, 21, nº 1, p. 1-7
https://doi.org/10.5802/crphys.15

A perspective of High Energy Physics from precision measurements
*La physique des Hautes Energies du point de vue des mesures de précision*

# A general perspective about high energy physics

## *Une perspective générale pour la physique des particules*

**Stéphane Monteil**[a] **and Marie-Hélène Schune**[*, b]

[a] Université Clermont Auvergne, CNRS/IN2P3, LPC, F-63000, Clermont-Ferrand, France

[b] Université Paris-Saclay, CNRS/IN2P3, IJCLab, Orsay, France.

*E-mails:* monteil@in2p3.fr (S. Monteil), schunem@lal.in2p3.fr (M.-H. Schune).

**Abstract.** This volume of Compte-Rendus proposes a discussion of an ensemble of precision measurements in particle physics. It provides an experimental state of the art review as well as perspectives for future measurements. We explore in this rapid overview the pillars of our knowledge, how they were established and draw some perspectives about the necessity of a new precision era to tackle the outstanding questions of the field.

**Résumé.** Ce dossier des Compte-Rendus de l'Académie des Sciences rassemble huit articles qui traitent chacun d'un thème de la physique des particules. Elle présente un état de l'art des mesures et des idées qui gouvernent aujourd'hui notre représentation physique de l'infiniment petit. Elle interroge aussi les perspectives du champ au travers des mesures de précision. Nous discutons dans cette introduction rapide les fondations de nos connaissances et comment une nouvelle ère de précision peut répondre aux questions fondamentales de la physique des particules moderne.

**Keywords.** Precision physics, Standard model, Quarks, Leptons, Bosons, Experimental diversity, Future projects.

**Mots-clés.** Physique de precision, Modèle standard, Quarks, Leptons, Bosons, Diversité expérimentale, Projets futurs.

### 1. Precision in physics

This series of articles will simultaneously describe the state of the art of key measurements and draw some perspectives for future experimental programs. Particle physics is experiencing a change of paradigm and we start this rapid overview by highlighting inspirational examples from Physics history where precision was instrumental in overcoming the central problems of the field.

[*] Corresponding author.

### 1.1. *The tools for precision: from accelerators and detectors to theory*

Since the first Wideroe's design of a particle accelerator in 1928, the understanding of the laws of physics in the previous century has been closely entangled with the evolution in energy and beam intensity of accelerators and the development of increasingly precise particle detectors (not mentioning the computing architectures to process the data). Their review is beyond the scope of this document and the interested reader can consult [1] for a comprehensive description of the progresses in theses domains. The discovery of the Brout–Englert–Higgs (BEH) boson at the Large Hadron Collider (LHC) experiments is an exemplary illustration of the concurrent and constructive achievements in these areas. The mid-term and long term projects of particle physics, and singularly the precision measurements, are still building on the concurrent progresses in these domains.

As we will see in all the articles published after this overview, there is a continuous need to match theory precision with experimental accuracy. An enlightening illustration is the anomalous magnetic moment. The magnetic moment of an elementary particle of charge $e$ and mass $m$ is aligned with its spin $\vec{s}$: $\vec{\mu} = g(e/2m)\vec{s}$. In 1928, Dirac predicted that the $g$-factor of elementary half-spin particles, is exactly 2. This value was in agreement with the experimental knowledge at that time. However in 1947, small deviations from the expectations were seen in the hyperfine structure of hydrogen and deuterium [2,3], $a^e_{\text{exp}} = 0.00126 \pm 0.00019$ and $a^e_{\text{exp}} = 0.00131 \pm 0.00025$, respectively. In 1948 Schwinger performed calculations at the one-loop level in Quantum Electro-Dynamics (QED) leading to a small shift in $g$: the so-called anomalous magnetic moment, $a^e_{\text{theory}} = (g-2)/2 = \alpha/(2\pi) = 0.00116$ [4]. Nowadays the precision on the measurement of the anomalous magnetic moment of the electron has improved by 9 orders of magnitude: $a^e_{\text{exp}} = 1159652180.91(26) \times 10^{-12}$ and the theoretical prediction has undergone a similar improvement in precision: in 2012 the QED calculation at the 5-loops level, involving the evaluation of more than 12000 Feynmann graphs has been published $a^e_{\text{theory}} = 1159652181.78(77) \times 10^{-12}$ [5]. Similar parallel developments in theory and experiments have taken place for the anomalous moment of the muon. In this case, due to the larger muon mass, not only the loops involving the $W$ and $Z$ weak bosons have be to taken into account but also the hadronic contributions. These last ones are very difficult to compute precisely and dominate the theoretical uncertainty budget on the prediction of $a_\mu$. The current experimental determination of $a^\mu_{\text{exp}} = 11659209.1(5.4)(3.3) \times 10^{-10}$ [1] is improved by a factor 14 with respect to the experiments from the 1970's [6]. The corresponding improvement in the theoretical prediction leads to $a^\mu_{\text{theory}} = 116591823(1)(34)(26) \times 10^{-11}$ [1], where the uncertainties are due to the electroweak, lowest-order hadronic, and higher-order hadronic contributions, respectively. There is a tension between these state-of-the-art prediction and measurement. Whether this tension is due to physics beyond what is known, overlooked uncertainties in the hadronic corrections or experimental issues, future results with increased precision will tell.

### 1.2. *$CP$-violation discovery*

Matching experimental accuracy with theory precision is necessary to produce sound tests of the theoretical predictions. Yet, there are many areas where the experimental precision is needed *per se*. Let's explore the first observation of a matter-antimatter physics difference. The first evidence of parity-symmetry ($P$) breaking in weak interactions [7], rapidly followed by the deeper observation that it is a maximal breaking concurrent with a maximal violation of the charge conjugation operation ($C$) [8], has laid the foundations of the electroweak standard model (SM) as we know it [9]. Only left-handed particles are interacting by the weak interaction. We will come back to that. It is a vibrant testimony to the necessity to experimentally test the first principles:

it then becomes clear that the laws of physics allow to make an absolute distinction between left-handed and right-handed coordinate systems, defeating the mirror reflection invariance. To overcome this intellectual discomfort, it was then advocated that the simultaneous operation of the charge conjugation and the space reflection, known as the $CP$ transformation must be an exact symmetry of the weak interaction. In the year 1961, an experiment at the JINR Synchrophasotron [10] was conducted to search in particular for $CP$-symmetry breaking effects ($K^0_{\rm L} \to \pi^+\pi^-$). The authors did not see an event out of the 255 recorded and reported a limit at 0.3%, remarkably close to the current world-average value of the branching fraction. They missed it by nothing! The decisive experiment [11] came a couple of years later at Brookhaven. Articulated with a comprehensive physics program, the primary objective of this experiment was to understand better the neutral kaon regeneration. The search for $CP$-violating $K^0_{\rm L} \to \pi^+\pi^-$ was presented as a secondary target. Yet, the simultaneous characteristic of the machine intensity and the use of novel efficient spark chamber detectors made the difference to observe for the first time a $CP$-symmetry breaking effect. Not only the weak interaction can absolutely distinguish right from left, but particles and antiparticles have different behaviours. Incidentally, this was the first manifestation of the existence of a third generation of quarks! There are several lessons to learn from the history of this scientific revolution. Certainly, a comprehensive and well-thought physics program is a must. We are keeping for the purpose of these articles that precise instruments and large statistics are key to understanding.

## 2. The two pillars of the Standard Model

The Standard Model (SM) of particle physics is an elegant gauge theory able to describe (almost[1]) all particle measurements performed to date up to the electroweak energy scale. It is remarkable to note that beyond the first principles of symmetry, it built up as an intertwined evolution of experimental and theoretical progresses. The absence or the smallness of the probability of the $K^0_{\rm L} \to \mu^+\mu^-$ decay triggered the hypothesis of the charm quark through the so-called GIM mechanism [12]; we have already discussed that the observation of $CP$ violation introduced the possibility of three generation of quarks [13]; the $B^0$ meson oscillation frequency [14] and the LEP electroweak precision observables required a heavy top quark and its discovery at this very mass at Tevatron was a validation of a complete SM [15]; the same consistency test pointed towards the existence of a light BEH scalar boson that was discovered at the LHC [16, 17]. We highlight in the following the two consistency checks which constitute the modern pillars of the SM.

### 2.1. *The electroweak observables consistency-test*

The number of related free parameters in the SM is relatively low, in particular when focusing to the electroweak part. This is in particular due to the quadratic dependence of the radiative corrections with the fermion masses, which makes the top-quark contributions overwhelmingly dominant. Precise test of the SM can thus be performed comparing a large number of precise measurements (partial widths of the $Z^0$ boson, mass ($m_W$) and full width of the $W$-boson, top-quark mass ($m_t$), BEH-boson mass ($m_H$), coupling constants) with parametric SM predictions computed at the same level of precision, provided with a given set of experimental inputs ($m_Z$, $G_F$ and $\alpha_{\rm EM}$). An exemplary plot is shown in Figure 1 where the $W$-boson mass is shown as a function of the top-quark mass. The 68% CL and 95% CL ellipses are the contours obtained from comparing the measurements with the predictions scanning the ($m_t$, $m_W$) 2D-space. The

[1] The nonvanishing masses of neutrinos are an example but would deserve a specific Compte-Rendu per se.

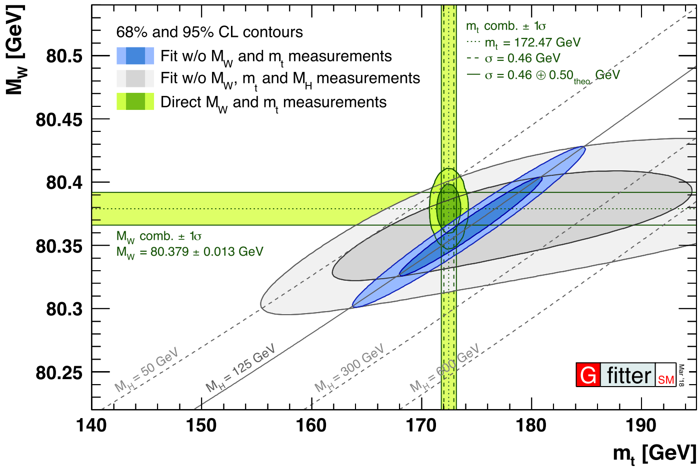


**Figure 1.** Contours of 68% and 95% confidence level obtained from scans of fits with fixed variable pairs $m_W$, $m_t$. The narrower blue and larger grey allowed regions are the results of the fit including and excluding the $m_H$ measurement, respectively. The horizontal and vertical bands indicate the $1\sigma$ regions of the $m_W$ and $m_t$ measurements [18].

narrower blue and larger grey allowed regions are the results of the fit including and excluding the $m_H$ measurement, respectively. The dependency of the radiative corrections with $m_H$ is logarithmic which explains the observed milder influence. The horizontal and vertical green bands indicate the one standard deviation regions of the $m_t$ and $m_W$ measurements. The fact that the blue ellipse overlaps with the measurements is one of the most powerful consistency check of the SM.

## 2.2. *The CKM consistency check*

Another stringent test of the SM can be performed in the quark sector. The weak charged-current transitions of different generations are encoded in the Cabibbo–Kobayashi–Maskawa (CKM) matrix, which can be parameterised with four independent parameters among which one is a phase; this is in the SM the unique source of $CP$ violation if one neglects the strong $CP$-phase and the neutrino masses effects. The tests consist in comparing a large number of experimental results with the corresponding predictions. Contrary to the gauge sector tests, since quarks are bounded into hadrons, an additional uncertainty comes from the estimations of the non-perturbative QCD effects that must be embodied in the fit. The set of observables considered in this global test of the SM hypothesis are selected to have clean theoretical uncertainties in their predictions and correspond to precise measurements. Remarkable progresses have been achieved in the last 20 years in the estimations of the hadronic matrix elements in particular in the framework of lattice QCD.

A graphical way to illustrate the outcome of this global fit is to represent the constraints on the ($\overline{\rho}$ and $\overline{\eta}$) 2D-space (while the SM fit has four parameters) to highlight the $\overline{\eta}$ parameter which governs the presence of $CP$ violation in the SM. Several groups using different statistical methods [19, 20] are performing those tests and in all cases the agreement between the measurements of $CP$-conserving and $CP$-violating observables (as well as the agreement between the tree-dominated and loop-dominated constraints) allows to conclude that the KM mechanism is the dominant source of $CP$ violation in $K$ and $B$ decays. In turn, beyond SM contributions are

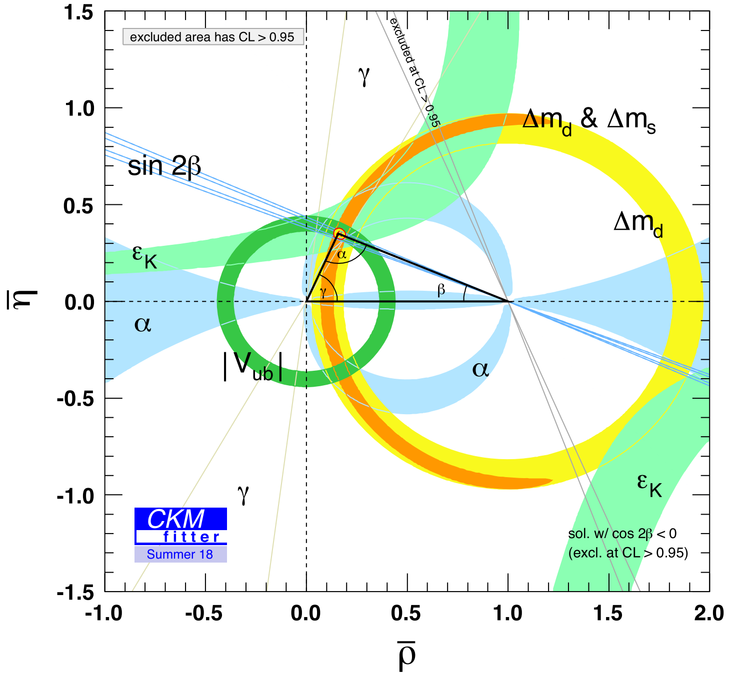


**Figure 2.** The consistency of the SM hypothesis is illustrated by the fact that the overlap region of the *CP*-conserving observables ($V_{ub}$, $\Delta m_d$ and $\Delta m_s$) coincides with the overlap region of the *CP*-depending observables ($\alpha$, $\beta$, $\gamma$ and $\epsilon_K$). The individual constraints are displayed for 95% C.L. exclusion. The red hashed region of the global combination corresponds to 68% C.L. exclusion.

constrained to be less than 20% as the article "*CP* violation in *B* decays" will discuss in details. An illustrative plot of the constraints on the CKM ($\overline{\rho}$ and $\overline{\eta}$) parameters is shown in Figure 2.

## 3. A perspective of HEP from precision measurements or precision as a perspective: finding the next energy scale

This series of articles is published at a time when a significant part of the analyses based on the LHC Run II data have been delivered. A new scalar particle consistent to date with the SM BEH boson has been discovered and no other new particle has been observed. Particle physics is therefore at a turning point of its history: there are compelling arguments that physics beyond SM must exist but we have not found a direct sign of its existence. Since there are no theoretical guidelines to infer the new physics energy scale, the balance is now towards building experimental facts.

As shown in the "Top-quark physics at the LHC" and "Higgs Physics" articles of this Compte-Rendu, the amount of produced particles already allow rather precise measurements of the heaviest fermion of the SM and of its unique spin-0 boson. In the future period of HL-LHC the precision will be dramatically increased and the results will certainly help to refine our understanding of the physics and might hopefully reveal inconsistencies. Beyond being a top quark factory, the LHC and the HL-LHC are also producing, in even larger amounts, charm and beauty quarks. For the first time, very precise measurements in this domain have been obtained at an hadronic collider. Consequently, the heavy flavour physics field is in a very healthy situation with precise information obtained in complementary experimental contexts: $pp$ collisions at 13 TeV (LHCb, ATLAS and CMS) and $e^+e^-$ collisions at 10.58 GeV (BaBar, Belle and Belle-II which is now starting to take data). This is highlighted in the articles on "tau and charm decays", "CP violation in B decays" and "Rare B Decays" of this issue. The latter article reports also observations of tensions with the SM predictions. None of them is significant enough to defeat the SM to date, but it is remarkable to notice that being put together, they are pointing towards a coherent beyond-SM scenario. It is thus of prime importance to collect more data in different experimental environments to clarify the picture. Furthermore detailed studies of the heaviest lepton of the SM ($\tau$) are also pursued, mostly at $e^+e^-$ colliders but also, for some specific modes at the LHC (see the article on "tau and charm decays").

With the discovery of a narrow scalar boson, consistent so far with the SM BEH boson, the LHC experiments have shaped an obvious case to study the properties of this particle at an equivalent precision that was achieved for the $Z$ and $W$ bosons at SLD, LEP and Tevatron machines. The HL-LHC facility will prolong this quest for precision and might reveal inconsistencies with the SM but there is a consensus in the particle physics community that an $e^+e^-$ machine is in order to address comprehensively this program. Among the projects thought so far, a large scale facility of circular colliders embraces the case for precision highlighted in this series of articles. At the intensity frontier, an $e^+e^-$ collider operated at the four electroweak energy thresholds $Z$, $WW$, $ZH$, $t\bar{t}$ will test the two pillars of the SM with unprecedented precision if an adequate matching of the experimental and theoretical uncertainties is achieved. At the energy frontier (>100 TeV), beyond the direct searches of new particles, a proton collider will ensure abundant production of self-coupled BEH bosons necessary to constrain the shape of the scalar potential.

A significant part of the particle physics program can only be conducted at colliders. Yet, finesse experiments, addressing the observation of forbidden or suppressed processes in the SM, that can be achieved with beam dump facilities or light flavour factories, as described in "Rare kaon decays" and "Precision experiments with muons and neutrons" are providing a complementary path to large scale collider experiments to comprehensively address the fundamental questions of the field. The selection of articles under this series of Compte-Rendu will hopefully underline the necessity and the richness of the diversity of experimental approaches.

## References


[1] Particle Data Group collaboration, M. Tanabashi *et al.*, "Review of particle physics", *Phys. Rev. D* **98** (2018), article ID 030001.

[2] J. E. Nafe, E. B. Nelson, I. I. Rabi, "The hyperfine structure of atomic hydrogen and deuterium", *Phys. Rev.* **71** (1947), p. 914-915.

[3] D. E. Nagle, R. S. Julian, J. R. Zacharias, "The hyperfine structure of atomic hydrogen and deuterium", *Phys. Rev.* **72** (1947), p. 971-971.

[4] J. Schwinger, "On quantum-electrodynamics and the magnetic moment of the electron", *Phys. Rev.* **73** (1948), p. 416-417.

[5] T. Aoyama, M. Hayakawa, T. Kinoshita, M. Nio, "Tenth-order qed contribution to the electron $g-2$ and an improved value of the fine structure constant", *Phys. Rev. Lett.* **109** (2012), article ID 111807.

[6] CERN-Mainz-Daresbury collaboration, J. Bailey *et al.*, "Final report on the CERN muon storage ring including the anomalous magnetic moment and the electric dipole moment of the muon, and a direct test of relativistic time dilation", *Nucl. Phys. B* **150** (1979), p. 1-75.

[7] C. S. Wu, E. Ambler, R. W. Hayward, D. D. Hoppes, R. P. Hudson, "Experimental test of parity conservation in beta decay", *Phys. Rev.* **105** (1957), p. 1413-1415.

[8] M. Goldhaber, L. Grodzins, A. W. Sunyar, "Helicity of neutrinos", *Phys. Rev.* **109** (1958), p. 1015-1017.

[9] S. Glashow, "Partial symmetries of weak interactions", *Nucl. Phys.* **22** (1961), p. 579-588.

[10] D. Neagu, E. O. Okonov, N. I. Petrov, A. M. Rosanova, V. A. Rusakov, "Decay properties of K-20 mesons", *Phys. Rev. Lett.* **6** (1961), p. 552-553.

[11] J. H. Christenson, J. W. Cronin, V. L. Fitch, R. Turlay, "Evidence for the $2\pi$ decay of the $K_2^0$ meson", *Phys. Rev. Lett.* **13** (1964), p. 138-140.

[12] S. Glashow, J. Iliopoulos, L. Maiani, "Weak interactions with lepton-hadron symmetry", *Phys. Rev. D* **2** (1970), no. 7, p. 1285-1292.
[13] M. Kobayashi, T. Maskawa, "CP violation in the renormalizable theory of weak interaction", *Prog. Theor. Phys.* **49** (1973), p. 652-657.
[14] ARGUS collaboration, H. Albrecht *et al.*, "Physics with ARGUS", *Phys. Rep.* **276** (1996), p. 223-405.
[15] G. 't Hooft, M. Veltman, "Regularization and renormalization of gauge fields", *Nucl. Phys. B* **44** (1972), p. 189-213.
[16] P. W. Higgs, "Broken symmetries and the masses of gauge bosons", *Phys. Rev. Lett.* **13** (1964), no. 16, p. 508-509.
[17] F. Englert, R. Brout, "Broken symmetry and the mass of gauge vector mesons", *Phys. Rev. Lett.* **13** (1964), p. 321-323.
[18] J. Haller, A. Hoecker, R. Kogler, K. Moenig, T. Peiffer, J. Stelzer, "Update of the global electroweak fit and constraints on two-Higgs-doublet models", *Eur. Phys. J. C* **78** (2018), article ID 675.
[19] A. Bevan *et al.*, "Standard model updates and new physics analysis with the unitarity triangle fit", 2014, preprint, https://arxiv.org/abs/1411.7233.
[20] J. Charles *et al.*, "Current status of the Standard Model CKM fit and constraints on $\Delta F = 2$ New Physics", *Phys. Rev. D* **91** (2015), article ID 073007.

*Comptes Rendus*
*Physique*
**2020**, 21, nº 1, p. 9-22
https://doi.org/10.5802/crphys.7

A perspective of High Energy Physics from precision measurements
*La physique des Hautes Energies du point de vue des mesures de précision*

# $W^{\pm}$ and $Z^0$ boson physics

## *La physique des bosons $W^{\pm}$ et $Z^0$*

**Frederic Teubert**[*, a] **and Pippa Wells**[a]

[a] European Organization for Nuclear Research (CERN), Geneva, Switzerland.
*E-mails:* frederic.teubert@cern.ch (F. Teubert), pippa.wells@cern.ch (P. Wells).

**Abstract.** Precision measurements of the weak bosons ($Z^0$ and $W^{\pm}$) at $e^+e^-$ and hadron colliders have allowed the Standard Model to be tested as a quantum field theory, requiring the inclusion of higher order quantum loop corrections. The agreement of these measurements with the Standard Model puts strong constrains on New Physics scenarios. To achieve such precision, a close collaboration between experimenters and theorists, as well as between experimenters in different collaborations was pioneered in the 90s. A superb control of the experimental systematic uncertainties as well as an unprecedented level of precision on the collider beam energy and intensity was required in many of these measurements. New accelerators are proposed in the future that could improve these tests of the Standard Model even further.

**Résumé.** Les mesures de précision effectuées sur les bosons $W^{\pm}$ et $Z^0$ aux collisionneurs $e^+e^-$ et hadroniques ont permis de tester le Modèle Standard en tant que théorie quantique des champs, c'est-à-dire incluant des corrections quantiques d'ordre élevé. L'accord entre ces mesures et le Modèle Standard contraint fortement les scenarii de nouvelle physique. Des collaborations étroites entre expérimentateurs et théoriciens ainsi qu'entre expérimentateurs des différentes expériences, telles que celles engagées dans les années 1990, sont indispensables pour atteindre une grande precision. Un excellent contrôle des incertitudes systématiques expérimentales ainsi qu'une détermination de l'énergie des faisceaux et de leur intensité avec un niveau de précision qui n'avait encore jamais été atteint ont été indispensables pour un grand nombre de ces mesures. De futurs accélérateurs sont actuellement proposés afin d'accroître encore la précision de ces tests du Modèle Standard.

**Keywords.** Large hadron collider, $Z^0$, $W^{\pm}$.

**Mots-clés.** Grand collisionneur de hadrons, $Z^0$, $W^{\pm}$.

## 1. Historical introduction

By the end of the 19th century several types of radioactivity had been discovered in heavy elements like Uranium, Thorium, Polonium and Radium. In 1899, Ernest Rutherford had separated radioactive emissions into two types: $\alpha$ and $\beta$-decays based on the penetration of objects and

* Corresponding author.

the ability to cause ionisation. While $\alpha$-rays could be stopped by thin sheets of aluminium, $\beta$-rays could penetrate several millimetres of aluminum. Later a third type of even more penetrating radiation, $\gamma$-rays, was identified. In 1900 Becquerel had measured the mass-to-charge ratio ($m/e$) for $\beta$ particles and found the same as for Thomson's electron, therefore concluding that $\beta$-rays were in fact electrons. The energy distribution of these $\beta$-rays was not a narrow peak (like for the other types of radiation) but a continuous distribution that forced Pauli in 1930 to propose the existence of a new extremely light neutral particle, the neutrino, in order to preserve the conservation of energy in the process.

To explain $\beta$-decays a new type of nuclear interaction was needed (Weak Interactions). Enrico Fermi came up in 1933 with a useful theory [1, 2] to explain the neutron $\beta$-decay by direct coupling of a neutron with an electron, a neutrino (later determined to be an antineutrino) and a proton. The Fermi interaction was the precursor to the theory for the weak interaction where the interaction is mediated by a virtual $W^\pm$ boson, of which Fermi theory is the low-energy effective field theory. In fact, following the success of the gauge field theory for electromagnetic interactions (QED) in the 1950s, Glashow, Weinberg and Salam (GWS) [3–5] efforts to replace Fermi's effective theory culminated around 1968 with a unified theory of electromagnetism and weak interactions. Their electroweak (EW) theory postulated not only the $W^\pm$ boson to explain $\beta$ decays, but also a new $Z^0$ boson that had never been observed and would induce neutral weak current interactions.

### 1.1. *Neutral current interactions in neutrino scattering experiments*

In 1973 neutral current interactions were indeed observed [6, 7] as predicted by theory. The huge "Gargamelle" bubble chamber made use of a neutrino beam produced from $\pi \to \mu\nu_\mu$ and $K \to \mu\nu_\mu$ decays, produced by a proton beam from the CERN Proton-Synchrotron (PS) accelerator. The Gargamelle collaboration discovered both leptonic neutral currents (events involving the interaction of an incoming neutrino with an electron), and hadronic neutral currents (events when an incoming neutrino is scattered from a nucleon). This experimental confirmation was crucial in establishing the GWS theory of electroweak interactions which is one of the pillars of the Standard Model (SM) today.

### 1.2. *Discovery of $Z^0$ and $W^\pm$ at CERN*

The discovery of the $W^\pm$ and $Z^0$ bosons themselves had to wait for the construction of a particle accelerator powerful enough to produce them. Within the framework of the SM, the observation of neutral currents in neutrino induced reactions allowed the first quantitative prediction for the mass of the weak bosons in the range 60 to 80 GeV for the $W^\pm$ and 75 to 92 GeV for the $Z^0$ bosons. In 1976 Rubbia, Cline and McIntyre proposed [8] the transformation of the new CERN Super-Proton-Synchrotron (SPS) accelerator into a $p\overline{p}$ collider as a quick and relatively cheap way to achieve collisions above threshold for $W^\pm$ and $Z^0$ production. By the end of 1982, the $p\overline{p}$ collision rate was high enough to permit the observation of $W \to e\nu_e$ decays [9, 10]. In a subsequent run during the spring of 1983, the decays $Z^0 \to e^+e^-$ and $Z^0 \to \mu^+\mu^-$ were also observed [11, 12], vindicating the GWS theory of Electroweak interactions. Figure 1 shows the invariant mass distribution of events recorded by the UA1 and UA2 Collaborations enabling the discovery of the $Z^0$ boson.

## 2. Theory context

In the context of the SM, any EW process can be computed at tree level from $\alpha$ (the fine structure constant measured at values of $q^2$ close to zero), $m_W$ (the $W^\pm$-boson mass), $m_Z$ (the

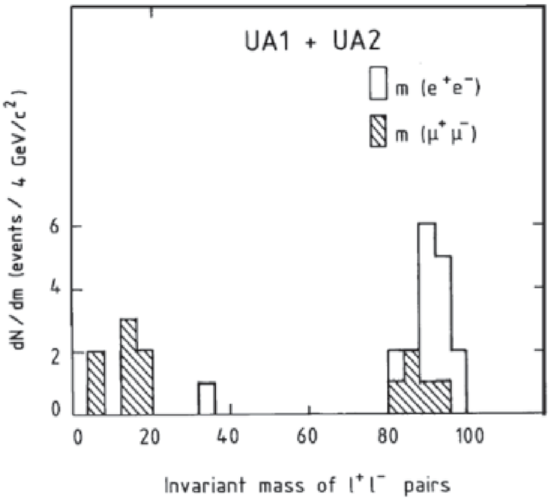


**Figure 1.** Invariant mass distribution of dilepton events from UA1 and UA2 experiments. A clear peak is visible at a mass of about 95 GeV (taken from http://www.nobelprize.org/).

$Z^0$-boson mass), and $V_{jk}$ (the Cabbibo–Kobayashi–Maskawa flavour-mixing matrix elements). When higher order corrections are included, any observable can be predicted in the "on-shell" renormalisation scheme as a function of:

$$O_i = f_i(\alpha, \alpha_s, m_W, m_Z, m_H, m_f, V_{jk})$$

and contrary to what happens with "exact gauge symmetry theories", like QED or QCD, the effects of heavy particles in the EW interactions do not decouple. Therefore, the SM predictions of the EW interactions at $q^2 \sim {m_Z}^2$ depend on the top quark mass ($(m_t^2 - m_b^2)/m_Z^2$) and to a lesser extent on the Higgs boson mass ($\log(m_H^2/m_Z^2)$), or to any kind of "heavy new physics".

The $W^{\pm}$ mass is one of the input parameters in the "on-shell" renormalisation scheme. As discussed later, $m_W$ is measured with a precision of about 0.015%, although the usual procedure is to take $G_\mu$ (the Fermi constant measured in the muon decay known with an even better precision of about 0.0009%) to predict $m_W$ as a function of the rest of the input parameters. The less well known input parameters are $\alpha_s$, $m_t$ and $m_H$, measured today with a precision of about 1%, 0.2% and 0.1% respectively. The value of $\alpha^{-1}(m_Z^2)$ is only known with a relative precision of about 0.01%, even though its value at $q^2 \sim 0$ is known with an amazing relative precision of $4 \times 10^{-9}$ due to the uncertainties in the calculation of the running of $\alpha$. In fact, given the accuracy already achieved and described in the next sections, an effort would be needed to improve the accuracy of the input parameters, and in particular $\alpha({m_Z}^2)$, if the precision of future measurements is not to be jeopardised.

From the point of view of EW radiative corrections we can divide the experimental measurements into four different groups: the $Z^0$ total and partial widths ($\Gamma_Z$), the partial width into $b$-quarks ($\mathrm{R}_b$), the $Z^0$ asymmetries ($\sin^2\theta_{\mathrm{eff}}^{\mathrm{lept}}$) and the $W^{\pm}$ mass ($m_W$). For instance, the $Z^0$ leptonic width is mostly sensitive to isospin-breaking loop corrections ($\Delta\rho$), the asymmetries are specially sensitive to radiative corrections to the $Z^0$ self-energy ($\Delta\kappa$ ), and $\mathrm{R}_b$ is mostly sensitive to vertex corrections ($\epsilon_b$) in the decay $Z^0 \to b\bar{b}$. One more parameter, $\Delta r$, is necessary to describe the radiative corrections to the relation between $G_\mu$ and $m_W$, and in fact it is the measured $\Delta r$ the most significant evidence for pure EW radiative corrections in agreement with the GWS theory.

## 2.1. *Definition of pseudo-observables at the $Z^0$ pole*

The shape of the resonance is completely characterised by three parameters: the position of the peak ($m_Z$), the width ($\Gamma_Z$) and the height ($\sigma^0_{f\bar{f}}$) of the resonance:

$$\sigma^0_{f\bar{f}} = \frac{12\pi}{m_Z^2}\frac{\Gamma_e\Gamma_f}{\Gamma_Z^2}.$$

The good capabilities of the LEP and SLC detectors to identify lepton flavours allows a measurement of the ratio of the different lepton species with respect to the hadronic cross-section, $R_\ell = \Gamma_h/\Gamma_\ell$. The large mass and long lifetime of the $b$ and $c$ quarks provides a way to perform flavour tagging. This allows for precise measurements of the partial widths of the decays $Z^0 \to c\bar{c}$ and $Z^0 \to b\bar{b}$. It is useful to normalise the partial width to $\Gamma_h$ by measuring the partial decay fractions with respect to all hadronic decays:

$$\mathrm{R}_c \equiv \frac{\Gamma_c}{\Gamma_h}, \quad \mathrm{R}_b \equiv \frac{\Gamma_b}{\Gamma_h}.$$

With this definition most of the radiative corrections appear both in the numerator and denominator and thus cancel out, with the important exception of the vertex corrections in the $Z^0 b\bar{b}$ vertex. This is the only relevant correction to $\mathrm{R}_b$, and within the SM basically depends on a single parameter, the mass of the top quark. The partial decay fractions of the $Z^0$ to other quark flavours, like $\mathrm{R}_c$, are only weakly dependent on $m_t$; the residual weak dependence is indeed due to the presence of $\Gamma_b$ in the denominator. The SM predicts $\mathrm{R}_c = 0.172$, valid over a wide range of the input parameters.

Parity violation in the weak neutral current is caused by the difference of couplings of the $Z^0$ to right-handed and left-handed fermions. If we define $A_f$ as

$$A_f \equiv \frac{2\left(\frac{g_V^f}{g_A^f}\right)}{1+\left(\frac{g_V^f}{g_A^f}\right)^2},$$

where $g^f_{V(A)}$ denotes the vector (axial-vector) coupling constants of the $Z^0$ and the corresponding fermion, one can write all the $Z^0$ asymmetries in terms of $A_f$.

Each process $e^+e^- \to Z \to f\bar{f}$ can be characterised by the direction and the helicity of the emitted fermion ($f$). Calling forward the hemisphere into which the electron beam is pointing, the events can be subdivided into four categories: FR, BR, FL and BL, corresponding to right-handed (R) or left-handed (L) fermions emitted in the forward (F) or backward (B) direction. Then, one can write three $Z^0$ asymmetries as:

$$A_{\mathrm{pol}} \equiv \frac{\sigma_{\mathrm{FR}}+\sigma_{\mathrm{BR}}-\sigma_{\mathrm{FL}}-\sigma_{\mathrm{BL}}}{\sigma_{\mathrm{FR}}+\sigma_{\mathrm{BR}}+\sigma_{\mathrm{FL}}+\sigma_{\mathrm{BL}}} = -A_f,$$
$$A_{\mathrm{pol}}^{\mathrm{FB}} \equiv \frac{\sigma_{\mathrm{FR}}+\sigma_{\mathrm{BL}}-\sigma_{\mathrm{BR}}-\sigma_{\mathrm{FL}}}{\sigma_{\mathrm{FR}}+\sigma_{\mathrm{BR}}+\sigma_{\mathrm{FL}}+\sigma_{\mathrm{BL}}} = -\frac{3}{4}A_e,$$
$$A_{\mathrm{FB}} \equiv \frac{\sigma_{\mathrm{FR}}+\sigma_{\mathrm{FL}}-\sigma_{\mathrm{BR}}-\sigma_{\mathrm{BL}}}{\sigma_{\mathrm{FR}}+\sigma_{\mathrm{BR}}+\sigma_{\mathrm{FL}}+\sigma_{\mathrm{BL}}} = \frac{3}{4}A_eA_f$$

and in case the initial state is polarised with some degree of polarisation ($P$), one can define:

$$A_{\mathrm{LR}} \equiv \frac{1}{P}\frac{\sigma_{\mathrm{Fl}}+\sigma_{\mathrm{Bl}}-\sigma_{\mathrm{Fr}}-\sigma_{\mathrm{Br}}}{\sigma_{\mathrm{Fr}}+\sigma_{\mathrm{Br}}+\sigma_{\mathrm{Fl}}+\sigma_{\mathrm{Bl}}} = A_e,$$
$$A_{\mathrm{FB}}^{\mathrm{pol}} \equiv -\frac{1}{P}\frac{\sigma_{\mathrm{Fr}}+\sigma_{\mathrm{Bl}}-\sigma_{\mathrm{Fl}}-\sigma_{\mathrm{Br}}}{\sigma_{\mathrm{Fr}}+\sigma_{\mathrm{Br}}+\sigma_{\mathrm{Fl}}+\sigma_{\mathrm{Bl}}} = \frac{3}{4}A_f$$

where r(l) denotes the right(left)-handed initial state polarisation. Assuming lepton universality, all these observables depend only on the ratio between the vector and axial-vector couplings between the $Z^0$ boson and the leptons. It is conventional to define the effective mixing angle $\sin^2\theta_{\text{eff}}^{\text{lept}}$ as

$$\sin^2\theta_{\text{eff}}^{\text{lept}} \equiv \frac{1}{4}\left(1-\frac{g_V^l}{g_A^l}\right)$$

and to convert all the asymmetry measurements into a single parameter $\sin^2\theta_{\text{eff}}^{\text{lept}}$.

## 3. Precision measurements at $e^+e^-$ colliders

### 3.1. *Precise energy determination at LEP*

Knowledge of the LEP beam energy is fundamental to the determination of the $Z^0$ mass and width [13], and the $W^\pm$ mass [14], and gradual unravelling of unexpected systematic effects took years in order to achieve the final precision.

Of historical interest, protons circulated around the ring for the first time in 1989, long before the advent of the LHC. Their speed at injection energy, 20 GeV, was inferred by comparing the radio-frequency needed to maintain protons and electrons on the LEP central orbit (through the centre of the focussing quadrupoles). This was extrapolated to 45 GeV using magnetic measurements to give a 20 MeV uncertainty on the $Z^0$ mass; the beam energy is proportional to the total magnetic field seen by the beam, $\oint B\cdot \mathrm{d}\ell$. However, the beam energy can be determined much more precisely with the technique of resonant depolarisation. The electron spin tends to align with the bending field due to synchrotron radiation, and significant polarisation can build up if the beam orbit is sufficiently smooth. The spins precess, with the number of precessions per orbit, $\nu_s$, given by:

$$\nu_s = \frac{g_e-2}{2}\frac{e}{2\pi m_e}\oint B\cdot \mathrm{d}\ell = \frac{g_e-2}{2}\frac{E_{\text{beam}}}{m_e}. \tag{1}$$

The polarisation is monitored, as the frequency of a fast sweeping horizontal magnetic field is varied. This depolarises the beam when the external field frequency matches $\nu_s$. The instantaneous precision on the beam energy is $\mathcal{O}(100)$ keV, but the technique can not be used when the beams are in collision. Instead the beam energy could be measured at the ends of fills. However, the beam energy was found to vary with time. In Figure 2, the results of several long term experiments to monitor the beam energy with resonant depolarisation were understood to be due to earth tides. The length of the beam orbit is fixed by the radio frequency (RF) accelerating cavities. The bulge of the earth due to tides changes the length of the tunnel by about 1 mm in 27 km, so the magnets move with respect to the beam. The extra contribution from the quadrupoles changes the beam energy with an amplitude of about 10 MeV.

In 1995, two NMR probes were installed in LEP dipoles to monitor the bending field on opposite sides of the ring. There was noise related to some unknown activity, with a quiet period over night, resulting in a general trend for the energy to increase during a fill. The beam energy measurement from the end of a fill was giving a bias of typically 5 MeV. This was eventually understood as being due to vagabond currents from the French high speed trains (TGV). A strong correlation was observed as a function of time between the current measured on the rail lines, the voltage on the LEP beam pipe, and the field measured by the NMRs. The return current from the trains from the nearest point labelled "Zimeysa" in Figure 2 flowed back to the power station in two directions round the ring, and then via a local river. A model to describe this average behaviour was derived and restrospectively applied to all the previous years' data [13]. This model took into account other effects including magnet temperatures, and interaction point dependent effects.

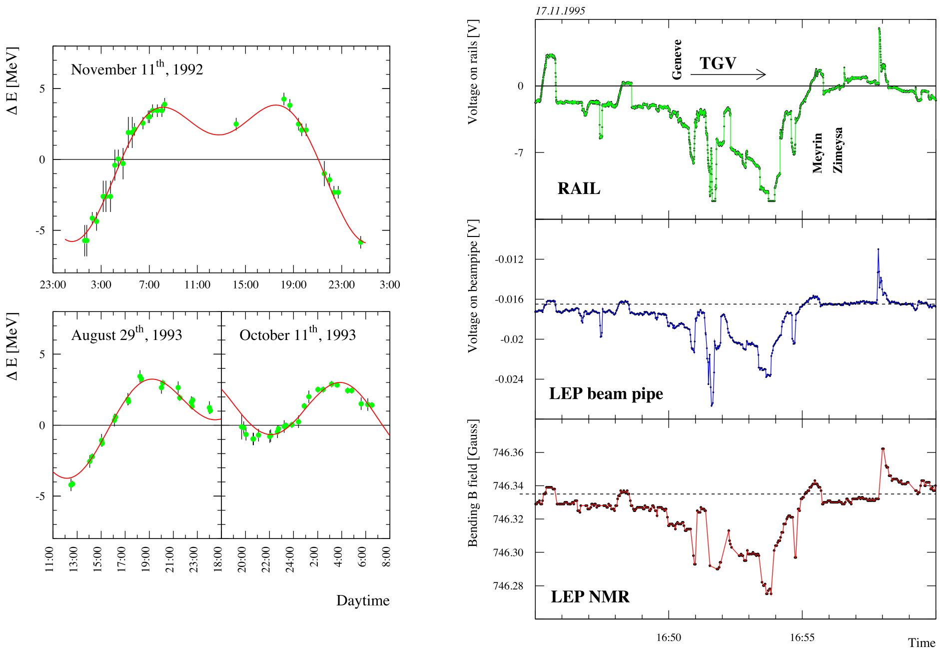


**Figure 2.** (left) Tides and polarisation measurement. Results from repeated beam energy measurements by resonant depolarisation (points), compared to the prediction of the energy taking into account earth tides (curves). (right) Simultaneous measurements of the current on the rail lines, the voltage on the LEP beam pipe, and the dipole magnetic field as a TGV leaves Geneva.

The collision energy was expected to be the same at all four interaction points, but already with the 1991 data, the results showed a trend for OPAL and L3 to have a lower value for the $Z^0$ mass than ALEPH and DELPHI. The discrepancy was traced to the positioning of the RF cavities. They were aligned to the wrong frequency, so that in practice the collision energy was higher in OPAL and L3. The exact configuration of the RF cavities was even more important as the beam energy increased during LEP2. In addition, the beam polarisation decreased as the beam energy increased, so for the measurement of the $W^\pm$ mass, magnetic extrapolation was again needed from resonant depolarisation measurements spanning up to 65 GeV and the full beam energy [14]. Additional NMR probes, two per octant, were installed, which also helped to validate the LEP1 beam energy model. A new spectrometer was also installed; a standard LEP dipole magnet was replaced by a shorter, precisely-mapped steel dipole magnet. Beam pickup monitors either side of this new dipole allowed a precise measurement of the bending angle to yield an independent measurement of the beam energy which was again cross-calibrated at lower energy with resonant depolarisation.

As a result of these very detailed studies and many careful cross checks, the final uncertainty due to the centre-of-mass energy was 1.7 MeV for the $Z^0$ mass, out of a total uncertainty of 2.1 MeV. The uncertainty increased to 10 MeV for the $W^\pm$ mass measurement, but this was still a relatively small component of the LEP combined 33 MeV uncertainty.

### 3.2. *Polarisation at SLC*

The SLC was the first $e^+e^-$ linear collider. The era of high precision measurements at SLC started in 1992 with the first longitudinally polarised beams. The polarisation was achieved by shining circularly polarised laser light on a gallium arsenide photo-cathode at the electron source. At that time, the electron polarisation was only $P \sim 22\%$. Shortly thereafter, improvements in the photocathodes allowed to increase the polarisation significantly, close to $P \sim 75\%$. Much work was invested in the SLC machine to maintain the electron polarisation at a very high value throughout the production, damping, acceleration and transfer through the arcs. The polarised beam physics programme at the SLC required additional instrumentation beyond the main SLD detector, most notably, precision polarimetry. A Compton-scattering polarimeter installed near the beam interaction point reached an ultimate precision of $\Delta P \sim 0.5\%$ which ensured that polarimetry systematics were never the leading contribution to the uncertainties.

### 3.3. *Detectors at LEP/SLC*

The designs of the LEP and SLC detectors are quite similar, although the details vary significantly among them. Starting radially from the interaction point, there is first a vertex detector, followed by a gas drift chamber to measure the parameters of charged tracks. Surrounding the tracking system is a calorimeter system, usually divided into electromagnetic and hadronic sections. Finally, an outer tracking system designed to measure the parameters of penetrating particles (muons) completes the system. The central part of the detector (at least the tracking chamber) is immersed in a solenoidal magnetic field to allow the measurement of the momentum of charged particles. In addition, particle identification systems may be installed, including $\mathrm{d}E/\mathrm{d}x$ ionisation loss measurements in the central chamber, time-of-flight, and ring-imaging Cherenkov detectors.

Special detectors extending to polar angles of ~25 mrad with respect to the beam axis detect small-angle Bhabha scattering events. The rate of these events was used for the luminosity determinations, as the small-angle Bhabha process is due almost entirely to QED, and the cross-section can be calculated precisely. All the LEP experiments replaced their first-generation luminosity detectors, which had systematic uncertainties at the percent level, with high-precision devices capable of pushing systematic uncertainties on the acceptance of small-angle Bhabha scattering events below one per-mille.

As a consequence of the improvements to the detectors and also in the understanding of the beam energy at LEP1, and the production of high beam polarisation at SLC, statistical and systematic uncertainties are much smaller for the later years of data taking, which hence dominate the precision achieved on the $Z^0$ parameters. All five detectors had almost complete solid angle coverage; the only holes being at polar angles below the coverage of the luminosity detectors.

### 3.4. *LEP/SLC combination and results*

The LEP electroweak working group was established in the early 1990s, including physicists from all four experiments to combine the cross-section and forward-backward asymmetry measurements at each energy point. The level of sophistication of the combinations was refined over the years as the statistical and systematic uncertainties improved. Correlations between experiments were carefully evaluated, including common effects coming from the LEP beam energy measurement, theoretical modelling of $Z^0$ decays and backgrounds, and Monte Carlo treatment of fragmentation and hadronisation.

In some areas, such as $Z^0$ decays to heavy-flavour quarks, this took detailed negotiations to agree on common treatments of systematic effects, and by 1994, results from the SLD heavy-flavour group were also included in a coherent way. While for the main lineshape and lepton asymmetry measurements, each experiment measured the same set of parameters, the situation was more complicated for heavy-flavour electroweak results. Different experiments used different tagging methods; some analyses made combined fits which included semileptonic branching

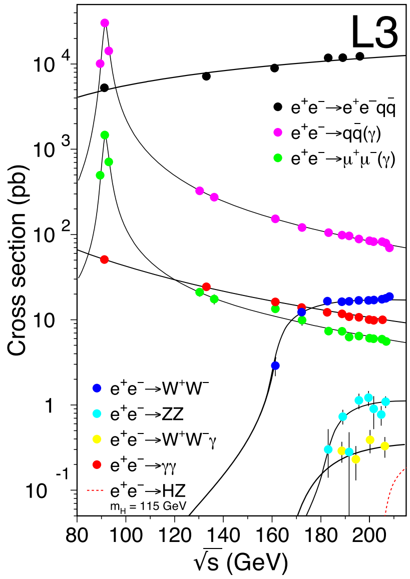


**Figure 3.** Measurements of various cross-sections in $e^+e^-$ collisions. This example is from the L3 collaboration, and indicates the precision around the $Z^0$ peak, and as $e^+e^- \to W^\pm W^\pm$ is accessible at higher centre-of-mass energies.

ratios and $B^0$ mixing parameters; the measurements could have an explicit dependence on other parameters such as the partial widths to $b$- and $c$-quarks, introducing additional correlations.

The results from 18 million $Z^0$ decays from the four LEP experiments, ALEPH, DELPHI, L3 and OPAL, and from the SLD experiment at SLC, provide numerous measurements of $Z^0$ boson properties, from inclusive hadron production, and from pair-production of charged leptons and heavy quarks. The production cross-sections and asymmetries as a function of centre of mass energies yield the combined results [15]

$$\begin{aligned}
m_Z &= 91.1875 \pm 0.0021\ \mathrm{GeV}/c^2,\\
\Gamma_Z &= 2.4952 \pm 0.0023\ \mathrm{GeV},\\
\rho_\ell &= 1.0050 \pm 0.0010,\\
\sin^2\theta_{\mathrm{eff}}^{\mathrm{lept}} &= 0.23153 \pm 0.00016,\\
N_\nu &= 2.9840 \pm 0082.
\end{aligned}$$

The sensitive test of lepton universality in $Z^0$ decays is demonstrated in Figure 4, comparing the combined left and right-handed couplings for the three types of charged lepton. The full set of combined measurements is listed in Figure 5, where the results are also compared to a global fit including other measurements at the time of the final LEP 1 publication [15].

The LEP measurements of the $W^\pm$-boson mass [16] are shown in Figure 6 where they are also compared with measurements from hadron colliders, which are discussed in the next section.

## 4. Precision measurements at hadron colliders

### 4.1. $W^\pm$ mass measurements

At hadron colliders, precision measurements of $W^\pm$ and $Z^0$ properties are limited to leptonic final states with electrons or muons. The main parameter of interest is the $W^\pm$ mass. Samples of $Z^0 \to$

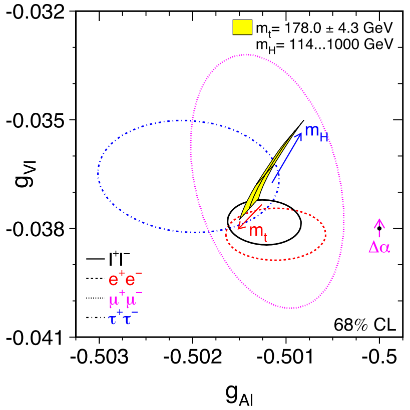


**Figure 4.** Comparison of the effective vector and axial-vector coupling constants for leptons. The shaded region shows the SM prediction with $m_t = 178.0 \pm 4.3$ GeV and $m_H = 300^{+700}_{-186}$ GeV.

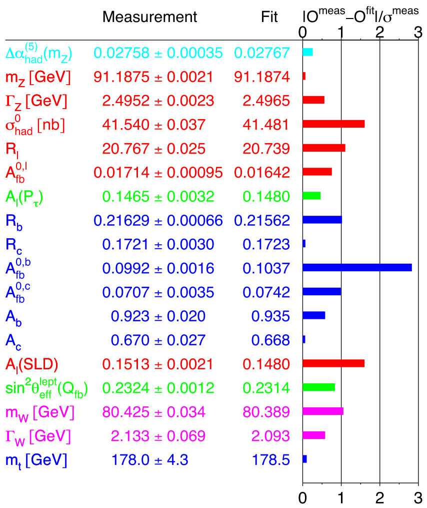


**Figure 5.** Comparison of measurements with the SM prediction from the best fit. Also shown is the pull of each measurement, defined as the difference between the measurement an expectation in units of the measurement uncertainty.

$e^+e^-$ or $\mu^+\mu^-$ are typically used to calibrate the energy or momentum response of the detector, normalising to the LEP measurement. $Z^0$ boson samples are also of use to control systematic uncertainties in the prediction of the $W^\pm$ transverse momentum spectrum. Production of $W^\pm$ and $Z^0$ bosons is dominated by quark-antiquark annihilation.

The $W^\pm$ mass is determined from fits to the distributions of the transverse momentum of the charged lepton, $p_T^\ell$, the neutrino, $p_T^\nu$, and of the transverse mass, $m_T$. The neutrino transverse momentum is taken to be the missing transverse momentum, $p_T^{miss}$, estimated from the negative vector sum of the transverse momenta of visible particles. The transverse mass is defined by $m_T^2 = 2p_T^\ell p_T^{miss}(1-\cos\Delta\phi)$, where $\Delta\phi$ the azimuthal opening angle between the charged lepton and missing transverse momentum. The kinematic distributions depend on detector effects, and also the modelling of the $W^\pm$ transverse momentum and parton distribution fuctions (PDFs).

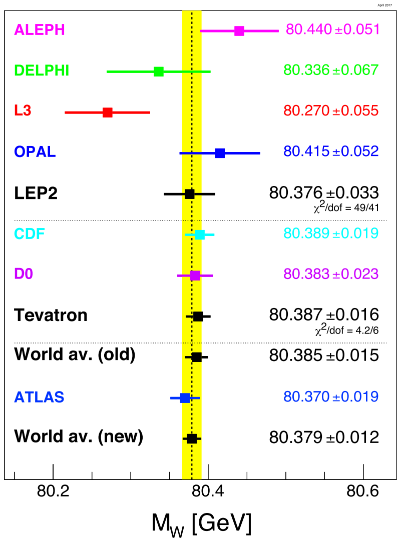


**Figure 6.** The latest world average $W^{\pm}$ mass from the Tevatron electroweak working group, and an update by the PDG including the new ATLAS result.

Valence (anti)quarks dominate at the Tevatron, while in higher-energy proton-proton collisions at the LHC, sea-quarks play a much more important role.

The Tevatron combined result is dominated by the most recent CDF and D0 measurements [17]. The CDF result uses $W \to \mu\nu$ and $W \to e\nu$ events in 2.2 fb$^{-1}$ recorded between 2002 and 2007. The momentum scale from $J/\psi$ and $\Upsilon$ decays to muon pairs yields a $Z^0$ mass consistent with the LEP average, so this is used as an additional constraint. The electromagnetic energy scale is determined from a fit to the $E/p$ distribution for electrons in $W^{\pm}$ and $Z^0$ decays. The $Z^0$ mass is again used as a consistency check and a constraint. The CDF measurement is obtained from a combination of all six observables, $p_T^{\ell}$, $p_T^{\nu}$ and $m_T$ for muons and for electrons. The most precise D0 measurement is from 4.3 fb$^{-1}$ recorded between 2006 and 2009, and only uses electrons. The energy scale is calibrated from $Z^0$ decays. The result combines the $p_T^e$ and $m_T$ distributions, and an earlier measurement using 1.0 fb$^{-1}$ recorded in 2002 to 2006.

The overall Tevatron combined precision is 16 MeV [17], compared to the combined LEP precision of 33 MeV, and leading to a world average $W^{\pm}$ mass from 2013 of $80.385 \pm 0.015$ GeV. This is displayed in Figure 6 [18].

ATLAS published their first $W^{\pm}$ mass measurement using the 7 TeV dataset recorded in 2011 [19]. The analysis uses $W \to e\nu$ and $W \to \mu\nu$ events, making template fits to the lepton $p_T$ or the transverse mass, $m_T$, of the $\ell\nu$ system. A sample of $Z \to \ell\ell$ events is also used for calibration; calibration of the leptons and of the hadronic recoil to the $W^{\pm}$ boson is the biggest experimental challenge in this measurement. The multijet background is evaluated from fits in bins of lepton isolation, which are then extrapolated to isolated leptons in the $W^{\pm}$ sample.

With the experimental uncertainties under control, physics modelling uncertainties dominate. These are also controlled by comparison to $W^{\pm}$ or $Z$ data in order to rule out large model variations, for example of the vector boson $p_T$ spectrum. Rapidity distributions and angular variables describing the decay products are reweighted to NNLO calculations. Angular variables are validated with $Z$ data including the larger 8 TeV sample from 2012.

Separate fits are performed according to lepton charge, lepton flavour ($e$ or $\mu$) and to the $p_T$ and $m_T$ distributions. The fit results also provide a closure test of the quality of modelling.

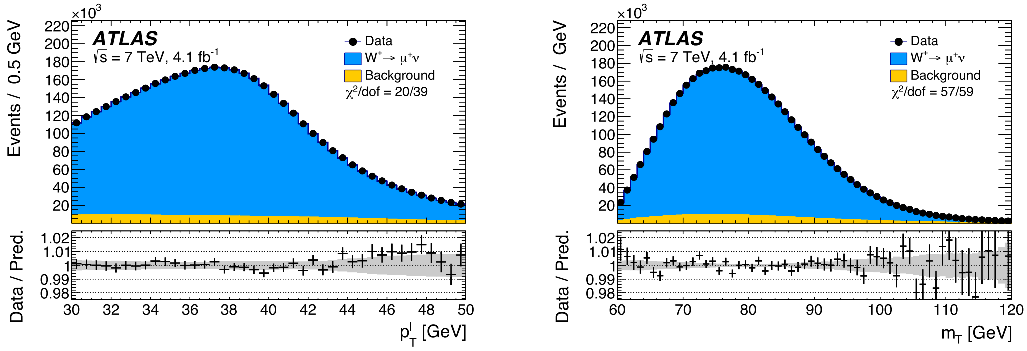


**Figure 7.** $W^{\pm}$ mass example fits to the $\mu^{+}$ $p_{\mathrm{T}}$ (left) and $m_{\mathrm{T}}$ (right) distributions.

**Table 1.** Systematic uncertainties in the $W^{\pm}$ mass measurements

| Uncertainty (MeV) | CDF (2.2 fb$^{-1}$) | D0 (4.3 fb$^{-1}$) | ATLAS (4.6 fb$^{-1}$) |
|---|---|---|---|
| Statistical | 12 | 13 | 7 |
| Experimental syst | 10 | 18 | 11 |
| QCD | n/a | n/a | 8 |
| PDF | 10 | 11 | 9 |
| QED | 4 | 7 | 6 |
| $p_{\mathrm{T}}(W)$ | 5 | 2 | n/a |

Two examples are shown in Figure 7. The final result is a weighted average, yielding $m_W = 80370 \pm 7(\mathrm{stat}) \pm 11(\mathrm{exp.\ syst.}) \pm 14(\mathrm{model})$ MeV, i.e. a combined precision of 19 MeV, equal to the CDF precision. The Particle Data Group [18] have made a new world average assuming 7 MeV common PDF uncertainty between the Tevatron and LHC results, as also shown in Figure 6.

The $W^{\pm}$ mass uncertainties are compared in Table 1, where the ATLAS uncertainties are taken from Table 11 of Ref. [19] for the combined result. To achieve a 10 MeV total uncertainty, the dominant PDF uncertainties will have to be reduced to about 5 MeV for the Tevatron results. With the huge samples of $W^{\pm}$ and $Z^{0}$ events at the LHC, there is scope to further reduce the experimental systematic uncertainties, and combining measurements with improved calculations to control the other modelling uncertainties.

### 4.2. *Weak mixing angle*

The forward-backward asymmetry of $Z^{0} \to \ell\ell$ decays at hadron colliders depends on the mixture of up- and down-type quarks, and therefore depends strongly on the proton PDFs in deriving a measurement of $\sin^2\theta_{\mathrm{eff}}^{\mathrm{lept}}$.

The combined Tevatron measurements of $\sin^2\theta_{\mathrm{eff}}^{\mathrm{lept}}$ achieve a precision of 0.00033, as shown in Figure 8. There are now also competitive results from CMS [20] using 8 TeV data and a preliminary measurement from ATLAS [21] using 7 TeV data. The CMS measurement derives $\sin^2\theta_{\mathrm{eff}}^{\mathrm{lept}}$ from template fits to the forward backward asymmetry in different rapidity regions. The ATLAS measurement is a fit to the full angular description of the differential cross-section $pp \to Z \to \ell\ell$. It includes central $\mu\mu$ and $ee$ events, and an additional category of central-forward $ee$ events which bring extra precision, since the asymmetry is larger in the forward region. Now that these measurements approach the precision of the LEP and SLD experiments, particular care

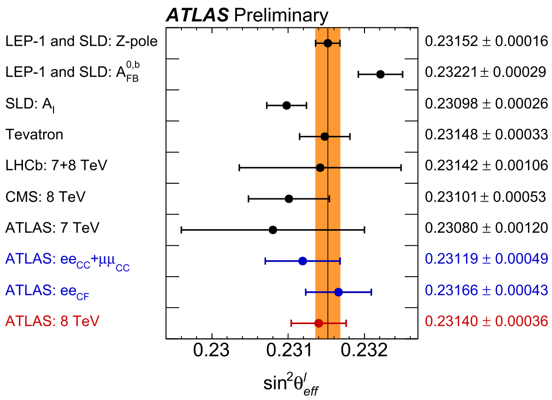


**Figure 8.** the most recent combinations of $\sin^2\theta_{\text{eff}}^{\text{lept}}$ measurements from LEP, SLD, the Tevatron and the LHC.

will be needed to be sure that consistent definitions of $\sin^2\theta_{\text{eff}}^{\text{lept}}$ are used, including QED and QCD corrections.

## 5. Future precision measurements

Several future $e^+e^-$ colliders are being discussed as worldwide projects that could contribute significantly to the precision measurements of the $Z^0$ and $W^\pm$ boson properties: the International Linear Collider (ILC) [22] which may be built in Japan, FCC-ee [23] a future circular collider proposed to be built at CERN and CEPC [24] a similar proposal to be built in China. Circular colliders will have several advantages: the most obvious one is extremely high statistics ($5\times10^{12}$ $Z^0$, $10^8$ $W^\pm W^\pm$) compared with the GigaZ scenario where the ILC would collect up to three orders of magnitude less statistics. However, probably even more important is the ability of the circular collider proposals (FCC-ee and CEPC) to determine with high precision (better than 100 keV!) the centre-of-mass energies at the $Z^0$ pole and $W^\pm W^\pm$ threshold, thanks to the availability of transverse polarisation and resonant depolarisation (see previous sections). In addition, the FCC-ee proposal includes an optimised run plan to allow a complete programme of ancillary measurements of input parameters that currently would limit the precision of EW tests, a crucial example being the direct measurement [25] of $\alpha(m_Z{}^2)$ from the $Z^0-\gamma$ interference in the process $e^+e^-\to\mu^+\mu^-$.

The ILC ability to have longitudinal polarised beams (up to 80%) in the GigaZ option could allow for a measurement of the left-right asymmetry at the level of $\Delta(A_{LR})\sim10^{-4}$ [26] (two orders of magnitude better than existing measurements) and competitive with what equivalent measurements of the $\tau$ forward-backward polarisation asymmetry could provide at the FCC-ee (or CEPC), both sets of measurements measuring the same combination of couplings.

It is clear, however, that the best ultimate precision in most of the relevant observables for precision measurements of the $Z^0$ and $W^\pm$ bosons would come from the future circular colliders proposals. As an example, Table 2 shows the expected sensitivities for some of the relevant observables expected from the ILC-GigaZ proposal and FCC-ee. The quoted uncertainties include the current estimation of the systematic uncertainties, which for many of the observables quoted in Table 2 dominate the total uncertainty.

## 6. Conclusions

The four LEP experiments, ALEPH, DELPHI, L3 and OPAL, and the SLD experiment at the SLC, took precision measurements of $W^\pm$ and $Z^0$ boson properties to an unprecedented level after

**Table 2.** Measurement of selected EW quantities at the FCC-ee compared with present precision and ILC-GigaZ precision taken from references [26, 27]

| Observable | Present value | ILC-GigaZ uncertainty | FCC-ee uncertainty |
|---|---|---|---|
| $m_Z$ (MeV) | $91186.7 \pm 2.2$ | 2.1 | 0.1 |
| $\Gamma_Z$ (MeV) | $2495.2 \pm 2.3$ | 1.0 | 0.1 |
| $R_\ell$ ($\times 10^3$) | $20767 \pm 25$ | 4 | 0.2–1.0 |
| $R_b$ ($\times 10^4$) | $2162.9 \pm 6.6$ | 1.2 | ~0.6 |
| $\sin^2\theta_{\text{eff}}^{\text{lept}}$ ($\times 10^5$) | $23148.0 \pm 16$ | 1.3 | 0.5 |
| $A_{LR}$ ($\times 10^3$) | $151.3 \pm 2.1$ | 0.1 | - |
| $A_{\text{pol}}^{\text{FB},\tau}$ ($\times 10^3$) | $149.8 \pm 4.9$ | - | ~0.2 |
| $m_W$ (MeV) | $80350 \pm 15$ | 5 | 0.5 |

their first observation at UA1 and UA2. There was very close collaboration with accelerator experts to ensure that the LEP beam energy and SLC beam polarisation were well understood. The LEP electroweak working group and SLD heavy-flavour group ensured that the measurements were combined taking into account statistical correlations and systematic uncertainties. This pioneering inter-experiment cooperation expanded to other areas, including flavour physics and searches, so that the experiments could provide robust combined results taking into account all the "inside" information. Experiments at hadron colliders, with much larger samples of $W^\pm$ and $Z^0$ events, for improve the precision, in particular of the $W^\pm$-boson mass in leptonic final states. There are exciting prospects for future machines, which will probe $W^\pm$ and $Z^0$ physics improving the sensitivity to physics beyond the Standard Model in the decades to come.

## References


[1] E. Fermi, "Attempt at a theory of β-rays", *Il Nuovo Cimento* **11** (1934), p. 1.

[2] E. Fermi, "Attempt at a theory of β-rays. 1.", *Z. Phys.* **88** (1934), p. 161-177.

[3] S. L. Glashow, "Partial-symmetries of weak interactions", *Nuclear Phys.* **22** (1961), p. 579-588.

[4] S. Weinberg, "A model of leptons", *Phys. Rev. Lett.* **19** (1967), p. 1264-1266.

[5] A. Salam, *Proc. 8th Nobel Symp.*, 1968, 367 pages.

[6] F. J. Hasert *et al.*, "Search for elastic $\nu_\mu$ electron scattering", *Phys. Lett. B* **46** (1973), p. 121-124, [5.11(1973)].

[7] F. J. Hasert *et al.*, "Observation of neutrino like interactions without muon or electron in the Gargamelle neutrino experiment", *Phys. Lett. B* **46** (1973), p. 138-140, [5.15(1973)].

[8] C. Rubbia, P. McIntyre, D. Cline, *Producing Massive Neutral Intermediate Vector Bosons with Existing Accelerators*, Vieweg+Teubner Verlag, Wiesbaden, 1977, 683-687 pages.

[9] G. Arnison *et al.*, "Experimental observation of isolated large transverse energy electrons with associated missing energy at $s = 540$ Gev", *Phys. Lett. B* **122** (1983), no. 1, p. 103-116.

[10] M. Banner *et al.*, "Observation of single isolated electrons of high transverse momentum in events with missing transverse energy at the cern pp collider", *Phys. Lett. B* **122** (1983), no. 5, p. 476-485.

[11] G. Arnison *et al.*, "Experimental observation of lepton pairs of invariant mass around 95-GeV/c**2 at the CERN SPS collider", *Phys. Lett. B* **126** (1983), p. 398-410, [7.55(1983)].

[12] P. Bagnaia *et al.*, "Evidence for $Z^0 \to e^+ e^-$ at the CERN anti-p p collider", *Phys. Lett. B* **129** (1983), p. 130-140, [7.69(1983)].

[13] R. Assmann *et al.*, "Calibration of center-of-mass energies at LEP-1 for precise measurements of Z properties", *Eur. Phys. J. C* **6** (1999), p. 187-223.

[14] R. Assmann *et al.*, "Calibration of centre-of-mass energies at LEP 2 for a precise measurement of the W boson mass", *Eur. Phys. J. C* **39** (2005), p. 253-292.

[15] "Precision electroweak measurements on the Z resonance", *Phys. Rep.* **427** (2006), no. 5-6, p. 257-454.

[16] "Electroweak measurements in electron-positron collisions at W-Boson-pair energies at LEP", *Phys. Rep.* **532** (2013), no. 4, p. 119-244.

[17] T. A. Aaltonen *et al.*, "Combination of CDF and D0 *W*-Boson mass measurements", *Phys. Rev. D* **88** (2013), no. 5, article ID 052018.

[18] M. Tanabashi *et al.*, "Review of particle physics", *Phys. Rev. D* **98** (2018), article ID 030001.
[19] "Measurement of the $W$-boson mass in pp collisions at $\sqrt{s} = 7$ TeV with the ATLAS detector", *Eur. Phys. J. C* **78** (2018), no. 2, article ID 110, [Erratum: *Eur. Phys. J.* C78 (2018) no. 11, 898].
[20] "Measurement of the weak mixing angle using the forward-backward asymmetry of Drell-Yan events in pp collisions at 8 TeV", *Eur. Phys. J. C* **78** (2018), no. 9, article ID 701.
[21] ATLAS Collaboration, "Measurement of the effective leptonic weak mixing angle using electron and muon pairs from $Z$-boson decay in the ATLAS experiment at $\sqrt{s} = 8$ TeV". Technical Report ATLAS-CONF-2018-037, CERN, Geneva, Jul 2018.
[22] H. Baer *et al.*, "The international linear collider technical design report - volume 2: Physics", 2013, preprint, https://arxiv.org/abs/1306.6352.
[23] A. Abada *et al.*, "Fcc-ee: the lepton collider", *Eur. Phys. J. Spec. Topics* **228** (2019), no. 2, p. 261-623.
[24] The CEPC Study Group, "CEPC conceptual design report: volume 1 - accelerator", 2018, preprint, https://arxiv.org/abs/1809.00285.
[25] P. Janot, "Direct measurement of $\alpha_{\mathrm{qed}}(mz^2)$ at the fcc-ee", *J. High Energy Phys.* **2016** (2016), no. 2.
[26] A. Irles, R. Pöschl, F. Richard, H. Yamamoto, "Complementarity between ILC250 and ILC-GigaZ", 2019, preprint, https://arxiv.org/abs/1905.00220.
[27] A. Abada *et al.*, "Fcc physics opportunities", *Eur. Phys. J. C* **79** (2019), no. 6, article ID 474.

*Comptes Rendus*
*Physique*
**2020**, 21, nº 1, p. 23-43
https://doi.org/10.5802/crphys.8

A perspective of High Energy Physics from precision measurements
*La physique des Hautes Energies du point de vue des mesures de précision*

# Higgs Physics

## *La Physique du Boson de Higgs*

**Heather Gray [a] and Patrick Janot [*, b]**

[a] Department of Physics, University of California, Berkeley, CA 94720, USA

[b] CERN, 1 Esplanade des Particules, CH-1217 Meyrin, Switzerland.

*E-mails:* heather.gray@berkeley.edu (H. Gray), patrick.janot@cern.ch (P. Janot).

**Abstract.** The existence of the Higgs boson was postulated more than 50 years ago, without any indication of its mass. The quest that followed, with several generations of particle physics experiments, culminated with the recent discovery of a new particle with a mass of 125 GeV. At least another half-century will be needed to map the properties of this particle with sufficient precision to understand its deepest origin.

**Résumé.** L'existence du boson de Higgs a été postulée il y a plus de 50 ans sans indication d'un ordre de grandeur pour sa masse. La longue recherche qui s'en suivit, impliquant plusieurs générations d'expériences de physique des particules a été enfin couronnée par la découverte récente d'une nouvelle particule de masse de 125 GeV. Il s'en faudra sans doute de cinquante années supplémentaires pour en découvrir les propriétés avec une précision suffisante pour comprendre la profonde origine physique de cette particule.

**Keywords.** Higgs, Discovery, Properties, Future, Colliders, New physics.

**Mots-clés.** Higgs, Découverte, Propriétés, Futur, Collisionneurs, Nouvelle physique.

## 1. Introduction

The Higgs mechanism [1–4] was proposed in 1964 as a theoretical way to provide mass to the gauge bosons, through their interactions with the Higgs field, while safeguarding the symmetries believed to underlie modern particle physics. This vital development enabled Glashow [5], Weinberg [6], and Salam [7] to independently propose a unified "electroweak" theory, with a massless photon for the electromagnetic interaction, and massive $Z$ and $W$ bosons for the weak interaction. In a summary talk for the ICHEP conference in 1974, John Iliopoulos presented, for the first time in a single report [8], the view of physics now called the Standard Model (SM). When applied in the SM, the Higgs mechanism predicts the existence of a scalar particle, the Higgs boson $H$, which directly couples to SM particles – including itself – proportionally to their masses, but with an unknown mass, $m_H$.

[*] Corresponding author.

ISSN (electronic) : 1878-1535 

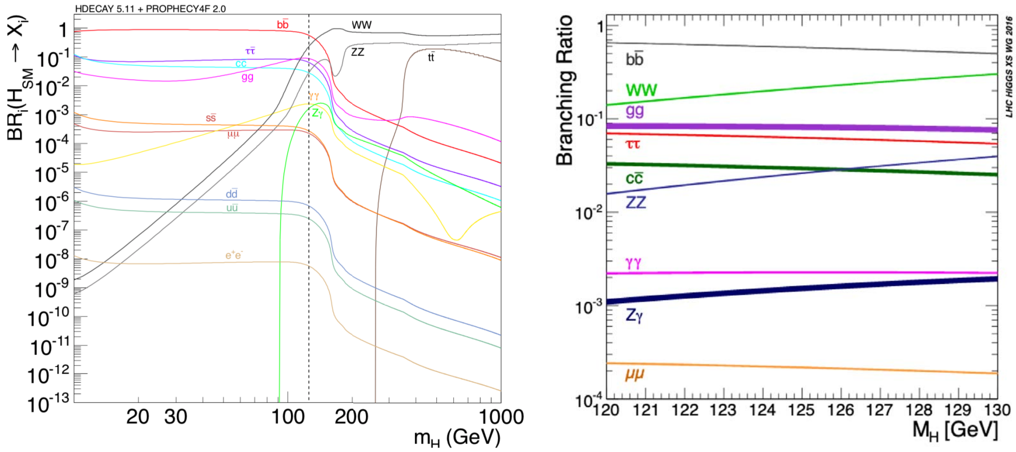


**Figure 1.** Predicted decay branching ratios of the SM Higgs boson over a wide mass range (left [9]) and close-up around $m_H = 125$ GeV (right [10]).

For any value of $m_H$, the production cross sections and decay rates of the SM Higgs boson can therefore be calculated accurately. For illustration, the predicted branching fractions are displayed in Figure 1 as a function of its mass. A campaign of searches for the SM Higgs boson was deployed over the following 50 years. This story, summarised in Section 2, culminated at LHC in 2012 with the discovery of a particle with a mass of 125 GeV, and with properties consistent with expectations for the SM Higgs boson.

With this discovery, the spectrum of particles and the interactions described by the SM are complete. Particle physics, however, must continue its investigations. On the one hand, many theoretical and experimental questions remained unanswered; on the other, the properties of the discovered particle are far from having been measured with the same precision as those of the other SM particles. It is essential to determine these properties with an accuracy order(s) of magnitude better than today, and to acquire sensitivity to the processes that, during the time span from $10^{-12}$ to $10^{-10}$ seconds after the Big Bang, led to the formation of today's Higgs vacuum field. Future hadron and lepton colliders are proposed to do exactly that. Their capabilities are reviewed and contrasted in Sections 3 to 5. Conclusions are offered in Section 6.

## 2. Current status of Higgs Physics

### 2.1. *Situation before LHC*

The first searches for a massless or light SM Higgs boson were performed in nuclear transitions and neutron-nucleon scattering [11, 12] in the early 1970s. They were followed in the 1980s by searches in the decays of pions [13], kaons [14], $B$ mesons [15], $J/\psi$'s and $\Upsilon$'s [16] (with a Higgs boson decay into $e^+e^-$ or $\mu^+\mu^-$) as discussed in Ref. [17], and a search by an original beam-dump experiment [18]. By 1989, a massless Higgs boson, and a Higgs boson with mass between 1 and 110 MeV, were excluded. A Higgs boson with a mass below 5–6 GeV was considered very unlikely, but not firmly excluded due to theoretical loopholes [17].

In the 20 years that followed, searches for a heavier Higgs boson were performed at the Large Electron-Positron collider (LEP) [19], located at CERN (Geneva, Switzerland) and at the Tevatron [20], located at Fermilab (Chicago, Illinois), benefiting from its large and unambiguously known couplings to the $Z$ and the $W$. At LEP, electrons and positrons collided at a centre-of-mass

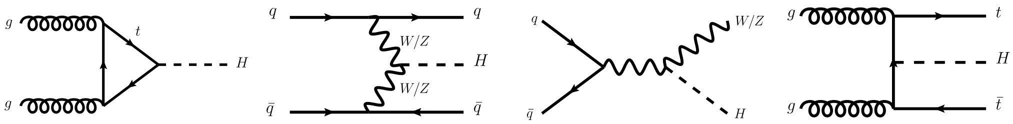


**Figure 2.** Higgs production modes with the largest cross section at LHC. From left to right, the production modes are gluon-gluon fusion; vector boson fusion; associated production with a vector boson; and associated production with a pair of top quarks.

energy around the $Z$ pole until 1995 (LEP1) and up to 209 GeV from 1996 to 2000 (LEP2). The Tevatron began colliding protons and anti-protons in 1985 initally at $\sqrt{s} = 1.8$ TeV and then from 2002 to 2011 at $\sqrt{s} = 1.96$ TeV.

Direct searches at LEP were performed using the Higgsstrahlung process, $e^+e^- \to HZ^{(*)}$, with the $Z$ decaying to a pair of charged leptons, neutrinos, or quarks. By the end of the LEP1 period, no such events had been found, and the mass range from 0.0 GeV to 65.6 GeV was excluded from these direct searches [21]. By the end of LEP2, a small excess of events was observed around 115 GeV in the last year of operation, and the lower limit on $m_H$ increased to 114.4 GeV [22]. Indirect effects of the Higgs boson on electroweak precision observables were also measured at LEP1, with almost 20 million recorded $Z$ decays. In combination with the direct determination of the $W$ and top masses at the Tevatron, these electroweak precision measurements constrained the SM Higgs boson mass in the range from 54 to 132 GeV [23]. Together with direct searches, the region between 114.4 and 132 GeV was thus favoured in the SM framework, at the 95% confidence level.

Direct searches for the SM Higgs boson produced in association with a vector boson, $q\bar{q} \to WH$ and $ZH$, were performed at the Tevatron. A small excess of events was found between 115 and 140 GeV, i.e. in the region still allowed by LEP precision measurements and direct searches, and Higgs boson masses between 149 and 182 GeV were excluded [24].

### 2.2. *Higgs discovery and measurements at LHC*

The Large Hadron Collider (LHC) [25] began colliding protons in 2009, reusing the existing LEP tunnel at CERN. At LHC, the most copious Higgs production mode is gluon-gluon fusion with a cross section of 17 pb at $\sqrt{s} = 7$ TeV [10]. Ordered by decreasing cross section, this mode is followed by vector boson fusion; associated production with a $W$ or $Z$ boson; and associated production with a pair of top quarks; as illustrated in Figure 2. A wide range of decay modes are accessible ranging from the high-resolution and low-background decays to four leptons (via $ZZ^*$ decay) and a pair of photons, through $WW^*$ and $\tau^+\tau^-$ decays, all the way to the low-resolution and high-background $b\bar{b}$ decay.

By the end of 2011, the ATLAS and CMS collaborations had collected approximately 5 $fb^{-1}$ of data at a centre-of-mass energy of 7 TeV. After all channels had been analysed and combined, the SM Higgs boson was excluded for all masses except for a small range around 125 GeV, where a modest excess of events with a significance of 2 to 3$\sigma$ was observed by each experiment [26, 27].

In 2012, the centre-of-mass energy increased from 7 to 8 TeV and the dataset doubled to 10 $fb^{-1}$ by the summer. At a joint seminar on 4 July 2012, the ATLAS and CMS collaborations reported the observation of a narrow resonance with a mass of approximately 126 GeV with statistical significance of 5.0$\sigma$ and 4.9$\sigma$ respectively [28, 29] and subsequently published this result in Refs. [30, 31]. Figure 3 shows two of the distributions contributing to this observation: $H \to ZZ^* \to 4\ell$ from ATLAS and $H \to \gamma\gamma$ from CMS.

Since the discovery in 2012, many of the properties of this new resonance have been measured and, so far, all these properties are consistent with the predictions for the SM Higgs boson. The

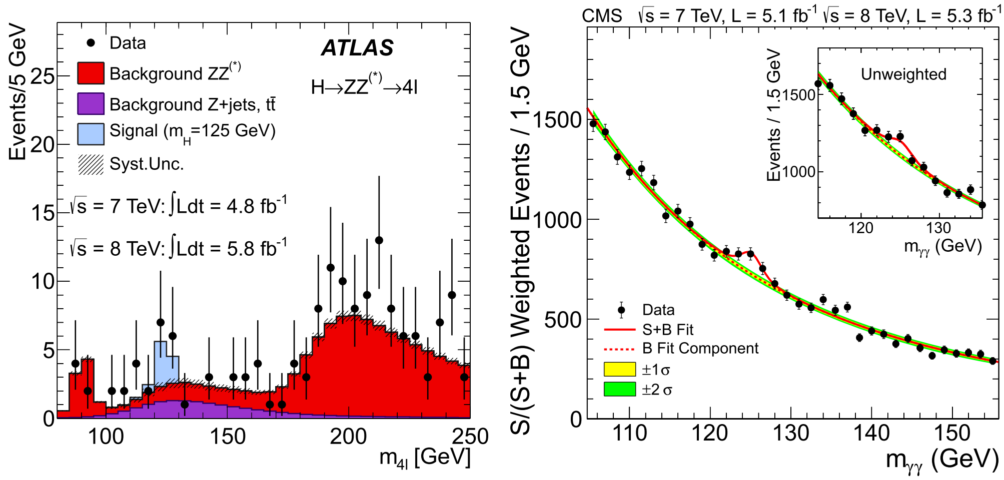


**Figure 3.** The invariant mass distribution in the $4\ell$ channel from the CMS experiment using 10.5 $\text{fb}^{-1}$ of data (left). The invariant mass distribution in the diphoton channel from the ATLAS experiment using 10.4 $\text{fb}^{-1}$ of data (right). From Refs. [30, 31].

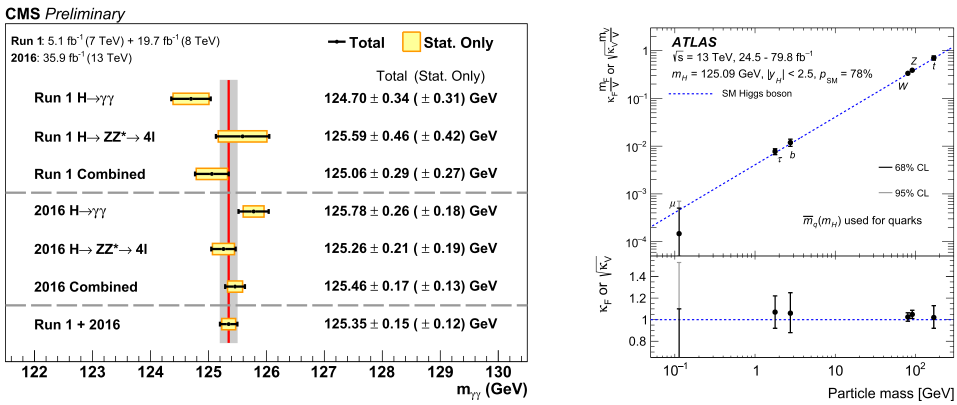


**Figure 4.** (Left) Summary of the measurements from the CMS experiment of the Higgs mass using the $H \to ZZ^* \to 4\ell$ and the $H \to \gamma\gamma$ channels. Results using data from Run1 and Run2 and their combination are shown. The total uncertainty is indicated in black and the systematic uncertainty in yellow. From Ref. [34]. The reduced coupling strength for fermions and bosons to the Higgs boson as a function of the particle mass from the ATLAS experiment using data recorded at 13 TeV. The blue dashed line is indicative of the prediction from the SM for either fermions or bosons. From Ref. [35].

mass is obtained by fitting the invariant mass in the $H \to ZZ^* \to 4\ell$ and $H \to \gamma\gamma$ channels, and was measured to be $m_H = 125.09 \pm 0.21(\text{stat.}) \pm 0.11(\text{syst.})$ [32] in the combination of the ATLAS and CMS measurements using the approximately 25 $\text{fb}^{-1}$ of data from Run1, which occurred from 2010 to 2012. Between 2015 and 2018, Run2 followed with a centre-of-mass energy of 13 TeV. The current measurements of the Higgs mass are $m_H = 124.97 \pm 0.24$ GeV [33] and $m_H = 125.35 \pm 0.15$ GeV [34] for ATLAS and CMS respectively using both Run1 and Run2 data. Figure 4 summarises the measurements of the Higgs mass made by the CMS experiment for each channel and each dataset. The $H \to ZZ^* \to 4\ell$ is statistically limited, but the $H \to \gamma\gamma$ measurement has statistical and systematic uncertainties of comparable size.

The Standard Model predicts that the width of a Higgs boson with mass of 125 GeV is 4.2 MeV [10]. Because hadron colliders can only measure the product of the production cross section and the branching ratio, the total width cannot be inferred without assumptions (see Section 4 for a discussion about the Higgs width measurement at lepton colliders). Direct measurements, e.g. from the width of the invariant mass distribution in the $H \to ZZ^* \to 4\ell$ channel, are sensitive to widths of 1–2 GeV, three orders of magnitude larger than the SM prediction. Indirect constraints on the width can be set by measuring the ratio of the cross section of on-shell (around the Higgs mass) to off-shell (higher invariant masses) Higgs production in vector boson decay channels [36–39]. These measurements of the off-shell production rate can also be used to set limits on the anomalous couplings of the Higgs boson.

The SM Higgs boson is predicted to have a zero total angular momentum, positive parity and positive charge parity. Due to the observation of the $H \to \gamma\gamma$ decay, the charge parity is known to be positive. The angular momentum and parity have been probed by measuring the angular distributions of the decay products on the Higgs boson using the $H \to \gamma\gamma$, $H \to WW^*$ and $H \to ZZ^*$ decays. The spin and parity measurements are independent of the measurements of the total rate in each channel. Constraints on the spin and $CP$ of the Higgs boson have also been set using the $H \to \tau^+\tau^-$ decay channels [40, 41].

Under certain assumptions, these results can be translated into model-dependent measurements of the coupling of the Higgs boson to the other SM particles as shown in Figure 4. (This model dependence can be lifted with the absolute measurement of the $HZZ$ coupling at a lepton collider, as explained in Section 4.) All major production modes have been observed. The cross section for Higgs production through gluon-gluon fusion has been measured to a precision of 10% [35, 42, 43] and the observation of the production of the Higgs boson in association with top quarks, with a cross section two orders of magnitude smaller was made by both ATLAS and CMS in 2018 [44, 45]. The strength of the coupling between the Higgs boson and the top quark is in agreement with indirect measurements. The decay of the Higgs boson has been observed in the following five channels: $H \to \gamma\gamma$, $H \to ZZ^* \to 4\ell$, $H \to WW^*$, $H \to \tau^+\tau^-$ and $H \to b\bar{b}$. The most recent observation has been the decay of the Higgs boson to bottom quarks in 2018 [46, 47]. No significant deviations from SM predictions have been observed in either the production or the decay modes.

The growing LHC dataset has also been used to set limits on channels with much smaller branching ratios. For example, the upper limit on the Higgs branching ratio to $Z\gamma$ is currently 1.4 times the SM prediction [48, 49]. So far, no observation has been made of the coupling of the Higgs bosons to fermions outside the third generation. The most promising channel, $H \to \mu\mu$, allowed an upper limit of 1.7 times the SM to be set [50, 51]. Searches for the decay of the Higgs boson to charm quarks have also been performed, but current limits are more than an order of magnitude above the SM prediction [52, 53].

The measurement of the self-coupling of the Higgs boson will be a key physics target for HL-LHC as discussed in Section 3.1, but searches for Higgs pair production ($HH$) are already being performed at LHC. A large number of final states are required to cover the different possible decay combinations of the two Higgs bosons. At LHC, the most sensitive modes are $HH \to b\bar{b}\tau^+\tau^-$ and $HH \to b\bar{b}\gamma\gamma$. The current observed (expected) upper limits on the Higgs pair production cross section are 6.9 (10) for ATLAS [54] and 12.8 (22.3) for CMS [55] times the SM prediction.

### 2.3. *Searches for Higgs Physics beyond the Standard Model*

The Higgs boson could be a portal to new physics in many ways. Selected examples are provided to illustrate the type of constraints obtained at LHC on Higgs physics beyond the Standard Model.

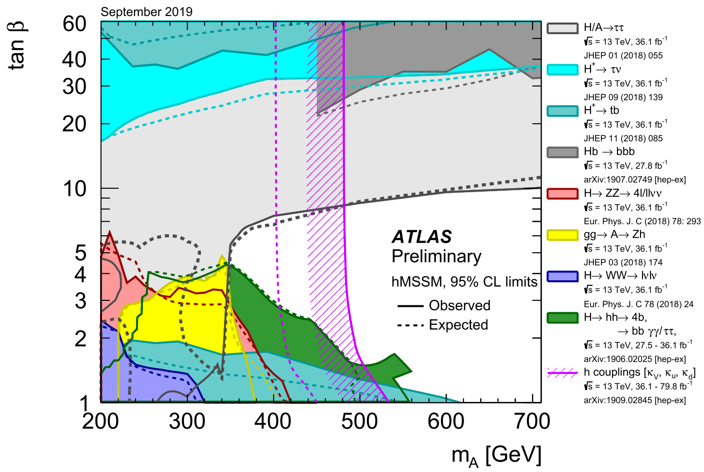


**Figure 5.** Regions of the $(m_A, \tan\beta)$ plane in the MSSM excluded by searches for additional Higgs bosons. Results from direct searches are indicated with solid shading and results from indirect searches are indicated with hatched shading. From Ref. [58].

Decays of the Higgs boson can be used to search for new particles with masses less than half that of the Higgs boson, either with direct searches or via a combined fit to all coupling measurements. Under the assumption that the Higgs couplings to the $Z$ and the $W$ are not larger than the SM prediction, ATLAS and CMS constrained the branching ratio of the Higgs boson to invisible or undetected particles, $\mathscr{B}_{\text{inv}}$, to be less than 34% [32]. Direct searches from ATLAS and CMS in the VBF production mode led to similar upper limits of $\mathscr{B}_{\text{inv}} < 37\%$ [56] and $\mathscr{B}_{\text{inv}} < 33\%$ [57].

Additional Higgs bosons can be searched for at LHC over a wide mass range in many decay channels. In minimal nonminimal versions of the Standard Model, two Higgs doublets are introduced to give mass to up-type and down-type quarks separately. In these models, the Higgs sector consists of five physical states: three neutral Higgs bosons (the SM-like Higgs boson $h$; another, heavier, $CP$-even state $H$; and a $CP$-odd state $A$), and a pair of charged Higgs bosons ($H^{\pm}$). The ratio of the vacuum expectations of the two Higgs doublets is denoted $\tan\beta$.

Figure 5 shows regions of the $(m_A, \tan\beta)$ plane in the minimal supersymmetric extension of the SM (MSSM), excluded by searches for such additional Higgs bosons. Direct searches have excluded high and low values of $\tan\beta$ and with the mass of one of the charged Higgs bosons, $m_A$, required to be above 350 GeV. Indirect limits from coupling fits are shown in pink and exclude $m_A$ below 500 GeV [58].

## 3. Higgs Physics at future hadron colliders

The highest energy elementary parton–parton collisions can be achieved, for the foreseeable future, with high-energy proton–proton colliders, for which a circular geometry is the only available option, at least for energies up to ≈150 TeV. In the LHC tunnel, the High-Luminosity LHC (HL-LHC) [59] will have a collision energy of 14 TeV and a luminosity 5 to 7 times larger than that of LHC. Three other hadron colliders are currently under study. The High-Energy LHC (HE-LHC) [60] would still use the LHC tunnel with upgraded dipole magnets, to reach a energy of 27 TeV. The FCC-hh [61] would collide protons at a centre-of-mass energy of at least 100 TeV in a new tunnel with a circumference of 100 km near CERN. A similar infrastructure, called Super

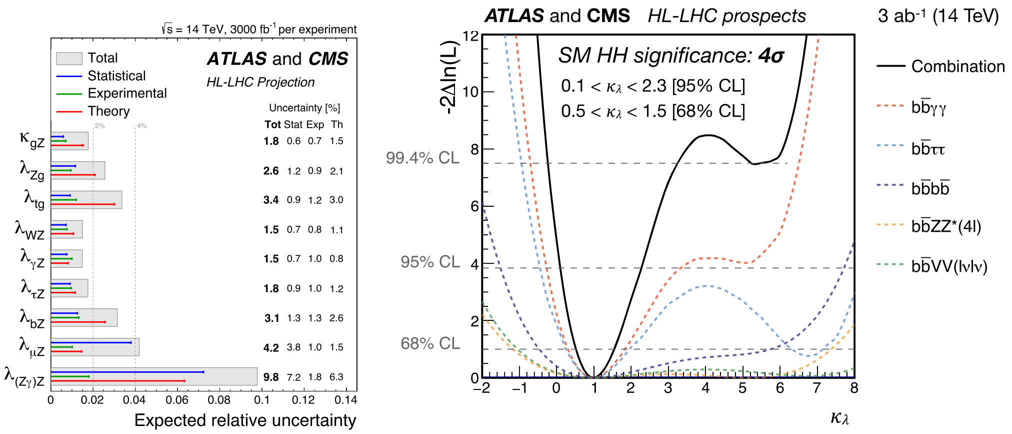


**Figure 6.** (Left) The expected uncertainty on the ratios of Higgs coupling modifiers, $\kappa$, from the combination of ATLAS and CMS at HL-LHC showing separately the statistical, experimental and theoretical uncertainties from Ref. [63]. (Right) The expected precision on the Higgs self-coupling, $\kappa_\lambda$ from HL-LHC shown as the minimum negative-log-likelihood distribution from the combination of all channels for ATLAS and CMS using the full HL-LHC dataset from Ref. [63]. The likelihoods for the individual channels are also shown.

proton–proton Collider (SppC [62]) is also proposed in China. In this note, the capabilities for Higgs physics of HL-LHC and FCC-hh are discussed.

### 3.1. *The luminosity frontier: HL-LHC*

The HL-LHC is expected to begin operation after 2027 to provide 3 ab$^{-1}$ of data. The large data sample will improve the precision of many LHC measurements, and open up new possibilities inaccessible at LHC.

The left panel of Figure 6 shows the expected uncertainty on the ratio of Higgs coupling modifiers, $\kappa$, with respect to the coupling of the Higgs boson to the $Z$ boson [63]. Projections are shown from the combination of the ATLAS and CMS results with the full dataset expected at HL-LHC. For many channels, HL-LHC measurements are expected to reach a precision better than 2%, typically dominated by theoretical uncertainties. Rare Higgs decays such as $H \to Z\gamma$ and $H \to \mu\mu$ are expected to be measured to a precision of 9.8% and 4.2% respectively. Under the assumption that $\kappa_{W,Z} \leq 1$, HL-LHC will be able to probe invisible and undetected decays of the Higgs boson with a precision of a few percent.

The HL-LHC is also expected to provide the first evidence for the Higgs self-coupling with the measurement of the Higgs pair inclusive and differential cross sections. The right panel of Figure 6 shows the expected precision on the Higgs self-coupling for the combination of ATLAS and CMS, with the full expected HL-LHC dataset. The expected significance from the combination of all channels and both experiments is $4\sigma$ [63] and the most sensitive channel is $b\bar{b}\gamma\gamma$ [63].

### 3.2. *The energy frontier: FCC-hh*

One of the key physics targets of FCC-hh will be studying the nature of the Higgs potential by measuring Higgs pair production with high precision. The leading order diagrams for Higgs

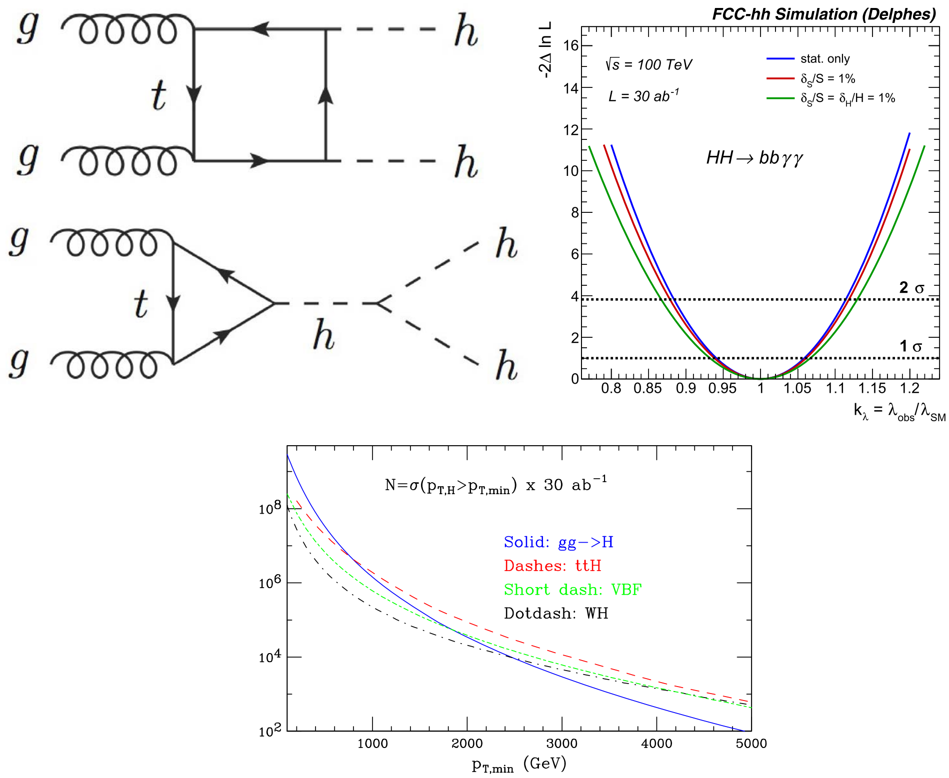


**Figure 7.** (Top left) Leading order Feynman diagrams for Higgs pair production at $pp$ colliders. (Top right) The expected precision on the Higgs self-coupling from FCC-hh in the $H \to b\bar{b}\gamma\gamma$ channel. The negative log-likelihood curves are shown for statistical uncertainties only (blue) and then under different assumptions on the systematic uncertainties (red, green). (Bottom) The number of Higgs bosons that are expected to be produced at FCC-hh as a function of the transverse momentum of the Higgs boson for various production modes. From Ref. [64].

pair production are shown in the upper-left panel of Figure 7. The lower diagram is the one sensitive to the Higgs self-coupling, while the upper diagram shows the most important SM background. The two diagrams have strong negative interference, which means that the cross section is very small and the accuracy of the measurement relies on both the high-energy and the high-luminosity of the collider. One of the most powerful channels to probe this coupling at FCC-hh will be the $HH \to b\bar{b}\gamma\gamma$ decay channel. The upper-right panel of Figure 7 shows the negative log-likelihood for this channel that is expected at FCC-hh, corresponding to an expected precision on $\kappa_\lambda$ of 6.5% [64]. A recent combination with other final states ($b\bar{b}\gamma\gamma$, $b\bar{b}\tau^+\tau^-$, $b\bar{b}b\bar{b}$, and $b\bar{b}ZZ$) improves the expected precision further, leading to a target of 3 to 4.5% on $\kappa_\lambda$ [65].

The $3 \times 10^{10}$ Higgs bosons that could be produced at FCC-hh would improve the precision of certain measurements and open up the possibility of new measurements. The transverse momentum distribution for the Higgs boson in a variety of production modes is shown in the lower panel of Figure 7. The many thousands of Higgs boson with momentum about 2 TeV will be produced in each of the production modes. This can be exploited at FCC-hh to measure ratios of Higgs coupling by selecting events with large transverse momentum which significantly reduces

**Table 1.** The expected FCC-hh precision on ratios of Higgs branching ratios and the branching ratio to invisible particles. From Ref. [64]

| Observable | Precision (stat) | Precision (stat + syst + lumi) |
|---|---|---|
| $B(H \to \mu\mu)/B(H \to 4\mu)$ | 0.33% | 1.3% |
| $B(H \to \gamma\gamma)/B(H \to 2e2\mu)$ | 0.17% | 0.8% |
| $\sigma(t\bar{t}H) \times B(H \to b\bar{b})/\sigma(t\bar{t}Z) \times B(Z \to b\bar{b})$ | 1.05% | 1.9% |
| $B(H \to \text{invisible})$ | $1 \times 10^{-4}$ | $2.5 \times 10^{-4}$ |

the backgrounds. In addition, the transverse momentum of the Higgs boson can be measured to search for contributions from new physics processes. Table 1 shows that the expected precision for the $H \to \mu\mu$ and $H \to \gamma\gamma$ channels would be approximately 1%. The coupling of the Higgs boson to top quarks can be measured to 1% accuracy by measuring the ratio of $t\bar{t}H$ to $t\bar{t}Z$ production. By fitting the missing energy distribution, FCC-hh could probe the branching ratio of the Higgs boson to invisible and undetected decay to the $10^{-4}$ level. Further details about these studies are available in Ref. [64].

## 4. Higgs Physics at future lepton colliders

In the present state of strategic discussions, a consensus emerges around the strong physics case for an $e^+e^-$ collider at the precision frontier, to measure the Higgs boson and the other particle properties with unprecedented accuracy. At the time of writing, four $e^+e^-$ collider projects are still on the table [66–72]. The physics case is summarised in the Physics Briefing Book [73].

The circular colliders (FCC-ee and CEPC) were conceived in 2011–2013, as soon as first hints for a light Higgs boson became publicly known [74]. Their luminosity curves provides the highest statistics at low energies, but is strongly limited by synchrotron radiation above 350–400 GeV. The proposed operation models comprise data taking at and around the $Z$ pole (91 GeV), at the $WW$ threshold (161 GeV), at the $ZH$ cross-section maximum (240 GeV), and, for FCC-ee, an extension at and above the top pair threshold (up to 365 GeV). The designs are sufficiently flexible to allow operation at other centre-of-mass energies (e.g., at $\sqrt{s} = m_H$, or well below the $Z$ peak), with unrivalled luminosities. Both colliders are planned to operate for 10–15 years with two IPs (A configuration with four IPs is being studied for FCC-ee.), and are considered to be a first, enabling step in a long-term plan towards a high-energy proton–proton collider (Section 3.2).

Linear colliders have been studied since 1975 [75], and are considered to be the only possible way towards higher-energy $e^+e^-$ collisions. The luminosity and power consumption grows linearly with energy. The proposed operation models include a first run at “low” energy, 250 GeV for ILC and 380 GeV for CLIC, for about a decade. Both colliders have an open-ended run plan, with possible extensions to 1 TeV (ILC) and 3 TeV (CLIC) in a run plan that extends over several decades.

At the top-pair threshold, FCC-ee, CLIC, and ILC are planned to deliver similar integrated luminosities, within a factor of two. A linear collider is the most effective option at 500 GeV (and the only possibility for higher energies), while a circular collider is more effective for any energy below 350–400 GeV. For example, at the $ZH$ cross-section maximum, FCC-ee is expected to produce 5 $ab^{-1}$ in about three years, while it would take between 20 and 30 years with ILC to reach the same figure. The integrated power for a circular machine is also five to ten times less per Higgs boson produced at the $ZH$ cross-section maximum.

In the longer term, $\mu^+\mu^-$ collisions could also be envisioned [76–78], once the considerable technological challenges related to muon production, cooling, acceleration, and decay backgrounds, have been solved. The reduced synchrotron radiation loss from muons – by a factor $10^9$

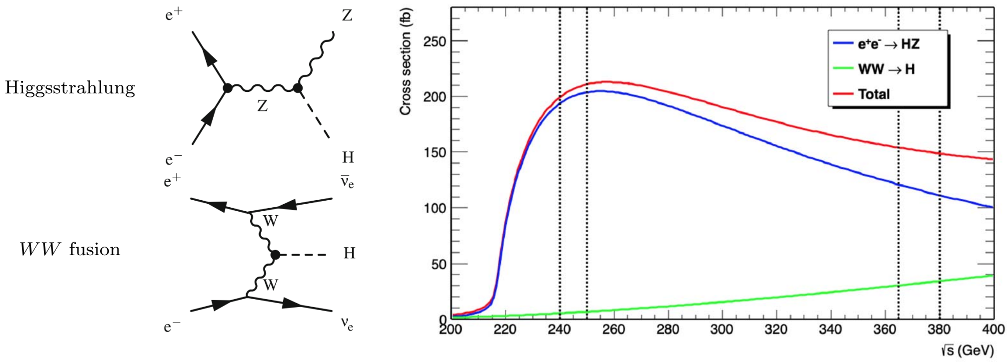


**Figure 8.** (Left) Feynman diagrams for the Higgsstrahlung (top) and the $WW$ fusion (bottom) processes. (Right) Unpolarised Higgs production cross section as a function of the centre-of-mass energy $\sqrt{s}$. Vertical dashed lines indicate the values of $\sqrt{s}$ foreseen for the four low-energy Higgs factories: FCC-ee (240 and 365 GeV), CEPC (240 GeV), ILC (250 GeV) and CLIC (380 GeV).

with respect to electrons – would then enable the construction of circular colliders either with much smaller radii at low energies, or with much higher design energies, typically 6 to 14 TeV. Possible operation models include a low-energy run at $\sqrt{s} = m_H$, in a ring of a few 100 m circumference, benefiting from a larger coupling to the Higgs boson and an exquisite energy definition; followed by multi-TeV collisions, e.g., in the LEP/LHC ring.

## 4.1. *The luminosity frontier: low-energy Higgs factories*

In $e^+e^-$ collisions at centre-of-mass energies from 240 to 380 GeV, the two main Higgs production mechanisms are the Higgsstrahlung process, $e^+e^- \to ZH$, and the $WW$ fusion process, $e^+e^- \to H\nu_e\bar{\nu}_e$, with Feynman diagrams and cross sections shown in Figure 8. With the integrated luminosities foreseen to be accumulated by each of the four colliders, over one million Higgs bosons would be collected at FCC-ee and CEPC, about 500,000 at ILC, and less than 200,000 at CLIC.

The total $ZH$ cross section, proportional to the Higgs coupling to the $Z$ boson $g^2_{HZZ}$, can be determined in a model-independent manner by counting events with an identified $Z$ (decaying into $e^+e^-$ or $\mu^+\mu^-$, for example), and for which the mass $m_R$ recoiling against the $Z$, given by $m_R^2 = s + m_Z^2 - 2\sqrt{s}(E_{\ell^+} + E_{\ell^-})$, clusters around 125 GeV. This absolute measurement of $g_{HZZ}$, unique to $e^+e^-$ colliders, can be used as a "standard candle" by all other measurements, including those made at HL-LHC and FCC-hh. The position of the recoil mass peak also provides an accurate measurement of the Higgs boson mass. Once $g_{HZZ}$ has been determined, the measurement of the cross sections for each exclusive Higgs boson decay, $H \to X\overline{X}$,

$$\sigma_{ZH} \times \mathscr{B}(H \to X\overline{X}) \propto \frac{g^2_{HZZ} \times g^2_{HXX}}{\Gamma_H} \quad \text{and} \quad \sigma_{H\nu_e\bar{\nu}_e} \times \mathscr{B}(H \to X\overline{X}) \propto \frac{g^2_{HWW} \times g^2_{HXX}}{\Gamma_H}, \tag{1}$$

gives access to all other couplings in a model-independent, absolute, way. For example, the ratio of the $WW$-fusion-to-Higgstrahlung cross sections for the same Higgs boson decay, proportional to $g^2_{HWW}/g^2_{HZZ}$, yields $g_{HWW}$, and the Higgsstrahlung rate with the $H \to ZZ$ decay, proportional to $g^4_{HZZ}/\Gamma_H$, provides a determination of the Higgs boson total decay width. The precision with which the Higgs mass, width and couplings can be measured at the various $e^+e^-$ colliders is given

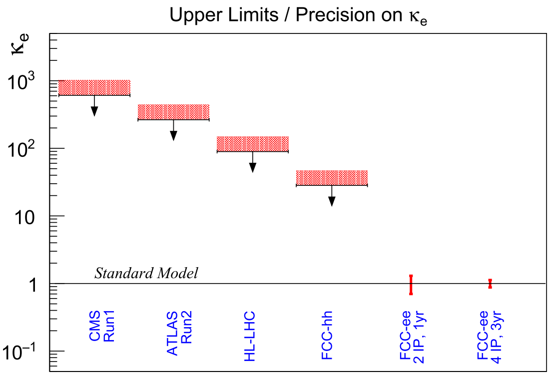


**Figure 9.** Current upper limits on the Higgs boson coupling modifier to electrons, $\kappa_e$, from CMS [80] and ATLAS [81]; projected $\kappa_e$ upper limits at HL-LHC and FCC-hh; and projected $\kappa_e$ precisions at FCC-ee in two different running configurations (one year with 2 IPs, or three years with 4 IPs).

in Section 5. The longitudinal beam polarisation, available at linear colliders, plays little role in this determination [68].

Several Higgs boson couplings, however, are not directly accessible from its decays, either because the masses involved, and therefore the decay branching ratios, are too small to allow for an observation within $10^6$ events or less – as is the case for the couplings to the particles of the first SM family: electron, up quark, down quark – or because the masses involved are too large for the decay to be kinematically open – as is the case for the top-quark Yukawa coupling and for the Higgs boson self coupling. Other methods are therefore required, as described below.

The ability of FCC-ee to provide the highest luminosities at lower centre-of-mass energies offers the unique opportunity to measure the Higgs boson coupling to electrons through the resonant production process $e^+e^- \to H$ at $\sqrt{s} = 125$ GeV [79]. A $2\sigma$ excess (with respect to a situation in which the Higgs boson does not couple to electrons) would be observed at FCC-ee after a year with two interaction points, and a precision of $\pm 15\%$ on the Higgs boson coupling to the electron can be observed after three years with four interaction points. A comparison with the hadron collider sensitivity is displayed in Figure 9.

The Higgs self-coupling can be obtained by two different methods [82]. The method with single Higgs production [83] at low-energy Higgs factories relies on the precise measurement of the $ZH$ cross section, which depends on the self-coupling via the diagrams shown in the left panel of Figure 10. This measurement provides a robust self-coupling determination from at least two sufficiently different energy points [84–86], e.g., 240 and 365 GeV. A precision of $\pm 34\%$ on the self-coupling can be achieved at FCC-ee (right panel of Figure 10), reduced to $\pm 24\%$ with four IPs instead of two [87]. No meaningful constraint can obtained with only a single centre-of-mass energy. The first $4\sigma$ demonstration of the existence of the Higgs self-coupling is therefore within reach in 15 years at FCC-ee.

Finally, the top Yukawa coupling will have been determined with a few percent precision – albeit with some model dependence – at HL-LHC, well before the advent of any $e^+e^-$ collider. The model-dependence of the HL-LHC measurement will be lifted off by the $g_{HZZ}$ absolute measurement made at low-energy Higgs factories. As mentioned in Section 3.2, the measurement of the $ttZ$ coupling (for example at FCC-ee$_{365}$ [88]) and the measurement of the cross section ratio $\sigma_{ttH}/\sigma_{ttZ}$ at FCC-hh will provide another significant improvement in precision for the top Yukawa coupling, to better than $\pm 1\%$.

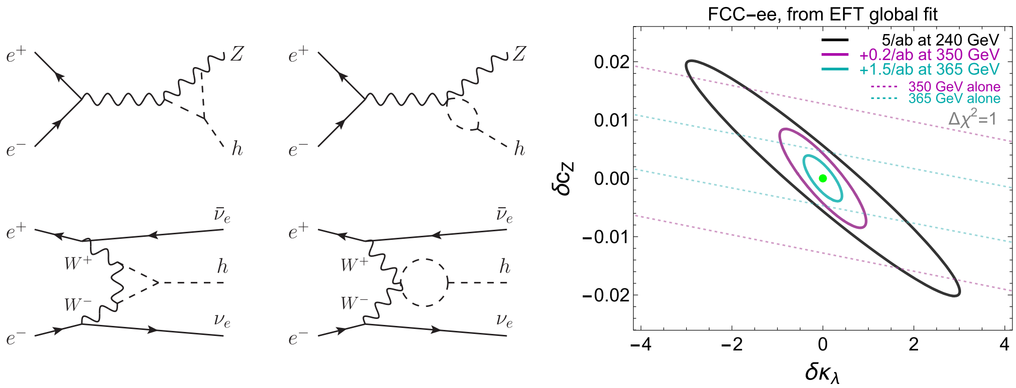


**Figure 10.** Left, from Ref. [84]: sample Feynman diagrams illustrating the effects of the Higgs self-coupling on single Higgs process at next-to-leading order. Right: FCC-ee precision in the simultaneous determination of the Higgs self-coupling $\kappa_\lambda$ and the $HZZ/HWW$ coupling $c_Z$, at 240 GeV (black ellipse), 350 GeV (purpled dashed), 365 GeV (green dashed), and by combining data at 240 and 350 GeV (purple ellipse), and at 240, 350, and 365 GeV (green ellipse).

All the above could in principle also be achieved with a low-energy muon collider ring of only 600 m circumference. The luminosity at a centre-of-mass energy of 240–250 GeV, however, is expected to be 10 (100) times smaller than at a linear (circular) $e^+e^-$ collider. This configuration is therefore inadequate for precision measurements of Higgs properties in any reasonable time. Interestingly, the resonant process $\mu^+\mu^- \to H$ at $\sqrt{s} = 125$ GeV has a cross section ~ 40,000 times larger than its $e^+e^-$ counterpart. Between 5,000 and 15,000 Higgs bosons could be produced every year in a scan of the Higgs lineshape. Such a scan does not provide a "standard candle" to hadron colliders, and is not competitive for the Higgs coupling precision, but it would be the only possibility to reveal substructure in the lineshape, e.g., due to two Higgs bosons almost degenerate in mass. In conclusion, a muon circular collider at $\sqrt{s} = 125$ GeV would be an elegant Higgs factory, but not necessarily the one needed for precision measurements (and therefore, for sensitivity to new physics).

## 4.2. *The energy frontier: Higgs physics at $\sqrt{s} \geq 500$ GeV*

### 4.2.1. *Study of the H(125) properties*

With their open-ended energy-upgrade plan, linear colliders progressively produce a larger number of Higgs bosons in the $WW$-fusion process and reach one million Higgs bosons after two or three additional decades of operation at 0.5 (1) TeV for ILC, and 1.5 (3) TeV for CLIC, with integrated luminosities of 4 (8) and 2.5 (5) ab$^{-1}$, respectively.

New Higgs production processes become available when the centre-of-mass energy exceeds 500 GeV, as shown in Figure 11. For example, the $ttH$ and $ZHH$ cross sections are just sufficient at 500 GeV (~100 ab) to enable independent measurements of the top Yukawa coupling and of the Higgs self-coupling with precisions of ±6% and ±27%, respectively. A slight increase of the centre-of-mass energy to 550 GeV would improve the top Yukawa coupling precision to ±4%, which would make $\mathrm{ILC}_{500}$ competitive with HL-LHC and FCC-ee for these two couplings. For these essential measurements, having both FCC-ee and $\mathrm{ILC}_{500}$ (or even better, $\mathrm{ILC}_{600}$ to get close to the maximum of the $ZHH$, $ttH$, and $ttZ$ cross sections) would provide important verification in case a discrepancy with the SM predictions is found, and improved precision altogether –

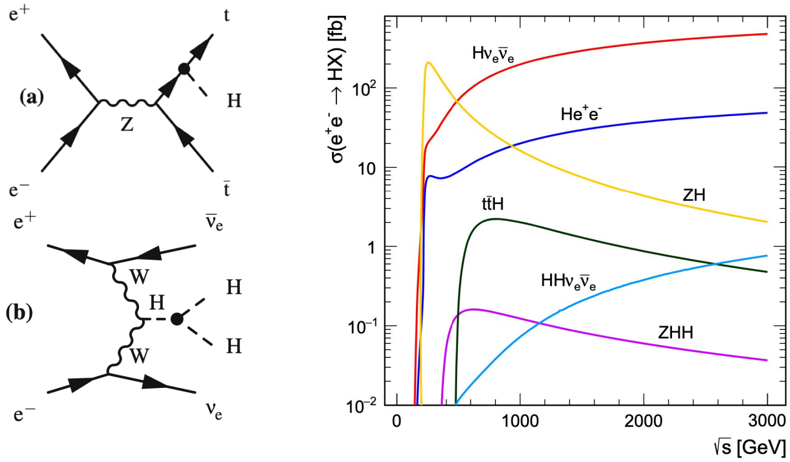


**Figure 11.** (Left) Feynman diagrams of the leading-order processes involving (a) the top Yukawa coupling $g_{Htt}$, and (b) the Higgs boson self-coupling $g_{HHH}$. (Right) Unpolarised production cross sections for the main Higgs production processes up to $\sqrt{s} = 3$ TeV. From Ref. [72].

i.e., new physics sensitivity to higher mass scale – with a combination of both sets of data. It is only with the highest energies and the full luminosity that $\text{ILC}_{1\,\text{TeV}}$ and $\text{CLIC}_{3\,\text{TeV}}$ would offer a precision of about ±10% on the Higgs self-coupling, with an analysis of the $HH\nu_e\bar{\nu}_e$ process.

At FCC, the current baseline strategy to access to double Higgs production is to not upgrade the energy FCC-ee to 500 GeV, but to move to proton–proton collisions at the much higher energy of 100 TeV (see Section 3.2). It has been recently realised, however, that FCC-ee could be, as an intermediate step towards FCC-hh, upgraded with the Energy-Recovery Linacs (ERL) technology, to reach an energy of 600 GeV with a luminosity 5 to 50 $\text{ab}^{-1}$ in 10 years of operation with one interaction point [89]. With such a luminosity, up to ten times that expected at a linear collider at the same energy, a measurement of the Higgs self-coupling with a 10% precision can be contemplated as well. Needless to say, the level of understanding of such a possibility is nowhere near that of the ILC or CLIC designs, and will require in depth feasibility and cost studies, comparable to that made for the well-established baseline ring-ring design at lower energies, to fully validate the concept.

### 4.2.2. *Search for additional Higgs states*

The new states in two-Higgs-doublet models, $H$, $A$, and $H^{\pm}$ can searched for with lepton colliders through their production in pairs: $e^+e^-$ or $\mu^+\mu^- \to HA$ or $H^+H^-$, with a sensitivity for discovery up to $\sqrt{s}/2$. The added value of a high-energy muon collider would be twofold in this respect. Firstly, the potentially higher centre-of-mass energy (up to 14 TeV) allows the pair production to be sensitive to additional Higgs states with masses up to 7 TeV. Secondly, the large $\text{H}\mu\mu$ coupling opens the possibility of an automatic mass scan of the neutral states up to $m_{H,A} = \sqrt{s}$, with the "radiative return" process: $\mu^+\mu^- \to H\gamma$ or $A\gamma$ [90]. For $\sqrt{s} = 3$ TeV, events selected with an isolated photon of energy above 10 GeV would have a recoil-mass distribution as displayed in the left panel of Figure 12, pointing clearly to the mass of a new neutral Higgs state. The collider centre-of-mass energy would then be tuned to the new state mass, in order to copiously produce both $CP$-even and $CP$-odd state through resonant production: $\mu^+\mu^- \to H$, $A$, as displayed in the right panel of Figure 12 [91], providing a unique laboratory for $H/A$ mixing and $CP$ violation studies [92].

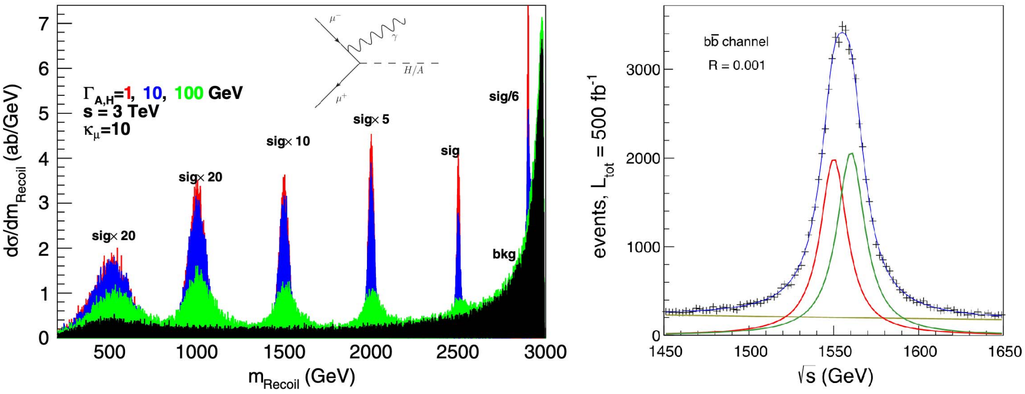


**Figure 12.** (Left, from Ref. [90]) Distribution of the mass recoiling against an isolated photon with momentum transverse to the beam in excess of 10 GeV, for heavy Higgs ($H$, $A$) masses of 0.5, 1, 1.5, 2, 2.5, and 2.9 TeV, with total width of 1 (red), 10 (blue), and 100 (green) GeV, at a 3 TeV muon collider. The beam energy resolution is assumed to amount to 0.1%. Signal and backgrounds have different multiplication factors for clarity. (Right, from Ref. [91]) Scan of the $H/A$ lineshape ($m_{H,A} \sim 1.55$ TeV) in the $\mu^+\mu^- \to b\bar{b}$ production with $\sqrt{s}$ from 1.45 to 1.65 TeV, with a centre-of-mass energy spread of 0.001 and a total luminosity of 0.5 ab$^{-1}$.

## 5. Projected results in $\kappa$ and EFT fits: discussion

In the SM, the Higgs boson coupling to a given particle $X$, denoted $g_{HXX}$, is uniquely fixed by its mass. The quantitative effect of new physics on these couplings requires a parametrisation of the induced deviations with respect to the SM predictions. Two such parametrisations are widely used, the $\kappa$ framework; and the effective field theory (EFT) approach.

The simpler $\kappa$ framework introduces multiplicative modifiers $\kappa_X = g_{HXX}/g^{\rm SM}_{HXX}$, for each of the tree-level couplings to SM particles, $\kappa_Z$, $\kappa_W$, $\kappa_b$, $\kappa_c$, $\kappa_\tau$, $\kappa_\mu$, and $\kappa_t$; and three effective modifiers for the loop-induced couplings, $\kappa_\gamma$, $\kappa_g$, and $\kappa_{Z\gamma}$; and one resulting modifier for the Higgs decay width, $\kappa_H$. The couplings $\kappa_s$, $\kappa_d$, $\kappa_u$ and $\kappa_e$, that are only weakly constrained from very rare decays, are currently not included in the combined $\kappa$-framework fits. The $\kappa$-framework also allows for the possibility of Higgs boson decays to invisible or "untagged" BSM particles, with the introduction of two additional branching ratio parameters, $\mathscr{B}_{\rm inv}$ and $\mathscr{B}_{\rm EXO}$. For colliders that can directly measure the Higgs width (such as FCC-ee), $\mathscr{B}_{\rm EXO}$ can be constrained together with $\kappa_X$ and $\mathscr{B}_{\rm inv}$ from a combined fit to the data. For colliders that cannot (such as HL-LHC), additional theoretical assumptions must be introduced (for example by fixing the width and other couplings to their SM prediction). The $\kappa$ framework makes no assumption on the new physics that modifies the couplings. Constraints derived in the $\kappa$ analysis can therefore be readily exploited to derive model-independent constraints on the new physics parameters. In certain new physics model, however, the $\kappa$ framework is sub-optimal in setting constraints, as it is blind to effects that do not change the coupling strengths, but change instead their helicity structure (which would modify, e.g., angular distributions).

To circumvent this shortcoming, the EFT approach is introduced to parametrise directly the new physics (rather than its effects) in terms of gauge invariant operators of dimension 6, 8, 10, etc, and calculated through an expansion in inverse powers of the new-physics mass scale $\Lambda$. Current EFT approaches typically only consider the supposedly dominant $\mathcal{O}(1/\Lambda^2)$ terms, carried by dimension-six operators. While more sensitive than the $\kappa$ framework to new physics effects,

**Table 2.** Precision on the Higgs boson couplings $g_{HXX}$, from Ref. [82] in the $\kappa$ framework (left) and in a global EFT fit to Higgs, diboson, and electroweak precision measurements (right), for the five low-energy Higgs factories ($\mu$Coll$_{125}$, ILC$_{250}$, CLIC$_{380}$, CEPC$_{240}$, and FCC-ee$_{240\to365}$), fixing the Higgs self-coupling $g_{HHH}$ to its SM value. For the $g_{HHH}$ fit, only the EFT global fit result is shown (with 2IPs and 4IPs for FCC-ee). For the muon collider, only the results of a standalone $\kappa$ fit are displayed. All numbers are in % and indicate 68% C.L. sensitivities. Also indicated in the $\kappa$ fit are the precision on the total decay width and the 95% C.L. sensitivity on the "invisible" and "exotic" branching fractions

| Collider | HL-LHC | $\mu$Coll$_{125}$ | ILC$_{250}$ | CLIC$_{380}$ | CEPC$_{240}$ | FCC-ee$_{240\to365}$ |
|---|---|---|---|---|---|---|
| Lumi (ab$^{-1}$) | 3 | 0.005 | 2 | 1 | 5.6 | 5 + 0.2 + 1.5 |
| Years | 10 | 6 to 10 | 11.5 | 8 | 7 | 3 + 1 + 4 |
| $g_{HZZ}$ (%) | 1.5/3.6 | SM | 0.29/0.39 | 0.44/0.50 | 0.18/0.45 | 0.17/0.26 |
| $g_{HWW}$ (%) | 1.7/3.2 | 3.9 | 1.0/0.41 | 0.73/0.50 | 0.88/0.43 | 0.41/0.27 |
| $g_{Hbb}$ (%) | 3.7/5.3 | 3.8 | 1.1/0.78 | 1.2/0.99 | 0.92/0.63 | 0.64/0.56 |
| $g_{Hcc}$ (%) | SM/SM | SM | 2.0/1.8 | 4.1/4.0 | 2.0/1.8 | 1.3/1.2 |
| $g_{Hgg}$ (%) | 2.5/2.3 | SM | 1.4/1.1 | 1.5/1.3 | 1.0/0.76 | 0.89/0.82 |
| $g_{H\tau\tau}$ (%) | 1.9/3.4 | 6.2 | 1.1/0.81 | 1.4/1.3 | 0.91/0.66 | 0.66/0.57 |
| $g_{H\mu\mu}$ (%) | 4.3/5.5 | 3.6 | 4.2/4.1 | 4.4/4.4 | 3.9/3.8 | 3.9/3.8 |
| $g_{H\gamma\gamma}$ (%) | 1.8/3.6 | SM | 1.4/1.3 | 1.4/1.4 | 1.3/1.3 | 1.3/1.2 |
| $g_{HZ\gamma}$ (%) | 10./11. | SM | 10./9.6 | 10./9.7 | 6.3/6.3 | 10./9.3 |
| $g_{Htt}$ (%) | 3.4/3.5 | SM | 3.1/3.2 | 3.2/3.2 | 3.1/3.1 | 3.1/3.1 |
| $g_{HHH}$ (%) | 50. | SM | 49. | 50. | 49. | 33./24. |
| $\Gamma_H$ (%) | SM | 6.1 | 2.2 | 2.5 | 1.7 | 1.1 |
| $\mathcal{B}_{\text{inv}}$ (%) | 1.9 | SM | 0.26 | 0.63 | 0.27 | 0.19 |
| $\mathcal{B}_{\text{EXO}}$ (%) | SM (0.0) | SM (0.0) | 1.8 | 2.7 | 1.1 | 1.0 |

this approach needs to make a number of assumptions on the underlying new physics. First, new physics is assumed to be heavy for the $1/\Lambda^n$ expansion to make sense, which excludes a whole class of new physics models that include light particles. Second, new physics must be described by only one mass scale – a criterion that is not satisfied by the standard model. Third, it is assumed that $\Lambda$ is large enough for dimension-six operators to dominate over all other operators, which restricts EFT analyses to an effective Lagrangian truncated to $1/\Lambda^2$ terms. Last by not least, only a small subset of the 2499 dimension-six operators is assumed to affect Higgs measurements and is included in EFT Higgs analyses. The physics implications of these strong assumptions are not transparent. It can be anticipated that further work will be needed for the Higgs analyses, similar to what was done at LEP to express the measurements in an observable-based, model-independent framework.

Projections have been obtained for both approaches in the context of the Symposium for the European Strategy Update in Granada, in May 2019. Updated results can be found in Ref. [82], and are displayed in Table 2 for Higgs coupling precisions at the different low-energy Higgs factories, when combined with the projected HL-LHC precisions [63]. The Higgs capabilities of their energy-frontier upgrades, still combined with the HL-LHC projections, are compared in Table 3. Such studies do not exist yet for a high-energy muon collider. After completion of their proposed operation models (up to 365 GeV for FCC-ee, up to 1 TeV for ILC, and up to 3 TeV for CLIC), a substantial part of the $e^+e^-$ collider Higgs physics programs is similar. There are, however, significant differences due to the variation of the production mode as a function of energy. Several remarks are in order.

**Table 3.** Precision on the Higgs boson couplings, from Ref. [82] in the $\kappa$ framework (left) and in a global EFT fit (right), for the combination of each low-energy Higgs factory ($\mathrm{ILC}_{250}$, $\mathrm{CLIC}_{380}$, and FCC-ee) and their proposed upgrades at higher energies: $\mathrm{ILC}_{500\,\mathrm{GeV}}$, $\mathrm{ILC}_{500+1000\,\mathrm{GeV}}$, $\mathrm{CLIC}_{1.4+3\,\mathrm{TeV}}$, and the complete FCC integrated programme. All numbers are in % and indicate 68% C.L. sensitivities. Also indicated are the precision on the total decay width, and the 95% C.L. sensitivity on the "invisible" and "exotic" branching fractions. A precision similar to that achieved at high-energy linear colliders is reached with FCC-hh in less than one year of operation for all couplings, except the Higgs self-coupling for which a precision of 10% is reached in about 3 to 5 years [65] (with respect to a couple decades for $\mathrm{ILC}_{1000}$ and CLIC)

| Collider | $\mathrm{ILC}_{500}$ | $\mathrm{ILC}_{1000}$ | CLIC | FCC |
|---|---|---|---|---|
| $g_{HZZ}$ (%) | 0.23/0.22 | 0.23/0.16 | 0.39/0.16 | 0.16/0.13 |
| $g_{HWW}$ (%) | 0.29/0.22 | 0.24/0.17 | 0.38/0.15 | 0.19/0.13 |
| $g_{Hbb}$ (%) | 0.56/0.52 | 0.47/0.43 | 0.53/0.38 | 0.48/0.44 |
| $g_{Hcc}$ (%) | 1.2/1.2 | 0.90/0.88 | 1.4/1.4 | 0.96/0.95 |
| $g_{Hgg}$ (%) | 0.85/0.79 | 0.63/0.55 | 0.86/0.75 | 0.50/0.49 |
| $g_{H\tau\tau}$ (%) | 0.64/0.58 | 0.54/0.49 | 0.82/0.73 | 0.46/0.46 |
| $g_{H\mu\mu}$ (%) | 3.9/3.9 | 3.6/3.5 | 3.5/3.5 | 0.43/0.42 |
| $g_{H\gamma\gamma}$ (%) | 1.2/1.2 | 1.1/1.1 | 1.2/1.1 | 0.31/0.34 |
| $g_{HZ\gamma}$ (%) | 10./6.8 | 10./6.7 | 5.7/3.7 | 0.70/0.70 |
| $g_{Htt}$ (%) | 2.8/2.9 | 1.4/1.5 | 2.1/2.1 | 0.96/1.6 |
| $g_{HHH}$ (%) | 27./27. | 10/10 | 9./n.a. | 3./4. |
| $\Gamma_H$ (%) | 1.1 | 1.0 | 1.6 | 0.91 |
| $\mathscr{B}_{\mathrm{inv}}$ (%) | 0.23 | 0.22 | 0.61 | 0.024 |
| $\mathscr{B}_{\mathrm{EXO}}$ (%) | 1.4 | 1.4 | 2.4 | 1.0 |

(i) Circular colliders operating at the maximum of the $ZH$ cross section are very efficient Higgs factories, requiring for example ~9 (5) GJ per Higgs boson for FCC-ee with 2 (4) IPs at 240 GeV, vs ~50 GJ for the proposed ILC run plan at 250 GeV. The measurement of the total $ZH$ cross section at FCC-ee provides the most precise determination of the $g_{HZZ}$ coupling. Linear colliders running at higher energies progressively obtain better measurement of $g_{HWW}$ from the $H\nu_e\bar{\nu}_e$ cross section. The synergistic combination of a circular and a linear colliders offers the best test of the SM relationship between the Higgs couplings to the $W$ and $Z$ boson, i.e., a test of the SU(2) custodial symmetry in the Higgs sector. The full integrated FCC (ee-hh-eh) could achieve this test with a similar precision.

(ii) Proton–proton collisions are qualitatively and quantitatively more effective to study the Higgs boson thoroughly at high energy, once the $g_{HZZ}$ and $ttZ$ couplings are determined in an absolute manner by (an) $\mathrm{e^+e^-}$ collider(s) operating at 240 GeV and above 350 GeV, respectively, and used as standard candles in $pp$ collisions. The FCC integrated plan yields precision consistently smaller than 1% for all the couplings to gauge bosons and to fermions shown in Table 3, for the invisible and exotic branching fractions, and for the Higgs boson total width. With $5 \times 10^{10}$ Higgs bosons produced, FCC-hh also gives the most sensitive measurements of the rare decays such as $\mu\mu, \gamma\gamma, Z\gamma$, and of the invisible width.

(iii) The Higgs self-coupling can be obtained by two different methods, as discussed in Ref. [82]. The method with single Higgs production relies on the precise measurement of the $ZH$ cross section, and provides a robust determination from at least two sufficiently different energy points [86]. The need for these two energies is satisfied by the current operation model of FCC-ee, but also provides a clear opportunity for a synergistic combination of a circular collider (operating up to 240 GeV) and a linear collider (operating above 350 GeV) [93].

(iv) A more precise determination of the Higgs self-coupling, to ±10%, can be obtained either with higher-energy $e^+e^-$ collisions from double Higgs production, at and above the $ZHH$ cross-section maximum – or at high-energy hadron colliders. This is the realm of excellence of ILC at 1 TeV or CLIC at 3 TeV, but could also be achieved with an upgrade of FCC-ee based on Energy Recovery Linacs. A precision of ±3% is possible at FCC-hh, which enjoys a wider phase space for double-Higgs production. For this important measurement, the different sources of systematic uncertainties in $e^+e^-$ and $pp$ collisions would also render their combination more robust than each individual result.

(v) On the other side of the spectrum, FCC-ee offers the unique opportunity to measure the Higgs boson coupling to electrons through the resonant production process $e^+e^- \to H$ at $\sqrt{s} = 125$ GeV [79]. A precision of ±15% on the Higgs boson SM coupling to the electron can be observed after three years with four interaction points. Because of the need of extremely high luminosity, combined with monochromatisation and continuous ppm centre-of-mass energy control, such a measurement is not possible with linear colliders. It is also out of reach of hadron colliders.

In summary, circular colliders provide both the highest luminosity and the best energy efficiency in $e^+e^-$ collisions for $\sqrt{s}$ up to 400 GeV, and the only possibility to deliver proton–proton collisions at 100 TeV and beyond. This interplay is essential for a broad spectrum of unique Higgs measurement, and makes the FCC complex a formidable tool of investigation. The combined sensitivity of FCC-ee and FCC-hh to deviations in the SM couplings and self-coupling, and to the production of new particles coupled to the Higgs, is a portal to physics beyond the SM, and can conclusively test the nature of the cosmological electroweak phase transition [64].

## 6. Outlook and conclusion

Particle physics has arrived at an important moment of its history. Half a century after having been proposed on purely theoretical grounds, the recent discovery of the Higgs boson with a mass of 125 GeV at LHC, exactly in the range from 114.4 to 132 GeV predicted by LEP and Tevatron precision measurements, completed the spectrum of particles and their interactions, which have constituted the Standard Model for several decades. This model has now become a consistent and predictive theory, which has so far proven successful in describing all phenomena accessible to collider experiments. In particular, today's measurements of the Higgs boson properties are consistent, within still large uncertainties, with the SM expectations.

This achievement does not stop the need for further exploration. Many questions remain unanswered, with the deep origin of the Higgs boson very high on the list. Is the Higgs boson an elementary particle, or is it a composite state of confined particles? What mechanism generates its mass and self-interaction, leading to electroweak symmetry breaking and to the generation of particle masses? What was the nature of the phase transition that led, in the early Universe, to electroweak symmetry breaking? Addressing these questions requires a detailed cartography of the Higgs boson and of the electroweak interactions above the weak scale, with the best possible precision to expose new dynamics.

High-energy lepton and hadron colliders are unique tools to study the Higgs boson in a controlled environment. The cornerstone of the Higgs measurement programme is the direct and model-independent determination of its coupling to the $Z$ boson. This measurement, unique to lepton colliders, is optimally performed at $\sqrt{s}$ around 240 GeV. The measurement of the $H \to ZZ^*$

decay then provide the total Higgs width. Absolute values of the other Higgs couplings follow, and can be done best with a high-energy hadron collider.

There is no doubt that a worldwide plan including both a lepton and a hadron collider will pose considerable challenges, but it would offer the particle physics community complementary and synergistic programs with a long-term vision, as well as answers to the fundamental questions that the discovery of the Higgs boson has brought to the forefront.

## References


[1] F. Englert, R. Brout, "Broken symmetry and the mass of gauge vector mesons", *Phys. Rev. Lett.* **13** (1964), no. 9, p. 321-323.

[2] P. W. Higgs, "Broken symmetries, massless particles and gauge fields", *Phys. Lett.* **12** (1964), no. 2, p. 132-133, https://cds.cern.ch/record/641590.

[3] P. W. Higgs, "Broken symmetries and the masses of gauge bosons", *Phys. Rev. Lett.* **13** (1964), p. 508-509.

[4] G. S. Guralnik, C. R. Hagen, T. W. B. Kibble, "Global conservation laws and massless particles", *Phys. Rev. Lett.* **13** (1964), no. 20, p. 585-587.

[5] S. L. Glashow, "Partial symmetries of weak interactions", *Nucl. Phys.* **22** (1961), no. 4, p. 579-588.

[6] S. Weinberg, "A model of leptons", *Phys. Rev. Lett.* **19** (1967), no. 21, p. 1264-1266.

[7] A. Salam, "Weak and Electromagnetic Interactions", *Conf. Proc. C* **680519** (1968), p. 367-377.

[8] J. Iliopoulos, "Progress in Gauge Theories", in *Proceedings, 17th International Conference of High Energy Physics (ICHEP), London, England, July 01–July 10, 1974*, 1974, p. III.89, http://inspirehep.net/record/3000/files/c74-07-01-p089.pdf.

[9] D. d'Enterria, "On the Gaussian peak of the product of decay probabilities of the standard model Higgs boson at a mass $m_H \sim 125$ GeV", 2012, preprint, https://arxiv.org/abs/1208.1993.

[10] D. de Florian *et al.*, "Handbook of LHC Higgs Cross Sections: 4. Deciphering the Nature of the Higgs Sector", 2016, preprint, https://arxiv.org/abs/1610.07922.

[11] D. Kohler, B. A. Watson, J. A. Becker, "Experimental search for a low-mass scalar boson", *Phys. Rev. Lett.* **33** (1974), p. 1628-1631.

[12] R. Barbieri, T. Ericson, "Evidence against the existence of a low mass scalar boson from neutron-nucleus scattering", *Phys. Lett. B* **57** (1975), no. 3, p. 270-272.

[13] SINDRUM collaboration, S. Egli *et al.*, "Measurement of the decay $\pi^+ \to e^+\nu_e e^+ e^-$ and search for a light Higgs boson", *Phys. Lett. B* **222** (1989), p. 533-537.

[14] G. D. Barr *et al.*, "Search for a neutral Higgs particle in the decay sequence $K_L^0 \to \pi^0 H^0$ and $H^0 \to e^+e^-$", *Phys. Lett. B* **235** (1989), no. 3-4, p. 356-362, https://cds.cern.ch/record/203195.

[15] CLEO collaboration, M. S. Alam *et al.*, "Search for a Neutral Higgs Boson in *B* Meson Decay", *Phys. Rev. D* **40** (1989), p. 712-720.

[16] CUSB collaboration, J. Lee-Franzini *et al.*, *Proc. of the XXIVth Int. Conf. of High Energy Physics, Munich, Germany, August, 1988*, 1988.

[17] M. Drees *et al.*, "Higgs search at LEP", in *LEP Physics Workshop Geneva, Switzerland, February 20, 1989*, 1989, p. 59.

[18] M. Davier, H. Nguyen Ngoc, "An unambiguous search for a light Higgs boson", *Phys. Lett. B* **229** (1989), p. 150-155.

[19] R. Aßmann, M. Lamont, S. Myers, "A brief history of the LEP collider", *Nucl. Phys. B Proc. Suppl.* **109** (2002), p. 17-31.

[20] H. T. Edwards, "The Tevatron energy doubler: a superconducting accelerator", *Ann. Rev. Nucl. Part. Sci.* **35** (1985), p. 605-660.

[21] P. Janot, "Searching for Higgs bosons at LEP1 and LEP2", in *Advanced Series on Directions in High Energy Physics*, World Scientific, Dec., 1997, p. 104-130.

[22] LEP Working Group for Higgs boson searches, ALEPH, DELPHI, L3, OPAL collaboration, R. Barate *et al.*, "Search for the standard model Higgs boson at LEP", *Phys. Lett. B* **565** (2003), p. 61-75.

[23] J. Haller *et al.*, "Update of the global electroweak fit and constraints on two-Higgs-doublet models", *Eur. Phys. J. C* **78** (2018), article ID 675.

[24] CDF, D0 collaboration, T. Aaltonen *et al.*, "Higgs boson studies at the Tevatron", *Phys. Rev. D* **88** (2013), article ID 052014.

[25] L. Evans, "The large hadron collider", *Ann. Rev. Nucl. Part. Sci.* **61** (2011), p. 435-466.

[26] ATLAS Collaboration, "Combined search for the Standard Model Higgs boson using up to 4.9 $fb^{-1}$ of *pp* collision data at $\sqrt{s} = 7$ TeV with the ATLAS detector at the LHC", *Phys. Lett. B* **710** (2012), no. 1, p. 49-66.

[27] CMS Collaboration, "Combined results of searches for the standard model Higgs boson in *pp* collisions at $\sqrt{s} =$ 7 TeV", *Phys. Lett. B* **710** (2012), p. 26-48.

[28] F. Gianotti, "Status of Standard Model Higgs Searches in ATLAS", 2012, *CERN Seminar*, https://indico.cern.ch/event/197461/contributions/1478916/attachments/290953/406671/ATLAS_Higgs-CERN-seminar-2012.pdf.

[29] J. Incandela, “Status of the CMS SM Higgs Search”, 2012, *CERN Seminar*, https://indico.cern.ch/event/197461/contributions/1478917/attachments/290954/406673/CMS_4July2012_Final.pdf.

[30] ATLAS Collaboration, “Observation of a new particle in the search for the Standard Model Higgs boson with the ATLAS detector at the LHC”, *Phys. Lett. B* **716** (2012), no. 1, p. 1-29.

[31] CMS Collaboration, “Observation of a new boson at a mass of 125 GeV with the CMS experiment at the LHC”, *Phys. Lett. B* **716** (2012), no. 1, p. 30-61.

[32] ATLAS and CMS Collaborations, “Combined Measurement of the Higgs Boson Mass in *pp* Collisions at $\sqrt{s} = 7$ and 8 TeV with the ATLAS and CMS Experiments”, *Phys. Rev. Lett.* **114** (2015), no. 19, article ID 191803.

[33] ATLAS Collaboration, “Measurement of the Higgs boson mass in the $H \to ZZ^* \to 4\ell$ and $H \to \gamma\gamma$ channels with $\sqrt{s} = 13$ TeV *pp* collisions using the ATLAS detector”, *Phys. Lett. B* **784** (2018), p. 345-366.

[34] CMS Collaboration, “A measurement of the Higgs boson mass in the diphoton decay channel”, Tech. Report CMS-PAS-HIG-19-004, CERN, Geneva, 2019.

[35] ATLAS Collaboration, “Combined measurements of Higgs boson production and decay using up to 80 $\mathrm{fb}^{-1}$ of proton-proton collision data at $\sqrt{s} = 13$ TeV collected with the ATLAS experiment”, (2019), https://arxiv.org/abs/1909.02845, preprint.

[36] N. Kauer, G. Passarino, “Inadequacy of zero-width approximation for a light Higgs boson signal”, *JHEP* **08** (2012), article ID 116.

[37] F. Caola, K. Melnikov, “Constraining the Higgs boson width with ZZ production at the LHC”, *Phys. Rev. D* **88** (2013), article ID 054024.

[38] J. M. Campbell, R. K. Ellis, C. Williams, “Bounding the Higgs width at the LHC using full analytic results for $gg \to e^- e^+ \mu^- \mu^+$”, *JHEP* **04** (2014), article ID 60.

[39] J. M. Campbell, R. K. Ellis, C. Williams, “Bounding the Higgs width at the LHC: complementary results from $H \to WW$”, *Phys. Rev. D* **89** (2014), article ID 053011.

[40] ATLAS Collaboration, “Test of *CP* Invariance in vector-boson fusion production of the Higgs boson using the *Optimal Observable* method in the ditau decay channel with the ATLAS detector”, *Eur. Phys. J. C* **76** (2016), article ID 658.

[41] CMS Collaboration, “Constraints on anomalous *HVV* couplings from the production of Higgs bosons decaying to $\tau$ lepton pairs”, *Phys. Rev. D* **100** (2019), article ID 112002.

[42] CMS Collaboration, “Measurements of properties of the Higgs boson in the four-lepton final state in proton-proton collisions at $\sqrt{s} = 13$ TeV”, Tech. Report CMS-PAS-HIG-19-001, CERN, 2019, preprint.

[43] CMS Collaboration, “Measurements of Higgs boson production via gluon fusion and vector boson fusion in the diphoton decay channel at $\sqrt{s} = 13$ TeV”, Tech. Report CMS-PAS-HIG-18-029, CERN, 2019, preprint.

[44] CMS collaboration, A. M. Sirunyan *et al.*, “Observation of $\mathrm{t\bar{t}H}$ production”, *Phys. Rev. Lett.* **120** (2018), article ID 231801.

[45] ATLAS Collaboration, “Observation of Higgs boson production in association with a top quark pair at the LHC with the ATLAS detector”, *Phys. Lett. B* **784** (2018), p. 173-191.

[46] ATLAS Collaboration, “Observation of $H \to b\bar{b}$ decays and *VH* production with the ATLAS detector”, *Phys. Lett. B* **786** (2018), p. 59-86.

[47] CMS Collaboration, “Observation of Higgs boson decay to bottom quarks”, *Phys. Rev. Lett.* **121** (2018), article ID 121801.

[48] CMS Collaboration, “Search for the decay of a Higgs boson in the $\ell\ell\gamma$ channel in proton–proton collisions at $\sqrt{s} = 13$ TeV”, *JHEP* **11** (2018), article ID 152.

[49] ATLAS Collaboration, “Searches for the $Z\gamma$ decay mode of the Higgs boson and for new high-mass resonances in *pp* collisions at $\sqrt{s} = 13$ TeV with the ATLAS detector”, *JHEP* **10** (2017), article ID 112.

[50] ATLAS Collaboration, “A search for the dimuon decay of the Standard Model Higgs boson in *pp* collisions at $\sqrt{s} = 13$ TeV with the ATLAS Detector”, Tech. Report ATLAS-CONF-2019-028, CERN, Geneva, Jul 2019.

[51] CMS Collaboration, “Search for the Higgs Boson Decaying to Two Muons in Proton–Proton Collisions at $\sqrt{s} = 13$ TeV”, *Phys. Rev. Lett.* **122** (2019), article ID 021801.

[52] ATLAS Collaboration, “Search for the decay of the Higgs boson to charm quarks with the ATLAS experiment”, *Phys. Rev. Lett.* **120** (2018), article ID 211802.

[53] CMS Collaboration, A. M. Sirunyan *et al.*, “A search for the standard model Higgs boson decaying to charm quarks”, *JHEP* **03** (2020), article ID 131.

[54] ATLAS Collaboration, G. Aad *et al.*, “Combination of searches for Higgs boson pairs in *pp* collisions at $\sqrt{s} = 13$ TeV with the ATLAS detector”, *Phys. Lett. B* **800** (2020), article ID 135103.

[55] CMS Collaboration, “Combination of searches for Higgs boson pair production in proton–proton collisions at $\sqrt{s} = 13$ TeV”, *Phys. Rev. Lett.* (2018), https://arxiv.org/abs/1811.09689.

[56] ATLAS Collaboration, “Search for invisible Higgs boson decays in vector boson fusion at $\sqrt{s} = 13$ TeV with the ATLAS detector”, *Phys. Lett. B* **793** (2019), p. 499-519.

[57] CMS Collaboration, A. M. Sirunyan *et al.*, “Search for invisible decays of a Higgs boson produced through vector boson fusion in proton–proton collisions at $\sqrt{s} = 13$ TeV”, *Phys. Lett. B* **793** (2019), p. 520-551.

[58] ATLAS Collaboration, "HBSM working group hMSSM summary plots", ATL-PHYS-PUB-2019-034 (2019).

[59] A. G. *et al.*, "High-Luminosity Large Hadron Collider (HL-LHC): Technical Design Report V. 0.1", 2017, CERN Yellow Reports: Monographs, CERN, Geneva, https://cds.cern.ch/record/2284929.

[60] FCC collaboration, A. Abada *et al.*, "HE-LHC: the high-energy large hadron collider volume", *Eur. Phys. J. ST* **228** (2019), p. 1109-1382.

[61] FCC collaboration, A. Abada *et al.*, "FCC-hh: the hadron collider", *Eur. Phys. J. ST* **228** (2019), p. 755-1107.

[62] C. S. Group, "CEPC Conceptual Design Report: Volume 1 - Accelerator", 2018, preprint, https://arxiv.org/abs/1809.00285.

[63] M. Cepeda *et al.*, "Report from Working Group 2", *CERN Yellow Rep. Monogr.* **7** (2019), p. 221.

[64] FCC collaboration, A. Abada *et al.*, "FCC physics opportunities", *Eur. Phys. J. C* **79** (2019), article ID 474.

[65] M. Selvaggi, "The Higgs self-coupling at FCC-hh", in *3rd FCC Physics and Experiments Workshop, January, 2020*, 2020, https://indico.cern.ch/event/838435/contributions/3635737/attachments/1970292/3277240/HH_fccphysicsWS.pdf.

[66] A. Abada *et al.*, "FCC physics opportunities", *Eur. Phys. J. C* **79** (2019), article ID 474.

[67] A. Abada *et al.*, "FCC-ee: the lepton collider", *Eur. Phys. J. Special Topics* **228** (2019), p. 261-623.

[68] N. A. Tehrani *et al.*, "FCC-ee: your questions answered", in *CERN Council Open Symposium on the Update of European Strategy for Particle Physics (EPPSU) Granada, Spain, May 13–16, 2019* (A. Blondel, P. Janot, eds.), 2019.

[69] CEPC Study Group collaboration, M. Dong *et al.*, "CEPC Conceptual Design Report: Volume 2 - Physics & Detector", 2018, preprint, https://arxiv.org/abs/1811.10545.

[70] K. Fujii *et al.*, "Physics case for the international linear collider", 2015, preprint, https://arxiv.org/abs/1506.05992.

[71] K. Fujii *et al.*, "Physics case for the 250 GeV stage of the international linear collider", 2017, preprint, https://arxiv.org/abs/1710.07621.

[72] H. Abramowicz *et al.*, "Higgs physics at the CLIC electron–positron linear collider", *Eur. Phys. J. C* **77** (2017), article ID 475.

[73] B. Heinemann *et al.*, "Physics Briefing Book: Input for the European Strategy for Particle Physics Update 2020", 2019, preprint, http://cds.cern.ch/record/2691414, https://arxiv.org/abs/1910.11775.

[74] A. Blondel, F. Zimmermann, "A High Luminosity $e^+e^-$ Collider in the LHC tunnel to study the Higgs Boson", 2011, preprint, https://arxiv.org/abs/1112.2518.

[75] U. Amaldi, "A possible scheme to obtain $e^-e^-$ and $e^+e^-$ collisions at energies of hundreds of GeV", *Phys. Lett. B* **61** (1976), no. 3, p. 313-315.

[76] M. Palmer, "Muon collider and neutrino factory", *ICFA Beam Dynamic Newsletter* (2011), no. 55, https://icfa-usa.jlab.org/archive/newsletter/icfa_bd_nl_55.pdf.

[77] R. Palmer, "Muon colliders", *Rev. Accelerator Sci. Technol.* **07** (2014), p. 137-159.

[78] J. P. Delahaye, M. Diemoz, K. Long, B. Mansoulié, N. Pastrone, L. Rivkin *et al.*, "Muon colliders", 2019, preprint, https://arxiv.org/abs/1901.06150.

[79] D. d'Enterria, "Higgs physics at the future circular collider", *PoS* **ICHEP2016** (2017), p. 434.

[80] CMS Collaboration, "Search for a standard model-like Higgs boson in the $\mu^+\mu^-$ and $e^+e^-$ decay channels at the LHC", *Phys. Lett. B* **744** (2015), p. 184-207.

[81] ATLAS Collaboration, G. Aad *et al.*, "Search for the Higgs boson decays $H \to ee$ and $H \to e\mu$ in pp collisions at $\sqrt{s} = 13$ TeV with the ATLAS detector", *Phys. Lett. B* **801** (2020), article ID 135148.

[82] J. de Blas *et al.*, "Higgs boson studies at future particle colliders", *JHEP* **01** (2020), article ID 139.

[83] M. McCullough, "An indirect model-dependent probe of the Higgs self-coupling", *Phys. Rev. D* **90** (2014), article ID 015001.

[84] S. Di Vita, G. Durieux, C. Grojean, J. Gu, Z. Liu, G. Panico *et al.*, "A global view on the Higgs self-coupling at lepton colliders", *JHEP* **02** (2018), article ID 178.

[85] F. Maltoni, D. Pagani, X. Zhao, "Constraining the Higgs self couplings at $e^+e^-$ colliders", 2018, preprint, https://arxiv.org/abs/1802.07616.

[86] J. Alison *et al.*, "Higgs boson pair production at colliders: status and perspectives", in *Double Higgs Production at Colliders Batavia, IL, USA, September 4, 2018–9, 2019* (B. Di Micco, M. Gouzevitch, J. Mazzitelli, C. Vernieri, eds.), 2019, https://lss.fnal.gov/archive/2019/conf/fermilab-conf-19-468-e-t.pdf.

[87] A. Blondel, P. Janot, "Future strategies for the discovery and the precise measurement of the Higgs self coupling", 2018, preprint, https://arxiv.org/abs/1809.10041.

[88] P. Janot, "Top-quark electroweak couplings at the FCC-ee", *JHEP* **04** (2015), article ID 182.

[89] V. N. Litvinenko, T. Roser, M. Chamizo-Llatas, "High-energy high-luminosity $e^+e^-$ collider using energy-recovery linacs", *Phys. Lett. B* **804** (2020), article ID 135394.

[90] N. Chakrabarty *et al.*, "Radiative return for heavy Higgs boson at a muon collider", *Phys. Rev. D* **91** (2015), article ID 015008.

[91] E. Eichten, A. Martin, "The muon collider as a $H/A$ factory", *Phys. Lett. B* **728** (2014), p. 125-130.

[92] M. Worek, "Higgs CP from $H/A0 \to \tau\tau$ decay", *Acta Phys. Polon. B* **34** (2003), p. 4549-4560.

[93] A. Blondel, P. Janot, "Circular and linear $e^+e^-$ colliders: another story of complementarity", 2019, preprint, https://arxiv.org/abs/1912.11871.

*Comptes Rendus*
*Physique*
**2020**, 21, nº 1, p. 45-60
https://doi.org/10.5802/crphys.9

A perspective of High Energy Physics from precision measurements
*La physique des Hautes Energies du point de vue des mesures de précision*

# Top quark physics at the LHC

## *La physique du quark top au LHC*

**Frédéric Déliot**[*, a] **and Petra Van Mulders**[b]

[a] CEA-Saclay, Université Paris-Saclay, DRF/Irfu/DPhP, France

[b] Vrije Universiteit Brussel, Belgium.

*E-mails:* frederic.deliot@cern.ch (F. Déliot), petra.van.mulders@vub.be (P. Van Mulders).

**Abstract.** An overview of the measurements and searches in the top quark sector at the LHC is presented. Due to the large amount of data recorded by the ATLAS and CMS experiments at a centre-of-mass energy of 13 TeV, top quark properties and couplings in production and decay can be studied with an unprecedented precision and compared to predictions of the standard model to shed light on the possible presence of new physics.

**Résumé.** Cet article donne un aperçu des mesures et des recherches au LHC dans le secteur du quark top. La grande quantité de données enregistrées par les expériences ATLAS et CMS à une énergie dans le centre de masse de 13 TeV, permet d'étudier avec une précision sans précédent les propriétés et les couplages du quark top lors de sa production et de sa désintégration. Les comparaisons avec les prédictions du modèle standard permettent de tester l'éventuelle présence d'une nouvelle physique.

**Keywords.** Top quark, LHC, Collisionner, Standard model, Couplings.

**Mots-clés.** Quark top, LHC, Grand collisionneur de hadrons, Modèle standard, Couplages.

### 1. Setting the top scene

The top quark was the last standard model (SM) fermion to be discovered in 1995. This up-type third-generation quark was first observed by the CDF and D0 Collaborations at the Tevatron collider. It is the heaviest SM particle and its mass plays a key role in the predictive power of the SM, e.g. in the consistency fits of the electroweak observables (see the article on the $W^{\pm}$ and $Z^0$ bosons physics), as well as in our understanding of the stability of the universe, i.e. the lifetime of the electroweak vacuum. Furthermore, the top quark is the only quark that decays before hadronisation, making top quark physics a unique playground to study a bare quark.

---

[*] Corresponding author.

ISSN (electronic) : 1878-1535 

Initial studies of the top quark production cross sections and the top quark properties have been performed at the Tevatron collider at a centre-of-mass energy $\sqrt{s} = 1.96$ TeV. The precision of these measurements was quickly surpassed when the LHC started colliding protons at $\sqrt{s} = 7$ TeV.

In proton collisions at the LHC top quarks are dominantly produced via the strong interaction, resulting in a top quark-antiquark pair ($t\bar{t}$). In the SM the top quark decays almost 100% of the time to a $b$ quark and a $W^+$ boson ($t \to bW^+$). The $W$ boson will subsequently decay to either two quarks ($W \to q\bar{q}'$), which are observed as jets of particles, or to a charged lepton and a neutrino ($W \to l\nu$). Typically three final state topologies are defined for $t\bar{t}$ events: $t\bar{t} \to bW^+\bar{b}W^- \to bl^+\nu\bar{b}l^-\bar{\nu}$ (dilepton), $t\bar{t} \to bW^+\bar{b}W^- \to bq\bar{q}'\bar{b}l^-\bar{\nu}$ or $l^+\nu\bar{b}q\bar{q}'\bar{b}$ (lepton+jets), and $t\bar{t} \to bW^+\bar{b}W^- \to bq\bar{q}'\bar{b}q_1\bar{q}_2$ (all-jets). In the following the charges of the particles will be omitted and charge conjugation will be implicitly assumed.

There are three main modes for producing single top (anti)quarks, which have all been observed. The $s$-channel (and $t$-channel) production mode has only been observed at the Tevatron. The $t$-channel and $tW$-channel production modes have been observed at the LHC. For the studies based on single top quark events the leptonic decay of the $W$ boson is typically considered.

## 2. Top quark production and modelling at the LHC

### 2.1. *Production of $t\bar{t}$ events*

The total $t\bar{t}$ production cross section has been measured in proton collision data at the LHC at four different centre-of-mass energies as shown in Figure 1, where the measurements are compared to the state-of-the-art prediction [1]. This prediction includes next-to-next-to-leading-order (NNLO) quantum chromodynamics (QCD) corrections supplemented with soft-gluon resummation with next-to-next-to-leading logarithmic (NNLL) accuracy. The scale uncertainty, which is used to estimate the impact of missing higher-order contributions, typically dominates the total uncertainty in the predictions. For the measurements the uncertainty is dominated by the systematic uncertainty for all considered final states. For the most precise measurements the uncertainty due to the luminosity is of the same size as all the other systematic uncertainties combined. The LHCb experiment observed the production of $t\bar{t}$ events in the forward region at different centre-of-mass energies. For the latest measurement the statistical and systematic uncertainties are of comparable size [2].

Apart from measuring the total $t\bar{t}$ production cross section, the accurate prediction and measurement of specific processes is crucial for precision physics. An example is the production of $t\bar{t}b\bar{b}$. Precise knowledge of this process is particularly important for studying the coupling between the top quark and the Higgs boson, which can be measured through the production cross section of $t\bar{t}H$ with the decay of the Higgs boson to $b\bar{b}$ being the dominant decay channel. Theoretically, the $t\bar{t}b\bar{b}$ process is challenging to compute because of the number of partons in the final state and the very different scales playing a role in producing the top and bottom quark pairs. There are several strategies to generate the $t\bar{t}b\bar{b}$ process. A first option is to use a next-to-leading-order (NLO) matrix element for the top quark pair and let the parton shower (PS) produce the bottom quark pair via gluon splitting. If the bottom quark pair is produced through gluon splitting the $b$ quarks are assumed to be massless. This is referred to as the 5-flavour scheme (5FS). Another option is to generate $t\bar{t}$ events at NLO with up to two additional jets, thereby also including $b$ quark jets. In this scheme the additional jets are produced through radiation and hence the 5FS is used. The third option is to use a $t\bar{t}+b\bar{b}$ matrix element at NLO. This last option assumes massive $b$ quarks and is referred to as the 4FS. Typically the uncertainty in the predictions is of the order of 30%. The $t\bar{t}b\bar{b}$ events generated via the different options yield similar distributions for the final-state observables within the uncertainties [4]. The $t\bar{t}b\bar{b}$ production cross section was measured at

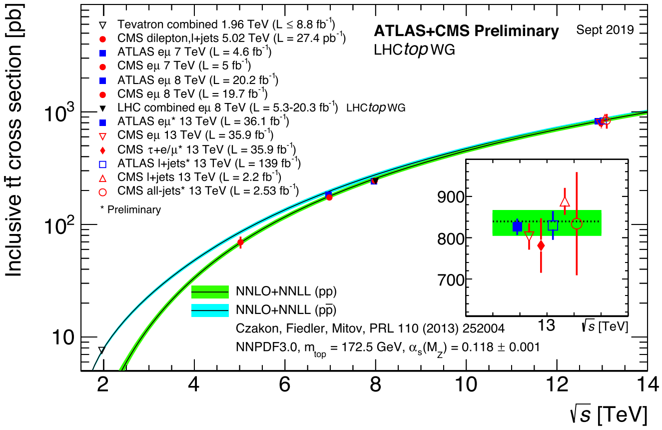


**Figure 1.** The $t\bar{t}$ production cross section at different centre-of-mass energies [3]. The prediction uses the NNPDF3.0 set for the parton distribution functions (PDFs), a top quark pole mass $m_t^{\text{pole}}$ of 172.5 GeV, and a strong coupling $\alpha_S(m_Z)$ of $0.118 \pm 0.001$.

$\sqrt{s} = 13$ TeV in each of the three $t\bar{t}$ decay channels [5–7]. The precision on these measurements is around 30% including both statistical and systematic uncertainties and the measured cross section is a factor 1.3–1.5 larger than the predictions.

The large amount of data also allows for precise differential cross section measurements and simultaneous measurements of the cross section and $m_t^{\text{pole}}$ or $\alpha_S$. Specific examples will be discussed in later sections.

## 2.2. *Production of events with a single top quark*

The cross sections for singly produced top quarks have been measured at the LHC at $\sqrt{s} = 7$, 8 and 13 TeV. These measurements are summarised in Figure 2. The $s$-channel process has not yet been observed at the LHC. However, evidence for this process has been achieved at the LHC in proton collisions at $\sqrt{s} = 8$ TeV [8]. For the $t$- and $tW$-channels, the amount of collected events is large enough so that differential cross section measurements are performed. The collected $t$-channel events are also used to measure properties, such as the top quark mass. The prediction for the $t$-channel production mode is at NNLO precision, while for the other modes, predictions are at NLO precision complemented with soft-gluon resummation at NNLL accuracy. The precision in the measured cross section is better than 20% for the $tW$-channel and 10% for the $t$-channel at $\sqrt{s} = 8$ TeV. The collision data to be analysed and/or to be collected will help to further constrain the systematic uncertainty at $\sqrt{s} = 13$, which limits the precision of the measurements.

The single top quark production cross section is particularly interesting to constrain new physics that would alter the $tWb$ coupling, which is a purely left-handed coupling in the SM, or change the production cross section when new particles or interactions are introduced. The single top quark production cross section is directly proportional to the square of the CKM matrix element $V_{tb}$ provided that there are no significant contributions from the $tWs$ and $tWd$ couplings. The size of the $tWb$ coupling can thus be directly measured using the single top quark production cross section measurements. In particular, the following quantity is measured: $|f_{\text{LV}} V_{tb}| = \sqrt{\sigma_{\text{meas}}/\sigma_{\text{theo}}(V_{tb} = 1)}$, where $f_{\text{LV}}$ parametrises the possible presence of anomalous left-handed vector couplings ($f_{\text{LV}} = 1$ in the SM), $\sigma_{\text{meas}}$ and $\sigma_{\text{theo}}$ are respectively the measured and predicted cross sections with the latter being calculated assuming $V_{tb} = 1$. In the expression, $|f_{\text{LV}} V_{tb}|$ does not depend on the unitarity of the CKM matrix nor on the assumed number

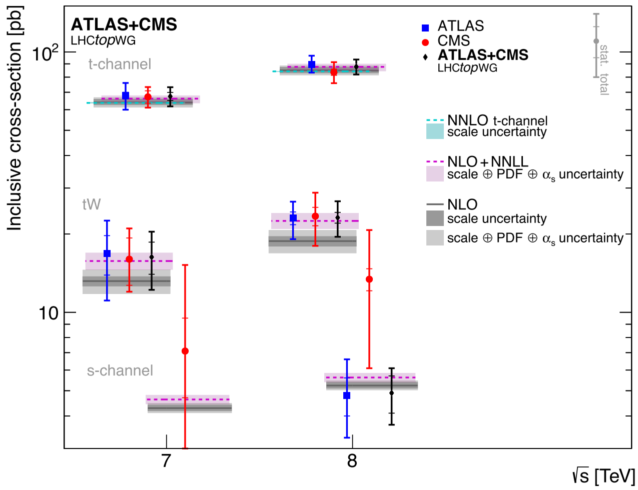


**Figure 2.** Single top quark production cross sections at different centre-of-mass energies [9].

of quark generations. The combination across experiments and centre-of-mass energies yields $|f_{\mathrm{LV}} V_{tb}| = 1.02 \pm 0.04(\mathrm{meas}) \pm 0.02(\mathrm{theo})$ [9], which is fully consistent with the SM expectation. The $t$-channel production mode dominates the precision of the combination.

## 2.3. *Modelling of events with top quarks*

The large amount of data collected at the LHC allows for (multi)differential cross section measurements as a function of a wide variety of observables. These measurements are then confronted with various state-of-the-art predictions from Monte Carlo (MC) event generators interfaced with a parton showering algorithm and hadronisation model. The events simulated in this way are typically at NLO accuracy. Deviations between the simulation and the measured distributions need to be carefully studied since observed differences could either be related to a mismodelling in the simulation, e.g. parameters that need further tuning or missing higher order corrections, or effects from new physics beyond the SM (BSM). Examples of how the differential cross section measurements are used to study specific top quark properties or search for new physics effects are presented in later sections. In this section we focus on comparisons of data with various predictions.

Differential cross section measurements are performed both for $t\bar{t}$ and single top quark production in the $t$- and $tW$-channels. In general all the MC predictions agree well with the data, with a well-studied exception the differential cross section of the top quark transverse momentum, $p_{\mathrm{T}}^{t}$. For the latter case, almost all MC predictions tend to be harder than the data as a function of $p_{\mathrm{T}}^{t}$. This has been observed by both experiments in different $t\bar{t}$ decay channels and at $\sqrt{s} = 8$ and 13 TeV [10–15]. The same trend is also seen in the single top $t$-channel at $\sqrt{s} = 8$ TeV by the ATLAS experiment [16], although it is noted that the NLO+NNLL prediction describes the data better than the MC predictions which are typically at NLO accuracy. The differential $p_{\mathrm{T}}^{t}$ cross section measurement in the single top $t$-channel performed by the CMS Collaboration at $\sqrt{s} = 13$ TeV [17] does not fully confirm the trend although it is worth noting in this context that both experiments use a different parton shower algorithm for their measurements. Similar measurements are also performed in the boosted top quark regime at 8 and 13 TeV [18–20]. It is clear that the description is improved with higher order MC predictions and that the uncertainties are still large in this part of the phase space. Measurements with more data and

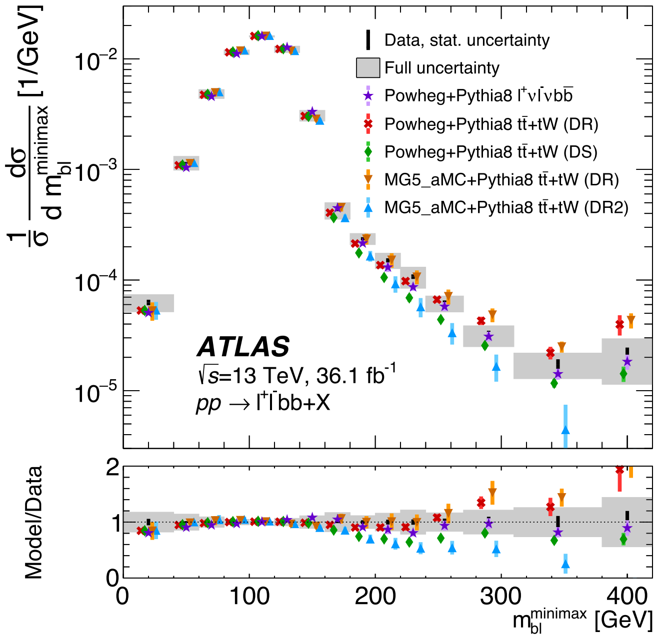


**Figure 3.** The differential $m_{bl}^{\text{minimax}}$ cross section compared with theoretical predictions with various implementations of interference effects. Uncertainties for each of the MC predictions correspond to variations of the parton distribution functions set and renormalisation and factorisation scales [21].

reduced systematic uncertainties are required to get a better understanding on whether this is a modelling issue for all top quark events, regardless of the production mode, and in the full phase space. Theoretical predictions will also continue to improve and be tested for this particular distribution.

When performing differential cross section measurements in the $t\bar{t}$ or tW production channels, it is particularly important to correctly subtract the tW or $t\bar{t}$ background, respectively. A different strategy would be to use differential cross section measurements to confront various prescriptions for modelling the interference between $t\bar{t}$ and tW production with the data. In this perspective a study was performed in the dilepton decay channel and reconstructing the invariant mass of the $b$-quark jet and charged lepton stemming from the same top quark decay. The ambiguity between the jets and the leptons is resolved by defining $m_{bl}^{\text{minimax}} = \min(\max(m_{b1,l1}, m_{b2,l2}), \max(m_{b1,l2}, m_{b2,l1}))$. The study demonstrates that the various prescriptions describe the unfolded normalised differential $m_{bl}^{\text{minimax}}$ cross section reasonably well [21] and the prediction that naturally incorporates the interference effects describes the data best. This can be seen from Figure 3. With more data it will become possible to constrain certain interference models and hence steer future model tuning and development.

Differential cross section measurements are also used to study the underlying event in $t\bar{t}$ events [22]. In that case, the normalised differential cross section is measured as function of the multiplicity and kinematic observables of charged-particle tracks. No deviation is observed from the hypothesis that underlying event is universal while tested here at high energy scales. An additional study was performed to tune the phenomelogical parameters and the value of $\alpha_S$ used in the simulation to the data [23]. This study showed that a lower value of $\alpha_S$ is preferred in the simulation. This was confirmed by a measurement of jet substructure observables [24] and resulted in a new set of underlying event tunes presented in [25].

Neutral strange particle production has been studied at $\sqrt{s}$ = 7 TeV in $t\bar{t}$ events in the dilepton decay channel [26] and compared to MC simulations with different hadronisation and fragmentation schemes, colour reconnection models and different tunes for the underlying event. The kinematic distributions are found to be well described by the MC models for strange particle production within jets, but not for strange particles produced outside jets.

Some initial studies on the jet fragmentation in top quark events have been performed at the LHC [27,28]. These studies show that the different fragmentation models adequately describe the proton collision data collected at $\sqrt{s}$ = 7 or 8 TeV. However, it is also clear that with more data the sensitivity will be significantly larger, which will allow constraining the fragmentation parameters in the near future.

Another interesting study is the differential cross section measurements of so-called jet-pull observables [29]. These observables are sensitive to the colour connections between the partons produced in the collision. The observables are measured at $\sqrt{s}$ = 13 TeV for the lepton+jets $t\bar{t}$ decay channel and for two dijet systems, i.e. the jets from the hadronic $W$ boson decay and the two $b$-quark jets from the top-quark decays. From the measured distributions it is clear that none of the current predictions is fully describing the data for all observables.

With the large amount of data still to be collected at the LHC more detailed studies will follow by both the ATLAS and CMS collaborations, which in turn will lead to significant progress for the modelling of top quark events.

## 3. Top quark properties

### 3.1. *Mesmerising mass*

One can not discuss the status of the top quark mass measurements without entering the discussion on how to interpret the mass measurements. Indeed, in quantum field theory the concept of mass has no absolute meaning. Quantum corrections affect the meaning of parameters such as the mass. To come to a physically meaningful definition divergent high-energy corrections need to be absorbed into the mass definition. This is achieved through so-called renormalisation techniques, for which several schemes exist. The mass parameter is thus dependent on the scheme. Masses in various schemes can be related to each other through a perturbative series. The so-called pole mass, $m_t^{\text{pole}}$, is conceptually closest to the rest mass of a classical particle, and it contains corrections from all energy scales down to zero momentum. Because of large corrections from QCD at low energies, $m_t^{\text{pole}}$ contains an intrinsic ambiguity of 110–250 MeV [30,31]. Other mass schemes have been introduced to avoid this ambiguity. These schemes define so-called short-distance masses and do not resum contributions from energy scales below some scale R, which implies that short-distance masses depend on the scale R. To avoid the ambiguity, the scale R is taken to be larger than $\Lambda_{\text{QCD}} \sim \mathcal{O}(200\ \text{MeV})$, which is the characteristic scale of confinement in QCD.

The most precise top quark mass measurements rely on the direct (partial) kinematic reconstruction of the top quark based on its decay products. A wide variety of techniques exists to extract the top quark mass from the decay products with different sources of systematic uncertainties limiting the precision of the measurements. The techniques rely on the simulated distributions of observables that are sensitive to the top quark mass parameter in the MC generator. In general terms one typically estimates the top quark mass from the peak position or the kinematic endpoint of these observable distributions. The direct measurements are thus limited by the accuracy of the MC generator for modelling these distributions and the corresponding conceptual meaning of the top quark mass parameter used in the MC generator, $m_t$. The CMS and ATLAS Collaborations have measured $m_t$ with a precision of about 500 MeV [32,33]. In these measurements the modelling uncertainties in the $t\bar{t}$ simulation are dominant. These are for instance the uncertainty in the colour reconnection model, the final-state radiation and the fragmentation, both of which impact the jet energy scale of light-quark-flavour and $b$ quark jets. In general the various $m_t$ measurements performed at the LHC agree very well with each other with $m_t$ being around 172.5 GeV. There is however one exception. The measurement performed using $t\bar{t}$ events in the lepton+jets channel based on a template fit to the invariant mass from the isolated charged lepton and the lepton required to be present in the decay chain of the beauty hadron in the $b$ quark jet yields $m_t = 174.48 \pm 0.40(\text{stat}) \pm 0.67(\text{syst})$ GeV [34]. This measurement provides an agreement at the level of about 2.2 standard deviations with other measurements performed at the LHC. The systematic uncertainty is dominated by the modelling of $t\bar{t}$ production and of the $b$ quark fragmentation and decay.

The high precision achieved by direct top quark mass measurements today, forces the debate on the interpretation of $m_t$ into a more quantitative discussion. To make quantitative statements, the questions that are raised are to which renormalisation scheme the extracted $m_t$ corresponds or how $m_t$ is related to standard schemes such as $m_t^{\text{pole}}$. In principle the top quark mass scheme used in the MC generators is fixed by the structure and theoretical precision of the PS algorithm. For example, the state-of-the-art PS algorithms are designed in the approximation of a stable top quark, i.e. the narrow width approximation. In addition, the PS algorithms are not uniformly precise for all observables, even with NLO matching. Recently a few studies have been performed to understand how some of these approximations affect $m_t$ [35–37]. Moreover, since the PS algorithms are developed in the collinear approach, i.e. in the boosted regime, a top quark mass measurement performed using boosted top quarks would be more straight-forward to interpret. Recently a measurement has been performed at $\sqrt{s} = 13$ TeV yielding $m_t = 172.56 \pm 2.47$ GeV [38].

A different approach is to use the $t\bar{t}$ production cross section to determine the top quark mass. Indeed, the $t\bar{t}$ production cross section is sensitive to the value of the top quark mass in a theoretically well-defined scheme, e.g. $m_t^{\text{pole}}$. This dependence can be calculated up to next-to-next-leading order (NNLO), including NNLL corrections in the production, and electroweak corrections in the production and the decay. Comparing the measured cross section with the calculated top quark mass dependence, the extracted top quark mass is achieving a precision of around 1.6 GeV for $m_t^{\text{pole}}$ [39–41]. Recently, a precision of less than 1 GeV was achieved using multidifferential cross section measurements [42]. It is worth noting that since the measurements of the cross section rely on MC generators for the selection of the event requirements, to determine the efficiency of these criteria, and for the extrapolation of the fiducial cross section to the full phase space, also these measurements are to some small extent model dependent and thus the extracted mass can not be fully unambigiously interpreted as $m_t^{\text{pole}}$ [43].

Over the last years, significant progress has been made from the theoretical side in an attempt to relate the $m_t$ measurements with $m_t^{\text{pole}}$ [44–46]. This progress is very promising and it is not unlikely that the question will be solved in the next decade.

Recently also the running of the top quark mass has been studied experimentally [47]. The measured running is probed up to a scale of the order of 1 TeV and found to be compatible with the scale dependence predicted by the renormalisation group equation.

### 3.2. *Width*

The top quark width $\Gamma_t$ can be measured indirectly using the $t$-channel production cross section for single top quarks and the ratio of the branching fraction to $b$ quarks to the branching fraction to any quark. The most precise indirect measurement corresponds to $\Gamma_t = 1.36 \pm 0.02(\text{stat})^{+0.14}_{-0.11}(\text{syst})$ GeV [48]. Both the ATLAS and CMS Collaborations also performed direct measurements of $\Gamma_t$. Among those, the most precise direct measurement is obtained using $t\bar{t}$ events in the dilepton final state collected at 13 TeV and results in $\Gamma_t = 1.9 \pm 0.5$ GeV for

$m_t$ = 172.5 GeV [49]. Both the direct and indirect measurements are fully consistent with the SM prediction at NLO, $\Gamma_t$ = 1.35 GeV, which has an uncertainty below 1% and which assumes $m_t$ = 173.3 GeV and $\alpha_S$ = 0.118 [48].

Given the large amount of data, a more natural strategy would be to measure the top quark mass and width simultaneously, which would allow taking into account the correlation between the width and the mass. However, in order to be able to clearly interpret these measurements the narrow width approximation in the PS algorithms would need to be lifted, as mentioned in the previous section.

### 3.3. *Spin correlations and polarisation*

The lifetime of the top quark ($\sim 10^{-25}$ s) is shorter than the hadronisation time ($\sim 10^{-23}$ s) and much shorter than the spin decorrelation time ($\sim 10^{-21}$ s). Therefore the top quark decays before hadronisation and its spin information is directly transferred to its decay products. This gives a unique opportunity to study the spin properties of a bare quark. Top quark pair production in QCD is parity invariant so at LO the top quarks and antiquarks produced at the LHC are not expected to be polarised. However, their spins are predicted to be correlated with an amount of correlation depending on the $t\bar{t}$ invariant mass, $m_{t\bar{t}}$. The amount of spin correlation in $t\bar{t}$ events could be affected by BSM physics, like e.g. the presence of scalar supersymmetric top squarks. To study spin correlations experimentally it is relevant to note that not all decay particles carry the same degree of spin information. The charged leptons arising from leptonically decaying $W$ bosons carry almost the full spin information of the parent top quark and spin correlation measurements are therefore often performed in the dilepton channel. The simplest sensitive observable that can be studied is the azimuthal opening angle, $\Delta\phi$, between the two charged leptons measured in the laboratory frame. The spin correlation is extracted from the absolute and normalised $t\bar{t}$ differential cross section measured as a function of $\Delta\phi$ in four bins of $m_{t\bar{t}}$ corrected for detector resolution and acceptance effects back to parton level [50]. The spin correlation measured by the ATLAS Collaboration inclusively over all the $m_{t\bar{t}}$ bins is found to be significantly higher than the NLO prediction including PS (see Figure 4). While NLO predictions including electroweak effects agree with data within its large scale uncertainties, the agreement disappears at NNLO in QCD. This observation is not confirmed by the CMS Collaboration [51]. It is clear that further measurements and developments for state-of-the-art predictions are required to understand the origin of the disagreement. Instead of using a single observable, it is also possible to measure the full spin density matrix, leading to 15 polarisation and spin correlation coefficients. In this case the top quark and antiquark kinematics need to be fully reconstructed, which gives rise to large uncertainties in the dilepton channel. The measured coefficients are found to be compatible with the SM expectation [51, 52] and are used to set limits on hypothetical BSM scenarios.

In single top quark production the SM assumes a $Wtb$ vector-axial-vector coupling leading to the production of highly polarised top quarks. The differential cross section of the top quark polarisation angle in the $t$-channel is studied and found to be in agreement with the SM predictions quoting a measurement with a 14% precision [54].

### 3.4. *Asymmetry*

At LO in QCD the top quark-antiquark production is symmetric under charge conjugation. However at NLO, interference in the amplitudes of the $q\bar{q}$ initiated processes lead to an asymmetry in $t$ versus $\bar{t}$ production. The $qg$ processes are also asymmetric (but to a smaller extent) while the $t\bar{t}$ production through gluon fusion remains symmetric at all orders. The consequence of this

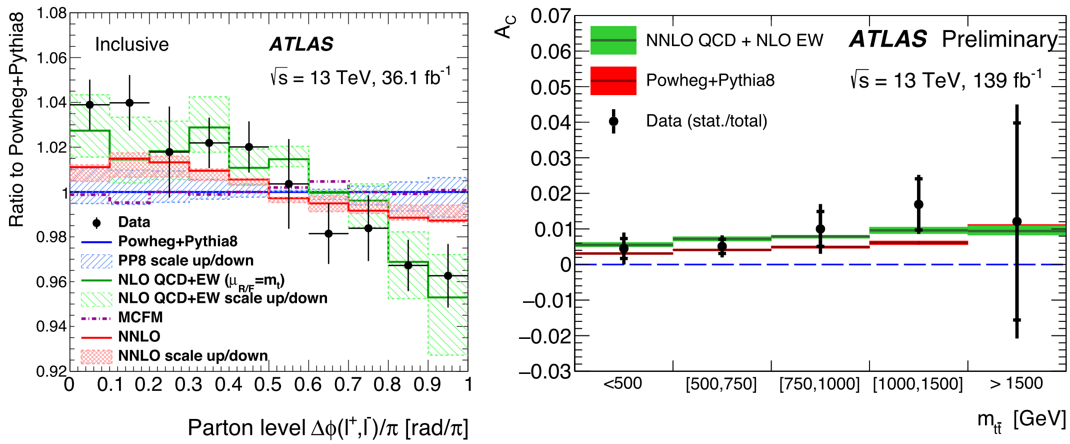


**Figure 4.** Comparison of the unfolded $\Delta\phi$ distribution normalised to the predictions from Powheg+Pythia with other theoretical predictions [50] (left). Measurement of the charge asymmetry as a function of $m_{t\bar{t}}$ compared to the SM predictions at different orders [53] (right).

asymmetry at NLO is that the top quarks (antiquarks) are produced preferentially in the direction of the incoming quark (antiquark). At the LHC which is a proton–proton collider, the colliding beams are symmetric so there is no preferential direction for the incoming quarks or antiquarks. Nevertheless due to the difference in the proton PDFs, the valence quarks carry on average a larger fraction of the proton momentum than the antiquarks from the sea. This results in top quarks being produced preferentially with higher absolute rapidity while top antiquarks are more centrally produced. Since the fraction of $q\bar{q}$ initiated $t\bar{t}$ production is only around 10% at $\sqrt{s} = 13$ TeV, this effect is predicted to be very small in the SM. Several BSM processes such as production of axigluons or heavy Z' bosons can enhance this asymmetry expecially in specific kinematic regions like large $m_{t\bar{t}}$ or large longitudinal boost of the $t\bar{t}$ system. A $t\bar{t}$ charge asymmetry is defined counting the number of events $N$ as:

$$A_C = \frac{N(\Delta|y| > 0) - N(\Delta|y| < 0)}{N(\Delta|y| > 0) + N(\Delta|y| < 0)},$$

where $\Delta|y| = |y_t| - |y_{\bar{t}}|$ is the absolute rapidity difference between the top quark and antiquark. Both the ATLAS and CMS Collaborations measured this quantity using data collected at 7 and 8 TeV. The inclusive and differential results obtained by both experiments in the lepton+jet channel have been combined [55], but the statistical uncertainties in the high $m_{t\bar{t}}$ region still limit the achievable precision. While the amount of $t\bar{t}$ events produced through $q\bar{q}$ annihilation is smaller at 13 TeV than at lower centre-of-mass energies, the large amount of data, especially in the boosted regime, permits to study the charge asymmetry more profoundly. The charge asymmetry is measured in the lepton+jets channel using a fully Bayesian unfolding method to correct for detector and acceptance effects simultaneously in the resolved and boosted topologies (see Figure 4) [53]. The methodology allows to constrain the larger systematic uncertainties in situ. The inclusive and differential measurements are found to be consistent with the SM predictions. The measured inclusive asymmetry differs from zero by 4 standard deviations. The differential cross sections measurements in the dilepton final state as a function of $\Delta|y| = |y_t| - |y_{\bar{t}}|$ at parton and particle levels can also be used to extract $A_C$ [15]. The measurements as a function of the lepton pseudo-rapidity $\Delta\eta_\ell = |\eta_\ell| - |\eta_{\bar{\ell}}|$ can be exploited to construct a similar asymmetry based only on the lepton angles. Such asymmetry is diluted compared to when using the reconstructed

$t\bar{t}$ event but it does not require the reconstruction of the top quark or antiquark kinematics. Both these measured observables are consistent with the SM expectations. Since the $q\bar{q}$ initiated production is enhanced in the forward region, it is expected that the LHCb Collaboration will provide interesting asymmetry measurements in the top quark sector at high luminosity [56]. The $b$ quark from the top quark decay can also be used to build other kind of asymmetries sensitive to CP violation [57]. So asymmetries in the top quark sector are still interesting to explore in the years to come.

## 4. Top quark couplings and rare processes

The large amount of data collected by the LHC at 13 TeV allows to establish and study top quark processes that were not accessible so far. With predicted cross sections around 1 pb or below, the production of top quarks in association with bosons ($W$, $Z$, $H$ or $\gamma$) becomes a tool to scrutinise the top quark couplings searching for any deviations from the SM expectations. The $Wtb$ coupling is for instance studied by measuring the $W$ helicity fractions with $\sqrt{s} = 8$ TeV data [58, 59]. The potential deviations from SM predictions are often parametrised within the framework of an effective field theory (EFT) in terms of Wilson coefficients of BSM dimension 6 operators [60]. Studies of the coupling between the top quark and Higgs boson are discussed in the Higgs Chapter.

### 4.1. *Top quark couplings to bosons*

Measurements of $t\bar{t}$ production in association with a $Z$ or a $W$ boson provide a direct probe of the weak couplings of the top quark. These couplings could be modified by the presence of BSM physics. Events containing two leptons of same charge (SS) are used to extract the $t\bar{t}W$ signal, while events with three or four charged leptons that include a same-flavour lepton pair compatible with the decay of a $Z$ boson are usually used to measure the $t\bar{t}Z$ cross section. In these channels, the efficiency of the trigger and of the isolated lepton selection requirements are crucial. The $t\bar{t}W$ signal is much more difficult to isolate than $t\bar{t}Z$ events because the SS dilepton final state suffers from a significant background from leptons with misidentified charge and from non-prompt leptons from hadron decays, photon conversions or jets misidentified as leptons. These type of backgrounds are evaluated using data driven techniques and validated in control regions. The main background in the $t\bar{t}Z$ analyses comes from at least one top quark produced in association with one or multiple $W$, $Z$, or Higgs bosons. The signal regions are split according to jet multiplicity and the number of $b$-tagged jets in the events. In the dilepton channel, a multivariate discriminant is introduced to further separate signal and background events. The amount of $t\bar{t}W$ and $t\bar{t}Z$ events are fitted in the signal and control regions to extract the individual cross sections as well as the 68 and 95% confidence level 2-dimensional contours. The latest $t\bar{t}W$ measurements [61, 62] reach a precision of around 22% still dominated by statistical uncertainties, while the inclusive $t\bar{t}Z$ cross section is now measured with a precision of 8% with equal contributions from statistical and systematic uncertainties [63]. For the first time, the large amount of data permits to measure absolute and normalised differential $t\bar{t}Z$ cross sections using signal-enriched regions [63]. These differential measurements are performed as a function of the transverse momentum of the $Z$ boson (see Figure 5) and other relevant kinematic observables. After correcting for detector and acceptance effects the distributions agree with the SM predictions and could then be used to put more stringent constraints on anomalous interactions.

The electroweak production of a single top quark in association with a $Z$ boson ($tZq$) is even trickier to isolate from the diboson, $t\bar{t}Z$ and non-prompt lepton backgrounds. However this

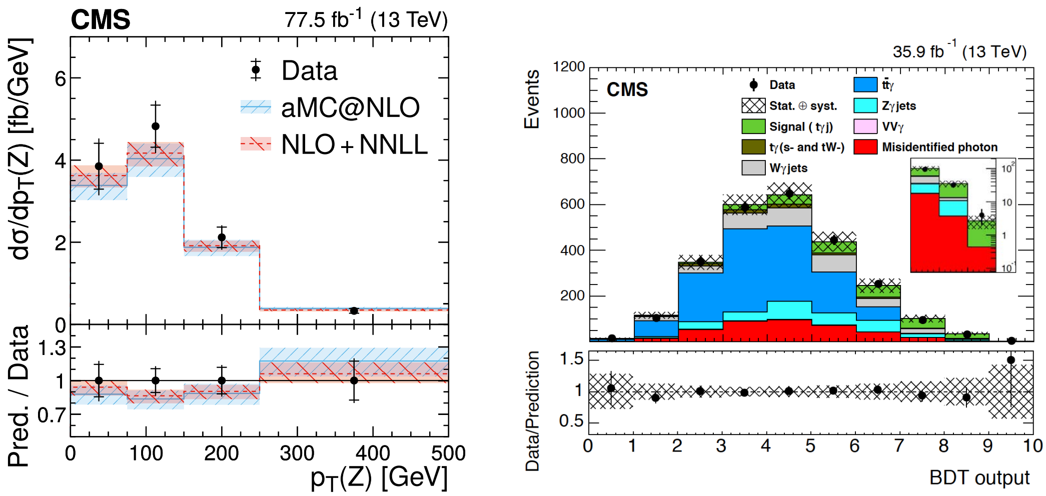


**Figure 5.** Measured differential $t\bar{t}Z$ production cross section in the full phase space as a function of the transverse momentum of the $Z$ boson [63] (left), multivariate discriminant used to isolate the $t\gamma$ signal [64] (right).

process is interesting to study since it provides sensitivity to the $WWZ$ triple-gauge coupling, which could be one of the production modes, and to modified interactions in a unique way. Final states where both the $W$ boson from the top quark decay as well as the $Z$ boson decay into leptons are explored leading to a three lepton signature. Events are categorised in different signal regions according to the number of jets and $b$-tagged jets. In each of the signal regions a multivariate discriminant is used to isolate $tZq$ events and fit the cross section value. The $tZq$ process has been observed with a significance of more than 5 standard deviations and is measured with an uncertainty of 15% [65, 66].

In order to probe the $t\gamma$ coupling, the production and kinematic properties of a top-quark pair produced in association with a photon ($t\bar{t}\gamma$) are studied. The inclusive and differential cross sections of this process are sensitive to BSM physics, for instance through anomalous dipole moments of the top quark affecting the transverse momentum spectrum of the $\gamma$ or through some of the Wilson coefficients in the context of an EFT. Backgrounds arise from electrons or hadronic processes that are reconstrued as photons. Also off-shell production of $Wt\gamma$ results in the same final state. The latest $t\bar{t}\gamma$ measurement uses the $e\mu$ channel and a likelihood fit to the scalar sum over all transverse momenta in the event to extract the inclusive cross-section in a fiducial volume. Normalised and absolute parton level differential cross sections are measured as a function of different characteristic observables and compared to MC simulations and NLO predictions [67], which are found to be in agreement. The first evidence for single top quark production in association with a photon in the $t$-channel has been reported [64]. Events with a muon are selected and the top quark kinematics is reconstructed. The multivariate discriminant distribution shown in Figure 5 is used to isolate the signal from the large $t\bar{t}\gamma$ background. This result paves the way for more precise measurements using the large amount of available or to be collected data.

## 4.2. *Four-top quark production*

The production of four top quarks ($t\bar{t}t\bar{t}$) is one of the most spectacular processes predicted by the SM and that could be studied at the LHC. With a cross section of only roughly 12 fb, it has not yet been observed. Therefore this observation would be a milestone for measuring rare processes at the LHC. Four top quarks could be copiously produced in many BSM like models with gluinos, heavy scalar bosons, axigluons, colour scalars and top compositeness, even in cases where top quark pairs are not. In the framework of EFT, $t\bar{t}t\bar{t}$ production has a larger constraining power than the $t\bar{t}$ process on the $qqtt$ operators. Therefore, the $t\bar{t}t\bar{t}$ process offers complementary handles to search for deviations from the SM in the top quark sector. Searches for the $t\bar{t}t\bar{t}$ process are performed in two different final states that have very different challenges. The channel with one lepton or two leptons with opposite charge corresponds to a large branching fraction but suffers from a large background coming mainly from $t\bar{t}$+light jets and $t\bar{t}b\bar{b}$ events. This background is usually evaluated using data driven techniques or from MC simulation validated in control regions. As the uncertainty on these backgrounds is very large, data in control regions is used to constrain these uncertainties by profiling the corresponding nuisance parameters in a likelihood fit. The channels with two leptons with the same charge or with at least three leptons, on the other hand, have small branching fractions but benefit from a low level of background mainly coming from fake or non-prompt leptons or from $t\bar{t}$ production with additional electroweak bosons. This is the most sensitive channel. The $t\bar{t}t\bar{t}$ topology also features high jet multiplicity and high $b$-jet multiplicity as well as high overall energy that could be quantified with a large value for the scalar sum of the transverse momenta of all reconstructed objects in the event. These observables are used in multivariate techniques to separate signal and background and enhance the sensitivity. The ATLAS Collaboration obtains an observed (expected) significance for the $t\bar{t}t\bar{t}$ signal of 2.8 (1.0) standard deviations [68] by combining the two final states. The latest result from the CMS Collaboration uses an extended dataset in the multilepton channel reaching 2.6 (2.7) standard deviations [69] for the $t\bar{t}t\bar{t}$ process above the background-only hypothesis. More data will allow the observation of this process at the LHC, although we might have to wait until the end of the LHC Run 3 in case the SM prediction is correct.

### 4.3. *Search for flavour-changing neutral currents in the top quark sector*

In the SM, flavour-changing neutral currents (FCNC) are forbidden at tree level and are strongly suppressed at higher orders by the Glashow–Iliopoulos–Maiani (GIM) mechanism. The SM predicts branching fractions for top quark FCNC decays of the order of $10^{-12}$–$10^{-16}$. However various extensions of the SM would result in a significant enhancement of the FCNC top quark decay rates. Hence any deviations from these heavily SM suppressed rates would be a sign of new physics. The anomalous vertices, $tqH$, $tq\gamma$, $tqg$ and $tqZ$, could be probed at the production or in the decays of single top quark or top quark pair production. Many searches for deviations are performed at the LHC for all possible production and decay modes. Often the analyses concentrate on one of such cases at a time. The searches rely on the reconstruction of the event kinematics, including the top quark decaying through an FCNC, and often utilise multivariate discriminant to separate signal and background. The $tqH$ vertex is probed with dedicated analyses for each signature according to the possible Higgs boson decay. In case of $H \to b\bar{b}$, the limits on the branching fraction of $t \to Hq$ are around $4 \times 10^{-3}$ [70, 71], while they are tighter for $H \to \tau\tau$ [71], $H \to WW^*/ZZ^*$ [72] or $H \to \gamma\gamma$ [73], which are both around $1$–$2 \times 10^{-3}$. The $tq\gamma$ vertex has been considered both in production and decay in the photon and one lepton final state leading to an upper limit on the $t \to q\gamma$ branching fraction at the 95% confidence level of $2$–$6 \times 10^{-5}$, depending on whether the assumed coupling is left-handed or right-handed. The upper limit on the $t \to c\gamma$ branching fraction is around $20 \times 10^{-5}$ [74]. The $tqZ$ vertex is explored in the trilepton final state and constrained to an upper limit on the $t \to qZ$ branching fraction of $2$–$4 \times 10^{-4}$ [75, 76]. The enormous amount of data expected in the high-luminosity phase of the LHC will permit to further improve these upper limits by at least an order of magnitude in case of no discovery [56].

Studying the top-quark couplings to bosons as well as rare processes involving the top quark is just at a start. These topics will be an important field of research in the coming years.

## 5. Perspectives

During the LHC Run 2 (2015–2018) an amount of proton–proton collisions corresponding to about 150 fb$^{-1}$ has been collected at $\sqrt{s} = 13$ TeV. Currently, many of the Run 2 measurements use only a fraction of the collected data (36 fb$^{-1}$). During the LHC Run 3 (2021–2023) 200 fb$^{-1}$ is expected to be collected at $\sqrt{s} = 13$–14 TeV. This means that by the end of Run 3, $\mathcal{O}(10)$ times more data will be available compared to what is used for the measurements today. This has two implications. First, some rare processes will potentially be observed for the first time at the LHC, e.g. the $t\bar{t}t\bar{t}$ process, leading to potentially new insights or constraints on beyond the standard model processes. Second, the uncertainty on all top quark precision measurements will be limited by systematic effects. For this reason, the focus is shifting towards reducing the systematic uncertainties, with the top quark mass and differential cross section measurements as the driving forces to achieve this goal. It is expected that significant progress will be made, both for the modelling of the top quark events in the simulation as for the prescription to assess the modelling uncertainties. After Run 3, the high-luminosity phase of the LHC is expected to deliver 3 ab$^{-1}$ bringing measurements and searches in top quark physics yet to another level [56]. In parallel, the theory community is developing new MC generators and better predictions for processes involving top quarks. These studies and the legacy measurements from the high-luminosity phase of the LHC will be the reference point for accelerators beyond the LHC.

A potential future $e^+e^-$ collider with $\sqrt{s} \geq 350$ GeV would enable to scrutinise the top quark properties with very high precision without suffering from significant uncertainties from PDF, QCD scales or collider luminosity. The precision of the theory predictions in leptonic collisions is around the per-mil level, allowing a comparison with measurements at the same level of precision. For instance, a scan of the top quark pair production cross section around the threshold will offer a precision in the top quark mass at the level of 25 MeV, including both statistic and systematic uncertainties. The theoretical uncertainty on the line shape prediction would allow a top quark mass extraction with a 50 MeV total theoretical uncertainty [77], providing the strong coupling constant is measured with sufficient precision. The precise measurement of the top quark mass and of other standard model parameters will be used in a global fit of the electroweak observables and provide the most stringent consistency test for the standard model. In addition, an $e^+e^-$ collider with a sufficiently large centre-of-mass energy allows for measuring the top quark Yukawa coupling precisely using the $t\bar{t}H$ final state, studying the $t\bar{t}Z$ and $t\bar{t}\gamma$ vertices at the per-mil level, and constraining anomalous operators an order of magnitude more stringently than what can be done at the HL-LHC [78, 79].

Clearly, depending on the chosen successor of the LHC, the top quark properties and couplings can be measured very precisely, and/or new physics can be probed in the top quark sector, e.g. using EFTs at a proton collider operating at much higher centre-of-mass energies.

## References

[1] M. Czakon, P. Fiedler, A. Mitov, "The total top quark pair production cross-section at hadron colliders through $\mathcal{O}(\alpha_S^4)$", *Phys. Rev. Lett.* **110** (2013), article ID 252004.

[2] LHCb Collaboration, "Measurement of forward top pair production in the dilepton channel in pp collisions at $\sqrt{s} = 13$ TeV", *JHEP* **08** (2018), article ID 174.

[3] LHCTopWG - LHC Top Physics Working Group, https://twiki.cern.ch/twiki/bin/view/LHCPhysics/LHCTopWG.

[4] T. Jezo, J. M. Lindert, N. Moretti, S. Pozzorini, "New NLOPS predictions for $t\bar{t} + b$-jet production at the LHC", *Eur. Phys. J. C* **78** (2018), article ID 502.

[5] ATLAS Collaboration, "Measurements of fiducial and differential cross-sections of $t\bar{t}$ production with additional heavy-flavour jets in proton–proton collisions at $\sqrt{s} = 13$ TeV with the ATLAS detector", *JHEP* **04** (2019), article ID 46.

[6] CMS Collaboration, "Measurements of $t\bar{t}$ cross sections in association with b jets and inclusive jets and their ratio using dilepton final states in pp collisions at $\sqrt{s} = 13$ TeV", *Phys. Lett. B* **776** (2018), p. 355-378.

[7] CMS Collaboration, "Measurement of the $t\bar{t}b\bar{b}$ production cross section in the all-jet final state in pp collisions at $\sqrt{s} = 13$ TeV", CMS Physics Analysis Summary, CMS-PAS-TOP-18-011.

[8] ATLAS Collaboration, "Evidence for single top-quark production in the s-channel in proton–proton collisions at $\sqrt{s} = 8$ TeV with the ATLAS detector using the Matrix Element Method", *Phys. Lett. B* **756** (2016), p. 228-246.

[9] ATLAS and CMS Collaborations, "Combinations of single-top-quark production cross-section measurements and $|f_{\rm LV} V_{tb}|$ determinations at $\sqrt{s} = 7$ and 8 TeV with the ATLAS and CMS experiments", *JHEP* **05** (2019), article ID 88.

[10] CMS Collaboration, "Measurement of the differential cross section for top quark pair production in pp collisions at $\sqrt{s} = 8$ TeV", *Eur. Phys. J. C* **75** (2015), article ID 542.

[11] ATLAS Collaboration, "Measurements of top-quark pair differential cross-sections in the lepton+jets channel in pp collisions at $\sqrt{s} = 8$ TeV using the ATLAS detector", *Eur. Phys. J. C* **76** (2016), article ID 538.

[12] ATLAS Collaboration, "Measurements of top-quark pair differential cross-sections in the eμ channel in pp collisions at $\sqrt{s} = 13$ TeV using the ATLAS detector", *Eur. Phys. J. C* **77** (2017), article ID 299.

[13] ATLAS Collaboration, "Measurements of differential cross sections of top quark pair production in association with jets in pp collisions at $\sqrt{s} = 13$ TeV using the ATLAS detector", *JHEP* **10** (2018), article ID 159.

[14] CMS Collaboration, "Measurement of differential cross sections for the production of top quark pairs and of additional jets in lepton+jets events from pp collisions at $\sqrt{s} = 13$ TeV", *Phys. Rev. D* **97** (2018), article ID 092005.

[15] CMS Collaboration, "Measurements of $t\bar{t}$ differential cross sections in proton–proton collisions at $\sqrt{s} = 13$ TeV using events containing two leptons", *JHEP* **02** (2019), article ID 149.

[16] ATLAS Collaboration, "Fiducial, total and differential cross-section measurements of t-channel single top-quark production in pp collisions at 8 TeV using data collected by the ATLAS detector", *Eur. Phys. J. C* **77** (2017), article ID 531.

[17] CMS Collaboration, "Measurement of differential cross sections and charge ratios for t-channel single top quark production at 13 TeV", CMS Physics Analysis Summary, CMS-PAS-TOP-17-023.

[18] CMS Collaboration, "Measurement of the integrated and differential $t\bar{t}$ production cross sections for high-$p_{\rm T}$ top quarks in pp collisions at $\sqrt{s} = 8$ TeV", *Phys. Rev. D* **94** (2016), article ID 072002.

[19] ATLAS Collaboration, "Measurement of the differential cross-section of highly boosted top quarks as a function of their transverse momentum in $\sqrt{s} = 8$ TeV proton–proton collisions using the ATLAS detector", *Phys. Rev. D* **93** (2016), article ID 032009.

[20] ATLAS Collaboration, "Measurements of $t\bar{t}$ differential cross-sections of highly boosted top quarks decaying to all-hadronic final states in pp collisions at $\sqrt{s} = 13$ TeV using the ATLAS detector", *Phys. Rev. D* **98** (2018), article ID 012003.

[21] ATLAS Collaboration, "Probing the quantum interference between singly and doubly resonant top-quark production in pp collisions at $\sqrt{s} = 13$ TeV with the ATLAS detector", *Phys. Rev. Lett.* **121** (2018), article ID 152002.

[22] CMS Collaboration, "Study of the underlying event in top quark pair production in pp collisions at 13 TeV", *Eur. Phys. J. C* **79** (2019), article ID 123.

[23] CMS Collaboration, "Investigations of the impact of the parton shower tuning in Pythia 8 in the modelling of $t\bar{t}$ at $\sqrt{s} = 8$ and 13 TeV", CMS Physics Analysis Summary, CMS-PAS-TOP-16-021.

[24] CMS Collaboration, "Measurement of jet substructure observables in $t\bar{t}$ events from proton–proton collisions at $\sqrt{s} = 13$ TeV", *Phys. Rev. D* **98** (2018), article ID 092014.

[25] CMS Collaboration, "Extraction and validation of a new set of CMS PYTHIA8 tunes from underlying-event measurements", *Eur. Phys. J. C* **80** (2020), no. 1, article ID 4.

[26] ATLAS Collaboration, "Measurement of $K^0_S$ and $\Lambda_0$ production in $t\bar{t}$ dileptonic events in pp collisions at $\sqrt{s} = 7$ TeV with the ATLAS detector", *Eur. Phys. J. C* **79** (2019), no. 12, article ID 1017.

[27] ATLAS Collaboration, "Measurement of jet shapes in top pair events at $\sqrt{s} = 7$ TeV using the ATLAS detector", *Eur. Phys. J. C* **73** (2013), article ID 2676.

[28] CMS Collaboration, "Measurement of the top quark mass using charged particles in pp collisions at $\sqrt{s} = 8$ TeV", *Phys. Rev. D* **93** (2016), article ID 092006.

[29] ATLAS Collaboration, "Measurement of colour flow using jet-pull observables in $t\bar{t}$ events with the ATLAS experiment at $\sqrt{s} = 13$ TeV", *Eur. Phys. J. C* **78** (2018), article ID 847.

[30] M. Beneke, P. Marquard, P. Nason, M. Steinhauser, "On the ultimate uncertainty of the top quark pole mass", *J. Phys. Lett. B* **10** (2017), p. 63-70.

[31] A. H. Hoang, C. Lepenik, M. Preisser, "On the light massive flavor dependence of the large order asymptotic behavior and the ambiguity of the pole mass", *JHEP* **09** (2017), article ID 99.

[32] CMS Collaboration, "Measurement of the top quark mass using proton–proton data at $\sqrt{s} = 7$ and 8 TeV", *Phys. Rev. D* **93** (2016), article ID 072004.

[33] ATLAS Collaboration, "Measurement of the top quark mass in the $t\bar{t} \to$ lepton+jets channel from $\sqrt{s} = 8$ TeV ATLAS data and combination with previous results", *Eur. Phys. J. C* **79** (2019), article ID 290.

[34] ATLAS Collaboration, "Measurement of the top quark mass using a leptonic invariant mass in pp collisions at $\sqrt{s} = 13$ TeV with the ATLAS detector", ATLAS-CONF-2019-046.

[35] S. F. Ravasio, T. Jazo, P. Nason, C. Oleari, "A theoretical study of top-mass measurements at the LHC using NLO+PS generators of increasing accuracy", *Eur. Phys. J. C* **78** (2018), article ID 458.

[36] G. Corcella, R. Franceschini, D. Kim, "Fragmentation uncertainties in hadronic observables for top quark mass measurements", *Nucl. Phys. B* **929** (2018), p. 485-526.

[37] G. Heinrich, A. Maier, R. Nisius, J. Schlenk, M. Schulze, L. Scyboz, J. Winter, "NLO and off-shell effects in top quark mass determinations", *JHEP* **07** (2018), article ID 129.

[38] CMS Collaboration, "Measurement of the jet mass distribution in highly boosted top quark decays in pp collisions at $\sqrt{s} = 13$ TeV", CMS Physics Analysis Summary, CMS-PAS-TOP-19-005.

[39] CMS Collaboration, "Measurement of the $t\bar{t}$ production cross section in the eμ channel in proton–proton collisions at $\sqrt{s} = 7$ and 8 TeV", *JHEP* **08** (2016), article ID 29.

[40] ATLAS Collaboration, "Measurement of lepton differential distributions and the top quark mass in $t\bar{t}$ production in pp collisions at $\sqrt{s} = 8$ TeV with the ATLAS detector", *Eur. Phys. J. C* **77** (2017), article ID 804.

[41] ATLAS Collaboration, "Measurement of the top-quark mass in $t\bar{t} + 1$-jet events collected with the ATLAS detector in pp collisions at $\sqrt{s} = 8$ TeV", *JHEP* **11** (2019), article ID 150.

[42] CMS Collaboration, "Measurement of $t\bar{t}$ normalised multi-differential cross sections in pp collisions at $\sqrt{s} = 13$ TeV, and simultaneous determination of the strong coupling strength, top quark pole mass, and parton distribution functions", *Eur. Phys. J. C* (2019) arXiv:1904.05237 (submitted).

[43] S. F. Ravasio, P. Nason, C. Oleari, "All-orders behaviour and renormalons in top-mass observables", 2019, preprint, https://arxiv.org/abs/1810.10931.

[44] M. Butenschoen *et al.*, "Top quark mass calibration for Monte Carlo event generators", *Phys. Rev. Lett.* **117** (2016), article ID 232001.

[45] A. H. Hoang, S. Mantry, A. Pathak, I. W. Stewart, "Extracting a short distance top mass with light grooming", 2017, preprint, https://arxiv.org/abs/1708.02586.

[46] A. H. Hoang, S. Plätzer, D. Samitz, "On the cutoff dependence of the quark mass parameter in angular ordered parton showers", *JHEP* **10** (2018), article ID 200.

[47] CMS Collaboration, "Running of the top quark mass from proton–proton collisions at $\sqrt{s} = 13$ TeV", *Phys. Lett. B* **803** (2020), article ID 135263.

[48] CMS Collaboration, "Measurement of the ratio $\mathscr{B}(t \to Wb)/\mathscr{B}(t \to Wq)$ in pp collisions at $\sqrt{s} = 8$ TeV", *Phys. Lett. B* **736** (2014), p. 33-57.

[49] ATLAS Collaboration, "Measurement of the top-quark decay width in top-quark pair events in the dilepton channel at $\sqrt{s} = 13$ TeV with the ATLAS detector", ATLAS-CONF-2019-038.

[50] ATLAS Collaboration, "Measurements of top-quark pair spin correlations in the $e$μ channel at $\sqrt{s} = 13$ TeV using $pp$ collisions in the ATLAS detector", *Eur. Phys. J. C* (2019) (submitted), https://arxiv.org/abs/1903.07570.

[51] CMS Collaboration, "Measurement of the top quark polarization and $t\bar{t}$ spin correlations using dilepton final states in proton–proton collisions at $\sqrt{s} = 13$ TeV", *Phys. Rev. D* **100** (2019), no. 7, article ID 072002.

[52] ATLAS Collaboration, "Measurements of top quark spin observables in $t\bar{t}$ events using dilepton final states in $\sqrt{s} = 8$ TeV pp collisions with the ATLAS detector", *JHEP* **1703** (2017), article ID 113.

[53] ATLAS Collaboration, "Inclusive and differential measurement of the charge asymmetry in $t\bar{t}$ events at 13 TeV with the ATLAS detector", ATLAS-CONF-2019-026.

[54] CMS Collaboration, "Measurement of differential cross sections and charge ratios for $t$-channel single top quark production in proton–proton collisions at $\sqrt{s} = 13$ TeV", *Eur. Phys. J. C* **80** (2020), no. 5, article ID 370.

[55] ATLAS and CMS Collaborations, "Combination of inclusive and differential $\mathrm{t\bar{t}}$ charge asymmetry measurements using ATLAS and CMS data at $\sqrt{s} = 7$ and 8 TeV", *JHEP* **04** (2018), article ID 33.

[56] HL-LHC Collaboration and HE-LHC Working Group, "Standard Model Physics at the HL-LHC and HE-LHC", 2019, preprint, https://arxiv.org/abs/1902.04070.

[57] ATLAS Collaboration, "Measurements of charge and CP asymmetries in $b$-hadron decays using top-quark events collected by the ATLAS detector in $pp$ collisions at $\sqrt{s} = 8$ TeV", *JHEP* **1702** (2017), article ID 71.

[58] ATLAS Collaboration, "Measurement of the W boson polarisation in $t\bar{t}$ events from pp collisions at $\sqrt{s} = 8$ TeV in the lepton + jets channel with ATLAS", *Eur. Phys. J. C* **77** (2017), article ID 264, Erratum: *Eur. Phys. J. C* **79** (2019).

[59] CMS Collaboration, "Measurement of the W boson helicity fractions in the decays of top quark pairs to lepton + jets final states produced in pp collisions at $\sqrt{s} = 8$ TeV", *Phys. Lett. B* **762** (2016), p. 512-534.

[60] B. Grzadkowski, M. Iskrzynski, M. Misiak, J. Rosiek, "Dimension-six terms in the standard model Lagrangian", *JHEP* **10** (2010), article ID 85.

[61] ATLAS Collaboration, "Measurement of the $t\bar{t}Z$ and $t\bar{t}W$ cross sections in proton–proton collisions at $\sqrt{s} = 13$ TeV with the ATLAS detector", *Phys. Rev. D* **99** (2019), article ID 072009.

[62] CMS Collaboration, "Measurement of the cross section for top quark pair production in association with a W or Z boson in proton–proton collisions at $\sqrt{s} = 13$ TeV", *JHEP* **08** (2018), article ID 11.
[63] CMS Collaboration, "Measurement of top quark pair production in association with a Z boson in proton–proton collisions at $\sqrt{s} = 13$ TeV", *JHEP* **03** (2020), article ID 56.
[64] CMS Collaboration, "Evidence for the associated production of a single top quark and a photon in proton–proton collisions at $\sqrt{s} = 13$ TeV", *Phys. Rev. Lett.* **121** (2018), article ID 221802.
[65] CMS Collaboration, "Observation of single top quark production in association with a $Z$ boson in proton–proton collisions at $\sqrt{s} = 13$ TeV", *Phys. Rev. Lett.* **122** (2019), article ID 132003.
[66] ATLAS Collaboration, "Observation of the associated production of a top quark and a Z boson in pp collisions at $\sqrt{s} = 13$ TeV with the ATLAS detector", ATLAS-CONF-2019-043.
[67] ATLAS Collaboration, "Measurements of inclusive and differential cross-sections of $t\bar{t}\gamma$ production in the $e\mu$ channel at 13 TeV with the ATLAS detector", ATLAS-CONF-2019-042.
[68] ATLAS Collaboration, "Search for four-top-quark production in the single-lepton and opposite-sign dilepton final states in pp collisions at $\sqrt{s} = 13$ TeV with the ATLAS detector", *Phys. Rev. D* **99** (2019), article ID 052009.
[69] CMS Collaboration, "Search for production of four top quarks in final states with same-sign or multiple leptons in proton–proton collisions at $\sqrt{s} = 13$ TeV", *Eur. Phys. J. C* **80** (2020), no. 2, article ID 75.
[70] CMS Collaboration, "Search for the flavor-changing neutral current interactions of the top quark and the Higgs boson which decays into a pair of b quarks at $\sqrt{s} = 13$ TeV", *JHEP* **06** (2018), article ID 102.
[71] ATLAS Collaboration, "Search for top-quark decays $t \to Hq$ with 36 fb$^{-1}$ of $pp$ collision data at $\sqrt{s} = 13$ TeV with the ATLAS detector", *JHEP* **05** (2019), article ID 123.
[72] ATLAS Collaboration, "Search for flavor-changing neutral currents in top quark decays $t \to Hc$ and $t \to Hu$ in multilepton final states in proton–proton collisions at $\sqrt{s} = 13$ TeV with the ATLAS detector", *Phys. Rev. D* **98** (2018), article ID 032002.
[73] ATLAS Collaboration, "Search for top quark decays $t \to qH$, with $H \to \gamma\gamma$, in $\sqrt{s} = 13$ TeV $pp$ collisions using the ATLAS detector", *JHEP* **10** (2017), article ID 129.
[74] ATLAS Collaboration, "Search for flavour-changing neutral currents in processes with one top quark and a photon using 81 fb$^{-1}$ of $pp$ collisions at $\sqrt{s} = 13$ TeV with the ATLAS experiment", *Phys. Lett. B* **800** (2020), article ID 135082.
[75] ATLAS Collaboration, "Search for flavour-changing neutral current top-quark decays $t \to qZ$ in proton–proton collisions at $\sqrt{s} = 13$ TeV with the ATLAS detector", *JHEP* **07** (2018), article ID 176.
[76] CMS Collaboration, "Search for flavour changing neutral currents in top quark production and decays with three-lepton final state using the data collected at $\sqrt{s} = 13$ TeV", *CMS Physics Analysis Summary*, CMS-PAS-TOP-17-017.
[77] F. Simon, "A first look at the impact of NNNLO theory uncertainties on top mass measurements at the ILC", 2016, preprint, https://arxiv.org/abs/1603.04764.
[78] M. S. Amjad *et al.*, "A precise characterisation of the top quark electro-weak vertices at the ILC", *Eur. Phys. J. C* **75** (2015), article ID 512.
[79] P. Janot, "Top-quark electroweak couplings at the FCC-ee", *JHEP* **04** (2015), article ID 182.

*Comptes Rendus*
*Physique*
**2020**, 21, nº 1, p. 61-74
https://doi.org/10.5802/crphys.11

A perspective of High Energy Physics from precision measurements
*La physique des Hautes Energies du point de vue des mesures de précision*

# *CP* violation in *B* decays

## *Brisure de la symétrie CP dans les désintégrations de mésons beaux*

**Yosef Nir** [a] **and Vincenzo Vagnoni** [*, b]

[a] Weizmann Institute, Department of Particle Physics and Astrophysics, Rehovot 7610001, Israel

[b] Istituto Nazionale di Fisica Nucleare, Sezione di Bologna, Italy.

*E-mails:* yosef.nir@weizmann.ac.il (Y. Nir), vincenzo.vagnoni@bo.infn.it (V. Vagnoni).

**Abstract.** The experimental study of *CP* violation in *B* decays has led to significant progress in our understanding of nature: (i) It demonstrated that the Kobayashi-Maskawa mechanism is the dominant source of *CP* violation in meson decays. (ii) It improved significantly the precision in the determination of the parameters of the Cabibbo–Kobayashi–Maskawa quark-mixing matrix. (iii) It proved that new physics that has order-one flavour-changing couplings to the $b$ quark should be characterised by a mass scale higher than $\mathcal{O}(10^3$ TeV). Further progress is expected from the Belle II and LHC experiments during the next decade and beyond. Present status and perspectives are here discussed.

**Résumé.** L'étude expérimentale de la brisure de la symétrie *CP* dans les désintégrations de mésons beaux ($B$) a apporté des contributions majeures à notre compréhension de la nature : (i) Elle a établi que le mécanisme de Kobayashi-Maskawa est la source dominante de brisure de la symétrie *CP* dans les systèmes des mésons $K$ et $B$. (ii) Elle a amélioré significativement la précision des paramètres qui décrivent la matrice de mélange des quarks Cabibbo–Kobayashi–Maskawa. (iii) Elle a prouvé que l'échelle d'énergie d'une nouvelle physique avec des couplages de changement de saveurs d'ordre unité, devait être supérieure à $\mathcal{O}(10^3$ TeV). Des progrès sont attendus, dans cette décennie et la suivante, des expériences du LHC et Belle II. L'état de l'art de cette Physique et les perspectives des expériences futures sont discutés dans cet article.

**Keywords.** Meson, Decay, LHC, Large Hadron Collider, CP symmetry violation.

**Mots-clés.** Méson, Désintégration, LHC, Grand collisionneur de hadrons, Violation de symétrie CP.

* Corresponding author.

## 1. Introduction

The noninvariance of the laws of nature under the combined action of charge conjugation ($C$) and parity ($P$) transformations, so-called $CP$ violation, is a well established experimental fact since several decades and is well known to be a necessary condition for the dynamical generation of the observed baryon asymmetry of the universe (BAU) [1]. The Standard Model (SM) of particle physics includes $CP$ violation through an irreducible complex phase in the Cabibbo–Kobayashi–Maskawa (CKM) quark-mixing matrix [2, 3]. However, the size of $CP$ violation in the SM appears to be too small to account for the observed BAU [4–6], suggesting the existence of sources of $CP$ violation beyond the SM.

The last two decades have seen enormous experimental progress in the study of $CP$ violation with beauty hadrons, first at the so-called $B$ factories and then at the Large Hadron Collider (LHC). Yet, no experimental findings leading to a major failure of the SM in the flavour sector (nor anywhere else) have emerged so far. In this paper, a brief review of the present experimental status and of future perspectives with $CP$ violation in $B$ decays, also including a historical reminder and a theoretical overview, is made.

## 2. Historical perspective

Flavour physics has played a prominent role in laying the foundations of what is known nowadays as the SM of particle physics. As a case in point, the existence of a third generation of quarks was predicted in a 1973 work by Kobayashi and Maskawa (KM) [3] by extending the Cabibbo [2] and the Glashow–Iliopoulos–Maiani [7] mechanisms. In the KM paper it was conjectured for the first time that the phenomenon of $CP$ violation, first revealed in a crucial experiment in 1964 using decays of neutral kaons [8], could be included into the model of weak interactions if six quarks existed in nature. Although at the time only hadrons made of the three lighter quarks were known, a new state made of a $c\bar{c}$ quark pair was discovered almost simultaneously at Brookhaven [9] and SLAC [10] one year later. The observation of the $b$ quark followed a few years later at FNAL [11], whereas the $t$ quark was observed for the first time, again at FNAL, only in 1995 [12], more than 20 years after the initial prediction. The KM model, formalised in the so-called Cabibbo–Kobayashi–Maskawa (CKM) quark-mixing matrix, became soon one of the main building blocks of the emerging SM theory.

The experimental proof of the validity of the KM mechanism became a question of utmost importance, and it was soon realised that an accurate test required $CP$-violation measurements to be performed with quarks heavier than the $s$ quark. At the beginning of the 1980's the CLEO experiment made first studies with $b$ quarks at CESR [13]. In the same period, the idea that $B^0 \to J/\psi K^0_S$ decays could exhibit large time-dependent $CP$-violating effects was put forward [14, 15]. However, the measurement of $CP$ violation in $B^0 \to J/\psi K^0_S$ decays presented remarkable experimental challenges. First of all, the production rate of $B^0$ mesons that was required to achieve a precise measurement was enormous with respect to what was conceivable at the time. Furthermore, it was not possible to perform a measurement of the $B^0$ decay time with $B^0$ mesons produced at rest at symmetric $e^+e^-$ colliders operating at the centre-of-mass energy of the $\Upsilon(4S)$. A fundamental physics advancement was made in 1987 owing to the ARGUS experiment at DESY, with the first measurement of the $B^0$–$\bar{B}^0$ mixing rate [16], as the relatively large mixing rate that was observed enhanced the feasibility of measuring $CP$ violation with $B^0 \to J/\psi K^0_S$ decays. In the same year, a proposal to realise a high-luminosity asymmetric $e^+e^-$ collider was made [17]: different energies of the colliding beams would have allowed $B^0$ mesons boosted towards the direction of the most energetic beam to be produced, enabling the measurement of the $B^0$ decay time by means of state-of-the-art silicon vertex detectors. The novel idea was then implemented a few years later with the the construction of two similar machines: PEP-II at SLAC and KEKB at KEK. The two machines were able to produce $\mathcal{O}(10^6)$ $b\bar{b}$ pairs per day, to be compared with a few tens at CESR, largely outscoring any previous record of luminosity at $e^+e^-$ colliders. The corresponding detectors, BaBar [18] at PEP-II and Belle [19] at KEKB, by the end of their programmes measured *CP* violation in $B^0 \to J/\psi K^0_S$ decays with a relative precision of about 3% [20,21], performing in addition a plethora of other very relevant measurements [22]. In the same period, relevant progresses were also made with hadronic collisions at the Tevatron, where, as an example, the first observation of $B^0_s$–$\overline{B}^0_s$ mixing was achieved [23]. It is also important to mention that, in the the course of the 1990's, some relevant $b$-physics measurements were made by LEP experiments at CERN [24] and SLD at SLAC [25], exploiting decays of $Z^0$ bosons to $b$-quark pairs.

While the BaBar and Belle detectors were under approval for construction, dedicated $b$-physics experiments at the LHC were also being proposed. The various proposals were eventually merged into a single one: the LHC beauty experiment, LHCb [26]. LHCb was designed as a single-arm forward spectrometer, thought to exploit the large $b\bar{b}$ production cross-section in proton-proton collisions at the LHC. The LHCb experiment was approved in 1998 and started taking data in 2009, performing amongst other things a wide range of high-precision measurements of *CP* violation. Although their detectors were designed for different principal purposes, the ATLAS [27] and CMS [28] experiments have also been making significant contributions to the $b$-quark sector, mainly using final states containing muon pairs.

Meanwhile, even before the LHC was turned on, proposals for constructing upgraded asymmetric $e^+e^-$ colliders capable of achieving two orders of magnitude larger instantaneous luminosity with respect to PEP-II and KEKB were put forward. Eventually, only one of such machines reached the construction phase: SuperKEKB. The associated detector, Belle II [29], started taking first data in 2018, and it is now expected to run for about another decade.

## 3. A *CP* violation primer

On the theoretical side, a Lagrangian is *CP*-violating if, when all freedom to redefine the phases of the fields is used, there remain couplings with irremovable phases. On the experimental side, *CP* violation is established if a pair of *CP*-conjugate processes (i.e., the initial and final particles in one process are the *CP*-conjugate of the initial and final particles in the other, respectively) proceed at different rates. A necessary condition for such a *CP* asymmetry to occur is that the process has contributions from two amplitudes which depend on (combinations of) couplings that carry different phases. When discussing *CP* violation in meson decays, one distinguishes three classes of *CP* asymmetries, depending on the nature of the interfering amplitudes.

***CP* violation in mixing.** Consider the transition amplitude from a neutral $B$ meson to $\overline{B}$ and the transition amplitude for the *CP*-conjugate transition, from $\overline{B}$ to $B$:

$$\langle B|\mathcal{H}|\overline{B}\rangle = M_{B\bar{B}} - \frac{\mathrm{i}}{2}\Gamma_{B\bar{B}}, \quad \langle\overline{B}|\mathcal{H}|B\rangle = M^*_{B\bar{B}} - \frac{\mathrm{i}}{2}\Gamma^*_{B\bar{B}}, \tag{1}$$

where $M$ and $\Gamma$ are associated with transitions via off-shell (dispersive) and on-shell (absorptive) intermediate states. The ratio between the two is given by

$$\left(\frac{q}{p}\right)^2 = \frac{M^*_{B\bar{B}} - \frac{\mathrm{i}}{2}\Gamma^*_{B\bar{B}}}{M_{B\bar{B}} - \frac{\mathrm{i}}{2}\Gamma_{B\bar{B}}}. \tag{2}$$

*CP* violation in mixing is the result of interference between $M_{B\bar{B}}$ and $\Gamma_{B\bar{B}}$, and corresponds to $\mathcal{I}m(\Gamma_{B\bar{B}}/M_{B\bar{B}}) \neq 0$ or, equivalently,

$$|q/p| \neq 1, \tag{3}$$

which implies that the two neutral $B$ mass eigenstates are not $CP$ eigenstates. It is the only possible source of $CP$ asymmetries in wrong-sign semi-leptonic neutral $B$ decays,

$$A_{\rm sl}^{d(s)} \equiv \frac{\Gamma(\overline{B}^0_{(s)}(t)\to \ell^+ X)-\Gamma(B^0_{(s)}(t)\to \ell^- X)}{\Gamma(\overline{B}^0_{(s)}(t)\to \ell^+ X)+\Gamma(B^0_{(s)}(t)\to \ell^- X)} = \frac{1-|q/p|^4}{1+|q/p|^4}. \tag{4}$$

Here $B^0_{(s)}(t)$ ($\overline{B}^0_{(s)}(t)$) is the time-evolved state that was purely $B^0_{(s)}$ ($\overline{B}^0_{(s)}$) at time $t=0$. $CP$ violation in $B^0_{(s)}-\overline{B}^0_{(s)}$ mixing has been experimentally shown to be a small effect, since it has not been observed yet.

***CP* violation in decay.** Consider the decay of a charged or neutral $B$ meson into a final state $f$, and the decay of $\overline{B}$ into the $CP$-conjugate final state $\overline{f}$. The amplitudes for these two processes are defined as

$$A_f = \langle f|\mathscr{H}|B\rangle, \quad \overline{A}_{\overline{f}} = \langle \overline{f}|\mathscr{H}|\overline{B}\rangle. \tag{5}$$

$CP$ violation in decay is the result of interference between two contributions to $A_f$ (such as tree and penguin operators) and it corresponds to

$$|\overline{A}_{\overline{f}}/A_f| \neq 1. \tag{6}$$

It is the only possible source of $CP$ asymmetries in charged $B$ decays,

$$\mathscr{A}_{f^\pm} \equiv \frac{\Gamma(B^-\to f^-)-\Gamma(B^+\to f^+)}{\Gamma(B^-\to f^-)+\Gamma(B^+\to f^+)} = \frac{|\overline{A}_{f^-}/A_{f^+}|^2-1}{|\overline{A}_{f^-}/A_{f^+}|^2+1}. \tag{7}$$

$CP$ violation in decay has been established (at a level higher than $5\sigma$) for $B$ decays into $\pi^+\pi^-$, $K^+\pi^-$, various $DK^+$ states and several three-body final states [30].

***CP* violation in interference of decays with and without mixing.** Consider the direct decay amplitude of a neutral $B$ meson to a final $CP$ eigenstate $f_{CP}$, $A_{f_{CP}}$. An additional contribution to this decay comes from a $B$ to $\overline{B}$ transition followed by $\overline{B}\to f_{CP}$ decay, $M_{B\bar{B}}\overline{A}_{f_{CP}}$. (We neglect here $\Gamma_{B\bar{B}}$ since it is experimentally established that $|\Gamma_{B\bar{B}}| \ll |M_{B\bar{B}}|$.) Define

$$\lambda_{f_{CP}} = \frac{M^*_{B\bar{B}}}{|M_{B\bar{B}}|}\frac{\overline{A}_{f_{CP}}}{A_{f_{CP}}}. \tag{8}$$

$CP$ violation in the interference of decays with and without mixing corresponds to

$$\mathscr{I}m(\lambda_{f_{CP}}) \neq 0. \tag{9}$$

It can be measured in $B^0$ decays into final $CP$ eigenstates,

$$\mathscr{A}_{f_{CP}}(t) \equiv \frac{\Gamma(\overline{B}^0(t)\to f_{CP})-\Gamma(B^0(t)\to f_{CP})}{\Gamma(\overline{B}^0(t)\to f_{CP})+\Gamma(B^0(t)\to f_{CP})} = \mathscr{I}m(\lambda_{f_{CP}})\sin(\Delta m_d t), \tag{10}$$

where $\Delta m_d$ is the mass difference between the masses of the two $B^0$ mass eigenstates. The final equality in (10) corresponds to the case that $CP$ violation in mixing and $CP$ violation in decay are neglected. The case of a $B^0_s$ meson is similar, but the non-negligible width difference between the mass eigenstates must also be taken into account generalising equation (10). $CP$ violation in the interference of decays with and without mixing has been established in neutral $B$ decays into $\psi K_{\rm S,L}$, $D^{(*)}h^0$, $\psi\pi^0$, $D^+D^-$, $D^{*+}D^{*-}$, $\phi K_{\rm S}$, $\eta' K_{\rm S}$, $f_0 K_{\rm S}$, $K^+K^-K_{\rm S}$ and $\pi^+\pi^-$. The average of the results for all charmonium states is subject to the cleanest theoretical interpretation, and it is

$$\mathscr{I}m(\lambda_{c\bar{c}K_{\rm S,L}}) = +0.699 \pm 0.017. \tag{11}$$

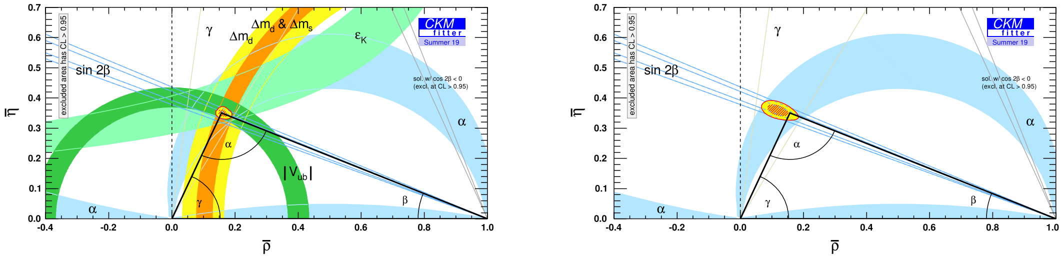


**Figure 1.** The constraints in the $(\bar\rho,\bar\eta)$ plane from (left) all relevant processes, and (right) from *CP*-violating asymmetries in *B* decays only [31].

## 4. The CKM mechanism and *CP* violation in beauty

The three-generation SM violates *CP*. Among the parameters of the SM Lagrangian, there is a single phase (or, equivalently, a single imaginary parameter), which appears in $V$, the CKM matrix that parametrises the $W^+$ interactions with $\overline{u}_{Li} d_{Lj}$ pairs (where $u_{1,2,3} = u, c, t$, and $d_{1,2,3} = d, s, b$)

$$\mathscr{L}_{W,q} = -\frac{g}{\sqrt{2}} \overline{u}_{Li} V_{ij} \not{W}^+ d_{Lj} + \text{h.c.} \tag{12}$$

The CKM matrix depends on three real and one imaginary parameters. The Wolfenstein parametrisation is particularly useful

$$V = \begin{pmatrix} 1-\frac{1}{2}\lambda^2 & \lambda & A\lambda^3(\rho - \mathrm{i}\eta) \\ -\lambda & 1-\frac{1}{2}\lambda^2 & A\lambda^2 \\ A\lambda^3(1-\rho-\mathrm{i}\eta) & -A\lambda^2 & 1 \end{pmatrix}. \tag{13}$$

The fact that all quark flavour-violating processes and all *CP*-violating processes depend on only three real $(\lambda, A, \rho)$ and one imaginary $(\mathrm{i}\eta)$ parameters makes the (C)KM mechanism of flavour and *CP* violation subject to stringent tests. Here, *CP*-violating processes play a special role. The fact that *CP* is a good symmetry of the strong interactions implies that *CP* asymmetries dominated by interference of decays with and without mixing are subject to a uniquely clean theoretical interpretation. Thus, for example, within the SM

$$\mathscr{I}m(\lambda_{\psi K_S}) = \frac{2\eta(1-\rho)}{\eta^2 + (1-\rho)^2}, \tag{14}$$

with hadronic uncertainties entering only at the level of a few permil corrections.

In the literature, one often defines $\bar\rho + \mathrm{i}\bar\eta = -(V_{ud}V_{ub}^*)/(V_{cd}V_{cb})$ which is valid to all orders in $\lambda$. The parameters $\rho$ and $\eta$ approximate $\bar\rho$ and $\bar\eta$ to order $\lambda^2$. The various constraints in the $(\bar\rho, \bar\eta)$ plane are presented in Figure 1. *CP* asymmetries in *B* decays are playing a major role: $\mathscr{A}_{\psi K_S}$, $\mathscr{A}_{\pi\pi}$ and the *CP* asymmetry in $B \to DK$ decays constrain with impressive accuracy the angles

$$\alpha \equiv \arg\left(-\frac{V_{td}V_{tb}^*}{V_{ud}V_{ub}^*}\right), \quad \beta \equiv \arg\left(-\frac{V_{cd}V_{cb}^*}{V_{td}V_{tb}^*}\right), \quad \gamma \equiv \arg\left(-\frac{V_{ud}V_{ub}^*}{V_{cd}V_{cb}^*}\right), \tag{15}$$

respectively. As there is a region in the $(\bar\rho, \bar\eta)$ plane that is consistent with all measurements, the CKM mechanism of flavour violation and the KM mechanism of *CP* violation provide a consistent explanation of all data.

## 5. Probing new physics with *CP* violation in *B* decays

The consistency of the measured *CP* violation in *B* decays with the SM predictions leads to strong constraints on new physics. In the previous section, we assumed that the various flavour-violating and *CP*-violating observables are accounted for by the CKM matrix, and tested the

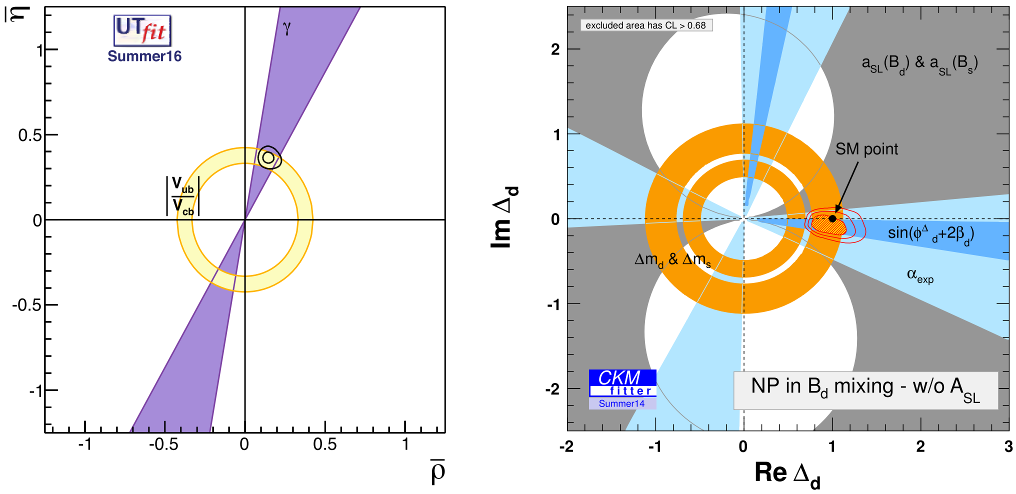


**Figure 2.** The constraints (left) in the $(\bar{\rho},\bar{\eta})$ plane and (right) in the $(\mathscr{R}e(\Delta_d),\mathscr{I}m(\Delta_d))$ plane from processes involving tree-level decays and $B^0-\overline{B}^0$ mixing only [31, 32].

self-consistency of this assumption. To constrain new physics, we here relax this assumption. While we still assume that new physics contributions can be neglected in tree-level flavour-changing processes, we allow new physics contributions to flavour-changing neutral-current processes (FCNC) to be of arbitrary size and phase. This will allow us to ask how much room there is for new physics in these processes.

The most relevant process for our purposes is $B^0-\overline{B}^0$ mixing, and the most general new physics contribution to this process can be represented by a single dimensionless complex parameter $\Delta_d$

$$M_{B\bar{B}} = M_{B\bar{B}}^{\rm SM}\Delta_d. \tag{16}$$

The constraints on $z_{bs}/\Lambda^2$ are somewhat weaker. Using only processes that involve no FCNC processes except, possibly, $B^0-\overline{B}^0$ mixing, one can constrain the four parameters $[\bar{\rho},\bar{\eta},\mathscr{R}e(\Delta_d),\mathscr{I}m(\Delta_d)]$, as shown in Figure 2. A similar analysis can be carried out for $B_s^0-\overline{B}_s^0$ mixing.

Thus new physics can contribute no more than $\mathscr{O}(20\%)$ ($\mathscr{O}(10\%)$) of $M_{B\bar{B}}$ if its phase is [mis]aligned with the SM phase. These bounds can be translated into constraints on new physics parameters and, in particular, on new *CP*-violating sources. It can be done for specific models or, assuming that the new degrees of freedom are much heavier than the electroweak-breaking scale, for higher-dimension terms in the SM effective field theory. Take, for example, the dimension-six term

$$\mathscr{L}_{\Delta B=2} = \frac{z_{bd}}{\Lambda^2}(\overline{Q}_{Lb}\gamma_\mu Q_{Ld})(\overline{Q}_{Lb}\gamma^\mu Q_{Ld}), \tag{17}$$

where $Q_{Lq}$ stands for the quark doublet that contains the $q$ quark. Then, for $z_{bd}$ aligned with the SM phase and of $\mathscr{O}(1)$, the lower bound on the scale of new physics is ~660 TeV. If, on the other hand, the relative phase with the SM amplitude is large, the lower bound is raised to close to $10^3$ TeV. Conversely, if the scale of new physics is of order TeV, then $\mathscr{R}e(z_{bd})\lesssim 2.2\times10^{-6}$ and $\mathscr{I}m(z_{bd})\lesssim 1.2\times10^{-6}$. The constraints on $z_{bs}/\Lambda^2$ are somewhat weaker.

The conclusion is that, if there is new physics that has tree-level $\bar{b}d$ coupling of $\mathscr{O}(1)$, then its scale must be at least four orders of magnitude above the weak scale, well above the reach

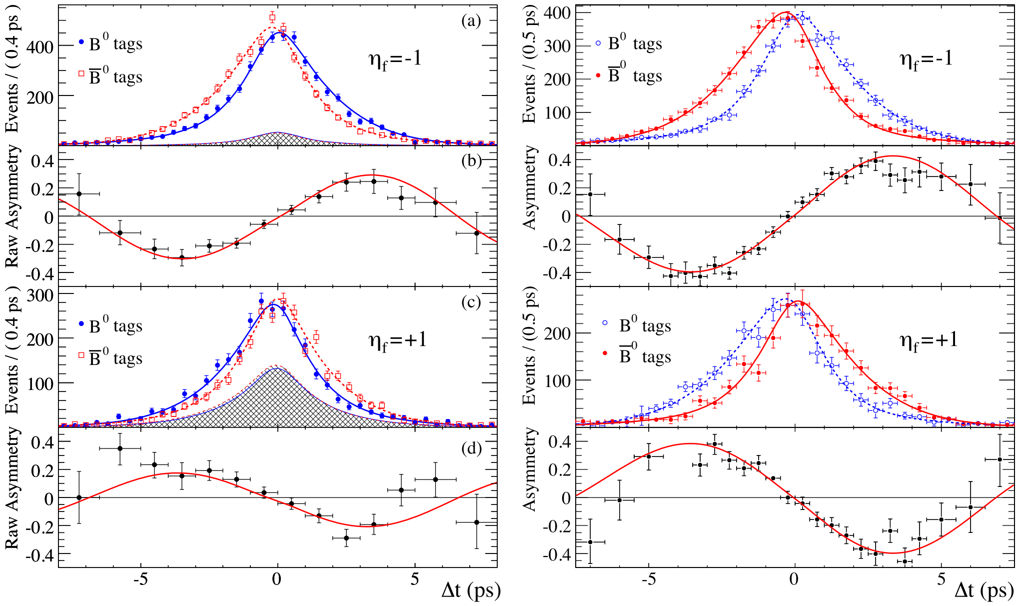


**Figure 3.** Flavour-tagged $\Delta t$ distributions (a, c) and raw $CP$ asymmetries (b, d) for the BaBar (left) and Belle (right) measurements of $\sin 2\beta$. The two plots at the top show the $B \to c\bar{c}K_S^0$ samples whereas those at the bottom the $B \to J/\psi K_L^0$ sample. The shaded regions for BaBar represent the fitted background, while the Belle distributions are background-subtracted. The plot is taken from Ref. [22].

of direct searches. If, on the other hand, there is new physics at the TeV scale, then its flavour-changing $\bar{b}d$ coupling must be smaller than $10^{-6}$, well below a loop suppression. We learn that $CP$ violation in $B$ decays is a powerful probe of physics at very high scales.

## 6. The legacy of $B$ factories

The measurement of time-dependent $CP$-violation in $B^0 \to J/\psi K_S^0$ decays was the main motivation for the construction of the $B$ factories. This is the so-called *golden mode*, belonging to a larger class of decays mediated by $b \to c\bar{c}s$ quark-level transitions, along with other relevant decays, such as $B^0 \to J/\psi K_L^0$. These decay modes have very clean experimental signatures and relatively large branching fractions. They also provide a clean determination of the angle $\beta$, as the pollution due to subleading contributions from penguin operators is expected to be at the few permil level.

The two $B$ factories have performed their legacy measurements using their entire data samples, with about $465 \times 10^6$ [20] and $772 \times 10^6$ [21] $B\overline{B}$ pairs. The average of the results from the two experiments gives

$$\sin 2\beta = 0.677 \pm 0.020, \tag{18}$$

corresponding to a 3% precision (which is further improved when considering also LHCb results, as in the world average of (11)). The time-dependent rates and the corresponding $CP$-violating asymmetries are shown in Figure 3.

But the $B$ factories were able to go well beyond the measurement of $\sin 2\beta$. In order to check the self-consistency of the KM mechanism of $CP$ violation, the measurement of the other two angles $\alpha$ and $\gamma$ was also of paramount importance. The angle $\alpha$ can be determined by measuring time-dependent *CP* asymmetries in charmless $b \to u\bar{u}d$ transitions. The interference between the tree amplitude and the $B^0$–$\overline{B}^0$ mixing amplitude provides sensitivity to $\alpha$. If the tree amplitude were the only one contributing, as in the case of the $B^0 \to J/\psi K^0_{\mathrm{S}}$ decay, the measurement of $\alpha$ using the $B \to \pi^+\pi^-$ decay would have been completely analogous to that of $\beta$. However, contributions from penguin operators to charmless $B$ decays cannot be neglected. The presence of such contributions is certainly a nuisance for the determination of $\alpha$, but it also means that new physics might affect the result due to new virtual particles circulating in the loops. As such, the comparison of high-precision measurements of $\alpha$ made with different decays can be exploited to search for possible new physics effects. To overcome the problem of the presence of sizeable penguin amplitudes, techniques which make use of the isospin symmetry of strong interactions have been adopted. One approach is to combine measurements of isospin-related decay modes, as $B^0 \to \pi^+\pi^-$, $B^+ \to \pi^+\pi^0$ and $B^0 \to \pi^0\pi^0$. Analogously, although the analysis is more complicated due to the presence of vector particles in the final states, $B^0 \to \rho^+\rho^-$, $B^+ \to \rho^+\rho^0$ and $B^0 \to \rho^0\rho^0$ decays can be used. Another approach is to perform a time-dependent Dalitz analysis of $B^0 \to \pi^+\pi^-\pi^0$ decays, using information from the interference between resonances in the corners of the Dalitz plot, also making use of isospin symmetry. All of these methods were pursued at the $B$ factories, and averaging all results the angle $\alpha$ was measured to be [22]

$$\alpha = (88 \pm 5)^\circ. \tag{19}$$

While $\alpha$ and $\beta$ were determined with precisions at the few percent level, a precise determination of $\gamma$ turned out to be more difficult, due to the small branching fractions of the relevant decay processes. The most important route to measure $\gamma$ relies on the interference between $b \to u\bar{c}s$ and $b \to c\bar{u}s$ quark-level amplitudes using $B \to D^{(*)}K^{(*)}$ decays. The interference is achieved by choosing common final states for $D$ and $\overline{D}$ mesons. As there are no penguin contributions for these decays, all hadronic unknowns are obtainable from data and the interpretation of the measurements in terms of $\gamma$ turns out to be extremely clean. Different methods have been adopted in $B$-factory analyses: the GLW method [33, 34], based on Cabibbo-suppressed $D^0$ decays to *CP* eigenstates, such as $K^+K^-$ or $K^0_{\mathrm{S}}\pi^0$; the ADS method [35, 36], where the $D^0$ meson decays to $K^-\pi^+$ (Cabibbo-favoured) or $K^+\pi^-$ (doubly Cabibbo-suppressed) final states; and the GGSZ method [37], which is based on a Dalitz-plot analysis of multibody $D$ decays, such as $D^0 \to K^0_{\mathrm{S}}\pi^+\pi^-$. By combining all available BaBar and Belle measurements, the resulting 1-CL curves for the angle $\gamma$ are shown in Figure 4. The overall average from the $B$ factories is [22]

$$\gamma = (67 \pm 11)^\circ. \tag{20}$$

As no evidence for inconsistencies in the CKM picture of *CP* violation have emerged from the analyses of the two $B$ factories, their most important legacy is the confirmation that the CKM matrix provides a leading-order description of *CP* violation in the quark sector. For this reason, the focus is now on the search for possible second-order *CP*-violating effects beyond the SM.

## 7. *CP* violation in beauty at the LHC

The great success of the $B$ factories marked the start of a new era in flavour physics. Experiments of the subsequent generation, owing to the huge $b\bar{b}$ production rate made available by the LHC, made it possible to perform measurements with unprecedented precisions, looking with renovated impetus for new sources of *CP* violation beyond the single phase of the CKM matrix.

Besides a $b\bar{b}$ cross-section much larger than that at the $B$ factories, one further big advantage of the LHC is the possibility to study decays of all $b$-hadron species, not limiting the search for new physics to $B^0$- and $B^+$-meson decays. For example, the large production cross-section of $B^0_s$ mesons and the ultimate capabilities of LHC detectors to resolve $B^0_s$ oscillations have

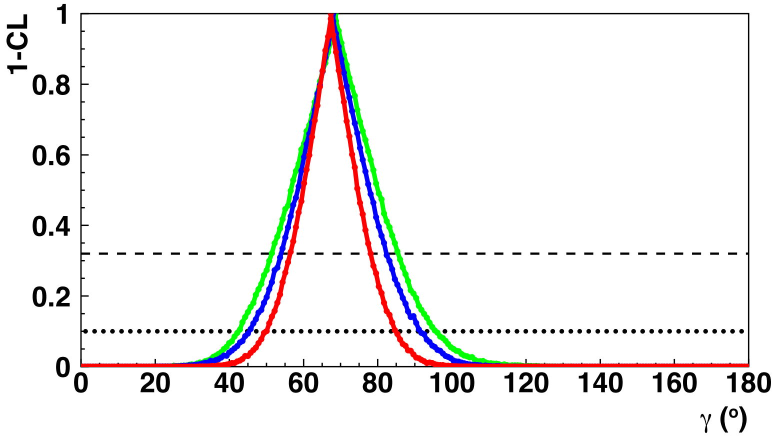


**Figure 4.** Combined constraint (red curve) on $\gamma$ obtained using relevant BaBar and Belle data from $B \to D^{(*)}K^{(*)}$ decays. The green (blue) curve represents the results using only the BaBar (Belle) data. The dashed (dotted) line indicates the lower limit of 68% (90%) confidence-level. The plot is taken from Ref. [22].

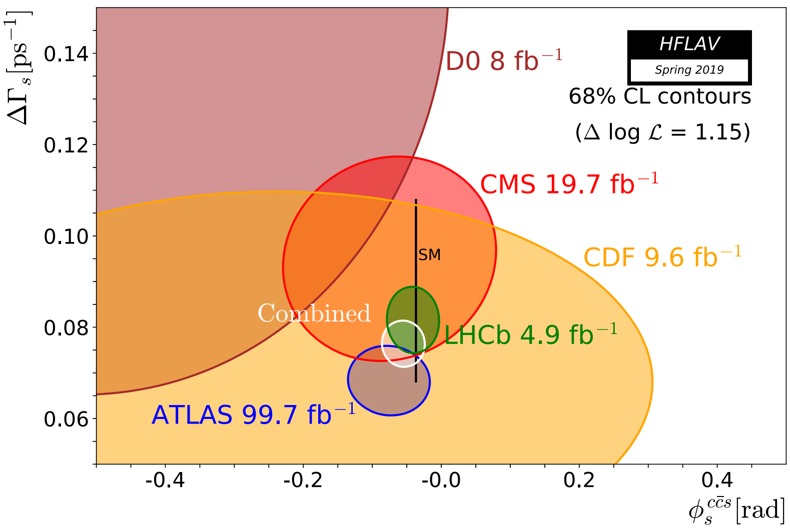


**Figure 5.** Experimental status for $\Delta\Gamma_s$ and $\phi_s^{c\bar{c}s}$ [42].

enabled precision measurements of the *CP*-violating phase $\phi_s^{c\bar{c}s}$, which in the SM is equal to $-2\beta_s \equiv \arg(-V_{ts}V_{tb}^*/V_{cs}V_{cb}^*)$ neglecting subleading penguin contributions, to be performed. The ATLAS, CMS and LHCb experiments measured $\phi_s^{c\bar{c}s}$, mainly using the decays $B_s^0 \to J/\psi K^+K^-$ [38–40] and $B_s^0 \to J/\psi\pi^+\pi^-$ [41]. Combining all available determinations, LHCb measured $\phi_s^{c\bar{c}s} = -0.041 \pm 0.025$ rad. By averaging ATLAS, CMS and LHCb results, the precision is further increased, obtaining

$$\phi_s^{c\bar{c}s} = -0.055 \pm 0.021 \text{ rad}. \tag{21}$$

The present experimental status, which is well compatible with the SM, is summarised in Figure 5.

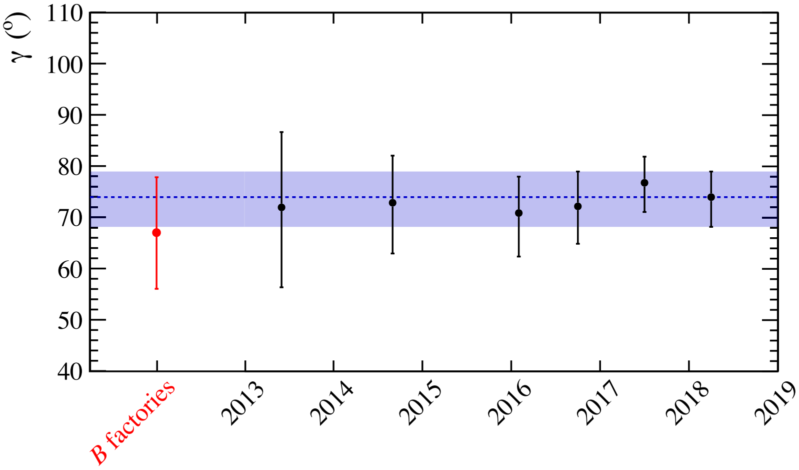


**Figure 6.** Central value and $1\sigma$ uncertainty of the LHCb $\gamma$ combination (black points with error bars) as a function of time. The blue line (band) shows the central value (68.3% CL). LHCb data points are taken from Ref. [43]. The legacy of $B$ factories is also reported for comparison (red point with error bar).

Concerning the measurement of the angle $\gamma$ from tree-level decays, the LHCb experiment largely outperforms the $B$ factories, owing to a much larger data sample of $B \to DK$ decays. The LHCb average is achieved by combining several independent measurements, namely from the time-integrated analyses of $B^+ \to DK^+$, $B^+ \to D^*K^+$, $B^+ \to DK^{*+}$, $B^0 \to DK^{*0}$, $B^0 \to DK^+\pi^-$ and $B^+ \to DK^+\pi^+\pi^-$ decays, and from time-dependent analyses of $B_s^0 \to D_s^{\mp}K^{\pm}$ and $B^0 \to D^{\mp}\pi^{\pm}$ decays [43]. The LHCb result is

$$\gamma = (74.0^{+5.0}_{-5.8})^{\circ}. \tag{22}$$

It is worth noting that this result is already twice more precise than the average from the $B$ factories, although obtained only with Run-1 and part of Run-2 data. Hence LHCb has still a vast growth potential to improve our knowledge of $\gamma$ in the upcoming Run 3 and subsequent LHC runs. The history of the $\gamma$ sensitivity from LHCb is shown in Figure 6.

An alternative route to $\gamma$ beyond tree-level decays has been investigated by LHCb. The amplitudes of the charmless decays $B \to hh$ with $h = \pi, K$ receive large contributions from penguin operators and are sensitive to $\gamma$. LHCb measured for the first time $CP$-violation in the $B_s^0 \to K^+K^-$ decay [44], updated later with more statistics in Ref. [45]. Following Refs. [46–48] and assuming U-spin symmetry, a combination of this and other results from $B \to \pi\pi$ modes allows the determination of $\gamma = (63.5^{+7.2}_{-6.7})^{\circ}$ [49]. The dependence on the amount of U-spin breaking is taken into account, allowing for a maximum of 50% breaking of the symmetry, and included in the overall uncertainty.

Large $CP$-violating asymmetries have been observed by LHCb also in other charmless $B$ decays, namely $B^+ \to h^+h^-h^+$ [50–53]. Particularly striking features of these decays are the very large asymmetries observed in small regions of the phase-space, which could be a sign of long-distance rescattering effects. Furthermore, LHCb performed a first amplitude analysis of the $B_s^0 \to K_S^0 K^+\pi^-$ decay, opening the avenue to a new class of amplitude analyses with three-body charmless $B_s^0$ decays [54].

The same-sign dimuon asymmetry measured some years ago by the D0 collaboration [55] and interpreted as a combination of the semileptonic asymmetries $A_{\rm sl}^d$ and $A_{\rm sl}^s$ in $B^0$ and $B_s^0$ decays, respectively, differs from the SM expectation by about $3\sigma$. LHCb has invested significant efforts to

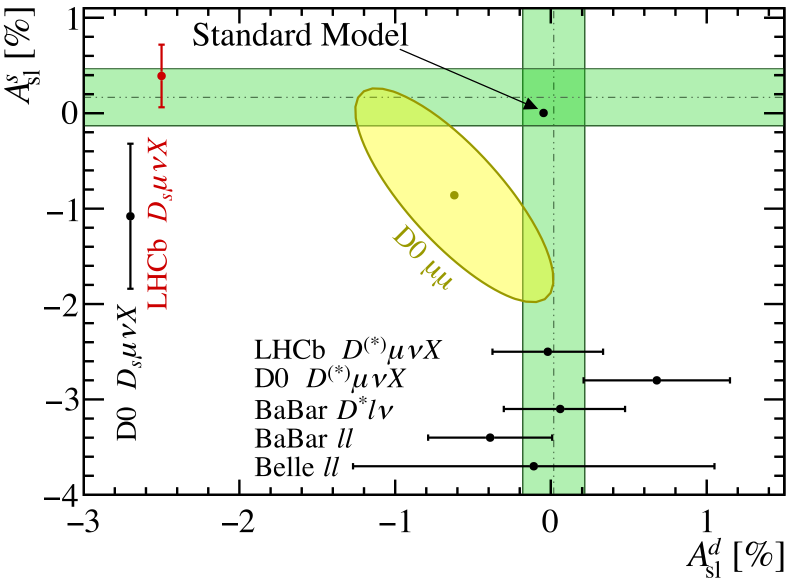


**Figure 7.** Experimental status on $A_{\rm sl}^d$ and $A_{\rm sl}^s$ from various experiments. The plot is taken from Ref. [57].

understand whether the hint of such a discrepancy was real, but has not been able to confirm the result so far. The measurements from LHCb look for *CP* asymmetries in partially reconstructed $B \to D\mu\nu$ decays, where the flavour of the $D$ meson identifies that of the $B$. The measured values are [56, 57]

$$A_{\rm sl}^s = [0.39 \pm 0.26\ (\text{stat.}) \pm 0.20\ (\text{syst.})]\%, \tag{23}$$

$$A_{\rm sl}^d = [-0.02 \pm 0.19\ (\text{stat.}) \pm 0.30\ (\text{syst.})]\%, \tag{24}$$

which are both consistent with the SM expectations. The world averages including measurements from the $B$ factories and D0 are shown in Figure 7. The overall results are marginally compatible with the measurement of the dimuon asymmetry by D0.

## 8. Future perspectives

Physics measurements of *CP* violation performed at the $B$ factories and then, to date, at the LHC have by far exceeded any initial expectation. Yet, in the next 10–15 years we expect huge improvements in statistical sensitivities of all key physics channels, which will bring tests of the (C)KM mechanism of flavour and *CP* violation to a new regime of precision.

In the forthcoming future, the upgraded LHCb and the new Belle II detectors are expected to outperform their previous incarnations. In particular, LHCb Upgrade I will start taking data with the LHCb Run 3 in 2021, whereas Belle II has just started its physics run at SuperKEKB, notably the first major collider to be built since the LHC. Both experiments will operate over the next decade with the LHCb Upgrade I planning to collect 50 fb$^{-1}$ of data in proton-proton collisions at 13–14 TeV, and Belle II 50 ab$^{-1}$ in $e^+e^-$ collisions at the $\Upsilon(4S/5S)$. The two facilities are highly complementary, with LHCb exploiting the availabilty of larger statistics in charged-track decay modes of all $b$-hadron species, and Belle II having unique capabilities to reconstruct $B^0$, $B^+$ and, with lower statistics, $B_s^0$ decays with neutral or missing particles in the final states. Phase-2 upgrades of ATLAS and CMS will follow in the LHC Run 4, with the main intention of fully exploiting the HL-LHC luminosity for high $p_{\mathrm{T}}$ physics. The ATLAS and CMS experiments will also continue to contribute to flavour physics, with particular emphasis on $b$-physics decays to final states containing muons.

In the longer term, a further upgrade of the LHCb experiment to reach an instantaneous luminosity up to $2 \times 10^{34}$ cm$^{-2}\cdot$s$^{-1}$ and collect more than 300 fb$^{-1}$ of data, to be compared with about 9 fb$^{-1}$ available today, is being planned to exploit the full potential of the HL-LHC in flavour physics [58–60]. The LHCb Upgrade II, along with the enhanced $B$-physics capabilities of the Phase-2 upgrades of ATLAS and CMS, will enable a host of measurements to be performed with unprecedented precision complementing and extending the reach of LHCb Upgrade I and Belle II. As an example, in the domain of *CP* violation the knowledge of the angle $\gamma$ will be improved by an order of magnitude at least, reaching the subdegree precision. Furthermore, the precision measurement of the $B_s^0$ weak mixing phase will be another key part of the programme, with an expected precision on $\phi_s^{c\bar{c}s}$ at the end of the HL-LHC period going below 3 mrad, again an order of magnitude better than today.

More recently, the idea that a Belle III project should be considered has also been put forward. The evident complementarity of the flavour-physics programmes at hadronic and $e^+e^-$ colliders makes such a possibility very appealing, extending, along with the LHCb Upgrade II, the horizon of flavour-physics and *CP* violation towards 2035 and beyond, also providing a bridge towards future larger-scale accelerators as FCC-*ee* and FCC-*hh*.

## 9. Conclusions

The study of *CP* violation in $B$ decays is one of the key subjects of modern research at the intensity frontier. Amongst the various motivations, it is worth mentioning the fact that the Kobayashi-Maskawa mechanism of *CP* violation embedded into the Standard Model appears to fail largely in accounting for the observed baryon asymmetry of the universe. For this reason, new sources of *CP* violation, beyond the Standard Model, must exist in nature. In the context of meson mixing and decays, *CP* is a good symmetry of the strong interactions. Therefore, *CP* asymmetries in meson decays are subject to uniquely clean theoretical interpretation.

The two $B$-factory experiments, BaBar and Belle, and then the LHC experiments, with LHCb as a front-runner, have measured a large number of *CP* asymmetries in $B$-meson decays. Although no striking evidence for deviations from Standard Model expectations have emerged so far, the experimental effort allowed some relevant conclusions to be drawn. The three *CP*-violating angles $\alpha$, $\beta$ and $\gamma$, along with other relevant *CP*-conserving observables, have been measured with great accuracy, and this allowed the Cabibbo–Kobayashi–Maskawa mechanism to be proved as the dominant source of flavour and *CP* violation in meson mixing and decay. New flavour- and *CP*-violating physics must either take place at a scale higher than about $10^3$ TeV or, if its scale is significantly lower, have a very strongly suppressed couplings to quarks.

The programme of precision measurements of *CP* violation in $B$ decays will continue to test the Standard Model and search for new physics in the Belle II/III and LHC experiments during the next decade and beyond, waiting for future colliders like FCC-*ee* and FCC-*hh* to grab the flavour-physics torch. Such a programme has the potential to provide crucial clues about the scale of new physics. In the event that no direct evidence for new physics will pop out of the LHC, such measurements can play a leading role in indicating the way for future research developments. Otherwise, they will be a fundamental ingredient to understand the structure of the beyond-the-Standard-Model Lagrangian.

In the current phase of our challenge to understand fundamental physics, it is necessary more than ever to have a programme as diversified as possible. The line of research discussed in this review must be pursued to the uttermost of our capacity, until cracks in the Standard Model will become eventually manifest.

## References


[1] A. D. Sakharov, "Violation of *CP* invariance, *C* asymmetry, and baryon asymmetry of the universe", *Pisma Zh. Eksp. Teor. Fiz.* **5** (1967), p. 32-35.

[2] N. Cabibbo, "Unitary symmetry and leptonic decays", *Phys. Rev. Lett.* **10** (1963), no. 12, p. 531-533.

[3] M. Kobayashi, T. Maskawa, "CP violation in the renormalizable theory of weak interaction", *Prog. Theor. Phys.* **49** (1973), p. 652-657.

[4] A. G. Cohen, D. B. Kaplan, A. E. Nelson, "Progress in electroweak baryogenesis", *Ann. Rev. Nucl. Part. Sci.* **43** (1993), p. 27-70.

[5] A. Riotto, M. Trodden, "Recent progress in baryogenesis", *Ann. Rev. Nucl. Part. Sci.* **49** (1999), p. 35-75.

[6] W.-S. Hou, "Source of *CP* violation for the baryon asymmetry of the universe", *Chin. J. Phys.* **47** (2009), p. 134-141.

[7] S. L. Glashow, J. Iliopoulos, L. Maiani, "Weak interactions with lepton-hadron symmetry", *Phys. Rev. D* **2** (1970), no. 7, p. 1285-1292.

[8] J. H. Christenson, J. W. Cronin, V. L. Fitch, R. Turlay, "Evidence for the $2\pi$ decay of the $K_2^0$ meson", *Phys. Rev. Lett.* **13** (1964), no. 4, p. 138-140.

[9] J. J. Aubert *et al.*, "Experimental observation of a heavy particle J", *Phys. Rev. Lett.* **33** (1974), no. 23, p. 1404-1406.

[10] J. E. Augustin *et al.*, "Discovery of a narrow resonance in $e^+e^-$ annihilation", *Phys. Rev. Lett.* **33** (1974), no. 23, p. 1406-1408.

[11] S. W. Herb *et al.*, "Observation of a dimuon resonance at 9.5-GeV in 400-GeV proton–nucleus collisions", *Phys. Rev. Lett.* **39** (1977), no. 5, p. 252-255.

[12] CDF collaboration, F. Abe *et al.*, "Observation of top quark production in $\bar{p}p$ collisions", *Phys. Rev. Lett.* **74** (1995), no. 14, p. 2626-2631.

[13] CLEO collaboration, D. Andrews *et al.*, "The CLEO detector", *Nucl. Instrum. Meth.* **211** (1983), no. 1, p. 47-71.

[14] A. B. Carter, A. I. Sanda, "*CP* violation in *B* meson decays", *Phys. Rev. D* **23** (1981), no. 7, p. 1567-1579.

[15] I. I. Y. Bigi, A. I. Sanda, "On $B^0$–$\overline{B}^0$ mixing and violations of *CP* symmetry", *Phys. Rev. D* **29** (1984), no. 7, p. 1393-1398.

[16] ARGUS collaboration, H. Albrecht *et al.*, "ARGUS: A universal detector at DORIS-II", *Nucl. Instrum. Meth. A* **275** (1989), no. 1, p. 1-48.

[17] P. Oddone, "Detector considerations", *eConf* **C870126** (1987), p. 423-446.

[18] BaBar collaboration, B. Aubert *et al.*, "The BaBar detector", *Nucl. Instrum. Meth. A* **479** (2002), no. 1, p. 1-116.

[19] A. Abashian *et al.*, "The Belle detector", *Nucl. Instrum. Meth. A* **479** (2002), no. 1, p. 117-232.

[20] BaBar collaboration, B. Aubert *et al.*, "Measurement of time-dependent *CP* asymmetry in $B^0 \to c\bar{c}K^{(*)0}$ decays", *Phys. Rev. D* **79** (2009), article ID 072009.

[21] I. Adachi *et al.*, "Precise measurement of the *CP* violation parameter $\sin 2\phi_1$ in $B^0 \to (c\bar{c})K^0$ decays", *Phys. Rev. Lett.* **108** (2012), article ID 171802.

[22] BaBar and Belle Collaborations, A. J. Bevan *et al.*, "The Physics of the *B* Factories", *Eur. Phys. J. X* **74** (2014), article ID 3026.

[23] CDF collaboration, A. Abulencia *et al.*, "Observation of $B_s^0$–$\overline{B}_s^0$ oscillations", *Phys. Rev. Lett.* **97** (2006), article ID 242003.

[24] G. J. Barker, " *b*-physics at LEP", p. 1-21, Springer Berlin Heidelberg, 2010.

[25] P. C. Rowson, D. Su, S. Willocq, "Highlights of the SLD physics program at the SLAC linear collider", *Ann. Rev. Nucl. Part. Sci.* **51** (2001), p. 345-412.

[26] LHCb collaboration, A. A. Alves Jr. *et al.*, "The LHCb detector at the LHC", *JINST* **3** (2008), article ID S08005.

[27] ATLAS collaboration, G. Aad *et al.*, "The ATLAS experiment at the CERN Large Hadron Collider", *JINST* **3** (2008), article ID S08003.

[28] CMS collaboration, S. Chatrchyan *et al.*, "The CMS experiment at the CERN LHC", *JINST* **3** (2008), article ID S08004.

[29] T. Abe *et al.*, "Belle II Collaboration, Belle II Technical Design Report", KEK Report 2010-1, 2010.

[30] Particle Data Group, M. Tanabashi *et al.*, "Review of particle physics", *Phys. Rev. D* **98** (2018), article ID 030001.

[31] CKMfitter Group, J. Charles *et al.*, " *CP* violation and the CKM matrix: Assessing the impact of the asymmetric *B* factories", *Eur. Phys. J. C* **41** (2005), p. 1-131, updated results and plots available at http://ckmfitter.in2p3.fr.

[32] UTfit Collaboration, M. Bona *et al.*, "Model-independent constraints on $\Delta F = 2$ operators and the scale of new physics", *J. High Energy Phys.* **0803** (2008), article ID 049, updated results and plots available at http://www.utfit.org.

[33] M. Gronau, D. Wyler, "On determining a weak phase from *CP* asymmetries in charged *B* decays", *Phys. Lett. B* **265** (1991), no. 1, p. 172-176.

[34] M. Gronau, D. London, "How to determine all the angles of the unitarity triangle from $B^0 \to DK_S^0$ and $B_s^0 \to D\phi$ ", *Phys. Lett. B* **253** (1991), no. 3-4, p. 483-488.

[35] D. Atwood, I. Dunietz, A. Soni, "Enhanced *CP* violation with $B \to KD^0$ ($\overline{D}^0$) modes and extraction of the CKM angle $\gamma$", *Phys. Rev. Lett.* **78** (1997), no. 17, p. 3257-3260.

[36] D. Atwood, I. Dunietz, A. Soni, "Improved methods for observing *CP* violation in $B^\pm \to KD$ and measuring the CKM phase $\gamma$", *Phys. Rev. D* **63** (2001), article ID 036005.

[37] A. Giri, Y. Grossman, A. Soffer, J. Zupan, "Determining $\gamma$ using $B^\pm \to DK^\pm$ with multibody $D$ decays", *Phys. Rev. D* **68** (2003), article ID 054018.

[38] ATLAS Collaboration, Measurement of the *CP* violation phase $\phi_s$ in $B_s \to J/\psi\phi$ decays in ATLAS at 13 TeV, ATLAS-CONF-2019-009.

[39] CMS Collaboration, V. Khachatryan *et al.*, "Measurement of the *CP*-violating weak phase $\phi_s$ and the decay width difference $\Delta\Gamma_s$ using the $B_s^0 \to J/\psi\phi(1020)$ decay channel in *pp* collisions at $\sqrt{s} = 8$ TeV", *Phys. Lett. B* **757** (2016), p. 97-120.

[40] LHCb Collaboration, R. Aaij *et al.*, "Updated measurement of time-dependent *CP*-violating observables in $B_s^0 \to J/\psi K^+K^-$ decays", *Eur. Phys. J. C* **79** (2019), article ID 706.

[41] LHCb Collaboration, R. Aaij *et al.*, "Measurement of the *CP*-violating phase $\phi_s$ from $B_s^0 \to J/\psi\pi^+\pi^-$ decays in 13 TeV *pp* collisions", *Phys. Lett. B* **797** (2019), article ID 134789.

[42] HFLAV Collaboration, Y. S. Amhis *et al.*, "Averages of *b*-hadron, *c*-hadron, and $\tau$-lepton properties as of 2018", 2019, preprint, updated results and plots available at https://hflav.web.cern.ch, https://arxiv.org/abs/1909.12524.

[43] LHCb Collaboration, Update of the LHCb combination of the CKM angle $\gamma$, LHCb-CONF-2018-002.

[44] LHCb Collaboration, R. Aaij *et al.*, "First measurement of time-dependent *CP* violation in $B_s^0 \to K^+K^-$ decays", *J. High Energy Phys.* **2013** (2013), article ID 183.

[45] LHCb Collaboration, R. Aaij *et al.*, "Measurement of *CP* asymmetries in two-body $B^0_{(s)}$-meson decays to charged pions and kaons", *Phys. Rev. D* **98** (2018), article ID 032004.

[46] R. Fleischer, "New strategies to extract $\beta$ and $\gamma$ from $B_d \to \pi^+\pi^-$ and $B_s \to K^+K^-$", *Phys. Lett. B* **459** (1999), p. 306-320.

[47] R. Fleischer, "$B^0_{s,d} \to \pi\pi, \pi K, KK$: Status and Prospects", *Eur. Phys. J. C* **52** (2007), p. 267-281.

[48] M. Ciuchini, E. Franco, S. Mishima, L. Silvestrini, "Testing the Standard Model and Searching for New Physics with $B_d \to \pi\pi$ and $B_s \to KK$ Decays", *J. High Energy Phys.* **1210** (2012), article ID 29.

[49] LHCb Collaboration, R. Aaij *et al.*, "Determination of $\gamma$ and $-2\beta_s$ from charmless two-body decays of beauty mesons", *Phys. Lett. B* **741** (2015), p. 1-11.

[50] LHCb Collaboration, R. Aaij *et al.*, "Measurements of *CP* violation in the three-body phase space of charmless $B^\pm$ decays", *Phys. Rev. D* **90** (2014), article ID 112004.

[51] LHCb Collaboration, R. Aaij *et al.*, "Amplitude analysis of $B^\pm \to \pi^\pm K^+ K^-$ decays", *Phys. Rev. Lett.* **123** (2019), article ID 231802.

[52] LHCb Collaboration, R. Aaij *et al.*, "Observation of several sources of *CP* violation in $B^+ \to \pi^+\pi^+\pi^-$ decays", *Phys. Rev. Lett.* **124** (2020), article ID 031801.

[53] LHCb Collaboration, R. Aaij *et al.*, "Amplitude analysis of the $B^+ \to \pi^+\pi^+\pi^-$ decay", *Phys. Rev. D* **101** (2020), article ID 012006.

[54] LHCb Collaboration, R. Aaij *et al.*, "Amplitude analysis of $B_s^0 \to K_S^0 K^\pm \pi^\mp$ decays", *J. High Energy Phys.* **2019** (2019), article ID 114.

[55] D0 Collaboration, V. M. Abazov *et al.*, "Study of *CP*-violating charge asymmetries of single muons and like-sign dimuons in $p\bar{p}$ collisions", *Phys. Rev. D* **89** (2014), article ID 012002.

[56] LHCb Collaboration, R. Aaij *et al.*, "Measurement of the semileptonic *CP* asymmetry in $B^0 - \overline{B}^0$ mixing", *Phys. Rev. Lett.* **114** (2015), article ID 041601.

[57] LHCb Collaboration, R. Aaij *et al.*, "Measurement of the *CP* asymmetry in $B_s^0 - \overline{B}_s^0$ mixing", *Phys. Rev. Lett.* **117** (2016), article ID 061803.

[58] LHCb Collaboration, Expression of Interest for a Phase-II LHCb Upgrade: Opportunities in flavour physics, and beyond, in the HL-LHC era, CERN-LHCC-2017-003.

[59] LHCb Collaboration, R. Aaij *et al.*, "Physics case for an LHCb Upgrade II - Opportunities in flavour physics, and beyond, in the HL-LHC era", CERN-LHCC-2018-027, 2018.

[60] A. Cerri *et al.*, "Opportunities in Flavour Physics at the HL-LHC and HE-LHC", *CERN Yellow Rep. Monogr.* **7** (2019), p. 867-1158.

*Comptes Rendus*
*Physique*
**2020**, 21, nº 1, p. 75-92
https://doi.org/10.5802/crphys.14

A perspective of High Energy Physics from precision measurements
*La physique des Hautes Energies du point de vue des mesures de précision*

# Tau and charm decays

## *Les désintégrations du $\tau$ et du charme*

**Evelina Gersabeck**[*, a] **and Antonio Pich**[b]

[a] University of Manchester, Oxford Road, Manchester, M13 9PL, UK

[b] IFIC, Universitat de València–CSIC, Catedrático José Beltrán 2, E-46980 Paterna, Spain.

*E-mails:* evelina.gersabeck@cern.ch (E. Gersabeck), pich@ific.uv.es (A. Pich).

**Abstract.** A summary of recent precise results in tau and charm physics is presented. Topics include leptonic and hadronic tau decays, lepton flavour and lepton number violation, charm mixing and *CP* violation, leptonic and semileptonic charm decays, rare decays and spectroscopy.

**Résumé.** Nous présentons une sélection de mesures précises et récentes des physiques du lepton $\tau$ et du quark charmé et leur interprétation. Nous examinons en particulier les désintégrations hadroniques et leptoniques du $\tau$, les recherches de violation du nombre leptonique et du nombre leptonique par famille, le mélange des mésons neutres charmés et l'observation de la brisure de la symétrie *CP*, les désintégrations leptoniques et semileptoniques des hadrons charmés, leurs désintégrations rares et les récentes découvertes spectroscopiques.

**Keywords.** Tau and charm physics, $D^0$ mixing, CP violation.

**Mots-clés.** La physique du charme et du tau, Oscillation du $D^0$, Violation de CP.

## 1. Introduction

The $\tau$ is a third generation lepton that decays into quarks and leptons of the first two families. A precision study of its dynamical properties could then shed some light in our understanding of the flavour problem: why fermions are replicated in three sequential generations with identical properties, except the values of their masses. Moreover, the $\tau$ lepton is heavy enough to have a rich variety of hadronic decays, providing a clean laboratory to tests QCD at low energies [1].

The charm is an up-type quark accessible to precision experiments. Being a member of the second family, it allows us to study the interplay of weak and strong interactions through its large diversity of weak decays: leptonic, semileptonic, Cabibbo favoured, Cabibbo suppressed,

* Corresponding author.

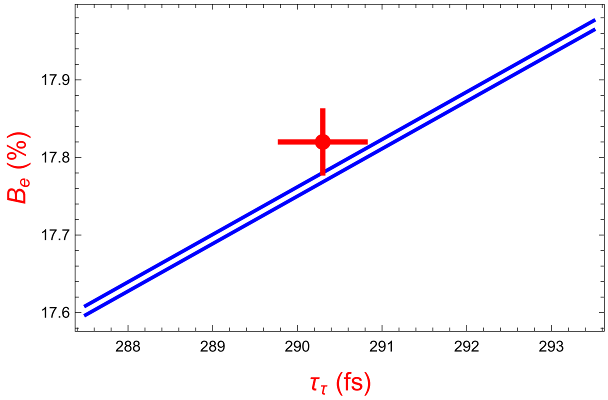


**Figure 1.** SM relation between the $\tau$ lifetime and $B_e \equiv B(\tau^- \to \nu_\tau e^- \bar{\nu}_e)$ (blue band), compared with the measured values (red cross). The band width reflects the current uncertainty on $m_\tau$.

doubly Cabibbo suppressed, and rare decays that are very suppressed (radiative decays, flavour-changing neutral-current transitions) or even forbidden in the Standard Model (SM). The investigation of $D^0$-$\bar{D}^0$ mixing and *CP*-violation phenomena in the up-type sector is of enormous interest to test the CKM quark-mixing mechanism. The confinement properties of QCD can also be analysed through the spectroscopy of open charm mesons and charm baryons.

The $\tau$ mass, $m_\tau = (1776.86 \pm 0.12)$ MeV, is very close to the lightest charmed-particle mass, $m_{D^0} = (1864.83 \pm 0.05)$ MeV [2]. Therefore, both types of particles have similar production mechanisms at $e^+e^-$ colliders, making the physics of $\tau$ and $c$ a common objective in many experiments. The electromagnetic (or $Z^0$ exchange) production cross section is usually maximised by running at some resonance peak that, moreover, decays to quantum correlated $\tau^+\tau^-$, $D^0\bar{D}^0$ or $D^+D^-$ pairs. The LEP-I experiments were running at the $Z^0$ peak, MARKIII (at SPEAR at SLAC), CLEO (at CESR-c) and BESIII (at BEPCII) utilise the $\psi(3770)$ resonance, and the $\Upsilon(4S)$ is the default choice at the b-factories, Belle (at KEKB) and BaBar (at PEP-II). The charm cross-sections at low-energy $e^+e^-$ colliders are at the order few nb. The charm production at hadron colliders occurs in very asymmetric collisions due to the fact that the protons are no longer point-like particles. At hadron colliders experiments LHCb (at LHC) and CDF (at Tevatron), the cross-sections for prompt and secondary production (from B decays) are significantly higher: they can reach about 2 mb for prompt $D^0$ at 13 TeV [3].

## 2. Leptonic tau decays

The $\tau$ lepton decays through the emission of a virtual $W^-$ boson, i.e., $\tau^- \to \nu_\tau W^{-*} \to \nu_\tau X^-$ with $X^- = e^-\bar{\nu}_e, \mu^-\bar{\nu}_\mu, d\bar{u}, s\bar{u}$. In the SM, the charged-current interaction has a universal strength that can be precisely measured in the analogous decay of the muon, $\mu^- \to \nu_\mu e^- \bar{\nu}_e$. Therefore, the leptonic decay width of the $\tau$ can be predicted with high accuracy or, equivalently, one gets a relation between the $\tau$ lifetime and its leptonic branching ratio that is in excellent agreement with the experimental values [2], shown in Figure 1. The main uncertainty originates in the current experimental error on the $\tau$ mass ($\Delta m_\tau / m_\tau = 0.7 \times 10^{-4}$) because $\Gamma_{\tau\to e}$ is proportional to $m_\tau^5$.

Alternatively, one can use the leptonic decay widths of the $\tau$ and the $\mu$ to test the predicted flavour universality of the $W^\pm$ couplings, i.e., that $g_e = g_\mu = g_\tau \equiv g$. The ratio $\Gamma_{\tau\to\mu}/\Gamma_{\tau\to e}$ is sensitive to $|g_\mu/g_e|$, while $\Gamma_{\tau\to e}/\Gamma_{\mu\to e}$ tests $|g_\tau/g_\mu|$. Table 1 shows the current experimental

**Table 1.** Experimental determinations of the ratios $g_\ell/g_{\ell'}$ [1,2]

| | | | | | |
|---|---|---|---|---|---|
| | $\Gamma_{\tau\to\mu}/\Gamma_{\tau\to e}$ | $\Gamma_{\pi\to\mu}/\Gamma_{\pi\to e}$ | $\Gamma_{K\to\mu}/\Gamma_{K\to e}$ | $\Gamma_{K\to\pi\mu}/\Gamma_{K\to\pi e}$ | $\Gamma_{W\to\mu}/\Gamma_{W\to e}$ |
| $\lvert g_\mu/g_e\rvert$ | 1.0018 (16) | 1.0021 (16) | 0.9978 (20) | 1.0010 (25) | 0.996 (10) |
| | $\Gamma_{\tau\to e}/\Gamma_{\mu\to e}$ | $\Gamma_{\tau\to\pi}/\Gamma_{\pi\to\mu}$ | $\Gamma_{\tau\to K}/\Gamma_{K\to\mu}$ | $\Gamma_{W\to\tau}/\Gamma_{W\to\mu}$ | |
| $\lvert g_\tau/g_\mu\rvert$ | 1.0011 (15) | 0.9962 (27) | 0.9858 (70) | 1.034 (13) | |
| | $\Gamma_{\tau\to\mu}/\Gamma_{\mu\to e}$ | $\Gamma_{W\to\tau}/\Gamma_{W\to e}$ | | | |
| $\lvert g_\tau/g_e\rvert$ | 1.0030 (15) | 1.031 (13) | | | |

constraints, together with the most precise tests from leptonic $\pi$, $K$ and $W^\pm$ decays. Charged-current universality has been successfully tested at low energies with a 0.15% precision. The direct leptonic decays of the $W^\pm$ suggest a slight excess of events in $W^-\to\tau^-\bar\nu_\tau$, implying a $2.5\sigma$ deviation from universality that is not compatible with the one order of magnitude more accurate constraints from $W$-mediated decays. Better $W^\pm$ data would be welcome.

The Lorentz structure of the $\ell^-\to\nu_\ell\ell'^-\bar\nu_{\ell'}$ interaction can be analysed in a model-independent way. The most general, local, derivative-free, lepton-number conserving, four-lepton interaction Hamiltonian, consistent with locality and Lorentz invariance contains ten possible structures with their corresponding complex couplings $g^n_{\epsilon\omega}$, where $n=S,V,T$ denotes the type of interaction (scalar, vector, tensor) and the subindices label the left or right chiralities of $\ell$ ($\omega$) and $\ell'$ ($\epsilon$) [1]. Taking out a common global factor that is determined by the total decay rate, the couplings are normalised so that they satisfy $|g^S_{\epsilon\omega}|\le 2$, $|g^V_{\epsilon\omega}|\le 1$ and $|g^T_{\epsilon\omega}|\le 1/\sqrt{3}$. In the SM, $g^V_{LL}=1$, while all other couplings are identically zero. Measuring the energy and angular distribution of the final charged lepton, complemented with polarisation information whenever available, it is possible to disentangle the contributions from the different operators.

In $\mu$ decay, where precise polarisation measurements have been performed of both $\mu$ and $e$, it has been experimentally proved that the bulk of the decay amplitude is indeed of the predicted $V-A$ type, $|g^V_{LL}|>0.960$ (90% C.L.) [2] (one needs also information from the inverse transition $\nu_\mu e^-\to\mu^-\nu_e$), and upper bounds on all other couplings have been set. Owing to its much shorter lifetime, the analysis of the $\tau$ interaction is more challenging. It is still possible to get polarisation information about the initial $\tau$, through the correlated distribution of $\tau^+\tau^-$ pairs produced in $e^+e^-$ annihilation. However, the polarisation of the secondary charged lepton from the $\tau$ decay has never been measured. Since the data agree with the SM, there exist upper bounds on those couplings corresponding to an initial right-handed $\tau$ [2], but the Lorentz structure of a left-handed decaying $\tau$ remains undetermined.

## 3. Hadronic tau decays

A large set of kinematically-allowed semileptonic decays can be accessed with $\tau$ decay data. Contrary to $e^+e^-$ annihilation that only tests the electromagnetic vector current, the decay $\tau^-\to\nu_\tau H^-$ probes the matrix elements of both vector and axial-vector currents between the vacuum and the given hadronic state $H^-$. Moreover, one can also disentangle the Cabibbo allowed ($\bar d u$) and suppressed ($\bar s u$) currents through the strangeness of the produced hadrons. The $\tau$ provides a very good data sample to investigate the dynamics of the QCD Goldstone bosons ($\pi$, $K$, $\eta$) in the resonance region, around 1 GeV.

For the lowest-multiplicity decays, $H^-=\pi^-,K^-$, the hadronic matrix elements are already known from $\pi^-\to\mu^-\bar\nu_\mu$ and $K^-\to\mu^-\bar\nu_\mu$, which makes possible to perform the universality tests in Table 1. One can also make a determination of $|V_{us}|$, but it is not yet competitive with those from $K\to\ell\nu$ and $K\to\pi\ell\nu$, owing to the currently larger uncertainties in $\tau^-\to K^-\nu_\tau$.

The $\pi^-\pi^0$, $\pi^-\bar{K}^0$ and $\pi^0 K^-$ final states give us access to an interesting variety of vector form factors with relevant dynamical information. The decay into the odd G-parity state $\pi^-\eta$ is strongly suppressed in the SM with an expected branching fraction around $10^{-5}$ [4, 5]; its observation above this level would imply new physics incorporating second-class currents. With the large data samples collected at the B factories, differential decay distributions with three hadrons in the final state have become available and branching ratios into high-multiplicity 3- and 5-prong decays have been measured [6]. However, several inconsistencies are known to exist in some branching fraction measurements [2] and errors are still large in the Cabibbo suppressed modes. Thus, there is ample room for improvements at Belle II.

The inclusive hadronic width of the $\tau$ can be rigorously computed in QCD. Its Cabibbo allowed component can be expressed in the form [7]

$$R_{\tau,V+A} \equiv \frac{\Gamma(\tau^- \to \nu_\tau + \text{hadrons}\,[\bar{d}u])}{\Gamma(\tau^- \to \nu_\tau e^- \bar{\nu}_e)} = N_C\,|V_{ud}|^2 S_{\rm EW}\{1+\delta_P+\delta_{\rm NP}\}, \tag{1}$$

with $N_C = 3$ the number of QCD colours and $S_{\rm EW} = 1.0201 \pm 0.0003$ [8–10] the electroweak radiative corrections. The non-perturbative correction $\delta_{\rm NP}$ is strongly suppressed by six powers of the $\tau$ mass [7] and, moreover, can be extracted from the invariant mass distribution of the final hadrons [11]. Detailed studies performed by ALEPH [12–16], CLEO [17] and OPAL [18] have confirmed that non-perturbative contributions are below 1%. The theoretical prediction of $R_{\tau,V+A}$ is then governed by the perturbative correction $\delta_P$ (~20%), which is known to $O(\alpha_s^4)$ [19] and is very sensitive to the strong coupling, making possible a quite accurate determination of $\alpha_s$ [7, 20, 21]. The main theoretical uncertainty originates in the unknown higher-order perturbative corrections [22, 23].

The most precise experimental determination, extracted from the ALEPH $\tau$ decay distributions, gives $\delta_{\rm NP} = -0.0064 \pm 0.0013$ and $\alpha_s^{(n_f=3)}(m_\tau^2) = 0.332 \pm 0.005_{\rm exp} \pm 0.011_{\rm th}$ [24]. Taking as input the ALEPH value of $\delta_{\rm NP}$, the strong coupling can be also determined from the total $\tau$ hadronic width (and/or lifetime); one gets $\alpha_s^{(n_f=3)}(m_\tau^2) = 0.331 \pm 0.013$ [1], in perfect agreement with the ALEPH result. An exhaustive phenomenological re-analysis of the ALEPH data has been recently performed, exploring all strategies previously considered in the literature and several complementary approaches. The results from all adopted methodologies are in excellent agreement, leading to a very robust and reliable value of the strong coupling [25]:

$$\alpha_s^{(n_f=3)}(m_\tau^2) = 0.328 \pm 0.013. \tag{2}$$

After evolution up to the scale $M_Z$, it implies $\alpha_s^{(n_f=5)}(M_Z^2) = 0.1197 \pm 0.0015$, which agrees perfectly with the direct measurement at $s = M_Z^2$ from the $Z^0$ hadronic width, $\alpha_s^{(n_f=5)}(M_Z^2) = 0.1196 \pm 0.0030$ [26]. The comparison of these two determinations, provides a beautiful test of the predicted QCD running:

$$\alpha_s^{(n_f=5)}(M_Z^2)|_\tau - \alpha_s^{(n_f=5)}(M_Z^2)|_Z = 0.0001 \pm 0.0015_\tau \pm 0.0030_Z. \tag{3}$$

The ratio of the inclusive $|\Delta S| = 1$ and $|\Delta S| = 0$ $\tau$ decay widths (normalised to the electronic width), $R_{\tau,S}/R_{\tau,V+A}$, provides a clean determination of $V_{us}$ [27, 28]. To a first approximation, the

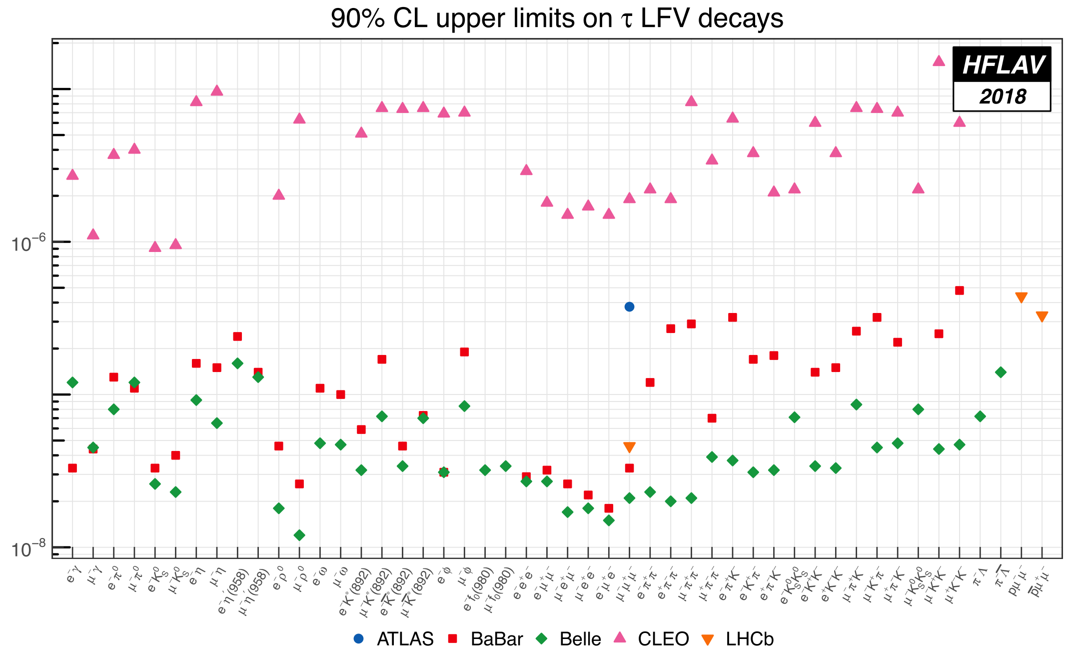


**Figure 2.** Experimental upper limits on $\tau$ LFV and LNV branching ratios [32].

experimental ratio directly measures $|V_{us}/V_{ud}|$. Taking into account the PDG value of $V_{ud}$ and the small SU(3)-breaking correction $\delta R_{\tau,\text{th}} = 0.242 \pm 0.033$ [29–31], one finds [32]

$$|V_{us}| = \left( \frac{R_{\tau,S}}{\frac{R_{\tau,V+A}}{|V_{ud}|^2} - \delta R_{\tau,\text{th}}} \right)^{1/2} = 0.2195 \pm 0.0019, \tag{4}$$

which is $2.9\sigma$ lower than the unitarity expectation $|V_{us}|^{\text{uni}} = \sqrt{1 - |V_{ud}|^2 - |V_{ub}|^2} = 0.2257 \pm 0.0009$. More precise measurements of the Cabibbo-suppressed $\tau$ branching fractions at Belle II are expected to clarify the current discrepancy [33].

## 4. Lepton flavour and lepton number violation in tau decays

The current experimental limits on neutrinoless lepton-flavour-violating (LFV) decays of the $\tau$ lepton are shown in Figure 2. Thanks to the large data samples collected at the B factories, sensitivities of a few times $10^{-8}$ have been achieved in many leptonic ($\tau \to \ell\gamma$, $\tau \to \ell'\ell^+\ell^-$) and semileptonic ($\tau \to \ell P^0$, $\tau \to \ell V^0$, $\tau \to \ell P^0 P^0$, $\tau \to \ell P^+ P'^-$) LFV decay modes. Competitive limits for some selected final states, such as $\tau \to 3\mu$, have been also set by LHCb. Belle II is expected to push these limits to the $10^{-9}$ level [33], increasing in a drastic way the sensitivity to new-physics scales.

Lepton-number violation (LNV) has been also searched for in $\tau$ decays. Very stringent upper limits in the range $(2.0 - 8.4) \times 10^{-8}$ (90% C.L.) have been set on the decay modes $\tau^- \to \ell^+ P^- P'^-$, with $\ell = e, \mu$ and $P, P' = \pi, K$ [34]. Worth mentioning is also the experimental limit $B(\tau^- \to \Lambda\pi^-) < 7.2 \times 10^{-8}$ (90% C.L.), which tests the violation of both lepton and baryon numbers [35].

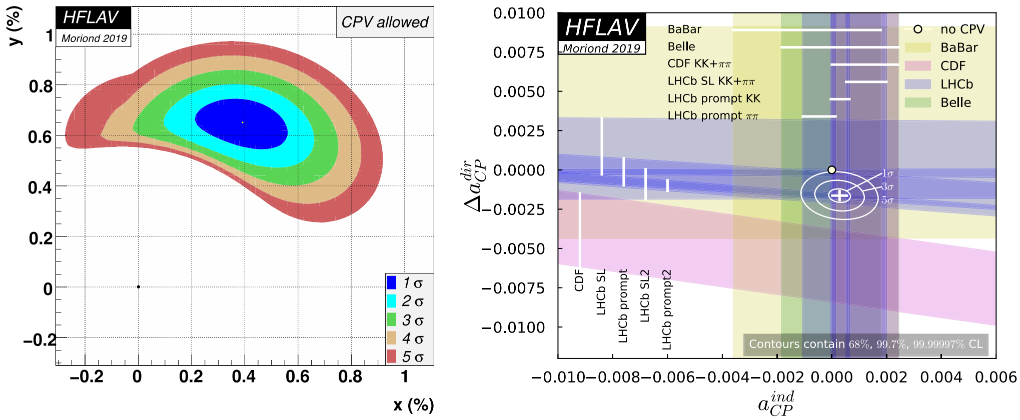


**Figure 3.** Left: The HFLAV averages for the mixing parameters $x$ and $y$; Right: The combination plot of $\Delta A_{CP}$ and $A_\Gamma$. The point of no *CP* violation (0,0) is shown as a filled circle [32].

## 5. Mixing and *CP* violation in charm decays

The phenomenon of *CP* violation is one of the keys to uncover why there is an overwhelming amount of matter over antimatter in our Universe, as postulated by Sakharov in 1967 [36]. The *CP* symmetry applies to processes invariant under the combined transformation of charge conjugation ($C$) under which a particle is exchanged with its own anti-particle, and spatial inversion (parity, $P$). The SM accommodates *CP* violation in a single complex phase of the CKM matrix which only appeared after introducing the third family of quarks. The *CP* violation has been well established in decays of $K^0(\bar{s}d)$, $B^0(\bar{b}d)$, $B_s^0(\bar{b}s)$ and $B^+(\bar{b}u)$ mesons. Unlike for the $b$-system where we expect sizeable effects, for D meson decays, SM *CP* violation effects are expected to be tiny because of the smallness of the imaginary component of the CKM elements involved in the relevant processes. *CP* violation in charm was only recently observed in decays of $D^0(c\bar{u})$ to a pair of charged kaons and to a pair of charged pions [37] and there is no agreement whether its size is compatible with the SM predictions [38–42].[1]

Neutral charm mesons can periodically change into their antimatter counterparts and back – they oscillate. As a result, the mass eigenstates, with well-defined masses and lifetimes, are linear combinations of flavour eigenstates, with well-defined quark composition: $|D_{1,2}\rangle = p|D^0\rangle \pm q|\bar{D^0}\rangle$. Here, $q, p$ are complex numbers that are related by $p^2 + q^2 = 1$. The mixing parameters $x$ and $y$ are defined as $y \equiv \Delta\Gamma/(2\Gamma)$, where $\Delta\Gamma = \Gamma_2 - \Gamma_1$ is the width difference of the charm mesons, and $x \equiv \Delta m/\Gamma$, where $\Delta m$ is their mass difference. The mixing process is suppressed in charm because the corresponding box diagrams contain down-type quarks in the internal lines: owing to the GIM cancellation, each virtual quark contribution is proportional to $m_q^2$, and the heaviest quark, $b$ is not quite as heavy as the top quark (which plays an important role in the B meson mixing) and has very small couplings with $c$ and $u$ quarks. This leads to very slow oscillation of the D mesons, and to very small values of $x$ and $y$, experimentally challenging to measure. The current world averages are displayed in Figure 3 (left) [32]. Including the latest LHCb result [43], the parameter $x$ related to the mass difference between neutral charm-meson eigenstates is measured to be greater than 0 with a significance exceeding 3 standard deviations for the first time.

[1]The theory predictions for charm mesons are particularly difficult because of the intermediate mass of the $c$ quark. Effective theories such as HQET (too light) and Chiral Perturbation Theory (too heavy) are not directly applicable.

The amplitude for the decay of a D hadron to a final state $f$ can be expressed as $A_f$, and the amplitude of the charge-conjugated process as $\bar{A}_{\bar{f}}$. There are several ways to generate a *CP* asymmetry. Direct *CP* violation occurs for a non-zero asymmetry in the decay amplitudes. This type of *CP* violation depends on the decay mode, and it can involve either charged or neutral particles. In order for direct *CP* violation to be realised the amplitudes $A_f$ and $\bar{A}_{\bar{f}}$ require interference of at least two different processes with different weak and strong phases, defined as the phase which changes its sign under *CP* transformation (the weak phase), and the one that does not (the strong phase). The indirect *CP* violation comprises the *CP* violation in mixing processes incorporating neutral particles, and *CP* violation in the interference between mixing and decay amplitudes. *CP* violation in mixing takes place if the transition probability of particles to antiparticles compared to the reverse process differs, and occurs when $|q/p| \neq 1$. This type of *CP* violation is universal and does not depend on the decay mode. *CP* violation in the interference between mixing and decay amplitudes is present if the imaginary part of $\lambda \equiv p\bar{A}_{\bar{f}}/(qA_f)$ is non-zero.

In two-body singly-Cabibbo-suppressed (SCS) charm decays, the direct *CP* violation is searched through measuring the time-integrated *CP* asymmetry in the decay rates of the charm mesons ($f = K^+K^-, \pi^+\pi^-$)

$$A_{CP} \equiv \frac{\Gamma(D \to f) - \Gamma(\bar{D} \to \bar{f})}{\Gamma(D \to f) + \Gamma(\bar{D} \to \bar{f})}, \tag{5}$$

where $\Gamma$ denotes the partial decay rate. Taking the difference of the asymmetries in two different final states, $\Delta A_{CP} = A_{CP}(D^0 \to K^+K^-) - A_{CP}(D^0 \to \pi^+\pi^-)$, has two advantages: the nuisance asymmetries originating from production and detection cancel, and the sensitivity to *CP* violation is enhanced as the *CP* asymmetries in these two channels are expected to be of similar magnitude but with opposite signs. $\Delta A_{CP}$ is mostly a measure of direct *CP* violation in charm. A study using the full Run 1 and Run 2 data of LHC yields $\Delta A_{CP}^{\mathrm{exp}} = (-15.4 \pm 2.9) \times 10^{-4}$, with a significance of more than five standard deviations [37]. A range of new SM predictions for $\Delta A_{CP}$ [38–42] argue whether beyond the SM (BSM) physics is necessary to explain this result, or whether it originates in a mild non-perturbative enhancement due to rescattering effects or to the presence of a nearby $0^{++}$ resonance such as $f_0(1710)$. Some papers suggest that resolving this tension within an extension of the SM includes a flavour violating $Z'$ that couples only to $\bar{s}s$ and $\bar{c}u$ quarks [38]. The value of $\Delta A_{CP}$ together with other experimental data can then be used to make predictions on CP violation in several $D^0 \to PP$ and $D^0 \to VP$ channels [42, 44].

This is the first observation of *CP* violation in the charm sector, and so far the only one. Several measurements in other two-body decays have greatly improved the precision of the asymmetries for the decay modes $D^0 \to K_S^0 K_S^0$, $D_{(s)}^+ \to K_S^0 h^+$, $D_{(s)}^+ \to \eta' h^+$, $D_{(s)}^+ \to \pi^+\pi^0$, $D^0 \to \pi^0\pi^0$, $D^0 \to K_S^0\pi^0$, $D^0 \to K_S^0\eta^{(\prime)}$, etc. [32]. From the theoretical point of view, a promising two-body decay to probe for *CP* violating effects is $D^0 \to KK^*$ [45]. In addition, various model-dependent and model-independent techniques probe for *CP* violation in multibody decays but the experimental results are so far compatible with *CP* symmetry conservation [32].

The asymmetry between the effective lifetimes,[2] $\hat{\Gamma}$, of mesons initially produced as $D^0$ and $\bar{D}^0$ and decaying into the *CP*-even final states $D \to hh$, where $h = K, \pi$, is a measure of indirect *CP* violation. The current best results from LHCb, combining the full Run 1 and Run 2 statistics [46], $A_\Gamma(KK) = (-4.4 \pm 2.3 \pm 0.6) \times 10^{-4}$ and $A_\Gamma(\pi\pi) = (2.5 \pm 4.3 \pm 0.7) \times 10^{-4}$ are compatible with no *CP* violation in charm mixing or the interference between mixing and decay. These are yet the

[2]The effective lifetime is the lifetime obtained from a single exponential fit to the decay-time distribution.

most precise experimental measurements of *CP* asymmetries. The interplay between direct and indirect *CP* violation in two-body charm decays is presented in Figure 3 (right) combining the $\Delta A_{CP}$ and $A_\Gamma$ results.

Two methods are employed in establishing mixing in charm decays. Firstly, the flavour of the neutral D meson at production has to be determined. Usually this is done by the charge of the pion in the strong decay of $D^{*+} \to D^0\pi^+$. Alternatively, the flavour of the secondary charm decays from $\bar{B} \to D^0\mu^-\nu_\mu X$ can be tagged by the charge of the muon. The second technique is used at the LHCb experiment only. Until 2012, the mixing in charm was established with more than 5 standard deviations significance only by a combination of three different experiments [47–50] done by HFLAV [32]. The mixing parameters can be extracted from the time-dependent ratio of $D^0 \to K^+\pi^-$ (also referred to as wrong-sign, WS) to $D^0 \to K^-\pi^+$ (also known as right-sign, RS) decay rates

$$R(t) = \frac{N_{WS}(t)}{N_{RS}(t)} \approx R_D + \sqrt{R_D}\, y' \frac{t}{\tau} + \frac{x'^2 + y'^2}{4}\left(\frac{t}{\tau}\right)^2. \qquad (6)$$

Here, $t/\tau$ is the decay time expressed in units of the average $D^0$ lifetime $\tau$, and $R_D$ is the ratio of doubly-Cabibbo-suppressed (DCS) to Cabibbo-favoured (CF) decay rates. Note that in (6), $x'$ and $y'$ are rotated by the strong phase difference between the CF and DCS amplitudes, $\delta$, compared to the $x$, $y$ parameters defined above. By observing a decay-time dependence of the ratio $R(t)$, and measuring the parameters $y'$ and $x'^2$, the LHCb experiment reported a first observation of $D^0 - \bar{D}^0$ oscillations in a single measurement [51]. Since then, more precise measurements have been reported [52]. Following a similar strategy, $D^0 - \bar{D}^0$ oscillations were observed in $D^0 \to K3\pi$ decays as well [53].

These measurements have been extremely useful in establishing that the neutral charm mesons oscillate. However, the golden mode for measuring the mixing parameters $x$ and $y$ without the strong phase rotation is $D^0 \to K^0_S hh$. This final state is accessible both through decays of $D^0$ and $\bar{D}^0$. The multiple CF and DCS interfering amplitudes enhance the sensitivity to $x$ and $y$. There are two techniques that can be employed to analyse these decays: a model-independent one where the decay-time evolution in bins of similar strong phase difference is studied, and a model-dependent one where the effective lifetimes of individual resonances are measured. The model-dependent technique where time-dependent amplitude analysis of self-conjugated decays allows for a direct measurement of $x$ and $y$, and a simultaneous search for *CP* violation in mixing, in the decay and in the interference between mixing and decay, was developed by the CLEO experiment [54], and was later extended by the BaBar and Belle experiments [55, 56]. The model-independent methods [57, 58] rely on external input for the strong phase differences between charm decay amplitudes from quantum correlated $D^0$ and $\bar{D}^0$ produced at threshold at the $\psi(3770)$ resonance at CLEO [59] or BESIII experiments. The most precise results come from BESIII [60, 61].[3] The latest LHCb measurement in [58], combined with previous measurements of the mixing parameters, yields the first evidence that the neutral charm meson masses are different, and $x$ is positive. An overview of how complex the state-of-art of the theory predictions for $x$ and $y$ is can be found in [63]. The mixing parameters can be extracted for $D^0$ and $\bar{D}^0$ which probes *CP* violation in charm mixing. To date, all results are compatible with *CP* symmetry and agree with the SM predictions.

[3] The current best results are based on a data sample of about 3 $\text{fb}^{-1}$ while the collaboration considers increasing this data sample to 20 $\text{fb}^{-1}$. In addition to improving our knowledge on charm mixing, these measurements play an important role in reducing systematic uncertainties on determinations of the CKM angle $\gamma$ allowing for sub-degree precision [62].

## 6. Leptonic and semileptonic charm decays

Purely leptonic charm decays $D^+_{(s)} \to \ell^+\nu_\ell$, where $\ell$ is a lepton, proceed through a $W^\pm$ annihilation diagram. In the SM at tree level, the decay width is given by

$$\Gamma(D^+ \to \ell^+\nu_\ell) = \frac{G_F^2 f_{D^+}^2}{8\pi}|V_{cd}|^2 m_\ell^2 m_{D^+}\left(1-\frac{m_\ell^2}{m_{D^+}^2}\right)^2 \tag{7}$$

where $G_F$ is the Fermi coupling constant, $m_\ell$ is the lepton mass, and $m_{D^+}$ is the $D^+$-meson mass. All these quantities are known with a very good accuracy [2]. An experimental measurement of the decay width (or the branching fraction) allows for a determination of the product of the decay constant, $f_{D^+}$, and the CKM element $V_{cd}$. The unique tagging technique and the excellent performance of the BESIII detector allows to reconstruct these decays. BESIII measured $B(D^+ \to \mu^+\nu_\mu) = (3.71 \pm 0.19 \pm 0.06) \times 10^{-4}$ [64]. This is the most precise result of this quantity to date, and determines $f_{D^+}|V_{cd}| = (45.75 \pm 1.20 \pm 0.39)$ MeV. The decay constant $f_{D^+}$ is obtained using as input the CKM matrix element $|V_{cd}| = 0.22520 \pm 0.00065$ from the global fit in the SM [65]. Alternatively, $|V_{cd}|$ is determined using $f_{D^+} = (207 \pm 4)$ MeV from lattice QCD (LQCD) as input. The results are: $f_{D^+} = (203.2 \pm 5.3 \pm 1.8)$ MeV, and $|V_{cd}| = 0.2210 \pm 0.0058 \pm 0.0047$.

Recently, the decay $D^+ \to \tau^+\nu_\tau$ was observed for a first time by the BESIII collaboration [66]. Its branching fraction was determined to be $B(D^+ \to \tau^+\nu_\tau) = (1.20 \pm 0.24 \pm 0.12) \times 10^{-4}$. Taking the world average result for $B(D^+ \to \mu^+\nu_\mu) = (3.74 \pm 0.17) \times 10^{-4}$, a test for lepton flavour universality (LFU) was reported:

$$R(D^+)_{\tau/\mu} = \frac{\Gamma(D^+ \to \tau^+\nu_\tau)}{\Gamma(D^+ \to \mu^+\nu_\mu)} = 3.21 \pm 0.64 \pm 0.43, \tag{8}$$

which is consistent with the SM expectation $R(D^+)_{\tau/\mu} = 2.67$.

The decays $D_s^+ \to \ell^+\nu_\ell$ have been studied by BESIII [67, 68], as well as by its predecessor CLEO [69], Belle [70] and BaBar [71] experiments. Analogously to the case above, the values $f_{D_s^+}$ and $|V_{cs}|$ were extracted and the most precise values are $252.9 \pm 3.7 \pm 3.6$ MeV and $0.985 \pm 0.014 \pm 0.014$, respectively [67]. These results are important to calibrate various theoretical predictions [72].

Similarly to $R(D^+)_{\tau/\mu}$, $R(D_s^+)_{\tau/\mu} = 10.2 \pm 0.5$ [73] is in agreement with the SM expectation. With a future sample of 20 $\mathrm{fb}^{-1}$ of data at 3.773 GeV at BESIII, the precision on $R(D^+)_{\tau/\mu}$ will be statistically limited to about 8%. Increasing the data sample at 4.178 GeV to 6 $\mathrm{fb}^{-1}$, the precision on $R(D_s^+)_{\tau/\mu}$ will be systematically limited to about 3%. The rate of the $D^+_{(s)} \to e^+\nu_e$ decay is helicity suppressed by a factor $m_e^2$ and is beyond the sensitivity of the BESIII experiment.

The measurements of $V_{cs(d)}$ from purely leptonic decays are the most precise ones. The projections with 20 $\mathrm{fb}^{-1}$ at BESIII [73] and 50 $\mathrm{ab}^{-1}$ of data at Belle II [74] indicate that their precision could be improved by an order of magnitude. An alternative way to measure $|V_{cs(d)}|$ is through the differential rate of semileptonic decays $D^0 \to K^-(\pi^-)\ell^+\nu_\ell$, which in the $m_\ell = 0$ limit takes the form

$$\frac{\mathrm{d}\Gamma}{\mathrm{d}q^2} = \frac{G_F^2}{24\pi^3}|V_{cs(d)}|^2|p_{K^-(\pi^-)}|^3|f_+^{K^-(\pi^-)}(q^2)|^2, \tag{9}$$

where $p$ is the three-momentum of the $K(\pi)$ meson in the rest frame of the D meson, and $f_+(q^2)$ represents the hadronic form factors which depend on the four-momentum transfer between the D meson and the final hadron. The form factors parameterise the strong interaction effects and can be calculated in LQCD. As the uncertainties in the predictions of the form factors shrink [75–77], experimental validation of the results becomes increasingly important. In [78, 79], using final states with electrons, the form factors are studied by fitting the differential decay rates with different shape parameters predicted by the various models, and the compatibility between the data and the calculations is interpreted. The best fit results in [79] for the form-factors at

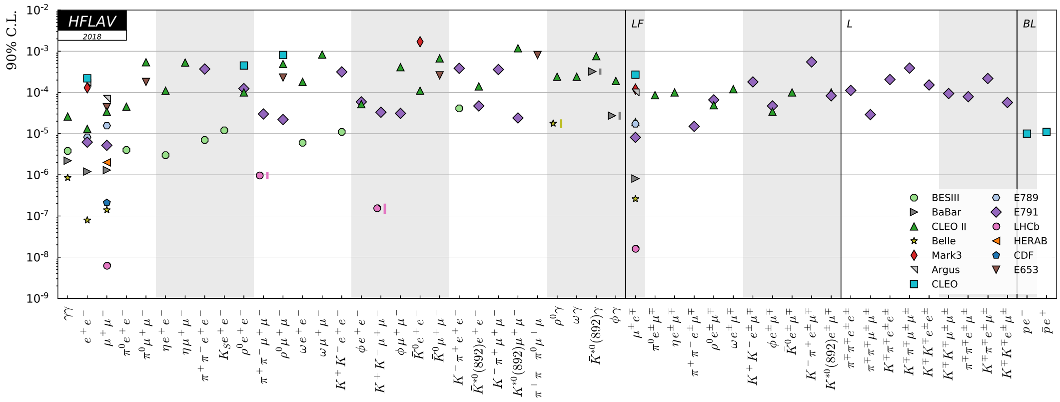


**Figure 4.** The current best 90% C.L. limits of rare $D^0$ decays. The different regions combine FCNC, LFV, LNV, BLN decays [32]. Similar summary plots for charged D mesons and charm baryons can be found in [32].

$q^2 = 0$ are $f_+^K(0) = 0.7368 \pm 0.0026 \pm 0.0036$ and $f_+^\pi(0) = 0.6372 \pm 0.0080 \pm 0.0044$. In analogy to the leptonic decays, $|V_{cs(d)}|$ are obtained using form-factor predictions as an input [75, 80] yielding $|V_{cs}| = 0.9601 \pm 0.0033 \pm 0.0047 \pm 0.0239$ and $|V_{cd}| = 0.2155 \pm 0.0027 \pm 0.0014 \pm 0.0094$.

The LFU tests with semileptonic decays indicate no deviation from the SM: $R_{\mu/e} = \Gamma(D^+ \to \bar{K}^0\mu^+\nu_\mu)/\Gamma(D^+ \to \bar{K}^0 e^+\nu_e) = 0.988 \pm 0.033$ [81] is consistent with the predicted value [82] within uncertainties; for $D^0 \to K^-\ell^+\nu_\ell$, the corresponding ratio $R_{\mu/e} = 0.974 \pm 0.007 \pm 0.012$ also agrees with the SM [77,83,84]; similarly, the ratios using $D^{0(+)} \to \pi^{-(0)} e^+\nu_e$ decays, $R^0_{\mu/e} = 0.922 \pm 0.030 \pm 0.022$ and $R^+_{\mu/e} = 0.964 \pm 0.037 \pm 0.026$, are in agreement with the SM [84] within $1.7\sigma$ and $0.5\sigma$, respectively. All these measurements are currently statistically limited and will be significantly improved with 20 fb$^{-1}$ of data taken at 3.773 GeV in the future, at BESIII [73], and 50 ab$^{-1}$ of data which is being collected by Belle II [33].

## 7. Rare charm decays or searches for BSM particles

The studies of charm rare decays provide a unique probe of BSM physics in the flavour sector, complementary to studies in K and B systems. These comprise studies of lepton flavour violation (LFV), lepton number violation (LNV), baryon number violation (BNV), flavour-changing neutral-current (FCNC) transitions, vector-meson-dominated (VMD) and radiative decays. The expected rates of these processes vary vastly, from forbidden, FCNC ($10^{-16}$ to $10^{-9}$), VMD ($10^{-8}$ to $10^{-6}$) to the not-so-rare radiative decays ($10^{-5}$ to $10^{-4}$).

Examples for such processes can be seen on Figure 4, together with the limits from different experiments. The most stringent limit on FCNC decays comes from $D^0 \to \mu^+\mu^-$ [85]; on LFV from $D^0 \to e^\pm\mu^\mp$ [86]; on LNV from $D^+_{(s)} \to \pi^+\mu^-\mu^-$ [87], and on BNV from $D^0 \to pe$ [88].

The FCNC processes are heavily suppressed in the SM. Short distance contributions to effective $c \to u$ transitions are rather small, therefore the branching fractions are dominated by long distance contributions. An enhancement of the predicted decay rates could signal the presence of new physics.

In the future, many of these limits will be pushed further by the precision experiments LHCb (Upgrade I and II) and Belle II. The large production cross sections will likely translate into world's best measurements. The BESIII experiment is complementary for decays which are difficult for LHCb and Belle, with missing neutrinos, neutral particles, etc., due to its unique capability to identify the flavour of the D meson at production in quantum correlated decays, e.g. decays such as $D^0 \to \pi^0 \nu\bar{\nu}$ or $D^{\pm,0} \to \pi^{\pm,0} a$, where $a$ is a light pseudoscalar. A future Super $\tau$-charm factory in Novosibirsk (or China) could further help in pushing the limits for rare and forbidden charm decays.

The rarest charm decay observed to date is the $D^0 \to K^+K^-\mu^+\mu^-$, studied along with $D^0 \to \pi\pi\mu\mu$ decays. It is observed away from the known resonances $\rho^0/\omega, \phi, \eta$ and its branching fraction, $\mathscr{B}(D^0 \to K^+K^-\mu^+\mu^-) = (1.54 \pm 0.27 \pm 0.09 \pm 0.16) \times 10^{-7}$ [89], is in agreement with the SM prediction [90, 91]. The *CP* asymmetries in the non-resonance regions for these two decays were determined as well [92], $A_{CP}(D^0 \to \pi^+\pi^-\mu^+\mu^-) = (4.9 \pm 3.8 \pm 0.7)\%$ and $A_{CP}(D^0 \to K^+K^-\mu^+\mu^-) = (0 \pm 11 \pm 2)\%$, and also agree with the SM expectations, which in turn imposes constrains on several BSM models [90, 91, 93–97].

## 8. Charm spectroscopy

Charm spectroscopy provides an excellent ground to study the dynamics of light quarks in the environment of a heavy quark. The theoretical framework for analysing decays of hadrons with one heavy quark is the Heavy Quark Effective Theory (HQET), making use of the limit $m_Q \to \infty$. Many of the exited states predicted in the 80's have not yet been observed [98]. Two of the lowest-lying (1S) states and four (1P) orbital excitations of the open charm mesons are known [2], both for non-strange and strange mesons. Recent experimental effort allows to study the properties (masses, widths) and to determine the quantum numbers such as the total angular momentum and parity of some of the newly observed states. A prompt production of the excited states allows to establish whether a state is natural ($J^P = 0^+, 1^-, 2^+, \ldots$) or unnatural ($J^P = 0^-, 1^+, 2^-, \ldots$). A secondary production of charmed mesons allows for a full spin-parity analysis. The excited states $D_{s1}(2536)^+(1^+)$, $D^*_{s2}(2573)^+(2^+)$, $D^*_{s1}(2700)^+(1^-)$ and $D^*_{s3}(2860)^+(3^-)$ were observed by [99–103], yielding information on their properties, including spin-parity assignments. In addition to the states reported above, an enhancement around $D^*_{sJ}(3400)^+$ was seen [103]. The most recent results from charm meson spectroscopy report the resonance parameters, quantum numbers and partial branching fractions of the $D_1(2420)$, $D_1(2430)$, $D_0(2550)$, $D^*_1(2600)$, $D_2(2740)$ and $D^*_3(2750)$ resonances, which are measured for the first time in a four-body amplitude analysis of the $B^- \to D^{*+}\pi^-\pi^-$ decays [104].

Singly charmed baryons consist of one heavy charm quark and two light $(u, d, s)$ quarks. The large mass difference between the charm quark and the lighter ones justifies the usage of HQET. Excited $\Lambda_c$, $\Sigma_z$ and $\Xi_c$ states have been well studied [2]. This was not the case for the heaviest of them, the $\Omega_c$ baryon with quark content *css* and quantum numbers $J^P = 1/2^+$, until not long ago. The first observed spin-excited $\Omega^*_c$ state was seen in a decay $\Omega^*_c \to \Omega_c\gamma$ [105, 106], presumed to be a $J^P = 3/2^+$ state. The LHCb experiment has reported the discovery of five new excited $\Omega$ states decaying to $\Omega^{**0}_c \to \Xi_c K^-$, with $\Xi_c \to pK^-\pi^+$ [107]. These five new very narrow states (with widths $\leq 10$ MeV) are $\Omega_c(3000)^0$, $\Omega_c(3050)^0$, $\Omega_c(3066)^0$, $\Omega_c(3090)^0$, and $\Omega_c(3119)^0$ (see Figure 5, left). In addition, a broad structure around 3188 MeV has been identified, which could be resolved with more data. Since these baryons were reconstructed using a two-body decay, their quantum numbers are not determined, and their masses are not compared to the theoretical predictions. A possible analysis of three-body final states can provide additional information. The first four of these states were confirmed using a smaller data sample by the Belle experiment, reporting the first observation of these states in $e^+e^-$ colliders [108]. These baryons have been interpreted as bound states of a c-quark and a P-wave ss-diquark [109]. An alternative interpretation is noted in which the heaviest two states are 2S excitations with $J^P = 1/2^+$ and $3/2^+$, while the lightest three are those with $J^P = 3/2^-, 3/2^-, 5/2^-$ expected to decay via D-waves. The lattice predictions of their masses are summarised in [110]. A molecular model has also been suggested for the interpretation of these states [111].

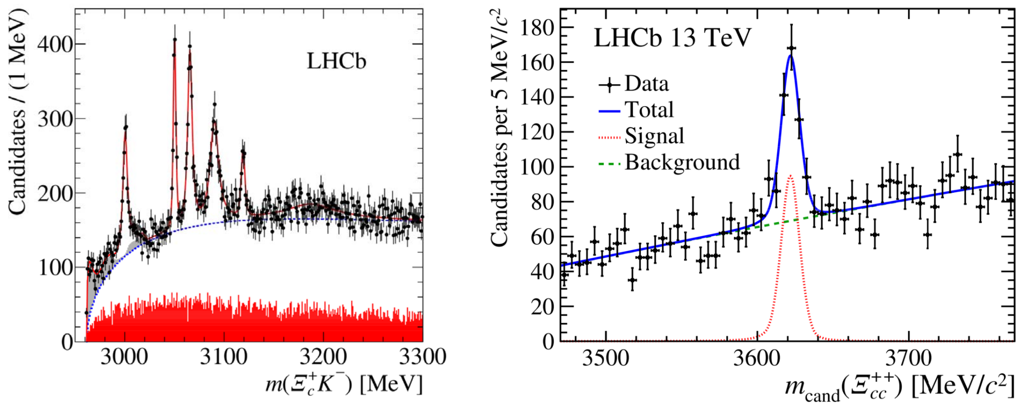


**Figure 5.** Left: The excited $\Omega_c(css)$ states observed by the LHCb collaboration [107]; Right: The first observation of $\Xi_{cc}^{++} \to \Lambda_c^+ K^- \pi^+ \pi^+$ [112].

The doubly charmed baryons are built of two $c$ quarks and a lighter quark: these are $\Xi_{cc}^{+}$(ccd), $\Xi_{cc}^{++}$(ccu) and $\Omega_{cc}^{+}$(ccs). The first two form an isospin doublet with quantum numbers $J^P = 1/2^+$ and $L = 0$. Many predictions of their masses in the range 3500 to 3800 MeV [113–124] and lifetimes from 0.1 to 1.5 ps [121, 122] exist. For the isospin doublet, the difference in the mass is not expected to exceed 1 MeV [120].

The SELEX collaboration [125, 126] observed a peak which was interpreted as a $\Xi_{cc}^{+}$ baryon in the final states $\Lambda_c^+ K^- \pi^+$ and $pD^+K^-$, with a measured mass of $(3518.7 \pm 1.7)$ MeV. The collaboration also reported a measurement of the $\Xi_{cc}^{++}$ meson mass to be 3460 MeV [127]. The mass difference is in conflict with the expected mass splitting of isospin doublets. The $\Xi_{cc}^{+}$ lifetime was experimentally measured to be less than 33 fs at the 90% C.L. which disagrees with the theoretical predictions. The $\Xi_{cc}^{+}$ observation has not been confirmed in searches performed at the FOCUS [128], BaBar [129], Belle [130], and LHCb [112, 131] experiments.

The doubly-charmed baryon $\Xi_{cc}^{++}$ was observed for the first time in the final state $\Xi_{cc}^{++} \to \Lambda_c^+ K^- \pi^+ \pi^+$ by the LHCb experiment [112] (see Figure 5). Its mass was determined as $(3621.40 \pm 0.72^{+0.024}_{-0.27} \pm 0.14)$ MeV [112], and its lifetime was measured to be $(0.256 \pm 0.022 \pm 0.014)$ ps [132]. Since the first observation, $\Xi_{cc}^{++}$ was also observed in the final state of $\Xi_{cc}^{++} \to \Xi_c^+ \pi^+$ [133]. The production cross-section of $\Xi_{cc}^{++}$ was determined relative to that of $\Lambda_c$ baryons to be $(2.22 \pm 0.27 \pm 0.29) \times 10^{-4}$ [134]. Currently, other decay modes of $\Xi_{cc}^{++}$ are investigated, and the searches for $\Xi_{cc}^{+}$ (to confirm the SELEX result), and $\Omega_{cc}^{+}$ are ongoing.

Measurements of lifetimes play an important role in validating effective models such as HQET and can be used to search for deviations from the SM predictions. Recently, the LHCb experiment reported the most precise measurements of the lifetimes of the charm baryons $\Omega_c$, $\Lambda_c^+$, $\Xi_c^+$ and $\Xi_c^0$ [135, 136]. While the last three agree with previous measurements, the lifetime of $\Omega_c^0$ is about four times larger (see Figure 6). It has been argued that the expected lifetime hierarchy, due to the higher-order contributions discussed above, should be $\tau(\Xi_c^+) > \tau(\Lambda_c^+) > \tau(\Xi_c^0) > \tau(\Omega_c^0)$ [113,137–141]. The current best measurements are inconsistent with this hierarchy. Possible interpretations of this deviation include constructive interference between the $s$ quark in the $c \to sW^+$ transition in the $\Omega_c^0$ decay and the spectator $s$ quark in the final state being smaller than expected, that the spin of the $ss$ system plays a larger role, or that additional higher-order contributions in the HQET need to be considered. However, according to [138], $\Omega_c^0$ can be either the most short-living or the most long-living among charmed baryons. For doubly charmed

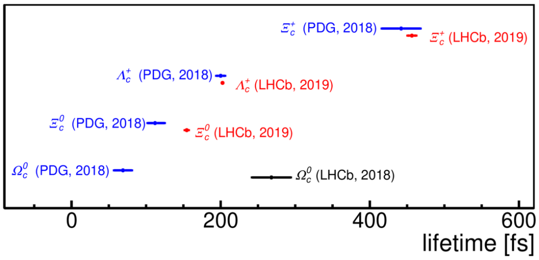


**Figure 6.** The tension in the charmed baryon lifetimes measurements [136].

baryons, the expected hierarchy is $\tau(\Xi_{cc}^{++}) \gg \tau(\Omega_{cc}^{+}) \approx \tau(\Xi_{cc}^{+})$ [137] which is why $\Omega_{cc}^{+}$ and $\Xi_{cc}^{+}$ are more difficult to discover at LHCb.

## 9. Summary

The investigation of the $\tau$ lepton properties has provided many beautiful tests of the SM and strong constraints on new physics scenarios. Belle II will significantly improve the current sensitivity to LFV, LNV and *CP*-violating phenomena in $\tau$ decays. Moreover, its huge data sample should allow for a more accurate scrutiny of SM properties, such as lepton universality, Lorentz structure of the charged-current interaction, quark mixing and QCD in the non-perturbative regime. Meanwhile, the $\tau$ has also become a superb experimental tool in the search for new physics at the LHC. At long term, the TeraZ option of a future FCC-ee collider running at the $Z^0$ peak would produce an enormous data sample of $1.7 \times 10^{11}$ $\tau^+\tau^-$ pairs in extremely clean kinematic (and background) conditions [142], opening a broad range of interesting opportunities in $\tau$ physics.

Charm physics covers a vast range of studies. In the past decade charm mixing and direct *CP* violation have been discovered. Intriguingly narrow excited $\Omega_c$ states have been seen and the doubly charmed baryons $\Xi_{cc}^{++}$ have been observed. The rarest charm decay's branching fraction measured is of the order $10^{-7}$. The LHCb experiment is currently undergoing its first major Upgrade. Several components of the detector will be replaced with new ones able to withstand the much higher rates and radiation doses in Run 3 of the LHC. A total of 300 fb$^{-1}$ of data is planned to be recorded. Belle II is currently taking data and has planned to collect a total of 50 ab$^{-1}$ of data. The BESIII experiment will increase its charm data samples at least by a factor 3. The longer term future of charm physics will be shaped by these three experiments and a possible Super Tau Charm factory.

## Acknowledgements

This work was supported by the Royal Society, UK [grant DH160214], by the Spanish Government and ERDF funds from the EU Commission [grant FPA2017-84445-P], and by the Generalitat Valenciana [grant Prometeo/2017/053].

## References

[1] A. Pich, "Precision tau physics", *Prog. Part. Nucl. Phys.* **75** (2014), p. 41-85.
[2] M. Tanabashi *et al.*, "Review of particle physics", *Phys. Rev. D* **98** (2018), no. 3, article ID 030001.
[3] R. Aaij *et al.*, "Measurements of prompt charm production cross-sections in *pp* collisions at $\sqrt{s} = 13$ TeV", *J. High Energy Phys.* **2016** (2016), article ID 159.

[4] A. Pich, "'Anomalous' $\eta$ production in tau decay", *Phys. Lett. B* **196** (1987), p. 561-565.
[5] R. Escribano, S. Gonzalez-Solis, P. Roig, "Predictions on the second-class current decays $\tau^- \to \pi^- \eta^{(\prime)} \nu_\tau$", *Phys. Rev. D* **94** (2016), no. 3, article ID 034008.
[6] A. J. Bevan *et al.*, "The physics of the B factories", *Eur. Phys. J. C* **74** (2014), article ID 3026.
[7] E. Braaten, S. Narison, A. Pich, "QCD analysis of the tau hadronic width", *Nucl. Phys. B* **373** (1992), p. 581-612.
[8] W. J. Marciano, A. Sirlin, "Electroweak radiative corrections to tau decay", *Phys. Rev. Lett.* **61** (1988), p. 1815-1818.
[9] E. Braaten, C.-S. Li, "Electroweak radiative corrections to the semihadronic decay rate of the tau lepton", *Phys. Rev. D* **42** (1990), p. 3888-3891.
[10] J. Erler, "Electroweak radiative corrections to semileptonic tau decays", *Rev. Mex. Fis.* **50** (2004), p. 200-202.
[11] F. Le Diberder, A. Pich, "Testing QCD with tau decays", *Phys. Lett. B* **289** (1992), p. 165-175.
[12] D. Buskulic *et al.*, "Measurement of the strong coupling constant using tau decays", *Phys. Lett. B* **307** (1993), p. 209-220.
[13] R. Barate *et al.*, "Measurement of the spectral functions of axial - vector hadronic tau decays and determination of $\alpha_s(M_\tau^2)$ ", *Eur. Phys. J. C* **4** (1998), p. 409-431.
[14] S. Schael *et al.*, "Branching ratios and spectral functions of tau decays: final ALEPH measurements and physics implications", *Phys. Rep.* **421** (2005), p. 191-284.
[15] M. Davier, A. Hocker, Z. Zhang, "The Physics of hadronic tau decays", *Rev. Mod. Phys.* **78** (2006), p. 1043-1109.
[16] M. Davier, S. Descotes-Genon, A. Hocker, B. Malaescu, Z. Zhang, "The determination of $\alpha_s$ from tau decays revisited", *Eur. Phys. J. C* **56** (2008), p. 305-322.
[17] T. Coan *et al.*, "Measurement of $\alpha_s$ from tau decays", *Phys. Lett. B* **356** (1995), p. 580-588.
[18] K. Ackerstaff *et al.*, "Measurement of the strong coupling constant $\alpha_s$ and the vector and axial vector spectral functions in hadronic tau decays", *Eur. Phys. J. C* **7** (1999), p. 571-593.
[19] P. A. Baikov, K. G. Chetyrkin, J. H. Kuhn, "Order $\alpha_s^4$ QCD corrections to Z and tau decays", *Phys. Rev. Lett.* **101** (2008), article ID 012002.
[20] S. Narison, A. Pich, "QCD formulation of the tau decay and determination of $\Lambda_{\mathrm{MS}}$", *Phys. Lett. B* **211** (1988), p. 183-188.
[21] E. Braaten, "The perturbative QCD corrections to the ratio R for tau decay", *Phys. Rev. D* **39** (1989), article ID 1458.
[22] F. Le Diberder, A. Pich, "The perturbative QCD prediction to $R_\tau$ revisited", *Phys. Lett. B* **286** (1992), p. 147-152.
[23] A. Pich, "Tau-decay determination of the strong coupling", *SciPost Phys. Proc.* **1** (2019), article ID 036.
[24] M. Davier, A. Höcker, B. Malaescu, C.-Z. Yuan, Z. Zhang, "Update of the ALEPH non-strange spectral functions from hadronic $\tau$ decays", *Eur. Phys. J. C* **74** (2014), no. 3, article ID 2803.
[25] A. Pich, A. Rodríguez-Sánchez, "Determination of the QCD coupling from ALEPH $\tau$ decay data", *Phys. Rev. D* **94** (2016), no. 3, article ID 034027.
[26] M. Baak, J. Cúth, J. Haller, A. Hoecker, R. Kogler, K. Mönig, M. Schott, J. Stelzer, "The global electroweak fit at NNLO and prospects for the LHC and ILC", *Eur. Phys. J. C* **74** (2014), article ID 3046.
[27] E. Gamiz, M. Jamin, A. Pich, J. Prades, F. Schwab, " $V_{us}$ and $m_s$ from hadronic tau decays", *Phys. Rev. Lett.* **94** (2005), article ID 011803.
[28] E. Gamiz, M. Jamin, A. Pich, J. Prades, F. Schwab, "Determination of $m_s$ and $|V_{us}|$ from hadronic tau decays", *J. High Energy Phys.* **01** (2003), article ID 60.
[29] E. Gamiz, M. Jamin, A. Pich, J. Prades, F. Schwab, "$|V_{us}|$ and $m_s$ from hadronic tau decays", *Nucl. Phys. Proc. Suppl.* **169** (2007), p. 85-89.
[30] A. Pich, J. Prades, "Strange quark mass determination from Cabibbo suppressed tau decays", *J. High Energy Phys.* **10** (1999), article ID 4.
[31] A. Pich, J. Prades, "Perturbative quark mass corrections to the tau hadronic width", *J. High Energy Phys.* **06** (1998), article ID 13.
[32] Y. S. Amhis *et al.*, "Averages of *b*-hadron, *c*-hadron, and $\tau$-lepton properties as of 2018", 2019, preprint, https://arxiv.org/abs/1909.12524.
[33] W. Altmannshofer *et al.*, "The Belle II physics book", *PTEP* **2019** (2019), no. 12, article ID 123C01.
[34] Y. Miyazaki *et al.*, "Search for lepton-flavor-violating and lepton-number-violating $\tau \to \ell h h'$ decay modes", *Phys. Lett. B* **719** (2013), p. 346-353.
[35] Y. Miyazaki *et al.*, "Search for lepton and baryon number violating tau- decays into $\bar{\Lambda}\pi^-$ and $\Lambda\pi^-$", *Phys. Lett. B* **632** (2006), p. 51-57.
[36] A. D. Sakharov, "Violation of *CP* Invariance, C asymmetry, and baryon asymmetry of the universe", *Pisma Zh. Eksp. Teor. Fiz.* **5** (1967), p. 32-35, *Usp. Fiz. Nauk* **161** (1991), no. 5, p. 61.
[37] R. Aaij *et al.*, "Observation of *CP* violation in charm decays", *Phys. Rev. Lett.* **122** (2019), article ID 211803.
[38] M. Chala, A. Lenz, A. V. Rusov, J. Scholtz, "$\Delta A_{CP}$ within the Standard Model and beyond", *J. High Energy Phys.* **07** (2019), article ID 161.
[39] H.-N. Li, C.-D. Lü, F.-S. Yu, "Implications on the first observation of charm CPV at LHCb", 2019, preprint, https://arxiv.org/abs/1903.10638.

[40] Y. Grossman, S. Schacht, "The emergence of the $\Delta U = 0$ rule in charm physics", *J. High Energy Phys.* **07** (2019), article ID 20.
[41] A. Soni, "Resonance enhancement of Charm *CP*", 2019, preprint, https://arxiv.org/abs/1905.00907.
[42] H.-Y. Cheng, C.-W. Chiang, "Revisiting CP violation in $D \to PP$ and *VP* decays", *Phys. Rev. D* **100** (2019), no. 9, article ID 093002.
[43] R. Aaij *et al.*, "Measurement of the mass difference between neutral charm-meson eigenstates", *Phys. Rev. Lett.* **122** (2019), article ID 231802.
[44] F. Buccella, A. Paul, P. Santorelli, " $SU(3)_F$ breaking through final state interactions and $CP$ asymmetries in $D \to PP$ decays", *Phys. Rev. D* **99** (2019), no. 11, article ID 113001.
[45] U. Nierste, S. Schacht, "Neutral $D \to KK^*$ decays as discovery channels for charm *CP* violation", *Phys. Rev. Lett.* **119** (2017), no. 25, article ID 251801.
[46] R. Aaij *et al.*, "Updated measurement of decay-time-dependent CP asymmetries in $D^0 \to K^+ K^-$ and $D^0 \to \pi^+ \pi^-$ decays", *Phys. Rev. D* **101** (2020), no. 1, article ID 012005.
[47] B. Aubert *et al.*, "Evidence for $D^0 - \bar{D}^0$ mixing", *Phys. Rev. Lett.* **98** (2007), article ID 211802.
[48] M. Starič *et al.*, "Evidence for $D^0$ - $\bar{D}^0$ mixing", *Phys. Rev. Lett.* **98** (2007), no. 21, article ID 211803, [**65** (2007)].
[49] T. Aaltonen *et al.*, "Evidence for $D^0 - \bar{D}^0$ mixing using the CDF II detector", *Phys. Rev. Lett.* **100** (2008), article ID 121802.
[50] B. Aubert *et al.*, "Measurement of $D^0 - \bar{D}^0$ mixing from a time-dependent amplitude analysis of $D^0 \to K^+ \pi^- \pi^0$ decays", *Phys. Rev. Lett.* **103** (2009), article ID 211801.
[51] R. Aaij *et al.*, "Observation of $D^0 - \bar{D}^0$ oscillations", *Phys. Rev. Lett.* **110** (2013), no. 10, article ID 101802.
[52] R. Aaij *et al.*, "Updated determination of $D^0$-$\bar{D}^0$ mixing and *CP* violation parameters with $D^0 \to K^+ \pi^-$ decays", *Phys. Rev. D* **97** (2018), no. 3, article ID 031101.
[53] R. Aaij *et al.*, "First observation of $D^0 - \bar{D}^0$ oscillations in $D^0 \to K^+ \pi^- \pi^+ \pi^-$ decays and measurement of the associated coherence parameters", *Phys. Rev. Lett.* **116** (2016), no. 24, article ID 241801.
[54] D. M. Asner *et al.*, "Search for $D^0$-$\bar{D}^0$ mixing in the Dalitz plot analysis of $D^0 \to K^0_{(S)}\pi^+\pi^-$ ", *Phys. Rev. D* **72** (2005), article ID 012001.
[55] T. Peng *et al.*, "Measurement of $D^0 - \bar{D}^0$ mixing and search for indirect *CP* violation using $D^0 \to K^0_S\pi^+\pi^-$ decays", *Phys. Rev. D* **89** (2014), no. 9, article ID 091103.
[56] P. del Amo Sanchez *et al.*, "Measurement of $D^0$-$\bar{D}^0$ mixing parameters using $D^0 \to K^0_{(S)}\pi^+\pi^-$ and $D^0 \to K^0_{(S)}K^+K^-$ decays", *Phys. Rev. Lett.* **105** (2010), article ID 081803.
[57] R. Aaij *et al.*, "Model-independent measurement of mixing parameters in $D^0 \to K^0_S\pi^+\pi^-$ decays", *J. High Energy Phys.* **04** (2016), article ID 33.
[58] R. Aaij *et al.*, "Measurement of the mass difference between neutral charm-meson eigenstates", *Phys. Rev. Lett.* **122** (2019), no. 23, article ID 231802.
[59] J. Libby *et al.*, "Model-independent determination of the strong-phase difference between $D^0$ and $\bar{D}^0 \to K^0_{S,L}h^+h^-$ $(h = \pi, K)$ and its impact on the measurement of the CKM angle $\gamma/\phi_3$", *Phys. Rev. D* **82** (2010), article ID 112006.
[60] M. Ablikim *et al.*, "Model-independent determination of the relative strong-phase difference between $D^0$ and $\bar{D}^0 \to K^0_{S,L}\pi^+\pi^-$ and its impact on the measurement of the CKM angle $\gamma/\phi_3$", *Phys. Rev. D* **101** (2020), no. 11, article ID 112002.
[61] M. Ablikim *et al.*, "Determination of strong-phase parameters in $D \to K^0_{S,L}\pi^+\pi^-$ ", *Phys. Rev. Lett.* **124** (2020), no. 24, article ID 241802.
[62] R. Aaij *et al.*, "Physics case for an LHCb Upgrade II - Opportunities in flavour physics, and beyond, in the HL-LHC era", 2018, preprint, https://arxiv.org/abs/1808.08865.
[63] A. A. Petrov, "Charm physics: theoretical review", *eConf* **C030603** (2003), MEC05, [**189** (2003)].
[64] M. Ablikim *et al.*, "Precision measurements of $B(D^+ \to \mu^+\nu_\mu)$, the pseudoscalar decay constant $f_{D^+}$, and the quark mixing matrix element $|V_{\rm cd}|$", *Phys. Rev. D* **89** (2014), no. 5, article ID 051104.
[65] J. Beringer *et al.*, "Review of Particle Physics (RPP)", *Phys. Rev. D* **86** (2012), article ID 010001.
[66] M. Ablikim *et al.*, "Observation of the leptonic decay $D^+ \to \tau^+\nu_\tau$", *Phys. Rev. Lett.* **123** (2019), no. 21, article ID 211802.
[67] M. Ablikim *et al.*, "Determination of the pseudoscalar decay constant $f_{D_s^+}$ via $D_s^+ \to \mu^+\nu_\mu$ ", *Phys. Rev. Lett.* **122** (2019), no. 7, article ID 071802.
[68] M. Ablikim *et al.*, "Measurement of the $D_s^+ \to \ell^+\nu_\ell$ branching fractions and the decay constant $f_{D_s^+}$ ", *Phys. Rev. D* **94** (2016), no. 7, article ID 072004.
[69] J. P. Alexander *et al.*, "Measurement of $B(D_s^+ \to \ell^+\nu)$ and the decay constant $f_{D_s^+}$ From 600 $\mathrm{pb}^{-1}$ of $e^\pm$ Annihilation Data Near 4170 MeV", *Phys. Rev. D* **79** (2009), article ID 052001.
[70] A. Zupanc *et al.*, "Measurements of branching fractions of leptonic and hadronic $D_s^+$ meson decays and extraction of the $D_s^+$ meson decay constant", *J. High Energy Phys.* **09** (2013), article ID 139.
[71] P. del Amo Sanchez *et al.*, "Measurement of the absolute branching fractions for $D_s^- \to \ell^-\bar{\nu}_\ell$ and extraction of the decay constant $f_{D_s}$", *Phys. Rev. D* **82** (2010), article ID 091103, [Erratum: *Phys. Rev. D* **91**, (2015), no. 1, 019901].

[72] S. Aoki *et al.*, "FLAG review 2019", *Eur. Phys. J. C* **80** (2020), no. 2, article ID 113.

[73] M. Ablikim *et al.*, "Future physics programme of BESIII", *Chin. Phys. C* **44** (2020), no. 4, article ID 040001.

[74] A. J. Schwartz, "Semileptonic and leptonic charm meson decays at Belle II", 2019, preprint, https://arxiv.org/abs/1902.07850.

[75] H. Na, C. T. H. Davies, E. Follana, J. Koponen, G. P. Lepage, J. Shigemitsu, " $D\to\pi,\ell\nu$ semileptonic decays, $|V_{cd}|$ and $2^{nd}$ row unitarity from lattice QCD", *Phys. Rev. D* **84** (2011), article ID 114505.

[76] R. Li *et al.*, "$D$ meson semileptonic decay form factors at $q^2 = 0$", *PoS* **LATTICE2018** (2019), article ID 269.

[77] V. Lubicz, L. Riggio, G. Salerno, S. Simula, C. Tarantino, "Scalar and vector form factors of $D\to\pi(K)\ell\nu$ decays with $N_f = 2+1+1$ twisted fermions", *Phys. Rev. D* **96** (2017), no. 5, article ID 054514, [Erratum: *Phys. Rev. D* **99**, (2019), no. 9, 099902].

[78] J. P. Lees *et al.*, "Measurement of the $D^0\to\pi^-\ e^+\nu_e$ differential decay branching fraction as a function of $q^2$ and study of form factor parameterizations", *Phys. Rev. D* **91** (2015), no. 5, article ID 052022.

[79] M. Ablikim *et al.*, "Study of dynamics of $D^0\to K^-\ e^+\nu_e$ and $D^0\to\pi^-\ e^+\nu_e$ decays", *Phys. Rev. D* **92** (2015), no. 7, article ID 072012.

[80] P. Ball, "Testing QCD sum rules on the light-cone in $D\to(\pi,K)\ell\nu$ decays", *Phys. Lett. B* **641** (2006), p. 50-56.

[81] M. Ablikim *et al.*, "Improved measurement of the absolute branching fraction of $D^+\to\bar{K}^0\mu^+\nu_\mu$", *Eur. Phys. J. C* **76** (2016), no. 7, article ID 369.

[82] J. G. Korner, G. A. Schuler, "Exclusive semileptonic heavy meson decays including lepton mass effects", *Z. Phys. C* **46** (1990), article ID 93.

[83] N. R. Soni, J. N. Pandya, "Decay $D\to K^{(*)}\ \ell^+\nu_\ell$ in covariant quark model", *Phys. Rev. D* **96** (2017), no. 1, article ID 016017, [Erratum: *Phys. Rev. D* **99** (2019), no. 5, 059901].

[84] L. Riggio, G. Salerno, S. Simula, "Extraction of $|V_{cd}|$ and $|V_{cs}|$ from experimental decay rates using lattice QCD $D\to\pi(K)\ell\nu$ form factors", *Eur. Phys. J. C* **78** (2018), no. 6, article ID 501.

[85] R. Aaij *et al.*, "Search for the rare decay $D^0\to\mu^+\mu^-$", *Phys. Lett. B* **725** (2013), no. 1-3, p. 15-24.

[86] R. Aaij *et al.*, "Search for the lepton-flavour violating decay $D^0\to e^\pm\mu^\mp$", *Phys. Lett. B* **754** (2016), p. 167-175.

[87] R. Aaij *et al.*, "Search for $D^+_{(s)}\to\pi^+\mu^+\mu^-$ and $D^+_{(s)}\to\pi^-\mu^+\mu^+$ decays", *Phys. Lett. B* **724** (2013), no. 4-5, p. 203-212.

[88] P. Rubin *et al.*, "Search for $D^0\to\bar{p}e^+$ and $D^0\to pe^-$", *Phys. Rev. D* **79** (2009), article ID 097101.

[89] R. Aaij *et al.*, "Observation of $D^0$ meson decays to $\pi^+\pi^-\mu^+\mu^-$ and $K^+K^-\mu^+\mu^-$ final states", *Phys. Rev. Lett.* **119** (2017), article ID 181805.

[90] L. Cappiello, O. Cata, G. D'Ambrosio, "Standard Model prediction and new physics tests for $D^0\to h^+\ h^-\ \ell^+\ \ell^-(h=\pi,K : \ell=e,\mu)$", *J. High Energy Phys.* **04** (2013), article ID 135.

[91] S. De Boer, G. Hiller, "Null tests from angular distributions in $D\to P_1\ P_2\ \ell^+\ \ell^-$, $\ell=e,\mu$ decays on and off peak", *Phys. Rev. D* **98** (2018), no. 3, article ID 035041.

[92] R. Aaij *et al.*, "Measurement of angular and *CP* asymmetries in $D^0\to\pi^+\pi^-\mu^+\mu^-$ and $D^0\to K^+K^-\mu^+\mu^-$ decays", *Phys. Rev. Lett.* **121** (2018), article ID 091801.

[93] S. Fajfer, S. Prelovsek, "Effects of littlest Higgs model in rare D meson decays", *Phys. Rev. D* **73** (2006), article ID 054026.

[94] I. I. Bigi, A. Paul, "On *CP* asymmetries in two-, three- and four-body D decays", *J. High Energy Phys.* **03** (2012), article ID 21.

[95] A. Paul, A. De La Puente, I. I. Bigi, "Manifestations of warped extra dimension in rare charm decays and asymmetries", *Phys. Rev. D* **90** (2014), no. 1, article ID 014035.

[96] S. Fajfer, N. Košnik, "Prospects of discovering new physics in rare charm decays", *Eur. Phys. J. C* **75** (2015), no. 12, article ID 567.

[97] S. de Boer, G. Hiller, "Flavor and new physics opportunities with rare charm decays into leptons", *Phys. Rev. D* **93** (2016), no. 7, article ID 074001.

[98] S. Godfrey, K. Moats, "Properties of excited charm and charm-strange mesons", *Phys. Rev. D* **93** (2016), no. 3, article ID 034035.

[99] J. P. Lees *et al.*, "Dalitz plot analyses of $B^0\to D^-\ D^0\ K^+$ and $B^+\to\bar{D}^0D^0K^+$ decays", *Phys. Rev. D* **91** (2015), no. 5, article ID 052002.

[100] J. Brodzicka *et al.*, "Observation of a new D(sJ) meson in $B^+\to\bar{D}^0D^0K^+$ decays", *Phys. Rev. Lett.* **100** (2008), article ID 092001.

[101] B. Aubert *et al.*, "Study of D(sJ) decays to D*K in inclusive $e^+\ e^-$ interactions", *Phys. Rev. D* **80** (2009), article ID 092003.

[102] B. Aubert *et al.*, "Observation of a new $D_s$ meson decaying to $DK$ at a mass of 2.86 GeV/$c^2$", *Phys. Rev. Lett.* **97** (2006), article ID 222001.

[103] R. Aaij *et al.*, "Study of $D^+_{sJ}$ mesons decaying to $D^{*+}K^0_S$ and $D^{*0}\ K^+$ final states", *J. High Energy Phys.* **02** (2016), article ID 133.

[104] R. Aaij *et al.*, "Determination of quantum numbers for several excited charmed mesons observed in $B^-\to D^{*+}\ \pi^-\ \pi^-$ decays", *Phys. Rev. D* **101** (2020), no. 3, article ID 032005.

[105] B. Aubert *et al.*, "Observation of an excited charm baryon $\Omega_c^*$ decaying to $\Omega_c^0\gamma$ ", *Phys. Rev. Lett.* **97** (2006), article ID 232001.
[106] E. Solovieva *et al.*, "Study of $\Omega_c^0$ and $\Omega_c^{*0}$ baryons at Belle", *Phys. Lett. B* **672** (2009), p. 1-5.
[107] R. Aaij *et al.*, "Observation of five new narrow $\Omega_c^0$ states decaying to $\Xi_c^+K^-$ ", *Phys. Rev. Lett.* **118** (2017), article ID 182001.
[108] J. Yelton *et al.*, "Observation of excited $\Omega_c$ charmed baryons in $e^+\ e^-$ collisions", *Phys. Rev. D* **97** (2018), no. 5, article ID 051102.
[109] M. Karliner, J. L. Rosner, "Very narrow excited $\Omega_c$ baryons", *Phys. Rev. D* **95** (2017), no. 11, article ID 114012.
[110] M. Padmanath, "Hadron spectroscopy and resonances: review", *PoS* **LATTICE2018** (2018), article ID 013.
[111] L. Tolos, R. Pavao, J. Nieves, "$\Omega_c$ excited states: a molecular approach with heavy-quark spin symmetry", *JPS Conf. Proc.* **26** (2019), article ID 022024.
[112] R. Aaij *et al.*, "Observation of the doubly charmed baryon $\Xi_{cc}^{++}$ ", *Phys. Rev. Lett.* **119** (2017), no. 11, article ID 112001.
[113] S. Bianco, F. L. Fabbri, D. Benson, I. Bigi, "A Cicerone for the physics of charm", *Riv. Nuovo Cim.* **26N7** (2003), p. 1-200.
[114] A. De Rujula, H. Georgi, S. L. Glashow, "Hadron masses in a gauge theory", *Phys. Rev. D* **12** (1975), p. 147-162.
[115] S. Fleck, J. M. Richard, "Baryons with double charm", *Prog. Theor. Phys.* **82** (1989), p. 760-774.
[116] R. Roncaglia, D. B. Lichtenberg, E. Predazzi, "Predicting the masses of baryons containing one or two heavy quarks", *Phys. Rev. D* **52** (1995), p. 1722-1725.
[117] S. S. Gershtein, V. V. Kiselev, A. K. Likhoded, A. I. Onishchenko, "Spectroscopy of doubly charmed baryons: $\Xi_{cc}^+$ and $\Xi_{cc}^{++}$ ", *Mod. Phys. Lett. A* **14** (1999), p. 135-146.
[118] S.-P. Tong, Y.-B. Ding, X.-H. Guo, H.-Y. Jin, X.-Q. Li, P.-N. Shen, R. Zhang, "Spectra of baryons containing two heavy quarks in potential model", *Phys. Rev. D* **62** (2000), article ID 054024.
[119] R. Lewis, N. Mathur, R. M. Woloshyn, "Charmed baryons in lattice QCD", *Phys. Rev. D* **64** (2001), article ID 094509.
[120] C. Itoh, T. Minamikawa, K. Miura, T. Watanabe, "Doubly charmed baryon masses and quark wave functions in baryons", *Phys. Rev. D* **61** (2000), article ID 057502.
[121] B. Guberina, B. Melic, H. Stefancic, "Inclusive decays and lifetimes of doubly charmed baryons", in *17th Autumn School: QCD: Perturbative or Nonperturbative? (AUTUMN 99)*, 1999, p. 363-368.
[122] V. V. Kiselev, A. K. Likhoded, A. I. Onishchenko, "Lifetimes of doubly charmed baryons: $\Xi_{cc}^+$ and $\Xi_{cc}^{++}$ ", *Phys. Atom. Nucl.* **62** (1999), p. 1940-1949, *Yad. Fiz.* **62** (1999), p. 2095.
[123] M. Karliner, J. L. Rosner, "Strange baryons with two heavy quarks", *Phys. Rev. D* **97** (2018), no. 9, article ID 094006.
[124] M. Karliner, J. L. Rosner, "Baryons with two heavy quarks: masses, production, decays, and detection", *Phys. Rev. D* **90** (2014), no. 9, article ID 094007.
[125] M. Mattson *et al.*, "First observation of the doubly charmed baryon $\Xi_{cc}^+$ ", *Phys. Rev. Lett.* **89** (2002), article ID 112001.
[126] A. Ocherashvili *et al.*, "Confirmation of the double charm baryon $\Xi_{cc}^+(3520)$ via its decay to $pD^+\ K^-$", *Phys. Lett. B* **628** (2005), p. 18-24.
[127] S. Koshkarev, V. Anikeev, "Production of the doubly charmed baryons at the SELEX experiment – the double intrinsic charm approach", *Phys. Lett. B* **765** (2017), p. 171-174.
[128] S. P. Ratti, "New results on c-baryons and a search for cc-baryons in FOCUS", *Nucl. Phys. Proc. Suppl.* **115** (2003), p. 33-36, [**33** (2003)].
[129] B. Aubert *et al.*, "Search for doubly charmed baryons $\Xi_{cc}^+$ and $\Xi_{cc}^{++}$ in BABAR", *Phys. Rev. D* **74** (2006), article ID 011103.
[130] R. Chistov *et al.*, "Observation of new states decaying into $\Lambda_c^+K^-\pi^+$ and $\Lambda_c^+K_S^0\pi^-$ ", *Phys. Rev. Lett.* **97** (2006), article ID 162001.
[131] R. Aaij *et al.*, "Search for the doubly charmed baryon $\Xi_{cc}^+$ ", *Sci. China Phys. Mech. Astron.* **63** (2020), no. 2, article ID 221062.
[132] R. Aaij *et al.*, "Measurement of the lifetime of the doubly charmed baryon $\Xi_{cc}^{++}$ ", *Phys. Rev. Lett.* **121** (2018), article ID 052002.
[133] R. Aaij *et al.*, "First observation of the doubly charmed baryon decay $\Xi_{cc}^{++}\to\Xi_c^+\pi^+$ ", *Phys. Rev. Lett.* **121** (2018), article ID 162002.
[134] R. Aaij *et al.*, "Measurement of $\Xi_{cc}^{++}$ production in $pp$ collisions at $\sqrt{s}=13$ TeV", *Chin. Phys. C* **44** (2020), no. 2, article ID 022001.
[135] R. Aaij *et al.*, "Measurement of the $\Omega_c^0$ lifetime", *Phys. Rev. Lett.* **121** (2018), article ID 092003.
[136] R. Aaij *et al.*, "Precision measurement of the $\Lambda_c^+$, $\Xi_c^+$, and $\Xi_c^0$ baryon lifetimes", *Phys. Rev. D* **100** (2019), article ID 032001.
[137] H.-Y. Cheng, "Charmed Baryons Circa 2015", 2015, preprint, https://arxiv.org/abs/1508.07233.
[138] B. Blok, M. A. Shifman, "Lifetimes of charmed hadrons revisited. Facts and fancy", in *3rd Workshop on the Tau-Charm Factory*, 1991.
[139] H.-Y. Cheng, "A Phenomenological analysis of heavy hadron lifetimes", *Phys. Rev. D* **56** (1997), p. 2783-2798.
[140] G. Bellini, I. I. Y. Bigi, P. J. Dornan, "Lifetimes of charm and beauty hadrons", *Phys. Rept.* **289** (1997), p. 1-155.

[141] M. A. Shifman, M. B. Voloshin, "Preasymptotic effects in inclusive weak decays of charmed particles", *Sov. J. Nucl. Phys.* **41** (1985), 120, [*Yad. Fiz.* **41** (1985), 187].
[142] A. Abada *et al.*, "FCC physics opportunities", *Eur. Phys. J. C* **79** (2019), no. 6, article ID 474.

*Comptes Rendus*
*Physique*
**2020**, 21, nº 1, p. 93-106
https://doi.org/10.5802/crphys.10

A perspective of High Energy Physics from precision measurements
*La physique des Hautes Energies du point de vue des mesures de précision*

# Rare $b$-hadron decays

## *Désintégrations rares des hadrons beaux*

**Ulrik Egede** [a] **and Justine Serrano** [*, b]

[a] School of Physics and Astronomy, Monash University, Melbourne, Australia

[b] Aix Marseille Univ, CNRS/IN2P3, CPPM, Marseille, France.

*E-mails:* ulrik.egede@monash.edu (U. Egede), serrano@cppm.in2p3.fr (J. Serrano).

**Abstract.** Rare $b$-hadron decays provide a rich environment to search for beyond Standard Model physics effects thanks to numerous observables. In the recent years, several tensions with the SM expectations have appeared. A review of the most important experimental results is presented together with their interpretation in the context of the effective Hamiltonian approach.

**Résumé.** Les désintégrations rares des hadrons beaux fournissent un environnement riche pour rechercher des effets de physique au-delà du Modèle Standard grâce à de nombreuses observables. Dans les dernières années, plusieurs tensions avec les prédictions du Modèle Standard sont apparues. Une revue des résultats expérimentaux les plus importants est présentée ainsi que leur interprétation dans le contexte de l'approche d'Hamiltonien effectif.

**Keywords.** Flavour physics, Rare decays, Penguin decays, Beyond standard model, B-hadron decays.

**Mots-clés.** Physique des saveurs, Désintégrations rares, Diagrammes pingouins, Physique au-delà du Modèle Standard, Désintégrations de hadrons beaux.

## 1. Introduction

Rare $b$-hadron decays are defined as flavour changing neutral current decays and have either photons or leptons in the final state. In the Standard Model (SM) these decays are proceeding through either electroweak penguin or box diagrams, with an example in Figure 1 for the decay $B^0 \to K^{*0}\ell^+\ell^-$, where $\ell = e, \mu, \tau$. In the SM these decays are suppressed by both the small CKM factor $V_{ts}$ (or the even smaller $V_{td}$) and a loop level suppression, while in beyond the Standard Model (BSM) scenarios neither of these suppressions might be present. Combined with a very clear final state signature for many of the decays, rare $b$-hadron decays one of the best possible places to search for BSM physics.

Measurements of rare $b$-hadron decays has over the past six years shown an increasing number of discrepancies between the SM expectation and the measurements. There is no firm con-

* Corresponding author.

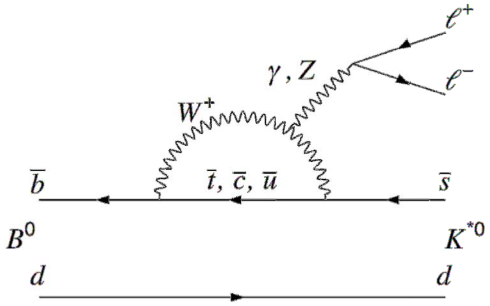


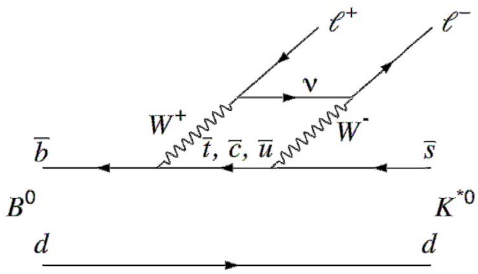


**Figure 1.** A penguin and a box diagram for the decay $B^0 \to K^{*0}\ell^+\ell^-$ in the Standard Model.

clusion yet if this is the result of BSM physics or a combination of experimental issues with the measurements, problems with the theoretical predictions and their uncertainties, and statistical uncertainties. After introducing the effective Hamiltonian approach and the experimental context, the sections below will outline the various experimental measurements and then move onto their interpretation in terms of effective couplings parametrising any possible BSM physics.

### 1.1. *The effective Hamiltonian approach*

To parametrise the branching fractions and angular distributions in rare $b$-hadron decays, the effective Hamiltonian [1]

$$\mathscr{H}_{\text{eff}} = \frac{4G_F}{\sqrt{2}}\left(\lambda_u^{(q)}\sum_{i=1}^{2}\mathscr{C}_i\mathscr{O}_i^u + \lambda_c^{(q)}\sum_{i=1}^{2}\mathscr{C}_i\mathscr{O}_i^c - \lambda_t^{(q)}\sum_{i=3}^{10}\mathscr{C}_i\mathscr{O}_i - \lambda_t^{(q)}\mathscr{C}_\nu\mathscr{O}_\nu + h.c\right) \tag{1}$$

can be used, where $q = d, s$ for processes based on the quark level $b \to d, s$ transitions and $\lambda_p^{(q)} = V_{pb}V_{pq}^*$. The long-distance effects, governed by non-perturbative theory, are encoded in the operators $\mathscr{O}_i$ while the short distance ones are proportional to the so-called Wilson coefficients $\mathscr{C}_i$.

The SM operators of interest for the rare $b$-hadron decays are the electromagnetic and chromomagnetic operators $\mathscr{O}_{7,8}$ and the semileptonic operators $\mathscr{O}_{9,10,\nu}$. Under the assumption that BSM physics arise from virtual particles with a mass much above the $b$-quark mass, it will only affect the effective Hamiltonian by modifying the Wilson coefficients of operators that may or may not already be present in the SM. New operators could be $\mathscr{O}'$ operators corresponding to a chirality flipped operator (right-handed current), lepton-flavour-dependent operators $(\mathscr{O}_{9,10,\nu})^\ell$ in case of lepton flavour universality violation, scalar or pseudoscalar operators involving two quarks and two leptons, $\mathscr{O}_{\mathscr{S},\mathscr{P}}$, and lepton flavour violating operators $\mathscr{O}_9^{\ell_i\ell_j}$. The effective Hamiltonian approach is very powerful in the sense that it allows to combine the measured observables in a model-independent way.

### 1.2. *Experimental context*

To investigate rare $B$ decays requires both a large number of $b$-hadrons produced as well as the ability to trigger and identify them with high efficiency. In the past this was achieved at the $e^+e^-$ $B$ Factories BaBar and Belle while it has been dominated in the past decade by the LHC experiments with the majority of results coming from LHCb [2,3] and a smaller number from ATLAS [4] and CMS [5]. The future will see upgraded detectors and increased integrated luminosity for the LHC experiments while data taking has just started at the Belle II [6] experiment.

In terms of access to rare $b$-hadron decays the different experiments have various strengths and weaknesses. The $B$ Factories have just a $B^0\overline{B}^0$ or $B^+B^-$ pair produced in an entangled state which gives an environment with a low number of particles in the final state and with kinematics that are constrained from the well defined initial state. This allows analysis of final states that include multiple neutral particles such as $K^0_S$ and $\pi^0$ as well as final states with neutrinos. The weakness is in the total number of $b$-hadrons produced which allowed for the limit $\mathscr{B}(B^0 \to \mu^+\mu^-) < 5.2\times10^{-8}$ to be set [7], and in the few $b$-hadron species accessible. A dedicated run above the $B_s\bar{B}_s$ threshold has been performed by Belle with a very limited statistics though allowing for limits on rare decays such as $B_s \to \gamma\gamma$ to be set.

The hadron collider experiments have the advantage of the large cross section for $b$-hadron production. The challenge is to trigger the events in the presence of the overwhelming background of events with only lighter hadrons produced. For final states involving only charged particles, background particles coming from the primary interaction vertex are not an issue but this is not the case for neutrals where the tracking system does not provide the means to distinguish between particles from a detached $b$-vertex and the primary vertex. In general, final states with more than one neutral particle are very difficult to reconstruct. Today the best limit set on a rare decay is $\mathscr{B}(B^0 \to \mu^+\mu^-) < 2.1 \times 10^{-10}$ [8]. The ATLAS and CMS experiments have a much smaller trigger bandwidth devoted to the decays of $b$-hadrons which means that they are only competitive with LHCb for a small number of final states.

The future will allow for the experimental understanding of rare decays to be further extended. The Belle II experiment [9] has just started taking data and will over the next eight years, in an environment similar to the $B$ Factories, acquire a dataset that is about a factor 50 larger than what Belle acquired. The ongoing upgrade I [10] of LHCb and upgrade II [11] planned for 2032 will allow for datasets of rare decays that are several orders of magnitude larger than what is analysed today. For ATLAS and CMS, the high luminosity LHC running conditions will be very challenging for rare decays but in particular for the $B^0 \to \mu^+\mu^-$ it might provide the first observation.

## 2. Radiative decays

Radiative decays, corresponding to $b \to s/d\gamma$ transitions, are generated by the electromagnetic dipole operator $\mathscr{O}_7$ in the SM. The contribution from the right-handed operator $\mathscr{O}'_7$ is suppressed by $m_{s/d}/m_b$, making the photon final state predominantly left-handed. Several observables such as the decay rate, photon helicity or *CP* and isospin asymmetries can be used to test the presence of BSM physics. From the theoretical point of view, inclusive decays, denoted $B \to X_{s/d}\gamma$, are much cleaner than exclusive ones, for which form factors and hadronic matrix elements have to be estimated. In particular the combined inclusive $(s+d)\gamma$ *CP* asymmetry is $\mathscr{O}(10^{-6})$ in the SM [12].

The inclusive branching fractions and *CP* asymmetries have been measured by the $B$ Factories using various techniques: reconstructing only the final state photon, adding leptonic or hadronic tagging of the other $b$-hadron, or summing together different exclusive decays. The current world averages from HFLAV are $\mathscr{B}(B \to X_s\gamma) = (3.32\pm15)\times10^{-6}$ and $\mathscr{B}(B \to X_d\gamma) = (9.2\pm3.0)\times10^{-6}$ [13], extrapolating the measurements to a photon energy larger than 1.6 GeV. These results are in good agreement with the SM predictions $\mathscr{B}(B \to X_s\gamma) = (3.36\pm0.23)\times10^{-6}$ and $\mathscr{B}(B \to X_d\gamma) = (1.73^{+0.12}_{-0.22})\times10^{-6}$ [14]. The measured *CP* asymmetries of the $s\gamma$ and $(s+d)\gamma$ final states are also found to agree with the SM with absolute uncertainties of 1 and 3% respectively.

Exclusive decays $B \to f\gamma$ are particularly interesting as they provide several methods to test the photon polarisation. The first one uses time-dependent tagged analyses to measure the $S_f$ and $C_f$ *CP* observables. The Belle and BaBar experiments have analysed various $B^0$ modes, the most precise result corresponding to the $K^*\gamma$ final state with an uncertainty of ~0.2 on $S_{K*\gamma}$ for a SM prediction of $\mathcal{O}(0.01)$. LHCb has recently obtained the first measurement of these parameters in a $B_s^0$ decay with Run1 data [15]. Another method consists in measuring the up-down asymmetry in $B \to K\pi\pi\gamma$ decays. This was performed by LHCb in four region of the $K\pi\pi$ system, obtaining a result inconsistent with 0 polarisation at more than $5\sigma$ [16]. The quantitative interpretation of this measurement in nevertheless complicated by the presence of different hadronic resonances. A last method to test the photon polarisation is to use angular distribution of radiative $\Lambda_b$ decays. The first step toward this goal has been done by LHCb that observed for the first time the $\Lambda_b \to \Lambda\gamma$ decay [17]. The photon polarisation is also accessible from an angular analysis of $B \to K^* ee$ decays at low masses of the di-electron system, where the rate is dominated by the electromagnetic dipole operator. Current measurements give a precision of around 0.15 on this [15].

Future measurements of inclusive decay rates will be performed by Belle II. The $\mathcal{B}(B \to X_s\gamma)$ results are systematically dominated and an uncertainty of about 3% should be achieved with the final Belle II dataset for a photon energy threshold $E_\gamma > 1.9$ GeV. Precision on the *CP* asymmetries of the $s\gamma$ and $(s+d)\gamma$ final states will be below 0.2 and 0.5% respectively, and the one of $S_{K*\gamma}$ is expected to be 0.03. With the Upgrade I and II, LHCb will improve the *CP* measurement in the $B_s^0 \to \phi\gamma$ channel and will also be competitive on the $B^0 \to K_s\pi^+\pi^-\gamma$ channel. Determination of the photon polarisation will also be improved thanks to baryonic $B$ decays and a $B \to K^* ee$ analyses.

## 3. Purely leptonic decays

The leptonic decays $B_q \to \ell^+\ell^-$, where $q = s, d$ are particularly rare in the SM. Indeed, in addition of being loop and CKM suppressed, they suffer from an additional helicity suppression, appearing when a pseudoscalar meson decay to two spin-1/2 particles. Within the framework of the effective Hamiltonian approach defined in (1), the SM branching fraction of $B_q \to \ell^+\ell^-$ can be expressed as

$$\mathcal{B}(B_q^0 \to \ell^+\ell^-)_{\mathrm{SM}} = \tau_{B_q} \frac{G_F^2\alpha^2}{16\pi^2} f_{B_q}^2 m_\ell^2 m_{B_q} \sqrt{1 - \frac{4m_\ell^2}{m_{B_q}^2}} |V_{tb}V_{tq}^*|^2 |\mathscr{C}_{10}^{\mathrm{SM}}|^2, \tag{2}$$

where $\tau_{B_q}$, and $m_{B_q}$ are the $B_q$ meson lifetime and mass, $\alpha$ is the electromagnetic constant, $m_\ell$ is the mass of the final state lepton, and $f_{B_q}$ is the $B_q$ meson decay constant. For the case of $B_s^0$ mesons, this expression, which is valid at $t = 0$, has to be corrected to take into account the fact that $B_s^0$ mesons oscillate before decay. The corresponding time-integrated branching fraction is expressed as [18]

$$\bar{\mathcal{B}}(B_s^0 \to \ell^+\ell^-)_{SM} = \frac{1 + y_s\mathcal{A}_{\Delta\Gamma}}{1 - y_s^2} \mathcal{B}(B_s^0 \to \ell^+\ell^-)_{SM}, \tag{3}$$

with $y_s = \Delta\Gamma_s/(2\Gamma_s) = 0.065 \pm 0.005$ [13] and $\mathcal{A}_{\Delta\Gamma} = 1$ in the SM. The SM predictions for the branching fractions are [19]

$$\begin{aligned}
\mathcal{B}(B^0 \to \mathrm{e}^+\mathrm{e}^-) &= (2.48 \pm 0.21) \times 10^{-15}, \bar{\mathcal{B}}(B_s^0 \to \mathrm{e}^+\mathrm{e}^-) = (8.54 \pm 0.55) \times 10^{-14}, \\
\mathcal{B}(B^0 \to \mu^+\mu^-) &= (1.06 \pm 0.09) \times 10^{-10}, \bar{\mathcal{B}}(B_s^0 \to \mu^+\mu^-) = (3.65 \pm 0.23) \times 10^{-9}, \\
\mathcal{B}(B^0 \to \tau^+\tau^-) &= (2.22 \pm 0.19) \times 10^{-8}, \bar{\mathcal{B}}(B_s^0 \to \tau^+\tau^-) = (7.73 \pm 0.49) \times 10^{-7}.
\end{aligned}$$

Their precision is limited by the knowledge of the hadronic decay constants and the CKM matrix elements.

In case where contributions from particles beyond the SM are allowed, the $|\mathscr{C}_{10}^{\ell SM}|^2$ factor of (2) is replaced by

$$|S|^2 \left(1 - \frac{4m_\ell^2}{m_{B_q}^2}\right) + |P|^2, \tag{4}$$

where

$$S = \frac{m_{B_q}^2}{2m_\ell}(\mathscr{C}_S^\ell - \mathscr{C}_S'^\ell), \quad \text{and} \quad P = (\mathscr{C}_{10}^\ell - \mathscr{C}_{10}'^\ell) + \frac{m_{B_q}^2}{2m_\ell}(\mathscr{C}_P^\ell - \mathscr{C}_P'^\ell). \tag{5}$$

From these equations, one can see that while $\mathscr{C}_{10}^{(\prime)\ell}$ is affected by the helicity suppression factor $m_\ell / m_{B_q}$, this is not the case for the scalar and pseudoscalar contributions. It is actually a unique property of the $B_q \to \ell^+\ell^-$ decay to be strongly helicity suppressed in the SM but not in the presence of BSM physics scalar operators, making it a 'golden channel' to search for new physics. One may note that a pseudoscalar contribution can also suppress the branching fraction in case of negative interference with $\mathscr{C}_{10}^\ell$. In case of BSM physics, $\mathscr{A}_{\Delta\Gamma}$ is expressed as

$$\mathscr{A}_{\Delta\Gamma} = \frac{\mathrm{Re}(P^2 - S^2)}{|P|^2 + |S|^2}. \tag{6}$$

The measurement of the branching fraction and $\mathscr{A}_{\Delta\Gamma}$, which is accessible through the measurement of the $B_s^0 \to \ell^+\ell^-$ effective lifetime, can therefore provide complementary information.

The experimental search for the $B_q \to \ell^+\ell^-$ decays started in the eighties with the CLEO, UA1 and Argus collaborations. The limits were then improved by the Tevatron and $B$ Factories experiments and are nowadays studied by the LHC experiments. Thanks to the high muon trigger and reconstruction efficiency of the LHC experiments, the analyses first focused on the muonic final state. The three experiments use a strategy based on a likelihood fit to the dimuon invariant mass in bins of a multivariate discriminant. The first evidence of the $B_s^0 \to \mu^+\mu^-$ decay has been obtained by LHCb in 2012 [20] and the first observation by a combined analysis of LHCb and CMS Run1 data [21]. The latest results from LHCb [22], ATLAS [8] and CMS [23] are based on data collected until 2016 and shown in Figure 2, where one can see a correlation between the $B_s^0$ and $B^0$ branching fractions due to the overlap of the two signals in the dimuon invariant mass. The highest significance is obtained by LHCb at $7.8\sigma$ with the measurement $\bar{\mathscr{B}}(B_s^0 \to \mu^+\mu^-) = (3.0 \pm 0.6^{+0.3}_{-0.2}) \times 10^{-9}$. A naive combination of the two-dimensional likelihoods leads to a compatibility with the SM expectation at the level of $\sim 2\sigma$. The $B^0 \to \mu^+\mu^-$ decay is still not observed and the most stringent limit is currently obtained by ATLAS at $2.1 \times 10^{-10}$ at 95% C.L. A measurement of the $B_s^0 \to \mu^+\mu^-$ effective lifetime was also obtained by the CMS and LHCb experiments, although still with a limited sensitivity to $\mathscr{A}_{\Delta\Gamma}$.

The electron modes are more difficult to study because of large Bremsstrahlung radiation. The current best limits are from the CDF collaboration at $8.3 \times 10^{-8}$ ($2.8 \times 10^{-7}$) for the $B^0$ ($B_s^0$) mode at 90% C.L [26], and are still about seven orders of magnitude larger than their SM prediction.

The tauonic modes are experimentally very challenging due to the $\tau$ decay which necessarily implies undetected final sates neutrinos. A first limit was obtained by BaBar on the $B^0$ mode, by fully reconstructing the event [27]. The LHCb experiment improved this result and obtained a first limit for the $\bar{\mathscr{B}}(B_s^0 \to \tau^+\tau^-)$ reconstructing both $\tau$ into the $3\pi\nu$ final state and performing a likelihood fit to the output of a boosted decision tree [28]. The corresponding limits are $2.1 \times 10^{-3}$ ($5.2 \times 10^{-3}$) for the $B^0$ ($B_s^0$) mode at 90% C.L.

Using Run3 data, LHCb will be able to measure the $B_s^0 \to \mu^+\mu^-$ branching fraction with a 8% uncertainty. If the Upgrade II is confirmed this number could be improved by a factor 2 at the end of the high luminosity LHC runs. Depending on their future trigger strategy, ATLAS and CMS will have measurements at 7–13% [29,30]. With this level of precision, it will be crucial to also improve the systematic uncertainties, which are up to now are dominated by the ratio of hadronisation fractions $f_s / f_d$. The $B^0 \to \mu^+\mu^-$ decay should be observed with the HL-LHC and the effective lifetime of the $B_s^0 \to \mu^+\mu^-$ decay could reach a precision of less than 0.1 ps, allowing to further constrain the BSM physics phase space.

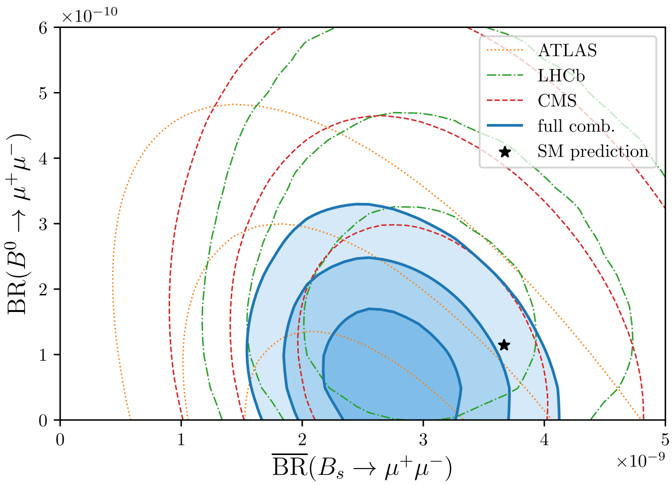


**Figure 2.** Two-dimensional likelihood contours in the space of the $B^0 \to \mu^+\mu^-$ and $B_s^0 \to \mu^+\mu^-$ branching ratios from individual measurements (thin contours), the naive combination (thick solid contours). Created using FLAVIO [24,25].

While LHCb will remain the only experiment being able to search for the $B_s^0 \to \tau^+\tau^-$ decay, with an expected limit at few $10^{-4}$ with 300 fb$^{-1}$, Belle II could be competitive for the $B^0 \to \tau^+\tau^-$ decay going below $10^{-4}$ [9].

## 4. Semileptonic decays

Semileptonic rare $b$-hadron decays are FCNC decays of the type illustrated in Figure 1. While the main measurements are coming from the decays $B^+ \to K^+\ell^+\ell^-$ and $B^0 \to K^{*0}\ell^+\ell^-$, the other $b \to s$ modes $B_s^0 \to \phi\mu^+\mu^-$, $\Lambda_b^0 \to \Lambda\mu^+\mu^-$, $B^+ \to K^{*+}\ell^+\ell^-$, $B^0 \to K_S^0\ell^+\ell^-$ and the rarer $b \to d$ modes $B^+ \to \pi^+\mu^+\mu^-$ and $\Lambda_b^0 \to p\pi\mu^+\mu^-$ have been measured as well. For several of them, the differential branching fraction measured in $q^2$ bins, where $q^2$ is the di-lepton invariant mass squared, tend to lie below the SM prediction [31–33]. The branching fraction of the decay $B^+ \to K^+\ell^+\ell^-$ is given as

$$\frac{\mathrm{d}\Gamma}{\mathrm{d}q^2} = \frac{G_F^2\alpha^2|V_{tb}V_{ts}^*|^2}{128\pi^5}|k|\beta\left\{\frac{2}{3}|k|^2\beta^2\left|\mathscr{C}_{10}f_+(q^2)\right|^2 + \frac{4m_\ell^2(m_B^2-m_K^2)^2}{q^2m_B^2}\left|\mathscr{C}_{10}f_0(q^2)\right|^2\right.$$
$$\left. + |k|^2\left[1-\frac{1}{3}\beta^2\right]\left|\mathscr{C}_9f_+(q^2)+2\mathscr{C}_7\frac{m_b+m_s}{m_B+m_K}f_T(q^2)\right|^2\right\}, \quad (7)$$

with $k$ the momentum of the kaon, $\beta = \sqrt{1-4m_\ell^2/q^2}$, and $f_0$, $f_+$, and $f_T$ the $B \to K$ scalar, vector and tensor form factors respectively. The expression in (7) is not the full story from an experimental point of view. The $K^+\ell^+\ell^-$ final state can also be reached through decays like $B^+ \to K^+\psi_X$ where $\psi_X$ represents any of the vector charmonium resonances that can subsequently decay to a pair of leptons. These decays are tree level Cabibbo favoured decays and thus several orders of magnitude more common than the $B^+ \to K^+\ell^+\ell^-$ decay. The $J/\psi$ and $\psi(2S)$ resonances are very narrow and can be excluded from any measurements by narrow vetos in the dilepton mass, but the $\psi$ resonances above the open charm threshold are wide, and while the resonances will predominantly decay to open charm there is still a component of decays to leptons that interfere with the semileptonic decay. In addition to this, the effect is not limited to the resonances and the influence of what is called *charm loops* is a hotly debated topic that

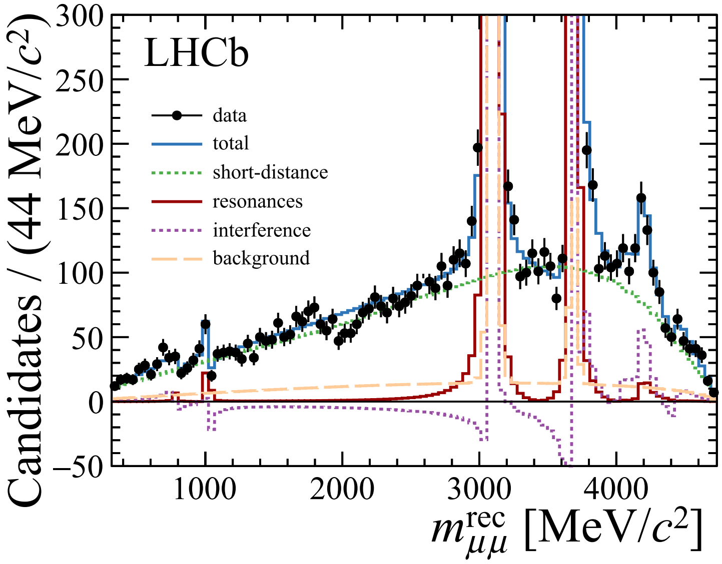


**Figure 3.** The differential branching fraction of the decay $B^+ \to K^+\mu^+\mu^-$ as a function of the dimuon mass. The contribution of the charmonium resonances (that reach far out through the top of the plot), including the interference with the semileptonic decay, can clearly be seen. From [37].

will have an influence on the decay even below the kinematic limit of two charm quark masses. To measure the Wilson coefficients from the branching fraction, two approaches can be taken. Either the measurement can be made in regions well away from the charmonium resonances, such that their contribution can be ignored [34–36]; or a fit, as seen in Figure 3, can be made that try to include all knowledge of how the charmonium decays will influence (7) and a fit made to the full range of dilepton masses [37]. While experimental measurements can provide some information about the form factors as a function of $q^2$, the overall scaling of the form factors is a purely theoretical calculation using light cone sum rules at low $q^2$ [38] and lattice QCD at high $q^2$ [39]. Measurements of the $B^+ \to K^+\ell^+\ell^-$ decay are thus mainly sensitive to the sum in quadrature of $\mathscr{C}_9$ and $\mathscr{C}_{10}$ and results in an overall uncertainty of the Wilson coefficients of around 6%.

The decay $B^0 \to K^{*0}\ell^+\ell^-$ with $K^{*0} \to K^+\pi^-$ provides as a four-body decay a much richer phenomenology than the $B^+ \to K^+\ell^+\ell^-$ decay. In the angular distribution of the decay products, the different Wilson coefficients contribute in different ways, making it possible to measure them with much lower relative correlation as well as becoming less sensitive to the overall normalisation of the form factors. The full expression for the angular distribution in regions not affected by charmonium resonances can be found in Ref. [40]. The coefficients of the angular distribution can be measured directly, but from a theoretical point of view it is better to experimentally measure a number of observables that are formed from the coefficients. The idea in the observables is to form ratios where the uncertainty is the forms factors are minimised [41–43]. The ATLAS [44], Belle [45], CMS [46] and LHCb [47] experiments have all measured these observables. The most famous one of these is the $P_5'$ observable as it, as seen in Figure 4, have shown a significant deviation from the SM prediction as calculated in Ref. [48]. The branching fraction is measured as the differential branching fractions in the regions well away from the charmonium regions in $q^2$, then normalised relative to the branching fraction of

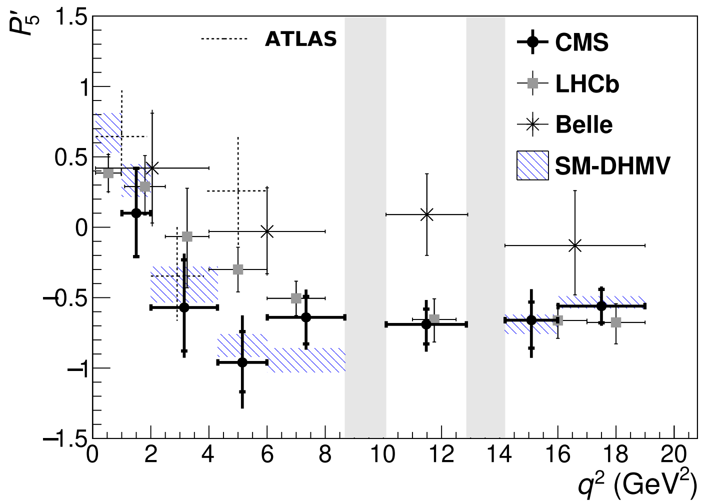


**Figure 4.** The $P_5'$ observable as measured in bins of $q^2$. All experimental measurements compared to a theoretical prediction. Figure adapted from [46].

$B^0 \to K^{*0} J/\psi$ as measured at the $B$ Factories and finally extended to the full $q^2$ region using a theoretical model for the interpolation. For $B^0 \to K^{*0}\mu^+\mu^-$, HFLAV [13] is calculating the average

$$\mathscr{B}(B^0 \to K^{*0}\mu^+\mu^-) = (1.05 \pm 0.07) \times 10^{-6}, \tag{8}$$

where the uncertainty is dominated by the normalisation.

Regarding the understanding of the charm loop effects, there is promising progress on the theoretical side based on an analytical dispersion relation which can take away the need to calculate the charm loop effect directly close to the charmonium resonances [49]. There is also a proposal to fit the angular distribution of $B^0 \to K^{*0}\mu^+\mu^-$ in an unbinned way as a function of $q^2$ and include the charmonium resonance regions [50].

To avoid the theoretical uncertainties from the charmonium resonances, it is also possible to look for decays of the type $B \to h\nu\overline{\nu}$ where $h$ represents a light-quark hadron. As the charmonium resonances only couple to $\nu\overline{\nu}$ through the weak force, the interference from those is insignificant and a measurement of the final state is a direct measurement of the semileptonic decay, independent of $q^2$. However, to identify a decay with two neutrinos in the final state is a challenge and only possible at the $B$ Factories where the full or partial reconstruction of one of the two $B$ mesons produced allows the kinematics of the other $B$ mesons to be fully constrained. Using this method, Belle [51] has with its full dataset put branching fraction limits in the region of $10^{-5}$ on a number of final states. The measurement of the decays with neutrinos, in connection with the decays to charged leptons as discussed above, gives detailed information on any type of BSM physics [52].

Semileptonic decays into $\tau$ leptons are still poorly known; only BaBar set a limit on the $\mathscr{B}(B \to K^+\tau^+\tau^-)$ at $2.25 \times 10^{-3}$ [53]. Both LHCb and Belle II should be able to study these decays in the future, reaching limits at the order of $10^{-5}$. The SM value of these decays should be reachable with a future high-luminosity $Z$ factory [54].

## 5. Test of lepton flavour universality

In the SM, the electroweak bosons couple equally to the leptons of different families. This lepton flavour universality (LFU) is an accidental property of the SM and could be violated by BSM

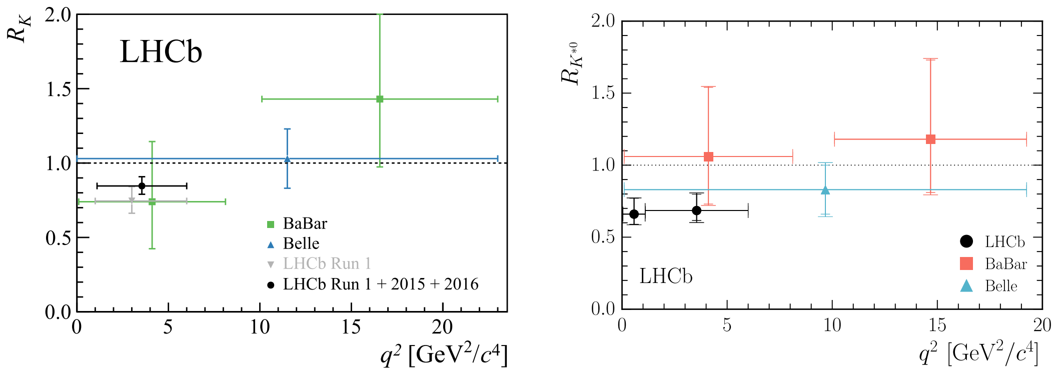


**Figure 5.** Comparison of the different experimental measurements of $R_K$ (left) and $R_K^*$ (right) as function of $q^2$. Figures from [55, 56]. A new preliminary measurement of $R_K^*$ by Belle II is also available in [58].

processes. Measurement of ratios of decay rates to different final state leptons, referred to as $R$-ratios, are expected to be 1 modulo phase-space factors related to the lepton masses, and thus provide very clean tests of the SM. In the past years some tensions in the $R_K$ and $R_K^*$ ratios, defined as

$$R_K^{(*)} = \mathscr{B}(B \to K^{(*)}\mu^+\mu^-)/\mathscr{B}(B \to K^{(*)}e^+e^-), \tag{9}$$

have appeared at the level of ~2.5$\sigma$. This is shown in Figure 5, where it can be seen that the LHCb measurements are below the SM expectation [55, 56]. While LHCb is using only the $K^+$ and $K^{*0}$ modes and actually measures double ratios to the resonant $B \to K^{(*)} J/\psi$ mode in order to mitigate the reconstruction differences between electrons and muons, the $B$ Factories also includes the $K_s^0$ and $K^{*\pm}$ channels [36, 57, 58]. Nevertheless, they have quite large statistical uncertainties and their results are both compatible with LHCb and the SM.

Belle also performed the first test of LFU with angular observable [45]. The results are limited by the size of the data sample but Belle II will be able to provide more stringent constraints.

These tensions triggered quite some excitement in the flavour community since similar discrepancies are also observed in test of LFU in charged currents as reviewed in Ref. [13]. More data are however necessary to confirm these effects and if the central values stay the same, both LHCb and Belle II will be able to confirm LFU violation in $b \to s\ell^+\ell^-$ processes around 2025 [59]. Search for LFU violation has been carried out in the $\Lambda_b^0 \to pK^-\ell^+\ell^-$ [60] and $B_s^0 \to \phi\ell^+\ell^-$ should appear in the coming years. The ATLAS and CMS experiments have improved their trigger for $B$ physics and plan to obtain first measurements of $R$-ratios with LHC Run 2 data.

## 6. Search for lepton flavour/number violating decays

Lepton number is a quantum number intrinsic to each elementary particle that is defined for each family (or flavour). In the SM and in absence of neutrino masses, lepton flavour number is conserved, even though this is not associated to a fundamental symmetry. However, the observation of neutrino mixing explicitly implies that lepton flavour is not conserved in the neutrino sector. It also implies a violation of lepton flavour in the charged sector through loop processes containing neutrinos, but at a rate far from reachable by any current and future experiment ($<10^{-40}$) as underlined in [61]. The observation of a lepton flavour violating process (LFV) in the charged sector would thus be an evident sign of BSM physics. Lepton number violating (LNV) processes such as $B^- \to \pi^+\mu^-\mu^-$ provide hints about the nature of the neutrinos, as they could occur if the neutrino is of Majorana type.

An exhaustive review of LFV and LNV decays can be found in [13]. Most of the $B^0$ results were obtained by BaBar at the level $10^{-5}$–$10^{-7}$, the weakest limits being for final states with $\tau$ leptons. The LHCb experiment put more stringent constraints on dimuon final states, for example in the $B^- \to \pi^+\mu^-\mu^-$ decays where limits at $\sim 10^{-9}$ are obtained. The best limits for the purely leptonic $e\mu$ and $\tau\mu$ final states are also from LHCb, at the level of few $10^{-9}$ and few $10^{-5}$, respectively.

In the future, improvements of these limits by 1 to 2 orders of magnitudes are foreseen by Belle II and LHCb. Tauonic modes will particularly benefit from an improved tagging method at Belle II [62], and improved trigger and tracking efficiency from the LHCb upgrade.

## 7. Interpretation

When considered all together, there are several hundred experimentally observed branching fractions, angular observables and asymmetries from rare $b$-hadron decays. Within the framework of the effective Hamiltonian as defined in Section 1.1, it is possible in what is called *global fits* to put all the measurements together, combine them with the theoretical uncertainties arising from QCD and fit for a consistent set of Wilson coefficients. Within the SM, the Wilson coefficients are well known, and it is thus possible in this way to ask if the data is compatible with a set of measurements from the SM or not. It can also be asked which set of Wilson coefficients are most likely to give the resulting experimental measurements.

A large number of papers has been published with global fits in recent years. The overall conclusion of these papers is that within our current understanding of the theoretical uncertainties, there is a tension between the SM prediction and the experimental results. The values of the Wilson coefficients that are giving the highest likelihood of the observed data are where a negative contribution to $\mathscr{C}_9^\mu$ and/or a positive contribution to $\mathscr{C}_{10}^\mu$ in addition to the SM contribution is allowed. An example [25] of such a global fit is seen in Figure 6(left). The measurements of $R_K$ and $R_{K^*}$ give a weaker indication that the Wilson coefficients for electrons and muons are different. Different global fits more or less agree on the Wilson coefficients that give the highest likelihood of the observed data and depending on the exact data used and theoretical assumptions made, make a BSM physics scenario favoured over the SM with significances of 4–7$\sigma$ [25, 63–65]. This large variation is dominated by the uncertainties that are assigned to the non-factorisable effects in the decay and due to the influence of charm loops in regions of $q^2$ where measurements are made for the semileptonic decays.

There has also been many papers that discuss which type of BSM physics could explain the observed pattern in the Wilson coefficients. These models are broadly divided up into models that introduce a new $U(1)$ symmetry to provide a new $Z'$ vector boson with a gauged $L_\mu - L_\tau$ symmetry [67, 68], and models that introduce leptoquarks [66, 69]. In [66], the flavour anomalies are analysed in the context of a simplified model with a vector leptoquark $U_1$ that can couple to both left and right-handed SM fields. Figure 6 (right) shows the preferred fit region in a plane representing different LFV decays. The current limits from $\tau \to \mu\gamma$ and $B_s^0 \to \tau\mu$ decays start to corner this model, demonstrating the interplay between semileptonic and LFV decays. An example of constraints from the $\bar{\mathscr{B}}(B_s^0 \to \mu^+\mu^-)$ measurement in the $U_1$ vector leptoquark scenario is shown in Figure 7 for current and future measurement [24]. One can see that this observable can constrain leptoquark masses well above what is reachable by direct LHC searches, and that the measurement of $\mathscr{A}_{\Delta\Gamma}$ allows to break the degeneracies.

## 8. Conclusion

Rare $b$-hadron decays have been extensively studied in the past decades at different facilities. Among the large number of measured observables, some mainly related to semileptonic $b \to s\ell\ell$

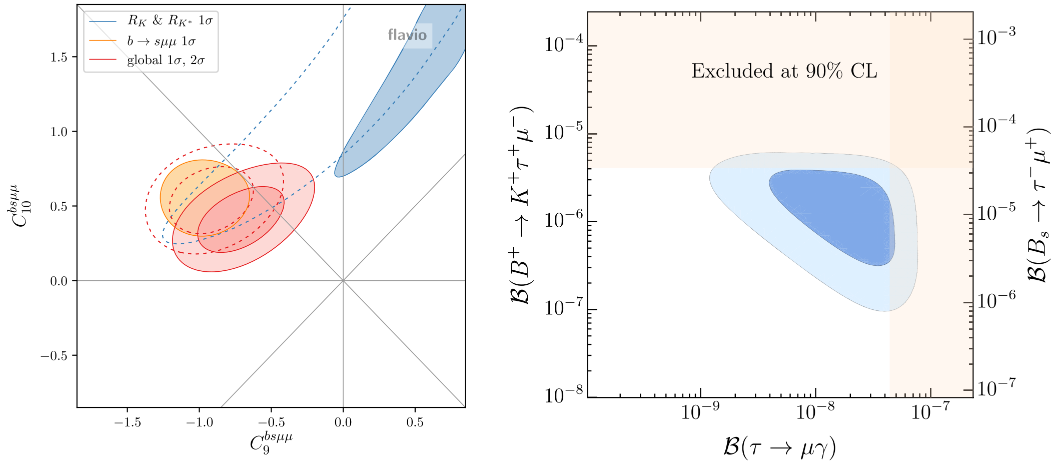


**Figure 6.** (left) Likelihood contours of the global fit and fits to subset of observables in the plane $\mathscr{C}_{10}^{\mu}$ vs $\mathscr{C}_9^{\mu}$ [25]. Solid (dashed) contours include (exclude) the Moriond 2019 results for $R_K$ and $R_K^*$. (right) Prefered fit region of a $U_1$ leptoquark model at 1 (light blue) and 2 (dark blue) $\sigma$ as function of different LFV decays [66].

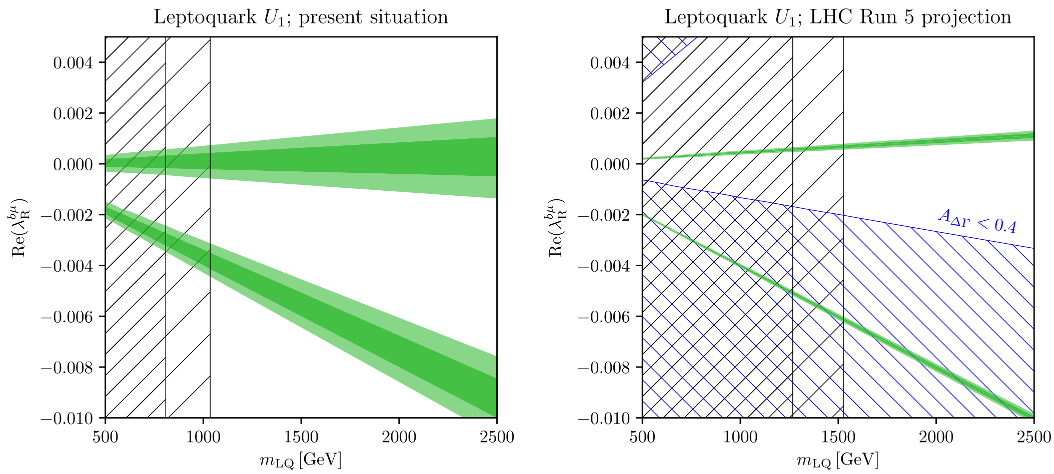


**Figure 7.** Current (left) and future (right) constraints from $B_s^0 \to \mu^+\mu^-$ decays in the plane defined by the mass and coupling for the LQs $U_1$. The green bands correspond to the regions allowed by $\bar{\mathscr{B}}(B_s^0 \to \mu^+\mu^-)$ at the 1 and 2$\sigma$ level. The black hatched regions show the exclusion from direct searches. The blue hatched region on the right plot shows the exclusion that would bring a measurement of $\mathscr{A}_{\Delta\Gamma}$ with SM-like central value. Figures from [24].

decays have shown tensions with respect to their SM prediction. The combination of smaller statistical uncertainties from the larger datasets analysed by LHCb and Belle II, a first measurement of the decay $B^0 \to \mu^+\mu^-$ and theoretical improvements in the understanding of the charm loop effects, it should be possible within the next decade to conclusively determine if the current indications of BSM physics are the first signs of a new sector of physics or if they are an interplay between statistical effects and issues with our current understanding of non-factorisable QCD. Improvements of measurements in radiative and LFV decays, as well as rare decays into $\tau$ leptons are also expected, which will allow to further reduce the BSM physics phase space.

## References


[1] T. Mannel, *Effective Field Theories in Flavour Physics*, Springer-Verlag, Berlin, Heidelberg, 2004.

[2] LHCb collaboration, A. A. Alves Jr. *et al.*, "The LHCb detector at the LHC", *JINST* **3** (2008), article ID S08005.

[3] LHCb collaboration, R. Aaij *et al.*, "LHCb detector performance", *Int. J. Mod. Phys. A* **30** (2015), article ID 1530022.

[4] ATLAS, G. Aad *et al.*, "The ATLAS experiment at the CERN large hadron collider", *JINST* **3** (2008), article ID S08003.

[5] CMS, S. Chatrchyan *et al.*, "The CMS experiment at the CERN LHC", *JINST* **3** (2008), article ID S08004.

[6] Belle II collaboration, T. Abe *et al.*, "Belle II Technical Design Report", 2010, preprint, https://arxiv.org/abs/1011.0352.

[7] BaBar collaboration, B. Aubert *et al.*, "Search for decays of $B^0 \to$ mesons into $e^+e^-$, $\mu^+\mu^-$, and $e^\pm\mu^\mp$ final states", *Phys. Rev. D* **77** (2008), article ID 032007.

[8] ATLAS collaboration, M. Aaboud *et al.*, "Study of the rare decays of $B_s^0$ and $B^0$ mesons into muon pairs using data collected during 2015 and 2016 with the ATLAS detector", *J. High Energy Phys.* **2019** (2019), article ID 98.

[9] Belle II collaboration, W. Altmannshofer *et al.*, "The Belle II Physics Book", 2018, preprint, https://arxiv.org/abs/1808.10567.

[10] LHCb collaboration, I. Bediaga *et al.*, "Framework TDR for the LHCb Upgrade: Technical Design Report", Tech. Report CERN-LHCC-2012-007. LHCb-TDR-12, 2012.

[11] LHCb collaboration, R. Aaij *et al.*, "Expression of Interest for a Phase-II LHCb Upgrade: Opportunities in flavour physics, and beyond, in the HL-LHC era", Tech. Report CERN-LHCC-2017-003, CERN, Geneva, 2017.

[12] T. Hurth, E. Lunghi, W. Porod, "Untagged $\bar{B} \to X_{s+d}\gamma$ CP asymmetry as a probe for new physics", *Nucl. Phys. B* **704** (2005), no. 1-2, p. 56-74.

[13] Heavy Flavor Averaging group (HFLAV), Y. S. Amhis *et al.*, "Averages of $b$-hadron, $c$-hadron, and $\tau$-lepton properties as of 2018", 2019, preprint, https://arxiv.org/abs/1909.12524.

[14] M. Misiak *et al.*, "Updated NNLO QCD predictions for the weak radiative B-meson decays", *Phys. Rev. Lett.* **114** (2015), article ID 221801.

[15] LHCb collaboration, R. Aaij *et al.*, "Observation of photon polarization in the $b \to s\gamma$ transition", *Phys. Rev. Lett.* **112** (2014), article ID 161801.

[16] LHCb collaboration, R. Aaij *et al.*, "First observation of the radiative decay $\Lambda_b^0 \to \Lambda\gamma$ ", *Phys. Rev. Lett.* **123** (2019), article ID 031801.

[17] LHCb collaboration, R. Aaij *et al.*, "Measurement of $CP$-violating and mixing-induced observables in $B_s^0 \to \phi\gamma$ decays", *Phys. Rev. Lett.* **123** (2019), article ID 081802.

[18] K. De Bruyn *et al.*, "Probing new physics via the $B_s^0 \to \mu^+\mu^-$ effective lifetime", *Phys. Rev. Lett.* **109** (2012), article ID 041801.

[19] C. Bobeth *et al.*, "$B_{s,d} \to l^+ l^-$ in the standard model with reduced theoretical uncertainty", *Phys. Rev. Lett.* **112** (2014), article ID 101801.

[20] LHCb collaboration, R. Aaij *et al.*, "First evidence for the decay $B_s^0 \to \mu^+\mu^-$", *Phys. Rev. Lett.* **110** (2013), article ID 021801.

[21] LHCb and CMS collaborations, V. Khachatryan *et al.*, "Observation of the rare $B_s^0 \to \mu^+\mu^-$ decay from the combined analysis of CMS and LHCb data", *Nature* **522** (2015), p. 68-72.

[22] LHCb collaboration, R. Aaij *et al.*, "Measurement of the $B_s^0 \to \mu^+\mu^-$ branching fraction and effective lifetime and search for $B^0 \to \mu^+\mu^-$ decays", *Phys. Rev. Lett.* **118** (2017), article ID 191801.

[23] CMS collaboration, "Measurement of properties of $B_s^0 \to \mu^+\mu^-$ decays and search for $B^0 \to \mu^+\mu^-$ with the CMS experiment", Tech. Report CMS-PAS-BPH-16-004, CERN, Geneva, 2019.

[24] W. Altmannshofer, C. Niehoff, D. M. Straub, "$B_s \to \mu^+\mu^-$ as current and future probe of new physics", *J. High Energy Phys.* **2017** (2017), article ID 76.

[25] J. Aebischer *et al.*, " $B$-decay discrepancies after Moriond 2019", *Eur. Phys. J. C* **80** (2020), article ID 252.

[26] CDF collaboration, T. Aaltonen *et al.*, "Search for the decays $B_s^0 \to e^+\mu^-$ and $B_s^0 \to e^+e^-$ in CDF run II", *Phys. Rev. Lett.* **102** (2009), article ID 201801.

[27] BaBar collaboration, B. Aubert *et al.*, "A search for the rare decay $B^0 \to \tau^+\tau^-$ at BABAR", *Phys. Rev. Lett.* **96** (2006), article ID 241802.

[28] LHCb collaboration, R. Aaij *et al.*, "Search for the decays $B_s^0 \to \tau^+\tau^-$ and $B^0 \to \tau^+\tau^-$", *Phys. Rev. Lett.* **118** (2017), article ID 251802.

[29] ATLAS collaboration, "Prospects for the $\mathscr{B}(B_{(s)}^0 \to \mu^+\mu^-)$ measurements with the ATLAS detector in the Run 2 and HL-LHC data campaigns", Tech. Report ATL-PHYS-PUB-2018-005, CERN, Geneva, 2018.

[30] CMS collaboration, Measurement of rare $B \to \mu^+\mu^-$ decays with the Phase-2 upgraded CMS detector at the HL-LHC.

[31] LHCb collaboration, R. Aaij *et al.*, “Differential branching fractions and isospin asymmetries of $B \to K^{(*)}\ \mu^+\ \mu^-$ decays”, *J. High Energy Phys.* **2014** (2014), article ID 133.
[32] LHCb collaboration, R. Aaij *et al.*, “Differential branching fraction and angular analysis of $\Lambda_b^0 \to \Lambda\mu^+\mu^-$ decays”, *J. High Energy Phys.* **2015** (2015), article ID 115, [Erratum: *J. High Energy Phys.* **09** (2018), 145].
[33] LHCb collaboration, R. Aaij *et al.*, “Angular analysis and differential branching fraction of the decay $B_s^0 \to \phi\mu^+\mu^-$”, *J. High Energy Phys.* **2015** (2015), article ID 179.
[34] LHCb collaboration, R. Aaij *et al.*, “Differential branching fraction and angular analysis of the $B^+ \to K^+\ \mu^+\ \mu^-$ decay”, *J. High Energy Phys.* **02** (2013), article ID 105.
[35] BaBar collaboration, B. Aubert *et al.*, “Direct CP, lepton flavor and isospin asymmetries in the decays $B \to K^{(*)}\ \ell^+\ \ell^-$”, *Phys. Rev. Lett.* **102** (2009), article ID 091803.
[36] Belle collaboration, J.-T. Wei *et al.*, “Measurement of the differential branching fraction and forward-backword asymmetry for $B \to K^{(*)}\ \ell^+\ \ell^-$”, *Phys. Rev. Lett.* **103** (2009), article ID 171801.
[37] LHCb collaboration, R. Aaij *et al.*, “Measurement of the phase difference between short- and long-distance amplitudes in the $B^+ \to K^+\ \mu^+\ \mu^-$ decay”, *Eur. Phys. J. C* **77** (2017), article ID 161.
[38] W. Altmannshofer *et al.*, “Symmetries and asymmetries of $B \to K^*\ \mu^+\ \mu^-$ decays in the standard model and beyond”, *J. High Energy Phys.* **2009** (2009), no. 01, article ID 19.
[39] J. A. Bailey *et al.*, “$B \to Kl^+\ l^-$ decay form factors from three-flavor lattice QCD”, *Phys. Rev. D* **93** (2016), article ID 025026.
[40] F. Kruger, L. M. Sehgal, N. Sinha, R. Sinha, “Angular distribution and *CP* asymmetries in the decays $\bar{B} \to K^-\pi^+e^-e^+$ and $\bar{B} \to \pi^-\pi^+e^-e^+$ ”, *Phys. Rev. D* **61** (2000), article ID 114028, [Erratum: *Phys. Rev. D* **63** (2001), 019901].
[41] A. Ali, T. Mannel, T. Morozumi, “Forward backward asymmetry of dilepton angular distribution in the decay $b \to sl^+\ l^-$”, *Phys. Lett. B* **273** (1991), no. 4, p. 505-512.
[42] U. Egede *et al.*, “New observables in the decay mode $\bar{B}_d \to \bar{K}^{*0} l^+ l^-$”, *J. High Energy Phys.* **2008** (2008), no. 11, article ID 032.
[43] S. Descotes-Genon, T. Hurth, J. Matias, J. Virto, “Optimizing the basis of $B \to K^*\ ll$ observables in the full kinematic range”, *J. High Energy Phys.* **2013** (2013), article ID 137.
[44] ATLAS collaboration, M. Aaboud *et al.*, “Angular analysis of $B_d^0 \to K^*\mu^+\mu^-$ decays in *pp* collisions at $\sqrt{s} = 8$ TeV with the ATLAS detector”, *J. High Energy Phys.* **2018** (2018), article ID 47.
[45] Belle collaboration, S. Wehle *et al.*, “Lepton-flavor-dependent angular analysis of $B \to K^*\ \ell^+\ \ell^-$”, *Phys. Rev. Lett.* **118** (2017), article ID 111801.
[46] CMS collaboration, A. M. Sirunyan *et al.*, “Measurement of angular parameters from the decay $\mathrm{B}^0 \to \mathrm{K}^{*0}\ \mu^+\ \mu^-$ in proton-proton collisions at $\sqrt{s} = 8$ TeV”, *Phys. Lett. B* **781** (2018), p. 517-541.
[47] LHCb collaboration, R. Aaij *et al.*, “Angular analysis of the $B^0 \to K^{*0}\ \mu^+\ \mu^-$ decay using 3 $\mathrm{fb}^{-1}$ of integrated luminosity”, *J. High Energy Phys.* **2016** (2016), article ID 104.
[48] S. Descotes-Genon, L. Hofer, J. Matias, J. Virto, “On the impact of power corrections in the prediction of $B \to K^*\ \mu^+\ \mu^-$ observables”, *J. High Energy Phys.* **2014** (2014), article ID 125.
[49] C. Bobeth, M. Chrzaszcz, D. van Dyk, J. Virto, “Long-distance effects in $B \to K^*\ \ell\ell$ from analyticity”, *Eur. Phys. J. C* **78** (2018), article ID 451.
[50] T. Blake *et al.*, “An empirical model to determine the hadronic resonance contributions to $\overline{B}^0 \to \overline{K}^{*0}\mu^+\mu^-$ transitions”, *Eur. Phys. J. C* **78** (2018), article ID 453.
[51] Belle collaboration, J. Grygier *et al.*, “Search for $B \to h\nu\bar{\nu}$ decays with semileptonic tagging at Belle”, *Phys. Rev. D* **96** (2017), article ID 091101, [Addendum: *Phys. Rev. D* **97** no.9, (2018), 099902].
[52] W. Altmannshofer, A. J. Buras, D. M. Straub, M. Wick, “New strategies for New Physics search in $B \to K^*\nu\bar{\nu}$, $B \to K\nu\bar{\nu}$ and $B \to X_s\nu\bar{\nu}$ decays”, *J. High Energy Phys.* **04** (2009), article ID 22.
[53] BaBar collaboration, J. P. Lees *et al.*, “Search for $B^+ \to K^+\tau^+\tau^-$ at the BaBar experiment”, *Phys. Rev. Lett.* **118** (2017), article ID 031802.
[54] FCC collaboration, A. Abada *et al.*, “FCC-ee: The lepton collider: Future circular collider conceptual design report volume 2”, *Eur. Phys. J. Spec. Top.* **228** (2019), p. 261-263.
[55] LHCb collaboration, R. Aaij *et al.*, “Search for lepton-universality violation in $B^+ \to K^+\ \ell^+\ \ell^-$ decays”, *Phys. Rev. Lett.* **122** (2019), article ID 191801.
[56] LHCb collaboration, R. Aaij *et al.*, “Test of lepton universality with $B^0 \to K^{*0}\ \ell^+\ \ell^-$ decays”, *J. High Energy Phys.* **2017** (2017), article ID 55.
[57] BaBar collaboration, J. P. Lees *et al.*, “Measurement of branching fractions and rate asymmetries in the rare decays $B \to K^{(*)}\ l^+\ l^-$”, *Phys. Rev. D* **86** (2012), article ID 032012.
[58] Belle collaboration, A. Abdesselam *et al.*, “Test of lepton flavor universality in $B \to K^*\ \ell^+\ \ell^-$ decays at Belle”, 2019, preprint, https://arxiv.org/abs/1904.02440.
[59] S. Bifani, S. Descotes-Genon, A. Romero Vidal, M.-H. Schune, “Review of lepton universality tests in *B* decays”, *J. Phys. G* **46** (2019), article ID 023001.

[60] LHCb collaboration, R. Aaij *et al.*, "Test of lepton universality with $\Lambda_b^0 \to pK^- \ell^+ \ell^-$ decays", *J. High Energy Phys.* **05** (2020), article ID 40.
[61] S. T. Petcov, "The processes mu → e Gamma, mu → e e anti-e, Neutrino' → Neutrino gamma in the Weinberg-Salam model with neutrino mixing", *Sov. J. Nucl. Phys.* **25** (1977), p. 340, [Erratum: *Sov. J. Nucl. Phys.* **25** (1977), 698, Erratum: *Yad. Fiz.* **25** (1977), 1336].
[62] T. Keck *et al.*, "The full event interpretation", *Comput. Softw. Big Sci.* **3** (2019), article ID 6.
[63] M. Alguero *et al.*, "Emerging patterns of New Physics with and without Lepton Flavour Universal contributions", *Eur. Phys. J. C* **79** (2019), article ID 714.
[64] A. Arbey *et al.*, "Update on the $b \to s$ anomalies", *Phys. Rev. D* **100** (2019), article ID 015045.
[65] M. Ciuchini *et al.*, "New Physics in $b \to s\ell^+ \ell^-$ confronts new data on Lepton Universality", *Eur. Phys. J. C* **79** (2019), article ID 719.
[66] C. Cornella, J. Fuentes-Martin, G. Isidori, "Revisiting the vector leptoquark explanation of the B-physics anomalies", *J. High Energy Phys.* **2019** (2019), article ID 168.
[67] X. G. He, G. C. Joshi, H. Lew, R. R. Volkas, "New $Z$-prime phenomenology", *Phys. Rev. D* **43** (1991), no. 1, p. R22-R24.
[68] W. Altmannshofer, P. Stangl, D. M. Straub, "Interpreting hints for lepton flavor universality violation", *Phys. Rev. D* **96** (2017), article ID 055008.
[69] J. C. Pati, A. Salam, "Unified lepton-hadron symmetry and a gauge theory of the basic interactions", *Phys. Rev. D* **8** (1973), no. 4, p. 1240-1251.

*Comptes Rendus*
*Physique*
**2020**, 21, nº 1, p. 107-119
https://doi.org/10.5802/crphys.12

A perspective of High Energy Physics from precision measurements
*La physique des Hautes Energies du point de vue des mesures de précision*

# Rare kaon decays

## *Les désintégrations rares des kaons*

**Augusto Ceccucci**[*, a] **and Cristina Lazzeroni**[b]

[a] EP Department, CERN, 1211 Geneva 23, CH, Switzerland

[b] School of Physics and Astronomy, University of Birmingham, UK.

*E-mails:* augusto.ceccucci@cern.ch (A. Ceccucci), cristina.lazzeroni@cern.ch (C. Lazzeroni).

**Abstract.** The article reviews the status of rare K decay physics. The explored area covers a broad program, ranging from precise tests of flavour theory and *CP*-violation to the searches for explicit violations of the standard model and the study of strong interactions at low energies.

**Résumé.** Cet article discute l'état de l'art de la physique des désintégrations rares des kaons. Tests de précision des transitions de saveurs de quarks et de la brisure de la symétrie *CP*, recherches explicites de brisure des lois de conservation du modèle standard et étude des interactions fortes à basse énergie forment le programme de cette revue.

**Keywords.** Kaon, Decay, CP symmetry violation, Rare processes, CKM tests, New physics searches.

**Mots-clés.** Kaon, Désintégration, Violation de la symétrie CP, Processus rares, Tests CKM, Recherches en Nouvelle Physique.

## 1. Introduction

The discovery of kaons and the study of their properties are seminal for the building of the Standard Model (SM). Strangeness, flavour mixing, *CP*-Violation, lack of flavour changing neutral currents (FCNC), GIM mechanism [1], all these pillars of the SM trace their origin in strange particles. We are still lacking a theory explaining why fundamental fermions appear in three families and many outstanding questions such as the baryon asymmetry of the Universe or the puzzle of dark matter remain unanswered. The interplay of symmetry violation, such as *CP*, and the mixing of quarks remains one of the most active areas of experimental research in high energy physics. To summarise the overarching strategy of flavour physics, one can say that in the SM:

* Corresponding author.

(i) The Higgs sector is the source of flavour violation. It is when the Higgs acquires a vacuum expectation value that the quarks get a physical mass and the charged-current $W^{\pm}$ interations couple to the quark interaction eigenstates with couplings given by the Cabibbo-Kobayashi and Maskawa (CKM) matrix [2, 3];
(ii) So far all manifestations of *CP* violation and quark mixing are compatible with the single complex phase of the CKM matrix;
(iii) Further experimental investment in the field of flavour physics is justified by the high energy scales addressed by these studies: in many cases they exceed the direct reach achievable at colliders.

The study of kaons are not only complementary to those performed with $B$ mesons but also mutually reinforcing: we need to over-constrain the CKM matrix with precise determinations of its parameters extracted independently from different quark systems. A discrepancy between the determinations of the parameters obtained from $K$ and $B$ would signal physics beyond the SM (BSM).

What makes rare $K$ decays special is the unique combination of precise theoretical predictions and the strong suppression of the SM contributions. These two factors make the detection of BSM contribution relatively plausible. The SM contribution to rare kaon decays are tiny and well predicted. In some cases they are not only absent at tree level but also suppressed at loop levels. Final states with a neutrino - antineutrino pair are the least affected by long distance contributions.

It should be emphasised that to explore the flavour structure, it is not enough to check the unitarity of CKM, which is such almost by construction: one has to study genuine [4] electro-weak FCNC processes. Among these, the $K \to \pi\nu\bar{\nu}$ ones described in the next section are a particularly interesting combination of theoretical cleanliness and experimental challenge.

## 2. $K \to \pi\nu\bar{\nu}$: gold-plated decays to test the CKM paradigm beyond the SM

The two decay modes $K^+ \to \pi^+\nu\bar{\nu}$ and $K_L^0 \to \pi^0\nu\bar{\nu}$ can be used to quantitatively check the description of quark mixing and *CP*-violation independently from information extracted from the $B$ system. To see why this is the case it is convenient to express the formulas for the branching fractions in terms of contributions from the different loop functions. Following [5] the SM predictions can be written as:

$$\mathscr{B}(K^+ \to \pi^+\nu\bar{\nu}) = \kappa_+(1+\Delta_{\rm EM})\left[\left(\frac{\mathscr{I}m\lambda_t}{\lambda^5}X(x_t)\right)^2 + \left(\frac{\mathscr{R}e\lambda_c}{\lambda}P_c(X) + \frac{\mathscr{R}e\lambda_t}{\lambda^5}X(x_t)\right)^2\right],$$

with $\Delta_{\rm EM} = -0.003$ the electromagnetic radiative corrections, $x_t = m_t^2/M_W^2$, $\lambda = |V_{us}|$, $\lambda_i = V_{is}^* V_{id}$ the relevant combinations of CKM matrix elements, $X$ and $P_c(X)$ the loop functions for the top and charm quark respectively, and

$$\kappa_+ = (5.173 \pm 0.025) \times 10^{-11}\left[\frac{\lambda}{0.225}\right]^8$$

the parameter encoding the relevant hadronic matrix elements extracted from a suitable combination of semi-leptonic rates. As the formula shows, $\mathscr{B}(K^+ \to \pi^+\nu\bar{\nu})$ depends on the sum of the square of the imaginary part of the top loop (*CP* violating) and the square of the sum of the charm contribution and the real part of the top loop.

The corresponding formulas for $K_L^0$ are:

$$\mathscr{B}(K_L^0 \to \pi^0\nu\bar{\nu}) = \kappa_L\left(\frac{\mathscr{I}m\lambda_t}{\lambda^5}X(x_t)\right)^2,$$

and

$$\kappa_L = (2.231 \pm 0.013) \times 10^{-10} \left[\frac{\lambda}{0.225}\right]^8.$$

The $\mathscr{B}(K_L^0 \to \pi^0 \nu\bar{\nu})$ depends only on the square of the imaginary part of the top loop which is *CP*-violating. The charm contributions drop out because $K_L^0$ is mostly an odd linear combination of $K^0$ and $\bar{K}^0$. This makes the theoretical prediction for the $K_L^0$ rate even cleaner than for the $K^+$. A measurement of the $K_L^0 \to \pi^0 \nu\bar{\nu}$ mode would amount to the measurement of the square of the *CP*-violating parameter $\eta$ in the Wolfenstein parametrisation [6] and directly related to the Jarlskog invariant $J$ [7], the unique measure of the magnitude of *CP*-Violation in the SM.

Inserting the numerical factors and making the dependence to the relevant CKM parameters explicit, one obtains:

$$\mathscr{B}(K^+ \to \pi^+ \nu\bar{\nu}) = (8.39 \pm 0.30) \times 10^{-11} \left[\frac{|V_{cb}|}{40.7 \times 10^{-3}}\right]^{2.8} \left[\frac{\gamma}{73.2^\circ}\right]^{0.74},$$
$$\mathscr{B}(K_L^0 \to \pi^0 \nu\bar{\nu}) = (3.36 \pm 0.05) \times 10^{-11} \left[\frac{|V_{ub}|}{3.88 \times 10^{-3}}\right]^2 \left[\frac{|V_{cb}|}{40.7 \times 10^{-3}}\right]^2 \left[\frac{\sin\gamma}{\sin 73.2^\circ}\right]^2.$$

In the above formulas the explicit numerical errors are the theoretical ones originating from QCD and electroweak uncertainties. They amount to 3.6% and 1.5% for the charged and the neutral mode respectively.

Taking $|V_{cb}|_{\text{avg}} = (40.7 \pm 1.4) \times 10^{-3}$, $|V_{ub}|_{\text{avg}} = (3.88 \pm 0.29) \times 10^{-3}$ and $\gamma = (73.2^{+6.3}_{-7.0})^\circ$ [8], one finds:

$$\mathscr{B}(K^+ \to \pi^+ \nu\bar{\nu}) = (8.4 \pm 1.0) \times 10^{-11},$$
$$\mathscr{B}(K_L^0 \to \pi^0 \nu\bar{\nu}) = (3.4 \pm 0.6) \times 10^{-11}.$$

The predictions are currently dominated by the parametric uncertainty that will plausibly be reduced by new measurements of $|V_{ub}|$, $|V_{cb}|$ and $\gamma$ by LHCb and Belle II.

With the discovery of the Higgs boson, the particle content of the SM is complete but we know that the SM itself cannot be the full story. There are many extensions of the SM where one could expect sizeable contributions, among which we can mention: Warped extra dimensions [9]; MSSM analyses [10–12]; Simplified Z and Z′ models [13], Littlest Higgs with T-Parity [14], Lepton Flavour Universality Violation models [15] and Lepto-quarks [16]. As an example of complementarity between $K \to \pi\nu\bar{\nu}$ and $B$-meson physics one can mention the case of $B_s \to \mu^+\mu^-$: the $B$ decay is sensitive to possible new pseudoscalar (e.g. charged Higgs) interactions while the $K$ rare decay is sensitive to possible new vector ones such as a $Z'$.

The SM theoretical precision is waiting to be matched experimentally. The experiments are difficult because the three-body final state lacks a significant signature and the $\nu\bar{\nu}$ pair cannot be detected. A long series of decay-at-rest searches for $K^+ \to \pi^+ \nu\bar{\nu}$ have culminated with the final results of the E878/E949 AGS experiments which have found strong evidence for the decay and quoted as final result [17]:

$$\mathscr{B}(K^+ \to \pi^+ \nu\bar{\nu})_{\text{exp}} = (17.3^{+11.5}_{-10.5}) \times 10^{-11}.$$

Although the mean value is about twice the SM prediction, the result is still consistent with the SM prediction because of the large statistical error. In addition to the purity of the separated kaon bean, the advantages of the stopped kaon technique include good kinematic constraint to kill backgrounds from two body kaon decays and the possibility to enforce good charged particle identification following the full $K^+ \to \pi^+ \to \mu^+ \to e^+$ decay chain. Limitations of the technique are the small acceptance once acceptable levels of muon and photon rejection levels are achieved and the presence of the material of the stopping target which leads to $\pi^+$ scattering and loss of energy.

An alternative method to study the decay is to let the kaon decay in flight, as done by the NA62 experiment at CERN [18]. High momentum (75 GeV/$c$), positively charged, secondary beams from the CERN SPS are well suited to provide a high flux of kaons and good immunity to backgrounds. A drawback is that the separation at beam level of kaons from the pion and proton components is practically impossible and because of this the main difficulty of the experiment is to track each particle of the beam before it enters the decay region. Only about 6% of the beam particles are kaons and of those only about 10% are usefully decaying in the fiducial volume. So for each useful $K$ decay NA62 has to track almost 200 particles. To be able to accumulate a sufficient number of decay the beam rate is very high (≃750 MHz). The SPS beam is delivered by a slow extraction to minimise the instantaneous beam intensity. The beam is not bunched as in collider experiments because otherwise the kaon decays occuring in the same bunch would veto each other. Nevertheless, even employing a slow extraction and an overall duty cycle of about 20%, the instantaneous beam intensity is so high that accidental activity in the beam tracker leads to the wrong association between a beam track (assumed to be the kaon) and the decay product. To avoid this problem and to correctly associate the kaon minimising mistags, NA62 has developed a novel Si pixel detector tracking detector [19] dubbed Gigatracker (GTK). The time resolution achieved with three GTK stations is as good as 65 ps. First results published by NA62 indicate that the novel in-flight technique is viable for $K^+ \to \pi^+ \nu\bar{\nu}$ [20].

Based on three candidate events (with an expected background of $1.65 \pm 0.31$), collected from the 2016–2017 data sample, the NA62 Collaboration reported [21]

$$\mathscr{B}(K^+ \to \pi^+ \nu\bar{\nu})_{\text{exp}} = (4.7^{+7.2}_{-4.7}) \times 10^{-11}$$

which, if interpreted as background leads to a 90% CL upper limit of [21]:

$$\mathscr{B}(K^+ \to \pi^+ \nu\bar{\nu}) < 18.5 \times 10^{-11}.$$

The NA62 result based on 2017 data excludes in practice the BNL mean value reported above. This is the first significant result obtained with the novel in-flight technique developed by NA62 [22]. NA62 has collected more data in 2018 and results based on this data sample will significantly improve the measurement. The overall kaon flux accumulated by NA62 so far ($\approx 6 \times 10^{12}$ kaons) corresponds to about 50 SM $K^+ \to \pi^+ \nu\bar{\nu}$ events for a nominal overall acceptance of 10%. The acceptance of the analysis on which the result presented above was obtained is of the order of ≈1% so lot of effort is underway to increase it towards the nominal value. To achieve the goal of 100 SM events NA62 will resume data taking after the CERN Long Shutdown 2 (LS2) in 2021. So far one extra year has been granted. Data taking may be further extended depending on the progress of the analysis. The possibility to further improve the measurement towards a 5% accuracy for a SM signal is being studied within NA62. Assuming that the infrastructure could be upgraded to take a factor of four more proton intensity, the detector would need to be upgraded in order to:

(i) Improve the time resolution of the beam tracker to less than 50 ps/station

The experiment is not limited by the number of protons deliverable by the SPS, but rather by the time resolution required to resolve the tracks in the beam tracker and to correctly match the kaon one to the pion reconstructed in the downstream tracker. As stated above, the NA62 Gigatracker has a time resolution of 120 ps per station, or 65 ps for the three stations combined. The NA62 GTK success has inspired several new R&D to develop Si pixel detectors with even better timing in the view of, for example, of the Upgrade 2 of LHCb [23]. A significant improvement of the time resolution would enable NA62 to operate efficiently with increased beam intensity.

(ii) Reduce material budget of the trackers

While any amount of material in the beam leads to unwanted scattering and interactions, for this experiment it is also important to minimise the thickness of the main pion tracker because particle scattered on detector material can mimic the weak signal signature. The NA62 straw tracker has a thickness of 1.2% of a radiation length. It is made of straws of 9.8 mm diameter. It is operated in the vacuum tank to minimise scattering. The main source of material is the plastic wall of the straw which amounts to 36 μm. Reducing the radius of the straw to approx. 5 mm opens the possibility to employ much thinner walls and reduce the material budget by about a factor of two. In addition, a shorter drift time will improve the high rate capability of the detector.

(iii) Faster EM calorimetry

One of the essential aspects of NA62 is the capability to detect photons with high efficiency. Increasing considerably the beam intensity will require faster veto counters in order to avoid large signal losses due to random veto.

While the experimental situation for $K^+ \to \pi^+ \nu\bar{\nu}$ shows that we have two independent experimental techniques able to reach SM sensitivities and beyond, the situation for the neutral mode is more complex. Progress has been hampered by the lack of experimental signature, as no redundancy is available once the $\pi^0$ mass is used as constraint to define the decay vertex.

On the experimental front for the neutral mode, the KOTO experiment at JPARC has published the 90% CL limit [24]:

$$\mathscr{B}(K_L^0 \to \pi^0 \nu\bar{\nu}) < 3 \times 10^{-9}.$$

KOTO builds on the experience of the E391a predecessor experiment which was performed at KEK. It is based on the technique of letting a very well collimated "pencil" beam enter the decay region surrounded by high performance photon vetoes. By vetoing extra photons and applying a transverse momentum cut (150 MeV/$c$) to eliminate residual $\Lambda \to n\pi^0$ decays KOTO plans to reach SM sensitivities by the mid of the next decade. The first step would be to improve the model independent 90% CL Grossman-Nir limit [25], which has been recently updated incorporating the latest NA62 result:

$$\mathscr{B}(K_L^0 \to \pi^0 \nu\bar{\nu})_{\text{Grossman−Nir}} < 8.14 \times 10^{-10}.$$

KOTO is starting to consider seriously a new experiment to reach 100 SM events (KOTO Step-2) [26]. The possibility to explore the neutral decay mode at CERN once NA62 is completed has been explored in the framework of the European particle physics strategy upgrade. The experiment under study (KLEVER) [27] is based on the same technique employed by KOTO but at much higher kaon energies. Higher kaon energies are expected to simplify the task of rejecting the photons from $K_L^0 \to \pi^0\pi^0$ which is the dominant source of background from kaon decays. One should notice that with respect to the charged mode, the two-pion branching ratio is $CP$-violating and therefore suppressed by a factor of about 200. Is this fact that makes the approach to study $K_L^0 \to \pi^0\pi^0$ at all thinkable. KLEVER expects to collect 60 SM events within five years of data taking after the CERN Long Shutdown 3 (from 2026 onward). KOTO and KLEVER are holding joint meetings to address issues of mutual interest.

In conclusion, what make the case to continue the study of these rare decays compelling, is that sensitivity beyond SM is there for most of the proposed extensions. Together with the study of muon rare decays and searches for electric dipole moments of elementary particles, rare kaon decays like $K^+ \to \pi^+ \nu\bar{\nu}$ and $K_L^0 \to \pi^0 \nu\bar{\nu}$ offer a genuine window of sensitivity to access high energy scales thanks to the absence of tree level contributions (CKM Unitarity), to the absence of long distance contributions ($\nu\bar{\nu}$ pair in the final state), and the hard GIM suppression at loop level in SM.

## 3. Other rare kaon decays

### 3.1. $K_S, K_L \to \mu^+\mu^-$ *and* $K_{L,S} \to l_1^+ l_1^- l_2^+ l_2^-$

The study of the rare process $K_L \to \mu^+\mu^-$ has played a crucial role in the understanding of the flavour content and structure of the standard model (SM) of electroweak interactions. The $K_S, K_L \to \mu^+\mu^-$ decays are dominated in the SM by long-distance two-photons contributions (LD), while the flavour-changing-neutral-current contributions provide information on short-distance (SD) dynamics of $\Delta S = 1$ transitions [28, 29]. The SM predictions for $K_S, K_L \to \mu^+\mu^-$ are [30]:

$$\mathscr{B}(K_S \to \mu^+\mu^-)_{\rm SM} = (5.18 \pm 1.50_{\rm LD} \pm 0.02_{\rm SD}) \times 10^{-12},$$
$$\mathscr{B}(K_L \to \mu^+\mu^-)_{\rm SM} = {}^{(6.85\pm0.80_{\rm LD}\pm0.06_{\rm SD})\times10^{-9}(+)}_{(8.11\pm1.49_{\rm LD}\pm0.13_{\rm SD})\times10^{-9}(-)}$$

where the SD contribution to the uncertainty includes the uncertainty on the CKM parameter ($\bar{\eta}$ and $\bar{\rho}$ respectively); the sign ambiguity for the $\mathscr{B}(K_L \to \mu^+\mu^-)_{\rm SM}$ depends on the (destructive or constructive) interference between short- and long-distance contributions which itself depends on the sign of an unknown low-energy constant [31]. The amplitude for the $K_L \to \mu^+\mu^-$ mode receives contributions from a complex long-distance amplitude generated by the two-photon exchange and a real amplitude induced by Z-penguin and box diagrams; the long-distance amplitude has a large absorptive (imaginary) part that provides the dominant contribution to the total rate; the uncertainty on the dispersive part of the two-photon amplitude is at present the dominant individual source of error [29]. The smallness of the total dispersive amplitude is well established thanks to precise experimental results on both $\Gamma(K_L \to \mu^+\mu^-)$ [8] and $\Gamma(K_L \to \gamma\gamma)$ [32]. The current experimental result for $K_L$ is based on over 6200 candidates from the BNL E871 Collaboration [33]:

$$\mathscr{B}(K_L \to \mu^+\mu^-) = (6.84 \pm 0.11) \times 10^{-9}$$

while for $K_S$ the limit from the 70 s [34] has been improved by upper limits at 90% CL by the LHCb experiment [35, 36]:

$$\mathscr{B}(K_S \to \mu^+\mu^-) < 2.1 \times 10^{-10}.$$

In the Phase-II upgrade during the High Luminosity LHC era, LHCb is expecting to collect around 300 fb$^{-1}$. If the trigger efficiency will be near 1, as can be achieved technically with the Phase-I full software trigger, LHCb will be able to explore branching fractions below $10^{-11}$ and could exclude values down towards the vicinity of the SM prediction [37].

The gap between the SM prediction and the current limit on $K_S, K_L \to \mu^+\mu^-$ leaves room for Beyond the Standard Model (BSM) contributions. The current limit already place constraints on leptoquark models [38, 39], supersymmetry [40, 41] and extensions of the SM [42]. Experiments using neutral kaon beams can address the *CP* asymmetry, which is also sensitive to BSM scenarios. Although both $K_S, K_L \to \mu^+\mu^-$ are almost *CP*-conserving decays, direct *CP* violation can be addressed by interference between $K_L$ and $K_S$ in the kaon beam, with the interference contribution affecting the $K_S$ SM predictions at the level of 60%; besides the unknown sign of the $K_L$ two-photon amplitude can be determined by a measurement of the interference [42].

The decays into 4 leptons are also of interest since the sign of the amplitude of $K_L \to \gamma\gamma$ affecting the determination of short-distance contributions to $K_L \to \mu^+\mu^-$ can be measured by studying $K_L$ and $K_S$ decays in four leptons [43]. The predicted branching ratios in the SM are of the order [44]:

$$\begin{aligned}
\mathscr{B}(K_S \to e^+e^-e^+e^-) &\sim 10^{-10},\\
\mathscr{B}(K_S \to \mu^+\mu^-e^+e^-) &\sim 10^{-11},\\
\mathscr{B}(K_S \to \mu^+\mu^-\mu^+\mu^-) &\sim 10^{-14},\\
\mathscr{B}(K_L \to e^+e^-e^+e^-) &\sim 10^{-10},\\
\mathscr{B}(K_L \to \mu^+\mu^-e^+e^-) &\sim 10^{-11},\\
\mathscr{B}(K_L \to \mu^+\mu^-\mu^+\mu^-) &\sim 10^{-14}.
\end{aligned}$$

The $K_S$ modes have never been observed and there are no experimental limits available in literature. The $K_L$ modes limits are from the KTeV and NA48 experiments [45, 46].

Recently LHCb has shown prospects for the $K_S$ modes [47]. Future high-intensity kaon experiments, with intensities around 5 times the most recent ones, could address all the modes with 2 or 4 electrons.

### 3.2. $K_S, K_L \to \pi^0 l^+ l^-$

In the SM, the process $K_S \to \pi^0 l^+ l^-$ is *CP*-conserving and dominated by a single photon exchange, while the $K_L$ decay is *CP*-violating, apart from a small *CP*-conserving contribution (mainly originating from two-photon process). In Chiral Perturbation Theory expansion beyond leading order, the $K_S$ decays can be expressed as:

$$\begin{aligned}
\mathscr{B}(K_S \to \pi^0 e^+e^-) &= (0.01 - 0.76 a_S - 0.21 b_S + 46.5 a_S^2 + 12.9 a_S b_S + 1.44 b_S^2) \times 10^{-10},\\
\mathscr{B}(K_S \to \pi^0 \mu^+\mu^-) &= (0.07 - 4.52 a_S - 1.50 b_S + 98.7 a_S^2 + 57.7 a_S b_S + 8.95 b_S^2) \times 10^{-11},
\end{aligned}$$

where $a_S$ and $b_S$ are free, real chiral-perturbation-theory parameters of the polynomial expansion of the EM form factor in terms of the di-lepton invariant mass $q^2$ (with $b_S$ being the coefficient of the linear term in $q^2$) [48]. The parameters $a_S$ and $b_S$ can be determined from data; avoiding assumptions from Vector Meson Dominance model is possible if a large enough statistics become available. For the $K_L$ process, *CP*-violating contributions can originate from $K^0 - \bar{K}^0$ mixing via a decay of the *CP*-even component of the $K_L$, and direct *CP*-violating contribution from short distance physics via loops sensitive to $\mathrm{Im}(\lambda_t) = \mathrm{Im}(V_{td} V_{ts}^*)$. The indirect and direct *CP*-violating contributions can interfere and the expression for the total *CP*-violating branching ratio can be written as [48]:

$$\mathscr{B}(K_L \to \pi^0 l^+ l^-)_{CPV} = \left[ C_{\mathrm{MIX}} \pm C_{\mathrm{INT}} \frac{\mathrm{Im}\lambda_t}{10^{-4}} + C_{\mathrm{DIR}} \left( \frac{\mathrm{Im}\lambda_t}{10^{-4}} \right)^2 \right] \times 10^{-12}$$

where $C_{\mathrm{INT}}$ is due to the interference between the direct ($C_{\mathrm{DIR}}$) and indirect ($C_{\mathrm{MIX}}$) *CP*-violating components. Here $C_{\mathrm{MIX}}$ and $C_{\mathrm{INT}}$ depend on $\mathscr{B}(K_S \to \pi^0 l^+ l^-)$ and $\sqrt{\mathscr{B}(K_S \to \pi^0 l^+ l^-)}$ respectively. The SM predictions for the branching ratios of $K_L \to \pi^0 l^+ l^-$ are:

$$\begin{aligned}
\mathscr{B}(K_L \to \pi^0 e^+e^-)_{\mathrm{SM}} &= (3.5 \pm 0.9, 1.6 \pm 0.6) \times 10^{-11},\\
B(K_L \to \pi^0 \mu^+\mu^-)_{\mathrm{SM}} &= (1.4 \pm 0.3, 0.9 \pm 0.2) \times 10^{-11}
\end{aligned}$$

for constructive (destructive) interference respectively [49]. Better measurements of the $K_S \to \pi^0 l^+ l^-$ decay rate would allow to improve the quoted errors, which are currently dominated by the uncertainty due to the chiral-perturbation-theory parameters $a_S$ and $b_S$. A joint study of the Dalitz plot variables and the components of the $\mu^+$ polarisation could directly allow the separation of the indirect, direct *CP*-violating and *CP*-conserving contributions [50].

The current experimental limits for $K_S$ modes come from NA48/1 [51, 52]:

$$\mathscr{B}(K_S \to \pi^0\mu^+\mu^-) = (2.9^{+1.5}_{-1.2} \pm 0.2) \times 10^{-9},$$
$$\mathscr{B}(K_S \to \pi^0 e^+ e^-) = (5.8^{+2.8}_{-2.3} \pm 0.8) \times 10^{-9},$$

together with the determination of two allowed regions for $a_S$ and $b_S$ from the combination of the two branching ratio measurements using a maximum likelihood method: $a_S = -1.6^{+2.1}_{-1.8}$ and $b_S = 10.8^{+5.4}_{-7.7}$, or $a_S = +1.9^{+1.6}_{-2.4}$ and $b_S = -11.3^{+8.8}_{-4.5}$. The 90% CL limits for the $K_L$ modes come from KTeV [53, 54]:

$$\mathscr{B}(K_L \to \pi^0 e^+ e^-) < 2.8 \times 10^{-10},$$
$$\mathscr{B}(K_L \to \pi^0\mu^+\mu^-) < 3.8 \times 10^{-10}.$$

The $K_L$ channel is sensitive to BSM models. Searches of extra-dimensions where enhancements of the branching ratio of both $K_L$ modes by a factor of about 5 are possible without violating any constraints [49]. Specific flavour structures can correlate effects in $K_S, K_L \to \pi^0 l^+ l^-$ with B-physics anomalies, for example LeptoQuark models with Rank-One Flavour violation [55, 56]. While future experiments using neutral kaon beams can address all the four channels, the LHCb experiment can significantly improve the precision on $\mathscr{B}(K_S \to \pi^0\mu^+\mu^-)$. LHCb can reach $0.25 \times 10^{-9}$ with 50 fb$^{-1}$ of integrated luminosity, assuming 100% trigger efficiency in LHC Run3; as the precision increases, the use of the $q^2$ dependence becomes a viable approach to avoid model dependence in the extraction of $a_S$ and LHCb can reach a precision of 0.10 on $a_S$ and 0.35 on $b_S$ with Phase II-Upgrade [57].

## 3.3. *Lepton Number/Flavour violation*

Rare kaon decays can be used to search for explicit violation of Lepton Number or Flavour. Both Lepton Number and Flavour are exact symmetries in the SM, and kaon decays $K \to (n\pi)\mu e$ contemplating their violation are null tests of the SM. However many extensions of the SM violate Lepton Flavour and Number. Violations can occur in BSM models, for example involving leptoquarks or the exchange of multi-TeV Gauge mediators, that can relate the observed anomalies in the B sector to observables in the kaon sector [58–63] with kaon branching ratios expected in the range $10^{-12}$–$10^{-13}$. Other models advocate Heavy Majorana Neutrinos as a source of Lepton Number violation [64, 65].

Limits (at 90% CL) on the branching fractions for the $K \to (n\pi)\mu e$ modes were achieved by BNL [66], KTeV [67], E865 [68, 69] in 1990–2000, and more recently by NA48/2 [70]:

$$\mathscr{B}(K_L \to e^\pm\mu^\mp) < 4.7 \times 10^{-12},$$
$$\mathscr{B}(K_L \to \pi^0 e^\pm\mu^\mp) < 7.6 \times 10^{-11},$$
$$\mathscr{B}(K^+ \to \pi^+ e^-\mu^+) < 1.3 \times 10^{-11},$$
$$\mathscr{B}(K^+ \to \pi^+ e^+\mu^-) < 5.2 \times 10^{-10},$$
$$\mathscr{B}(K^+ \to \pi^- e^+\mu^+) < 5.0 \times 10^{-10},$$
$$\mathscr{B}(K^+ \to \pi^-\mu^+\mu^+) < 8.6 \times 10^{-11},$$
$$\mathscr{B}(K^+ \to \pi^- e^+ e^+) < 6.4 \times 10^{-10}.$$

The NA62 experiment has already improved on some of these limits [71]:

$$\mathscr{B}(K^+ \to \pi^-\mu^+\mu^+) < 4.2 \times 10^{-11},$$
$$\mathscr{B}(K^+ \to \pi^- e^+ e^+) < 2.2 \times 10^{-10},$$

and has prospects to push the limits for the $K^+$ modes to the range of $10^{-12}$ to $10^{-11}$, considering the data taking foreseen after 2021. These modes can be also pursued at LHCb in the Upgrade phase, benefiting from the large strange-production cross-section and the improved efficiency for kaon decays; LHCb may be able to update the existing limits and probe a sizeable part of the parameter space suggested by the discrepancies in B physics [72].

### 3.4. $K^+ \to \pi^+ l^+ l^-$

The decays $K^+ \to \pi^+ l^+ l^-$ ($l = \mu, e$) are Flavour-Changing-Neutral-Current processes; their short-distance contribution is described by $Z, \gamma$ penguins and box diagram, with the amplitude depending on the logarithm-like GIM mechanism.

The decays $K^+ \to \pi^+ l^+ l^-$ are dominated by long-distance contributions involving one photon exchange ($K^+ \to \pi^+ \gamma \to \pi^+ l^+ l^-$), and their branching fraction can be derived within the framework of Chiral Perturbation Theory in terms of a vector-interaction form factor, which describes the single-photon exchange and characterises the di-muon invariant-mass spectrum. The form factor includes a small contribution from the two-pion-loop intermediate state and is dominated by a term phenomenologically described as a first-order polynomial ($a_+ + b_+ z$), where $z = (m_{\mu\mu}/M_K)^2$ and $a_+$ and $b_+$ are free parameters, used to describe the non-perturbative QCD effects in the chiral expansion [73, 74]. In order to obtain both the parameters and the corresponding branching fraction, the differential decay rate spectrum must be reconstructed from experimental data.

Similarly to $B \to K l^+ l^-$, this process can be described by an effective Lagrangian with no-zero Wilson coefficients for the semi-leptonic operators $Q_{7V}$ and $Q_{7A}$ [75], and new physics processes can be interpreted as deviations from the Standard Model Wilson coefficients $C_{7V}$, $C_{7A}$. In particular, the Wilson coefficient $C_{7A}$ can be related to $a_+$, making the form factor measurement a test of beyond-the-SM effects [76]. Beside, Lepton Flavour Universality implies the free parameters to be the same for both the electron and muon channels. Their comparison would provide a test of Lepton Flavour Universality, with any deviation being a sign of short-distance new physics dynamics [77].

The current best experimental measurements of the $K^+ \to \pi^+ l^+ l^-$ branching ratios are from the NA48/2 collaboration [78, 79]:

$$\mathscr{B}(K^+ \to \pi^+ e^+ e^-) = (3.11 \pm 0.04_{\text{stat}} \pm 0.12_{\text{syst}}) \times 10^{-7},$$
$$\mathscr{B}(K^+ \to \pi^+ \mu^+ \mu^-) = (9.62 \pm 0.21_{\text{stat}} \pm 0.13_{\text{syst}}) \times 10^{-7}.$$

Both the NA48/2 and E865 [80, 81] have extracted the free parameters $a_+$ and $b_+$ for muon and electron channels, placing limits on Lepton Flavour Universality violation. However, such test is at present limited by the uncertainties of the measurements, especially in the muon channel.

At NA62 both larger and significantly cleaner samples of both channels are expected to be collected over the lifetime of the experiment because of vast increases in instantaneous rate, improved tracking and larger field-integrals. The LHCb mass resolution is sufficient to separate the muon decay from the kinematically similar three-pion decay; the experiment can collect of order $10^4$ decays in the muon channel per year of upgraded-LHCb data taking. Similar considerations apply to the electron channel, where a reduced reconstruction efficiency is somehow compensated by the larger branching fraction [82].

## 4. HNL and exotics

The long lifetime of kaons opens the interesting possibility to investigate with good sensitivity decays of kaons in exotic final states including heavy neutral leptons (HNL) or exotics such as $K^+ \to \pi^+ X$ where X is a long-lived boson. As by-product of the $K^+ \to \pi^+ \nu\bar{\nu}$ analysis, one can search for new stable neutral bosons in two body decays of the type: $K^+ \to \pi^+ X$ and $K_L^0 \to \pi^0 X$.

A generic possibility of $k$ new sterile neutrino mass states can be written as

$$\nu_\alpha = \sum_{i=1}^{3+k} U_{\alpha i}\nu_i, \quad (\alpha = e, \mu, \tau).$$

On general grounds, the extension of the neutrino sector is motivated by its relation to the neutrino mass generation mechanism. The $\nu$MSM [83, 84] is the most economical theory accounting for neutrino masses and oscillations, baryogenesis, and dark matter. Three heavy neutral leptons (HNLs) are posited to provide a Dark Matter candidate ($m_1 \approx 10$ keV/$c^2$) while two more massive neutrinos could exist with $m_{2,3} \approx 1$ GeV/$c^2$.

The production of Heavy Neutral Leptons [84–86] can be searched in $K^+ \to l^+\nu$ as a peak search over a well know, well modelled background, independently of the HNL decay mode. While pion decays allow one to explore the mass region between 60 and 135 MeV/$c^2$ [87], kaons decays enable us to extend a very sensitive search up ≈450 MeV/$c^2$. In particular, both the rare decay $K^+ \to e^+\nu$ and the abundant $K^+ \to \mu^+\nu$ have been successfully used to set limits in the mass range up to about 450 MeV/$c^2$.

Limits at 90% CL on the square of the mixing angle extend down to about $10^{-8}$ for $K^+ \to \mu^+ N$ [88] and close to $10^{-9}$ for $K^+ \to e^+ N$ [89]. NA62 foresees to reach a sensitivity of order $10^{-9}$ and $10^{-8}$ on the electron coupling and muon coupling respectively, with the existing full data set.

This is part of a broader programme covering searches for feebly-interacting long-lived particles at LHC experiments and possible future facilities [90], with an interplay between the exploration of large masses and relatively strong couplings at colliders, and masses in the MeV–GeV region and low couplings in meson decays and at future beam-dump facilities.

## 5. Outlook

What makes the case to continue the study of rare kaon decays compelling, is their sensitivity beyond SM of most of the proposed extensions, offering a genuine window of sensitivity to access high energy scales. The NA62 experiment at CERN will resume data taking after LS2 to complete its physics programme for $K^+ \to \pi^+\nu\nu$ and a variety of other rare kaon decays and exotic searches. The possibility of high-intensity kaon beams, both charged and neutral, at CERN after LS3 is being explored, with a broad physics case covering the most interesting kaon decays as well as the golden channels $K \to \pi\nu\nu$. In Japan, the KOTO experiment plans to reach the SM sensitivity for $K_L \to \pi^0\nu\nu$ by the middle of the next decade, and is considering a new experiment to reach 100 SM events (KOTO Step-2). The LHCb experiment at CERN has a programme of rare kaon decays; in the Phase-II upgrade during the High Luminosity LHC era, the experiment will be able to explore branching ratios below $10^{-11}$ thanks to a large strange-production cross-section and an improved efficiency for kaon decays.

## References


[1] S. L. Glashow, J. Iliopoulos, L. Maiani, "Weak interactions with Lepton-Hadron symmetry", *Phys. Rev. D* **2** (1970), p. 1285-1292.

[2] N. Cabibbo, "Unitary symmetry and leptonic decays", *Phys. Rev. Lett.* **10** (1963), no. 12, p. 531-533.

[3] M. Kobayashi, T. Maskawa, "CP violation in the renormalizable theory of weak interaction", *Prog. Theor. Phys.* **49** (1973), no. 2, p. 652-657.

[4] R. Barbieri, "Quark masses and weak couplings in the standard model and beyond", *Int. J. Mod. Phys. A* **17** (2002), no. 22, p. 3059-3067.

[5] A. J. Buras, D. Buttazzo, J. Girrbach-Noe, R. Knegjens, "$K^+ \to \pi^+\nu\bar{\nu}$ and $K_L \to \pi^0\nu\bar{\nu}$ in the Standard Model: status and perspectives", *J. High Energy Phys.* **1511** (2015), article ID 33.

[6] L. Wolfenstein, "Parametrization of the Kobayashi–Maskawa matrix", *Phys. Rev. Lett.* **51** (1983), no. 21, p. 1945-1947.

[7] C. Jarlskog, "Commutator of the quark mass matrices in the standard electroweak model and a measure of maximal CP violation", *Phys. Rev. Lett.* **55** (1985), no. 10, p. 1039-1042.
[8] M. Tanabashi *et al.* (Particle Data Group), "Review of Particle Physics", *Phys. Rev. D* **98** (2018), article ID 030001, and 2019 update.
[9] M. Blanke, A. J. Buras, B. Duling, K. Gemmler, S. Gori, "Rare K and B decays in a warped extra dimension with custodial protection", *J. High Energy Phys.* **2009** (2009), no. 03, p. 108-108.
[10] M. Tanimoto, K. Yamamoto, "Probing SUSY with 10 TeV stop mass in rare decays and CP violation of kaon", *PTEP* **2016** (2016), no. 12, article ID 123B02.
[11] T. Blažek, P. Maták, "Left–left squark mixing, $K^+ \to \pi^+ \nu\bar{\nu}$ and minimal supersymmetry with large $\tan\beta$", *Int. J. Mod. Phys. A* **29** (2014), no. 27, article ID 1450162.
[12] G. Isidori, F. Mescia, P. Paradisi, C. Smith, S. Trine, "Exploring the flavour structure of the MSSM with rare K decays", *J. High Energy Phys.* **0608** (2006), article ID 64.
[13] A. J. Buras, D. Buttazzo, R. Knegjens, "$K \to \pi\nu\overline{\nu}$ and $\epsilon'/\epsilon$ in simplified new physics models", *J. High Energy Phys.* **1511** (2015), article ID 166.
[14] M. Blanke, A. J. Buras, S. Recksiegel, "Quark flavour observables in the Littlest Higgs model with T-parity after LHC Run 1", *Eur. Phys. J. C* **76** (2016), no. 4, article ID 182.
[15] M. Bordone, D. Buttazzo, G. Isidori, J. Monnard, "Probing Lepton Flavour Universality with $K \to \pi\nu\bar{\nu}$ decays", *Eur. Phys. J. C* **77** (2017), no. 9, article ID 618.
[16] S. Fajfer, N. Košnik, L. Vale Silva, "Footprints of leptoquarks: from $R_{K^{(*)}}$ to $K \to \pi\nu\bar{\nu}$", *Eur. Phys. J. C* **78** (2018), no. 4, article ID 275.
[17] A. V. Artamonov *et al.* [E949 Collaboration], "New measurement of the $K^+ \to \pi^+\nu\bar{\nu}$ branching ratio", *Phys. Rev. Lett.* **101** (2008), article ID 191802.
[18] NA62 Technical Design Document, NA62-10-07, https://cds.cern.ch/record/1404985?ln=en.
[19] G. Aglieri Rinella *et al.*, "The NA62 GigaTracKer: a low mass high intensity beam 4D tracker with 65 ps time resolution on tracks", *JINST* **14** (2019), article ID P07010.
[20] E. Cortina Gil *et al.* [NA62 Collaboration], "First search for $K^+ \to \pi^+\nu\bar{\nu}$ using the decay-in-flight technique", *Phys. Lett. B* **791** (2019), p. 156-166.
[21] G. Ruggiero for the NA62 Collaboration, "Latest measurement of $K^+ \to \pi^+\nu\bar{\nu}$ with the NA62 experiment at CERN", Presented at the International Conference on Kaon Physics, Perugia, Italy, 10–13 September 2019.
[22] E. Cortina Gil *et al.* [NA62 Collaboration], "The Beam and detector of the NA62 experiment at CERN", *JINST* **12** (2017), no. 05, article ID P05025.
[23] I. Bediaga *et al.*, "Physics case for an LHCb Upgrade II", CERN-LHCC-2018-027, LHCB-PUB-2018-009.
[24] J. K. Ahn *et al.* [KOTO Collaboration], "Search for the $K_L \to \pi^0\nu\overline{\nu}$ and $K_L \to \pi^0\ X^0$ decays at the J-PARC KOTO experiment", *Phys. Rev. Lett.* **122** (2019), no. 2, article ID 021802.
[25] Y. Grossman, Y. Nir, " $K(L) \to \pi^0$ neutrino anti-neutrino beyond the standard model", *Phys. Lett. B* **398** (1997), no. 1-2, p. 163-168.
[26] T. Nomura, "A future $K_L^0 \to \pi^0\nu\bar{\nu}$ experiment at J-PARC", Presented at the International Conference on Kaon Physics, Perugia, Italy, 10–13 September 2019.
[27] F. Ambrosino *et al.* [KLEVER Project Collaboration], "KLEVER: An experiment to measure $\mathrm{BR}(K_L \to \pi^0\nu\bar{\nu})$ at the CERN SPS", 2019, preprint, https://arxiv.org/abs/1901.03099.
[28] M. Gorbahn, U. Haisch, *Phys. Rev. Lett.* **97** (2006), article ID 122002.
[29] G. Isidori, R. Unterdorfer, *J. High Energy Phys.* **2004** (2004), no. 01, article ID 009.
[30] G. D'Ambrosio, T. Kitahara, *Phys. Rev. Lett.* **119** (2017), article ID 201802.
[31] J. M. Gerard, C. Smith, S. Trineb, *Nucl. Phys. B* **730** (2005), no. 1-2, p. 1-36.
[32] A. Lai *et al.* [NA48 Collaboration], *Phys. Lett. B* **551** (2003), no. 1-2, p. 7-15.
[33] D. Ambrose *et al.* [BNL E871 Collaboration], "Improved Branching Ratio Measurement for the Decay $K_L^0 \to \mu^+\mu^-$", *Phys. Rev. Lett.* **84** (2000), p. 1389-1392.
[34] S. Geisdal *et al.*, *Phys. Lett. B* **44** (1973), no. 2, p. 217-220.
[35] R. Aaij *et al.* [LHCb Collaboration], "Search for the rare decay $K_S \to \mu^+\mu^-$", *J. High Energy Phys.* **2013** (2013), no. 1, article ID 90.
[36] R. Aaij *et al.* [LHCb Collaboration], LHCB-CONF-2019-002.
[37] A. A. Alves Junior *et al.*, "Prospects for Measurements with Strange Hadrons at LHCb", *J. High Energy Phys.* **2019** (2019), article ID 48.
[38] C. Bobeth, A. J. Buras, "Leptoquarks meet $\varepsilon'/\varepsilon$ and rare Kaon processes", *J. High Energy Phys.* **2018** (2018), no. 2, article ID 101.
[39] V. Gherardi, D. Marzocca, M. Nardecchia *et al.*, "Rank-one flavor violation and B-meson anomalies", *J. High Energ. Phys.* **2019** (2019), article ID 112.
[40] M. E. Toru, T. Kitahara, S. Mishima, D. Ueda, K. Yamamoto, *J. High Energy Phys.* **04** (2018), article ID 19.

[41] V. Chobanova, G. D'Ambrosio, T. Kitahara, M. Lucio Martìnez, D. Martìnez Santos, I. Suárez Fernández, K. Yamamoto, *J. High Energy Phys.* **05** (2018), article ID 24.

[42] G. D'Ambrosio, T. Kitahara, *Phys. Rev. Lett.* **119** (2017), article ID 201802.

[43] G. D'Ambrosio, D. Greynat, G. Vulvert, *Eur. Phys. J. C* **73** (2013), article ID 2678.

[44] V. Cirigliano, G. Ecker, H. Neufeld, A. Pich, J. Portolés, "Kaon decays in the standard model", *Rev. Mod. Phys.* **84** (2012), p. 399-447.

[45] A. Alavi-Harati *et al.* [KTeV Collaboration], *Phys. Rev. Lett.* **90** (2003), article ID 141801.

[46] V. Fanti *et al.* [NA48 Collaboration], *Phys. Lett. B* **458** (1999), no. 4, p. 553-563.

[47] C. Marin Benito, *J. Phys.: Conf. Ser.* **800** (2017), article ID 012031.

[48] G. D'Ambrosio, G. Ecker, G. Isidori, J. Portoles, *J. High Energy Phys.* **08** (1998), article ID 4.

[49] M. Bauer, S. Casagrande, U. Haisch, M. Neubert, *J. High Energy Phys.* **09** (2010), article ID 17.

[50] M. V. Diwan, H. Ma, T. L. Trueman, *Phys. Rev. D* **65** (2002), article ID 054020.

[51] J. R. Batley *et al.* [NA48/1 Collaboration], *Phys. Lett. B* **576** (2003), no. 1-2, p. 43-54.

[52] J. R. Batley *et al.* [NA48/1 Collaboration], *Phys. Lett. B* **599** (2004), no. 3-4, p. 197-211.

[53] A. Alavi-Harati *et al.* [KTeV/E799 Collaboration], *Phys. Rev. Lett.* **93** (2004), article ID 021805.

[54] A. Alavi-Harati *et al.* [KTEV Collaboration], "Search for the Decay $K_L \to \pi^0 \mu^+ \mu^-$", *Phys. Rev. Lett.* **84** (2000), p. 5279-5282.

[55] V. Gherardi, D. Marzocca, M. Nardecchia *et al.*, "Rank-one flavor violation and B-meson anomalies", *J. High Energ. Phys.* **2019** (2019), article ID 112.

[56] B. Gripaios, M. Nardecchia, S. A. Renner, "Composite leptoquarks and anomalies in $B$-meson decays", *J. High Energy Phys.* **2015**, no. 5, article ID 6.

[57] A. A. Alves Junior *et al.*, *J. High Energy Phys.* **1905** (2019), article ID 048.

[58] A. Crivellin, G. D'Ambrosio, M. Hoferichter, L. C. Tunstall, *Phys. Rev. D* **93** (2016), article ID 074038.

[59] V. Cirigliano, A. Crivellin, M. Hoferichter, *Phys. Rev. Lett.* **120** (2018), no. 18, article ID 141803.

[60] S. L. Glashow, D. Guadagnoli, K. Lane, *Phys. Rev. Lett.* **114** (2015), article ID 091801.

[61] G. Hiller, D. Loose, K. Schonwald, *J. High Energy Phys.* **12** (2016), article ID 27.

[62] D. Buttazzo, A. Greljo, G. Isidori, D. Marzocca, *J. High Energy Phys.* **11** (2017), article ID 44.

[63] M. Bordone, C. Cornella, J. Fuentes-Martìn, G. Isidori, *J. High Energy Phys.* **10** (2018), article ID 148.

[64] A. Atre, T. Han, S. Pascoli, B. Zhang, *J. High Energy Phys.* **0905** (2009), article ID 30.

[65] L. S. Littenberg, R. Shrock, *Phys. Lett. B* **491** (2000), p. 285-290.

[66] D. Ambrose *et al.* [BNL E871 Collaboration], "New Limit on Muon and Electron Lepton Number Violation from $K_L^0 \to \mu^\pm e^\mp$ Decay", *Phys. Rev. Lett.* **81** (1998), no. 26, p. 5734-5737.

[67] E. Abouzaid *et al.* [KTeV Collaboration], *Phys. Rev. Lett.* **100** (2008), article ID 131803.

[68] A. Sher *et al.* [E865 Collaboration], *Phys. Rev. D* **72** (2005), article ID 012005.

[69] R. Appel *et al.* [E865 Collaboration], "Search for Lepton Flavor Violation in $K^+$ Decays into a Charged Pion and Two Leptons", *Phys. Rev. Lett.* **85** (2000), no. 14, p. 2877-2880.

[70] J. R. Batley *et al.* [NA48/2 Collaboration], *Phys. Lett. B* **769** (2017), p. 67-76.

[71] E. Cortina Gil *et al.* [NA62 Collaboration], *Phys. Lett. B* **797** (2019), article ID 134794.

[72] M. Borsato, V. Gligorov, D. Guadagnoli, D. Martinez Santos, O. Sumensari, *Phys. Rev. D* **99** (2019), article ID 055017.

[73] G. D'Ambrosio, G. Ecker, G. Isidori, J. Portoles, *J. High Energy Phys.* **08** (1998), article ID 4.

[74] A. Z. Dubnickova, S. Dubnicka, E. Goudzovski, V. N. Pervushin, M. Secansky, "Radiative kaon decay in the chiral perturbation theory", *Phys. Part. Nucl. Lett.* **5** (2008), no. 2, p. 76-84.

[75] G. Ecker, A. Pich, E. de Rafael, *Nucl. Phys. B* **291** (1987), p. 692-719.

[76] A. Crivellin, G. D'Ambrosio, M. Hoferichter, L. C. Tunstall, *Phys. Rev. D* **93** (2016), no. 7, article ID 074038.

[77] L. C. Tunstall, A. Crivellin, G. D'Ambrosio, M. Hoferichter, *J. Phys.: Conf. Ser.* **800** (2017), no. 1, article ID 012014.

[78] J. R. Batley *et al.* [NA48 Collaboration], *Phys. Lett. B* **677** (2009), p. 246-254.

[79] J. R. Batley *et al.* [NA48 Collaboration], *Phys. Lett. B* **697** (2011), no. 2, p. 107-115.

[80] R. Appel *et al.* [E865 Collaboration], "New Measurement of the Properties of the Rare Decay $K^+ \to \pi^+ e^+ e^-$", *Phys. Rev. Lett.* **83** (1999), no. 22, p. 4482-4485.

[81] R. Appel *et al.* [E865 Collaboration], "Search for Lepton Flavor Violation in $K^+$ Decays into a Charged Pion and Two Leptons", *Phys. Rev. Lett.* **85** (2000), no. 14, p. 2877-2880.

[82] A. A. Alves Junior *et al.*, *J. High Energ. Phys.* **2019** (2019), article ID 48.

[83] T. Asaka, M. Shaposhnikov, "The $\nu$MSM, dark matter and baryon asymmetry of the universe", *Phys. Lett. B* **620** (2005), no. 1-2, p. 17-26.

[84] T. Asaka, S. Blanchet, M. Shaposhnikov, "The nuMSM, dark matter and neutrino masses", *Phys. Lett. B* **631** (2005), no. 4, p. 151-156.

[85] R. E. Shrock, "New tests for and bounds on neutrino masses and lepton mixing", *Phys. Lett. B* **96** (1980), no. 1–2, p. 159-164.

[86] A. Canetti, M. Drewes, T. Frossard, M. Shaposhnikov, *Phys. Rev. D* **87** (2013), article ID 093006.

[87] A. Aguilar-Arevalo *et al.* [PIENU Collaboration], "Improved search for heavy neutrinos in the decay $\pi \to e\nu$", *Phys. Rev. D* **97** (2018), no. 7, article ID 072012.
[88] A. V. Artamonov *et al.* [E949 Collaboration], "Search for heavy neutrinos in $K^+ \to \mu^+ \nu_H$ decays", *Phys. Rev. D* **91** (2015), no. 5, article ID 052001, [Erratum: *Phys. Rev. D* **91** (2015) no. 5, 059903].
[89] E. Goudzovski, for the NA62 Collaboration, "HNL production and exotic searches at NA62", Presented at the International Conference on Kaon Physics, Perugia, Italy, 10–13 September 2019.
[90] J. Beacham *et al.*, "Physics Beyond Colliders at CERN: Beyond the Standard Model Working Group Report", *J. Phys. G* **47** (2020), article ID 010501, CERN-PBC-REPORT-2018-007.

*Comptes Rendus*
*Physique*
**2020**, 21, nº 1, p. 121-134
https://doi.org/10.5802/crphys.13

A perspective of High Energy Physics from precision measurements
*La physique des Hautes Energies du point de vue des mesures de précision*

# Precision experiments with muons and neutrons

## *Expériences de précision avec les muons et les neutrons*

**Yoshitaka Kuno** [a] **and Guillaume Pignol** [*, b]

[a] Osaka University, Machikaneyama, Toyonaka, Osaka, 560-0043, Japan

[b] Univ. Grenoble Alpes, CNRS, Grenoble INP, LPSC-IN2P3, 38000 Grenoble, France.

*E-mails:* kuno@phys.sci.osaka-u.ac.jp (Y. Kuno), guillaume.pignol@lpsc.in2p3.fr (G. Pignol).

**Abstract.** The precision experiments with muons and neutrons are described. The topics selected cover the anomalies of the muon $g_\mu - 2$ and the neutron lifetime, and searches for charged lepton flavour violation CLFV of $\mu^- \to e^-$ transition and the neutron electric dipole moment (EDM). These physics programs are anticipating significant improvements of experimental sensitivities, by a factor of ten to more than 10,000 with novel ideas and methods. They would provide a unique discovery potential to new physics beyond the Standard Model of particle physics, and is complementary to the collider and neutrino physics programs.

**Résumé.** Une sélection d'expériences de précision employant des muons ou des neutrons sont décrites. Cette sélection couvre les anomalies dans les mesures du facteur $g_\mu - 2$ du muon et de la duré de vie du neutron, ainsi que les recherches de violation de saveur pour les leptons chargés (CLFV) des transitions $\mu^- \to e^-$ et du moment dipolaire électrique (EDM) du neutron. Ces programmes promettent des améliorations significatives de la sensibilité expérimentale, les facteurs d'améliorations sont compris entre 10 et 10,000, avec des nouvelles idées et méthodes. Le potentiel de découverte de nouvelle physique au-delà du Modèle Standard de la physique des particules est complémentaire aux recherches sur collisionneurs et aux programmes avec les neutrinos.

**Keywords.** Neutron, Muon, Neutron lifetime, Muon magnetic moment, Muon anomaly, Lepton flavor violation, Electric dipole moment.

**Mots-clés.** Neutron, Muon, Temps de vie du neutron, Moment magnétique du muon, Anomalie du muon, Violation de la saveur leptonique, Moment dipolaire électrique.

[*] Corresponding author.

## 1. Muons and neutrons at the intensity frontier

About twenty large nuclear facilities dedicated to neutron and/or muon production are presently being operated in the world. These are fission nuclear reactors producing neutrons (and neutrinos), and accelerators to make spallation sources producing neutrons, pions and muons. Concerning nuclear reactors, there are about 15 research reactors accessible to scientific users in operation. One of the world center for neutron science is the high flux 48 MW reactor at the Institut Laue Langevin in France, with a thermal flux of $10^{15}$ $n\,\mathrm{cm}^{-2}\cdot\mathrm{s}^{-1}$ delivering neutrons to 45 instruments in parallel. In a spallation source, a high intensity (~mA) proton beam (~GeV) is shot at a target made with heavy elements such as lead, tungsten or mercury. By destroying nuclei, spallation reactions liberate typically 20 neutrons and several pions per incoming proton. The muons are indirectly produced by the decays of pions. Large spallation sources are currently operated at Paul Sherrer Institute (PSI) in Switzerland, SNS in the US and the Japan Proton Accelerator Research Complex (J-PARC) in Japan. The European Spallation Source (ESS) is currently under construction in Sweden. Concerning muon beam facilities, there are proton cyclotrons which produce a continuous muon beam such as PSI and TRIUMF, and proton synchrotrons which provide a pulsed muon beam such as ISIS/RAL and J-PARC. The time structure of a muon beam is important and should be chosen appropriately for an experiment. Among the facilities, PSI and J-PARC can deliver a proton beam of about 1 MW power, providing good opportunities for muon particle physics.

These installations are multidisciplinary facilities. Chemists and solids state physicists make good use of the neutron or muon beams as a probe of a sample of condensed or soft matter they wish to characterize. By contrast, particle physicists study the neutron and muon themselves to do precision experiments at the intensity frontier which are of two types: metrology measurements and quasi-null tests.

- *Metrology measurements.* This class of experiments aim at an accurate measurement of a non-zero quantity. Experiments with muons in this category include the measurement of the muon lifetime $\tau_\mu$ used to extract the Fermi constant, and the muon magnetic moment anomaly $(g_\mu-2)/2$. Neutrons are obviously used to measure the neutron lifetime $\tau_n$ and the various correlation coefficients in the three-body decay of the neutron.
- *Quasi-null tests.* These aim at testing symmetries – exact or approximate – of the Standard Model. Current or planned experiments are sensitive probes of new physics, because in general the new physics could violate these approximate symmetries. With muons, one can probe charged lepton flavour violation (CLFV) processes such as the $\mu^+ \to e^+\gamma$ decay. It is not strictly speaking a null test because neutrino oscillations violate the conservation of lepton flavor, but in the charged lepton sector the effect of the PMNS matrix is much too small to be measured, it is a quasi-null test. With neutrons, one can test baryon number conservation by measuring the neutron-antineutron oscillation. If $n-\bar{n}$ oscillation is observed, it would violate not only B conservation but also $B-L$. It is therefore a strict null test because $B-L$ is strictly conserved in the SM. Finally, the measurement of the Electric Dipole Moment (EDM) of the neutron is a test of time reversal symmetry, and therefore of *CP* symmetry according to the *CPT* theorem. Although *CP* violation is allowed in the SM, flavor-diagonal *CP* violation (the case of the EDM) is largely suppressed. The search for the neutron EDM is in fact a quasi-null test.

It is impossible to cover all aspects of precision experiments with neutrons and muons in this short review. Not only because of space limitations, but also because of the incompetence of the authors. Instead we choose to develop topics which, in our biased opinion, are the most interesting. In the second section we will report on the current status of the two persisting discrepancies ($4\sigma$), namely the disagreement between the experimental and theoretical values for the $(g_\mu-2)/2$, and the neutron lifetime puzzle. Sadly, we will not cover the more recent "proton radius puzzle", in which a muon experiment play a key role. Next we will cover the CLFV processes with muons in Section 3 and the search for the neutron EDM in Section 4. To cover the gaps in this review we refer to the following review on particle physics with neutrons [1] and reviews on muon particle physics [2,3].

## 2. Two persisting discrepancies

### 2.1. *Status of the muon ($g_\mu - 2$) anomaly*

Since the muon is a Dirac particle, the $g$ factor of its magnetic moment is two (2), when quantum corrections are not included. Here, the $g$ factor is defined as

$$\vec{\mu} = g\frac{e}{2m}\vec{s}, \tag{1}$$

where $\vec{\mu}$ is the magnetic moment vector, $\vec{s}$ is the spin vector, $e$ and $m$ are the electric charge and the mass respectively. A deviation from two, namely $(g-2)$, arises by quantum corrections, which can be calculated precisely in the SM. They are divided into higher-order QED corrections, hadronic vacuum polarization (HVP), hadronic light-by-light (HLbL) and electroweak (EW) contributions. For instance, one of the recent updates of theoretical calculations on $a_\mu = (g_\mu - 2)/2$ for the muon [4] gives

$$a_\mu^{\mathrm{QED}} = 11658471.90(0.01) \times 10^{-10}, \tag{2}$$

$$a_\mu^{\mathrm{HVP}} = 684.69(2.4) \times 10^{-10}, \tag{3}$$

$$a_\mu^{\mathrm{HLbL}} = 9.80(2.60) \times 10^{-10} \quad \text{and} \tag{4}$$

$$a_\mu^{\mathrm{EW}} = 15.36(0.10) \times 10^{-10}. \tag{5}$$

By adding the above contributions, the SM prediction is

$$\begin{aligned} a_\mu^{\mathrm{SM}} &= a_\mu^{\mathrm{QED}} + a_\mu^{\mathrm{HVP}} + a_\mu^{\mathrm{HLbL}} + a_\mu^{\mathrm{EW}} \\ &= 11659182.05(3.56) \times 10^{-10}. \end{aligned} \tag{6}$$

On the other hand, the present experimental value of $a_\mu$ is given by BNL E821 [5],

$$a_\mu^{\exp} = 11659208.9(6.3) \times 10^{-10} \quad (\pm 540\ \mathrm{ppb}). \tag{7}$$

The experimental value has about $+3.7\sigma$ deviation from the SM prediction. It is not known yet whether this deviation is due to new physics beyond the SM or not.

Experimentally the $(g_\mu - 2)$ is measured by the frequency ($\omega_a$) of muon spin precession with respect to the muon momentum vector in a muon storage ring. The Larmor frequency of the muon spin precession ($\omega_s$) and the cyclotron frequency of the muon motion ($\omega_c$) are given respectively as follows,

$$\omega_s = \frac{eB}{m_\mu\gamma}\left[1 + \frac{g_\mu - 2}{2}\gamma\right] \quad \text{and} \quad \omega_c = \frac{eB}{m_\mu\gamma}, \tag{8}$$

$$\omega_a \equiv \omega_s - \omega_c = \frac{a_\mu eB}{m_\mu}. \tag{9}$$

A new experiment E989 at Fermilab [6] is now running to improve an accuracy by a factor of four, reaching 140 ppb. The E989 experiment utilizes the same muon $(g_\mu - 2)$ storage ring used in BNL E821 with several significant improvements on a muon beam and detectors. Another experimental program at J-PARC is under preparation (J-PARC E34) [7]. It uses a low-emittance slow $\mu^+$ beam produced from laser ionization of a muonium, allowing a compact storage ring without electric focusing of muons. J-PARC E34 is expected to have different systematic uncertainties, and therefore it would provide a good cross-check of the BNL E821 result. It is noted that the electron $(g_e - 2)$ has also about $2\sigma$ deviation from the SM prediction, but an opposite sign [8].

## 2.2. *Status of the neutron lifetime puzzle*

The neutron decays due to the weak interaction process $n \to p e^- \bar{\nu}$. Given its importance in particle physics and cosmology, the neutron lifetime $\tau_n$ has been measured by more than 20 experiments since the 1950's. There is now a persistent disagreement between the two classes of methods to measure the lifetime, the so called "beam" and "bottle" methods [9].

In the "beam" method [10], one counts the rate of appearance $\dot{N}$ of protons in a neutron beam within a fiducial volume containing $N$ neutrons. One gets the neutron lifetime from the relation $\dot{N} = N/\tau_n$. This method requires an absolute measurement of the neutron flux to determine $N$ and also requires to know the efficiency of the detector counting the protons. The "beam" average is

$$\tau_n^{\text{beam}} = 888.0 \pm 2.0 \text{ s.} \tag{10}$$

In the "bottle" method, one uses trapped ultracold neutrons (UCNs). UCNs are neutrons with kinetic energy lower than about 200 neV. In this extremely low energy range, the neutrons are reflected off material surfaces at any angle of incidence (in contrast with cold neutrons which are reflected only at grazing incidence from the surface). Therefore UCNs can be trapped in evacuated material containers called "bottles". The method of the experiment consists in loading a bottle with UCNs and counting how many remain after some time $t$. By repeating the measurement for various times $t$, the storage time $\tau_n^{\text{bottle}}$ is extracted from a fit of the storage curve $N(t) = N_0 e^{-t/\tau_n^{\text{bottle}}}$. The experiments with UCNs are consistently reporting a lifetime shorter than the "beam" average. In UCN experiments one has to control all the neutron losses in the bottle which come in addition to the beta decay. In particular a correction for the losses due to wall collisions has to be applied, it was about 15 s in the most recent experiment of this type [11]. It was tempting to attribute the lifetime discrepancy to unaccounted errors in the wall losses correction. However, in the more recent experiments [12, 13], UCNs are contained in magnetic bottles (the magnetic potential barrier is 60 neV/T for neutrons) and never hit any material surfaces. These magnetic storage experiments confirmed the results with material traps, which makes the neutron lifetime puzzle more puzzling. The "bottle" average is now

$$\tau_n^{\text{bottle}} = 879.4 \pm 0.6 \text{ s.} \tag{11}$$

The discrepancy is as large as $\tau_n^{\text{beam}} - \tau_n^{\text{bottle}} = 8.6 \pm 2.1$ s (4 standard deviations).

Interestingly, the "bottle" method measures the total decay rate of the neutron whereas the "beam" method measures the partial decay to protons. The discrepancy could be explained by an invisible decay channel for the neutron with a branching ratio of about 1%. However this possibility has been ruled out [14, 15] by comparing the results with the theoretical predictions. In the Standard Model, $\tau_n$ can be calculated from the masses of the particles, the Fermi constant $G_F$ (accurately determined from the muon lifetime), the CKM matrix element $V_{ud}$, and $\lambda = g_A/g_V$ the ratio of the axial to vector coupling of the nucleon. The value of $\lambda$ could in principle be calculated from QCD, but the precision of lattice calculations of order 1% is presently insufficient. Instead, $\lambda$ is extracted from neutron decay correlation coefficients. It turns out that the SM prediction [15]

$$\tau_n^{\text{SM}} = 879.4 \pm 1.0 \text{ s} \tag{12}$$

agrees very well with the "bottle" average and is incompatible with the "beam" average. This rules out the invisible channel hypothesis, which predicts the contrary.

The situation with the neutron lifetime puzzle is serious. It must be settled experimentally, in particular with an improved beam experiment measuring the proton rate [16], and with a new beam experiment measuring the electron rate at J-PARC [17].

## 3. Lepton flavor violating processes with muons

### 3.1. *Physics motivation of charged lepton flavour violation (CLFV)*

In the minimal SM, neutrinos are massless and lepton flavor is conserved separately for each generation. However it has been known and confirmed that neutrinos are not massless and mixed by the observation of neutrino oscillation. Therefore lepton flavor is not conserved in the SM. The SM contribution to the CLFV rates, such as $\mu^+ \to e^+\gamma$ can be estimated by [18]

$$B(\mu^+ \to e^+\gamma) = \frac{3\alpha}{32\pi}\left|\sum_{\ell=1}^{3}(V_{\mathrm{MNS}})^*_{\mu\ell}(V_{\mathrm{MNS}})_{e\ell}\frac{m^2_{\nu_\ell}}{M_W^2}\right|^2 \sim \mathcal{O}(10^{-54}) \tag{13}$$

where $V_{\mathrm{MNS}}$ is the PMNS lepton mixing matrix element in the SM. $m_{\nu_\ell}$ ($\ell = 1,3$) and $M_W$ is the neutrino masses and the W boson mass respectively. The SM contribution is thus very small, providing a large window of experimental searches for new physics beyond the SM (BSM) without SM backgrounds.

The sensitivity of CLFV can be estimated, for instance, by using an effective field theory (EFT) approach. The effective Lagrangian ($\mathscr{L}$) is given by

$$\mathscr{L} = \mathscr{L}_{SM} + \sum_{d>4}\frac{C^{(d)}}{\Lambda^{d-4}}\mathcal{O}^{(d)}, \tag{14}$$

where $\mathscr{L}_{SM}$ is the Standard Model Lagrangian, $C^{(d)}$ is the coupling constant, $\Lambda$ is the energy scale of new physics, $\mathcal{O}^{(d)}$ is an operator of dimension $d$. For instance, the current upper bound of $B(\mu^+ \to e^+\gamma) < 4.2 \times 10^{-13}$ at 90% C.L. could yield $\Lambda \sim \mathcal{O}(10^4)$ TeV for the coupling constant of $C \sim \mathcal{O}(1)$ [19, 20]. Its sensitivity to energy scale of BSM has already reached to significantly high, well above that the current and planned accelerators can directly reach. Furthermore, as mentioned later, the currently-planned experiments are expecting sensitivity improvements of a factor of more than 10,000 from the current limits. With the dimension-six operators, the rate is proportional to $1/\Lambda^4$, suggesting that the energy reach of new physics can be extended by additional factor of ten, to $\mathcal{O}(10^5)$ TeV in the future. Also there are many theoretical models to predict sizable CLFV rates, some of which are just below the current experimental limits. They are, for example, the models with neutral heavy leptons, extra-dimension, $Z'$, leptoquark, supersymmetry and so on.

### 3.2. *Phenomenology of CLFV*

The most sensitive studies of CLFV are made by experiments to search for $\mu \to e$ transitions by utilizing highly intense muon beams. They are $\mu^+ \to e^+\gamma$, $\mu^+ \to e^+e^-e^+$, and $\mu^- \to e^-$ conversion in a muonic atom.

$\mu^+ \to e^+\gamma$ *decay:* The effective Lagrangian for the $\mu^+ \to e^+\gamma$ amplitude is given by

$$\mathscr{L}_{\mu\to e\gamma} = -\frac{4G_F}{\sqrt{2}}[m_\mu A_R \overline{\mu_R}\sigma^{\mu\nu}e_L F_{\mu\nu} + m_\mu A_L \overline{\mu_L}\sigma^{\mu\nu}e_R F_{\mu\nu} + \mathrm{h.c.}], \tag{15}$$

where $A_R$ and $A_L$ are coupling constants that correspond to the processes of $\mu^+ \to e^+_R\gamma$ and $\mu^+ \to e^+_L\gamma$, respectively. $\mu_{R(L)}$ is a right-handed (left-handed) positive muon, and $e_{R(L)}$ is a right-handed (left-handed) positron, $G_F$ is the Fermi coupling constant and $F_{\mu\nu}$ is the electromagnetic tensor. This Lagrangian presents a dipole-type interaction with photons, but changing lepton flavor. Then the branching fraction ($\mathscr{B}$) is given by

$$\mathscr{B}(\mu^+ \to e^+\gamma) = \frac{\Gamma(\mu^+ \to e^+\gamma)}{\Gamma(\mu^+ \to e^+\nu\overline{\nu})} = 384\pi^2(|A_R|^2 + |A_L|^2). \tag{16}$$

The event signature of $\mu^+ \to e^+\gamma$ decay at rest is a positron and a photon are moving back-to-back in coincidence with their energies equal to half that of the muon mass ($m_\mu/2 = 52.8$ MeV). The searches in the past were made by using positive muons at rest to fully utilize its kinematics. Negative muons have not been used because they are captured by a nucleus when they are stopped in a material. There are two major backgrounds to the search for $\mu^+ \to e^+\gamma$ decay. One of them is a physics background from radiative muon decay, $\mu^+ \to e^+\nu\overline{\nu}\gamma$ when $e^+$ and photon are emitted back-to-back with the two neutrinos carrying off a small amount of energy. The other background is an accidental coincidence of a positron in a normal muon decay accompanied by a high energy photon. Possible sources of the high energy photon would be either $\mu^+ \to e^+\nu\overline{\nu}\gamma$ decay, annihilation-in-flight or external bremsstrahlung of $e^+$s from a normal muon decay. To reduce accidental background events, an instantaneous rate of incident muons should be kept low, and thus a continuous muon beam should be utilized.

$\mu^+ \to e^+e^-e^+$ *decay:* The $\mu^+ \to e^+e^-e^+$ decay could have not only the dipole-type photonic contribution but also four-fermion contributions. The effective Lagrangian for $\mu^+ \to e^+e^-e^+$ can have two dipole operators and six four-fermion operators with different combinations of lepton chirality. If only the dipole-type photonic diagrams contribute to $\mu^+ \to e^+e^-e^+$ decay, a model-independent relation between the two branching ratios can be derived, $\mathscr{B}(\mu^+ \to e^+e^-e^+)/\mathscr{B}(\mu^+ \to e^+\gamma) \simeq 0.006$ [2].

The event signature of $\mu^+ \to e^+e^-e^+$ decay is kinematically well constrained, since all particles in the final state are detectable with high precision. Muon decay at rest has been used in all past experiments. In this case, the conservation of momentum sum ($|\sum_i \vec{p}_i| = 0$) and energy sum ($\sum_i E_i = m_\mu$) could be effectively used together with the timing coincidence between two $e^+$s and one $e^-$, where $\vec{p}_i$ and $E_i$ ($i = 1,3$) are respectively the momentum and energy of each of the $e$'s. One of the physics background processes is the allowed muon decay $\mu^+ \to e^+\nu\overline{\nu}e^+e^-$ ($\mathscr{B} = (3.4 \pm 0.4) \times 10^{-5}$), which becomes a serious background when $\nu_e$ and $\overline{\nu}_\mu$ have very small energies. The other background is an accidental coincidence of an $e^+$ from normal muon decay with an uncorrelated $e^+e^-$ pair, where a $e^+e^-$ pair could be produced either from Bhabha scattering of $e^+$, or from the external conversion of the photon in $\mu^+ \to e^+\nu_e\overline{\nu}_\mu\gamma$ decay. As has been discussed for the $\mu^+ \to e^+\gamma$ search, to reduce accidental background events, a continuous muon beam should be utilized.

$\mu^- \to e^-$ *conversion:* The third important $\mu \to e$ transition process is neutrino-less conversion of a negative muon to an electron in the field of a nucleus of a muonic atom. When a negative muon is stopped in some material, it is trapped by an atom, and a muonic atom is formed. After it cascades down energy levels in the muonic atom, the muon is bound in its $1s$ ground state. The fate of the muon is then either decay in orbit ($\mu^- N(A,Z) \to e^-\nu_\mu\overline{\nu}_e N(A,Z)$) or nuclear muon capture, namely, $\mu^- N(A,Z) \to \nu_\mu N(A,Z-1)$, for a nucleus $N(A,Z)$ of mass number $A$ and atomic number $Z$. However, in the context of BSM, the CLFV process of neutrino-less muon capture, such as

$$\mu^- N(A,Z) \to e^- N(A,Z), \tag{17}$$

is also expected. This process is called $\mu^- \to e^-$ conversion in a muonic atom. The final state of the nucleus $N(A,Z)$ could be either the ground state or one of the excited states. In general, the transition to the ground state, which is called coherent conversion, is dominant. The rate of the coherent capture over non-coherent capture is enhanced by a factor approximately equal to the number of nucleons in the nucleus. The conversion rate of $\mu^- \to e^-$ conversion is defined as $\mathrm{CR}(\mu^- N \to e^- N) \equiv \Gamma(\mu^- N \to e^- N)/\Gamma(\mu^- N \to \text{all})$, where $\Gamma$ is the rate. The time distribution of $\mu^- \to e^-$ conversion follows a lifetime of a muonic atom, which depends on a nucleus.

The event signature of $\mu^- \to e^-$ conversion in a muonic atom is a mono-energetic single electron emitted from the conversion with an energy ($E_{\mu e}$) of $E_{\mu e} = m_\mu - B_\mu - E_{\text{recoil}}$, where $m_\mu$ is the muon mass, and $B_\mu$ is the binding energy of the $1s$ muonic atom. $E_{\text{recoil}}$ is the nuclear recoil energy. Since $B_\mu$ varies for various nuclei, $E_{\mu e}$ could be different. For instance, $E_{\mu e} = 104.9$ MeV for aluminium (Al), $E_{\mu e} = 104.3$ MeV for titanium (Ti), and $E_{\mu e} = 94.9$ MeV for lead (Pb). The potential background sources for $\mu^- \to e^-$ conversion can be grouped into three. The first group is intrinsic physics backgrounds which come from muons stopped in the muon-stopping target, such as electrons from muon decays in orbit and radiative muon capture. The second is beam-related backgrounds which are caused by beam particles in a muon beam. To eliminate beam-related backgrounds, a pulsed proton beam is used and the measurement will be made between the beam pulses. The third is backgrounds coming from cosmic-ray muons, fake tracking events, and so on.

The effective Lagrangian of $\mu^- \to e^-$ conversion can be expressed by dipole, scalar, vector, pseudo-scalar, axial-vector and tensor interactions. Among these effective interactions, the dipole, scalar and vector operators contribute to the spin independent (SI) $\mu^- \to e^-$ conversion processes, whereas the axial, tensor and pseudo-scalar operators contributes to the spin dependent (SD) $\mu^- \to e^-$ conversion [21]. The SI process is a coherent process which does benefit from nucleon-number-squard enhancement, but the SD process does not. The rates of the SI processes for various nuclei were calculated, showing the dependence of atomic charge $(Z)$ could be used to discriminate different type of effective interactions [22, 23].

### 3.3. *Current limits and future prospects*

$\mu^+ \to e^+\gamma$ *decay:* The present experimental upper limit is $\mathscr{B}(\mu^+ \to e^+\gamma) < 4.2 \times 10^{-13}$ at 90% CL [24], which was obtained by the MEG experiment at PSI from data collected from 2009–2013. The MEG used a monochromatic beam (of 28 MeV/$c$) of surface positive muons, which are produced by pion decays at rest at the surface of a proton target. The MEG detector consisted of drift chambers to detect $e^+$s and a scintillation detector of 900 l of liquid xenon to measure photons. The detectors were placed inside a superconducting solenoid with a graded magnetic field along the beam axis.

The MEG II experiment [25] has a better $e^+$ spectrometer with a new cylindrical drift chamber and pixelated precision timing counter, and a liquid xenon photon detector read out by new silicon photomultipliers (at the central region) and photomultipliers (at the forward/backward regions). Fine segmentation of silicon photomultipliers would improve the position and angular resolution of photon detection. Additional detector to eliminate $\mu^+ \to e^+\nu\bar{\nu}\gamma$ backgrounds is newly introduced. The detector construction is complete. Each of the upgraded detectors is expected to provide resolutions roughly a factor of two better than MEG, allowing them to use the full muon beam intensity at PSI. The MEG II aims to achieve a factor of ten improvement, reaching $6 \times 10^{-14}$.

$\mu^+ \to e^+e^-e^+$ *decay:* The current experimental limit of $\mathscr{B}(\mu^+ \to e^+e^-e^+) < 1 \times 10^{-12}$ at 90% CL was obtained by the SINDRUM experiment from data collected from 1983–1986 [26]. This limit was obtained by assuming the constant matrix element of the $\mu^+ \to e^+e^-e^+$ decay.

The Mu3e experiment [27] is aiming at $\mathscr{B}(\mu^+ \to e^+e^-e^+) < 5 \times 10^{-15}$ at 90% CL in its first stage at the existing $\pi$E5 beamline at PSI. The Mu3e detector consists of ultra-thin, monolithic, silicon pixel tracking detectors based on the HV-MAPS technology, and a scintillating fiber system to measure timing in a sub-nanosecond resolution. All the detectors are located in a superconducting solenoid of 1 T magnetic field. After three years of operation, Mu3e Phase-I will reach the aimed sensitivity. This sensitivity is limited by the muon rate at the $\pi$E5 at PSI. At PSI, a new High Intensity Muon Beamline, HiMB, has been investigated. It would provide $1.3 \times 10^{10}$ surface $\mu^+$s/s. Mu3e Phase-II, the second stage of the experiment, will utilize a highly intense muon beam at the HiMB, aiming at another factor of ten improvement, to $\mathscr{B}(\mu^+ \to e^+e^-e^+) < 1 \times 10^{-16}$ at 90% CL.

$\mu^- \to e^-$ *conversion:* The past experimental searches for $\mu^- \to e^-$ conversion were made with five different materials of muon stopping target, such as sulphur ($Z = 16$), titanium ($Z = 22$), copper ($Z = 39$), gold ($Z = 79$), and lead ($Z = 82$). Among them, the best limit is $\mathrm{CR}(\mu^-\mathrm{Au} \to e^-\mathrm{Au}) < 7 \times 10^{-13}$ at 90% CL, which was obtained by the SINDRUM-II experiment, from data collected from 2000 [28].

There are two new experiments to search for $\mu^- \to e^-$ conversion under preparation; one is the Mu2e experiment in the US and the other is the COMET experiment in Japan.

The Mu2e experiment [29] at Fermilab is aiming at $\mathrm{CR}(\mu^-\mathrm{Al} \to e^-\mathrm{Al}) < 8 \times 10^{-17}$ at 90% CL with an aluminium target for 690 days of operation. 8 GeV protons with 8 kW from the Fermilab Booster with 1.7 µs intervals are delivered to a proton target of tungsten placed inside the high magnetic-field solenoids. The muons from pion decays are transported through two 90° curved solenoids in the opposite bending direction, forming a "S" shape, where momentum and charge of muons are selected by collimators located after the first 90° bend, and the second 90° bend brings the muons to the center of the beamline. Then the muons are delivered to a muon stopping target, which is placed in a graded magnetic field. The detector consists of straw tube drift chambers and an electron calorimeter of pure CsI crystals in a constant magnetic field region. The whole detector is covered by the scintillator based cosmic veto system. The Mu2e experiment can be upgraded to Mu2e-II [30], to take advantage of the high intensity proton beam available at the PIP-II project in the future. The PIP-II linac, under consideration at Fermilab, would provide 1.6 MW of 0.8 GeV protons. The Mu2e-II will utilize 100 kW of protons from PIP-II to increase its sensitivity by a factor of ten or more.

The COMET experiment has taken a two-staged approach. The COMET Phase-I [31, 32], the first stage of the experiment, is aiming at $\mathrm{CR}(\mu^-\mathrm{Al} \to e^-\mathrm{Al}) < 7 \times 10^{-15}$ at 90% C.L. for 150 days of operation. 8 GeV protons with 3.2 kW from the J-PARC main ring will be delivered to a proton target made of graphite inside the 5 T pion capture solenoid. The muon transport consists of a 90° curved solenoids, together with dipole coils installed inside the solenoids, providing momentum and charged selection by changing a dipole magnetic field. The detector to search for $\mu^- \to e^-$ conversion in COMET Phase-I is a cylindrical drift chamber. And low-mass straw tube drift chambers and a LYSO crystal calorimeter, which are the COMET Phase-II detector, will be used for beam measurement in COMET Phase-I. The COMET Phase-I will be extended to COMET Phase-II [33], the second stage, whose sensitivity is $\mathrm{CR}(\mu^-\mathrm{Al} \to e^-\mathrm{Al}) < 6 \times 10^{-17}$ at 90% CL with 56 kW proton beam power for 230 days of operation. The proton target for Phase-II is made of tungsten. The muon transport at Phase-II consists of two 90° curved solenoids with the same bending direction, forming a "C" shape, where continuous 180° bend will be fully utilized to make twice better momentum and charge separation than single 90° bend. The electron transport, which is installed between the muon target and the detector, has a 180° curved solenoid to select 105 MeV/$c$ electrons and eliminate positive-charged particles (such as protons from muon capture) and low energy electrons from normal muon decays. This curved electron transport also eliminates a direct sight from the detector to the muon target to remove neutron and $\gamma$-ray backgrounds, which would otherwise cause serious high detector rates. Recently, further improvements of sensitivity by one order of magnitude, yielding a sensitivity of $\mathscr{O}(10^{-18})$, from refinements to the experimental design and operation are being considered [34].

*High intensity muon beam sources:* Expected significant improvements in high intensity frontier with muons would benefit from the planned muon sources with their intensities of more than $10^{10}\mu^\pm$/s. At PSI, the HiMB with $1.3 \times 10^{10}$ surface muons/second is being considered with new capture and beamline solenoids at the Target M station. The Mu2e and COMET muon beams could produce $10^{10}$–$10^{11}$ $\mu^-$s/s with 8 GeV proton beams of 8 kW and 56 kW beam power, respectively. These high intensity muon beams can be realized with a 5 T pion capture solenoid system surrounding a proton target, followed by a curved solenoid magnet which provides a charge and momentum-selected muon beam to an experiment. Furthermore, the muon beam system adopted in Mu2e and COMET was originally proposed by Lobashev and Dzhilkibaev in 1989 [35]. The first experimental demonstration of the feasibility of the method was achieved at the Research Center of Nuclear Physics, Osaka University in 2011 [36]. In the long term future, a cooled muon beam of smaller beam emittance can be considered to make better CLFV measurements. The cooled muon beams can be made based on some novel techniques of phase rotation and ionizing cooling, which have been developed in the R&D of a muon collider and a neutrino factory. The PRISM concept [37] utilizing phase rotation of muons in a muon storage ring was considered and tested in Japan. The development of a new high-intensity muon beam of better emittance would be a key to make further significant progress in this field.

## 4. The neutron electric dipole moment

### 4.1. *nEDM as a probe of new CP-violating physics*

The electric dipole moment $d$ of a fermion $f$, from the point of view of relativistic field theory, is the coupling constant of the *CP* violating interaction with the electromagnetic field $F_{\mu\nu}$:

$$\mathscr{L}_{\mathrm{EDM}} = -\frac{\mathrm{i}d}{2}\bar{f}_L\sigma^{\mu\nu}f_R F_{\mu\nu} + \mathrm{h.c.} \tag{18}$$

where $f_L$ and $f_R$ are the left and right chirality components of the fermion. This effective non-renormalizable interaction is generated by virtual effects, as depicted generically in Figure 1(a). In fact the imaginary part of the diagram generate the EDM whereas the real part generate the anomalous magnetic moment. A specific loop diagram involving a scalar boson of mass $M$ and with a complex coupling $g$ to the fermion is shown in Figure 1(b). It generates an EDM of $d \approx e\hbar c\,\mathrm{Im}(g^2)/(4\pi)^2\, m_f/M^2$. This pedagogical example can be used to estimate the EDM of the first generation fermions – say the $d$ quark ($m_f = 5$ MeV) – induced by a boson at the TeV scale ($M \approx 1$ TeV and $\mathrm{Im}(g^2)/(4\pi) \approx 10^{-2}$). We get $d \approx 10^{-25}$ $e$ cm, a value in the reach of neutron[1] EDM experiments given that the current upper limit is [38]

$$|d_n| < 3\times 10^{-26}\ e\,\mathrm{cm}\ (90\%\ \mathrm{C.L.}). \tag{19}$$

The Standard Model contains two sources of *CP* violation: the complex phase in the CKM matrix and the strong phase $\theta_{\mathrm{QCD}}$. Due to the peculiar flavour structure of the electroweak theory, the neutron EDM induced by the CKM phase is undetectably small: $d_n \sim 10^{-32}$ $e$ cm. This is because only diagrams involving all three generations of quarks in the loops can contribute to the imaginary part of the interaction Figure 1(a). A nonzero strong phase, on the contrary, would induce a large neutron EDM. The limit (19) translates to the bound $|\theta_{\mathrm{QCD}}| < 10^{-10}$, a severe fine-tuning known as the *strong CP problem*. It is believed that physics beyond the Standard Model is at play to set this phase to zero with an Axion mechanism.

Then, EDMs are sensitive probes of *CP* violation effects beyond the Standard Model with practically zero background. As a illustrative example let us consider the search for *CP*-violating couplings of the Higgs boson $h$ to fermions. The Higgs couplings are generically parameterized by the following lagrangian

$$\mathscr{L}_h = -\frac{y_f}{\sqrt{2}}(\kappa_f\bar{f}fh + \mathrm{i}\tilde{\kappa}_f\bar{f}\gamma_5 fh), \tag{20}$$

[1] The EDM of the light quarks generate a neutron EDM with coefficients of order unity.

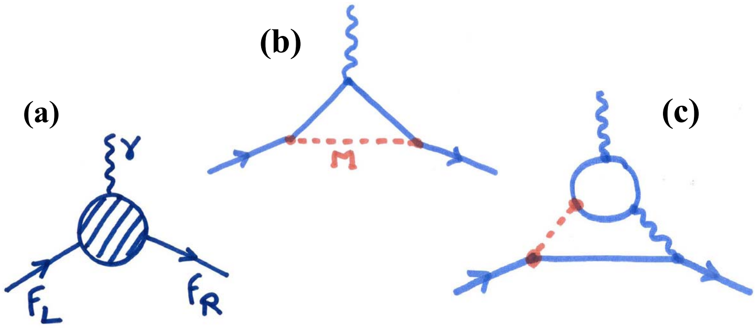


**Figure 1.** (a) Feynman diagram corresponding to the EDM coupling (18). (b) Example of a one-loop diagram contributing to the fermion EDM. (c) Two-loop Barr-Zee diagram contributing to the fermion EDM.

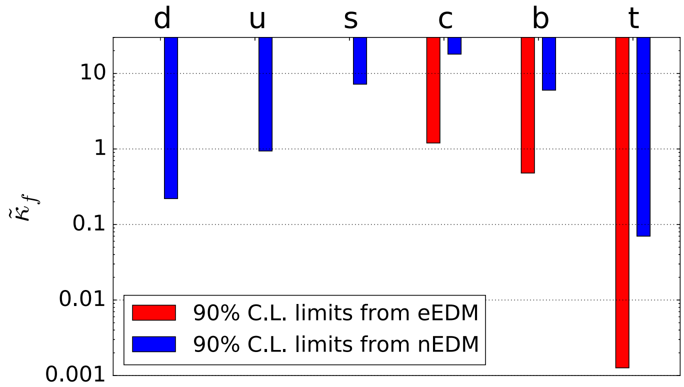


**Figure 2.** Current limits on the *CP*-violating couplings of the Higgs boson for the six quark flavours derived from the electron EDM (red bars) and from the neutron EDM (blue bars), adapted from [39–41].

where $y_f$ is the Yukawa coupling of the fermion $f$, $\kappa_f$ and $\tilde{\kappa_f}$ are the *CP*-conserving and *CP*-violating coupling constants. The Standard Model predicts $\kappa_f = 1$ and $\tilde{\kappa}_f = 0$. This coupling generates EDMs though the two-loops diagram shown in Figure 1(c). The limits on the *CP*-violating couplings to the quarks derived from the neutron and electron EDM bounds are shown in Figure 2. This plot illustrates the complementarity of EDM searches: the electron EDM is more sensitive to $\tilde{\kappa}$ of the heavy quarks while the neutron EDM is more sensitive to $\tilde{\kappa}$ of the light quarks. It also illustrates the great sensitivity of EDM searches: fundamental *CP*-violating couplings of order unity, relative to *CP*-conserving couplings, are already excluded except for the $s$ quark. Next generations of EDM experiments will push these limits down by an order of magnitude, or perhaps discover a signal induced by small *CP*-violation in the Higgs sector.

Extra *CP* violation is a generic feature of models extending the SM, which inevitably come with additional complex (therefore *CP*-violating) free parameters. Also, a new source of *CP* violation is required to explain the matter-antimatter asymmetry. Indeed *CP* violation is one of Sakharov's necessary condition to generate dynamically the baryon asymmetry in the early Universe. EDM limits are highly relevant for the *Electroweak baryogenesis* scenario. In this class of models, baryogenesis occurred at the electroweak phase transition epoch of the Universe, at a temperature of about 100 GeV. See [42] for a recent discussion on the subject. For baryogenesis

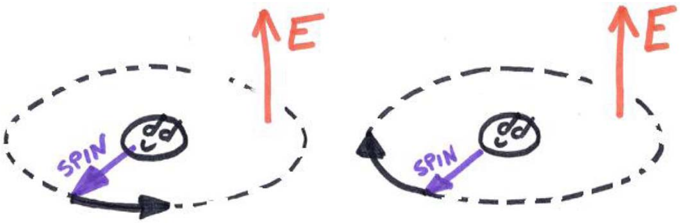


**Figure 3.** (a) Evolution in an electric field of a particle spin with a non-zero – negative in this case – EDM. (b) Time-reversed version of the evolution (a). The fact that (a) and (b) are different constitutes a violation of time reversal symmetry.

to work, new *CP*-violating interactions must have been active at this temperature, therefore the mass of the new particles could not be much heavier than 1 TeV and and the *CP*-violating interaction they mediate should be sufficiently strong. The models therefore also predict sizable EDMs and the future EDM experiments will either discover a nonzero EDM or exclude most of electroweak baryogenesis models.

## 4.2. *State of the art of the experiments and future prospects*

In the non-relativistic limit the lagrangian density (18) reduces to the following Hamiltonian:

$$\hat{H} = -d\,\hat{\vec{\sigma}} \cdot \vec{E}, \tag{21}$$

where $\hat{\vec{\sigma}}$ are the Pauli matrices acting on the fermion's spin sates and $\vec{E}$ is the applied external electric field. The electric dipole moment quantifies the coupling between the spin and the electric field, in the same way that the magnetic moment $\mu$ quantifies the coupling between the spin and the magnetic field. The time evolution is shown in Figure 3: the spin precesses around the field at an angular frequency given by $\hbar\omega = 2dE$. As Figure 3(b) shows, the existence of a non-zero EDM would constitute a violation of time reversal symmetry. It is consistent with the fact that the lagrangian (18) violates the *CP* symmetry, because $T$-violation is equivalent to *CP*-violation in any local relativistic quantum field theory.

The basic idea to measure the neutron EDM is to use polarized neutrons and measure precisely the spin precession frequency $f$ in parallel or antiparallel magnetic and electric fields:

$$f = \frac{\mu}{\pi\hbar} B_0 \pm \frac{d}{\pi\hbar} E. \tag{22}$$

The EDM term can be separated from the much larger magnetic term by taking the difference of the frequency measured in parallel and antiparallel configurations. The EDM term, if it exists, is extremely small ($dE/\pi\hbar \approx 10^{-7}$ Hz for $d = 10^{-26}$ $e$ cm and $E = 15$ kV/cm) compared to the magnetic term (typically, $f = 29$ Hz for $B_0 = 1$ μT).

To detect such a minuscule coupling, one needs (i) a long interaction time of the neutrons with the electric field, (ii) a high flux of neutrons and (iii) a precise control of the magnetic field. In the first experiment [43] Smith, Purcell and Ramsey used a beam of thermal neutrons passing in the electric field during $T \approx 1$ ms. In the 1980s, the precession time could be greatly increased by using *ultracold neutrons* (UCNs). These are neutrons with a kinetic energy smaller than the neutron optical potential of solid materials, typically 100 neV. These neutrons can therefore be stored in material traps because they undergo total reflection upon collision with the walls of the trap. In the best previous measurement [38] performed at ILL in the period 1998–2002, UCNs were stored in a chamber permeated by a weak magnetic field and a strong electric field during

**Table 1.** List of active ongoing nEDM projects [45]

| Project | Location | Concept | Reference |
|---|---|---|---|
| nEDM@SNS | Oak Ridge spallation source | UCN in superfluid helium with $^{3}$He comagnetometer | [46] |
| n2EDM | PSI spallation source | UCN large double chamber with $^{199}$Hg comagnetometer | [47] |
| nEDM@LANL | Los Alamos spallation source | UCN double chamber with $^{199}$Hg comagnetometer | [48] |
| panEDM | ILL reactor Grenoble | UCN double chamber | [52] |
| TUCAN | TRIUMF spallation source | UCN double chamber with $^{199}$Hg or $^{129}$Xe comagnetometer | [49] |
| PNPI nEDM | ILL - PNPI | UCN double chamber | [50] |
| beam nEDM | ESS spallation source | Pulsed cold neutron beam | [51] |

$T \approx 100$ s. Although the systematic error is also a big concern, this measurement was limited by the statistical error and thus by the intensity of the ILL/PF2 UCN source. New higher intensity UCN sources are now coming online at several major neutron factories worldwide, which are exploited by several nEDM projects. In particular, the nEDM experiment has collected data [44] in 2015–2016 at the PSI UCN source, which will result in a marginally improved measurement of the neutron EDM (the analysis is still ongoing at the time of writing). Other ongoing nEDM projects [45–51] are listed in Table 1, they are all at a different stage of readiness and they aim at an improvement in sensitivity by a factor 10 to 100 compared to the previous measurement [38] in the next decade. These projects to measure the neutron EDM are an important part of a global search for fundamentals EDMs. A variety of programmes with different systems are being pursued [45], with free neutrons, diamagnetic atoms, paramagnetic systems, charged particles (muons, protons, deutons) in storage rings and heavy unstable particles (lepton $\tau$, hyperons and charmed baryons) at particle colliders.

## 5. Conclusion

This precision physics programs of muons and neutrons are presently very productive and active, even after their long history of over 80 years. There are many new experiments being under preparation or planned. The anomalies of the muon $(g_\mu - 2)$ and the neutron lifetime would be hopefully resolved in a coming few years to address new physics. Over next years, currently planned experiments searching for CLFV $\mu^- \to e^-$ transitions would improve their sensitivities by a factor of 10 to more than 10,000. The experiments to search for the neutron EDM would improve their sensitivities by a factor of 10 to 100 over the current limit.

In summary, the physics with muons and neutrons, in particular the muon CLFV and the neutron EDM, provide an unique discovery potential to new physics beyond the SM. They are expected to play a leading role in the search for BSM, and offer extraordinary opportunities for exploring new phenomena which would otherwise be directly inaccessible at future high-energy colliders.

## References

[1] D. Dubbers, M. G. Schmidt, “The neutron and its role in cosmology and particle physics”, *Rev. Mod. Phys.* **83** (2011), no. 4, p. 1111-1171.

[2] Y. Kuno, Y. Okada, “Muon decay and physics beyond the standard model”, *Rev. Mod. Phys.* **73** (2001), p. 151-202.

[3] L. Calibbi, G. Signorelli, "Charged lepton flavour violation: An experimental and theoretical introduction", *Riv. Nuovo Cimento* **41** (2018), no. 2, p. 71-174.

[4] A. Keshavarzi, D. Nomura, T. Teubner, "Muon g-2 and (MZ2): a new data-based analysis", *Phys. Rev. D* **97** (2018), article ID 114025.

[5] G. W. Bennett *et al.* (Muon g-2 collaboration), "Final report of the E821 muon anomalous magnetic moment measurement at BNL", *Phys. Rev. D* **73** (2006), article ID 072003.

[6] J. Grange *et al.* (Muon g-2 Collaboration), "Muon (g-2) Technical Design Report", 2019, preprint, https://arxiv.org/abs/1501.06858.

[7] M. Abe *et al.* (J-PARC muon/edm collaboration), "A new approach for measuring the muon anomalous magnetic moment and electric dipole moment", *Progr. Theoret. Exp. Progress* **2019** (2019), article ID 053C02.

[8] D. Hanneke, S. F. Hoogerheide, G. Gabrielse, "Cavity control of a single-electron quantum cyclotron: measuring the electron magnetic moment", *Phys. Rev. A* **83** (2011), article ID 052122.

[9] F. E. Wietfeldt, "Measurements of the neutron lifetime", *Atoms* **6** (2018), no. 4, article ID 70.

[10] A. T. Yue, M. S. Dewey, D. M. Gilliam, G. L. Greene, A. B. Laptev, J. S. Nico, W. M. Snow, F. E. Wietfeldt, "Improved determination of the neutron lifetime", *Phys. Rev. Lett.* **111** (2013), no. 22, article ID 222501.

[11] A. P. Serebrov *et al.*, "Neutron lifetime measurements with a large gravitational trap for ultracold neutrons", *Phys. Rev. C* **97** (2018), no. 5, article ID 055503.

[12] V. F. Ezhov *et al.*, "Measurement of the neutron lifetime with ultra-cold neutrons stored in a magneto-gravitational trap", *JETP Lett.* **107** (2018), no. 11, p. 671-675.

[13] R. W. Pattie Jr. *et al.*, "Measurement of the neutron lifetime using a magneto-gravitational trap and in situ detection", *Science* **360** (2018), no. 6389, p. 627-632.

[14] A. Czarnecki, W. J. Marciano, A. Sirlin, "Neutron lifetime and axial coupling connection", *Phys. Rev. Lett.* **120** (2018), no. 20, article ID 202002.

[15] D. Dubbers, H. Saul, B. Märkisch, T. Soldner, H. Abele, "Exotic decay channels are not the cause of the neutron lifetime anomaly", *Phys. Lett. B* **791** (2019), p. 6-10.

[16] F. E. Wietfeldt, G. Darius, M. S. Dewey, N. Fomin, G. L. Greene, J. Mulholland, W. M. Snow, A. T. Yue, "A path to a 0.1 s neutron lifetime measurement using the beam method", *Phys. Proc.* **51** (2014), p. 54-58.

[17] N. Nagakura *et al.*, "Precise neutron lifetime experiment using pulsed neutron beams at J-PARC", *PoS INPC* **2016** (2017), article ID 191.

[18] S. T. Petcov, "The processes mu → e Gamma, mu → e e anti-e, Neutrino' → Neutrino gamma in the Weinberg–Salam model with neutrino mixing", *Sov. J. Nucl. Phys.* **25** (1977), p. 340.

[19] F. Feruglio, P. Paradisi, A. Pattori, "Lepton flavour violation in composite Higgs models", *Eur. Phys. J. C* **75** (2015), article ID 579.

[20] G. M. Pruna, A. Singer, "The mu → e gamma decay in a systematic effective field theory approach with dimension 6 operators", *JHEP* **1410** (2014), article ID 014.

[21] V. Cirigliano, S. Davidson, Y. Kuno, "Spin-dependent $\mu \to$ e conversion", *Phys. Lett. B* **771** (2017), p. 242-246.

[22] R. Kitano, M. Koike, Y. Okada, "Detailed calculation of lepton flavor violating muon-electron conversion rate for various nuclei", *Phys. Rev. D* **66** (2002), article ID 096002, [Erratum *Phys. Rev. D* **76** (2017), 059902].

[23] V. Cirigliano, R. Kitano, Y. Okada, P. Tuzon, "Model discriminating power of $\mu \to$ e conversion in nuclei", *Phys. Rev. D* **80** (2009), article ID 013002.

[24] A. Baldini *et al.* (MEG Collaboration), "Search for the lepton flavour violating decay $\mu^+ \to e^+ \gamma$ with the full dataset of the MEG experiment", *Eur. Phys. J. C* **76** (2016), article ID 434.

[25] A. Baldini *et al.* (MEG II Collaboration), "The design of the MEG II experiment", *Eur. Phys. J. C* **78** (2018), article ID 380.

[26] U. Bellgardt *et al.* (SINDRUM Collaboration), "Search for the decay $\mu^+ \to e^+ e^+ e^-$", *Nucl. Phys. B* **299** (1988), no. 1, p. 1-6.

[27] A. Blondel *et al.* (Mu3e Collaboration), "Research Proposal for an Experiment to Search for the Decay $\mu \to eee$", 2013, preprint, https://arxiv.org/abs/1309.7679.

[28] W. Bertl *et al.* (SINDRUM-II Collaboration), "A search for muon to electron conversion in muonic gold", *Eur. Phys. J. C* **47** (2006), article ID 337.

[29] L. Bartoszek *et al.* (Mu2e Collaboration), "Mu2e Technical Design Report", 2015, preprint, https://arxiv.org/abs/1501.05241.

[30] F. Abusalma *et al.* (Mu2e-II Collaboration), "Expression of Interest for Evolution of the Mu2e Experiment", 2018, preprint, https://arxiv.org/abs/1802.02599.

[31] R. Abramishvili *et al.* (COMET collaboration), "COMET Phase-I technical design report", *PTEP* **2020** (2020), no. 3, article ID 033C01.

[32] Y. Kuno, (COMET collaboration), "A search for muon-to-electron conversion at J-PARC: the COMET experiment", *Progr. Theoret. Exp. Progress* **2013** (2013), article ID 022C01.

[33] Y. G. Cui *et al.* (COMET collaboration), "J-PARC PAC E21 Proposal", 2009, unpublished.

[34] J. C. Angélique *et al.* (COMET collaboration), "COMET – A submission to the 2020 update of the European Strategy for Particle Physics on behalf of the COMET collaboration", 2018, preprint, https://arxiv.org/abs/1812.07824.
[35] R. M. Dzhilkibaev, V. M. Lobashev, "On the search for $\mu \to e$ conversion on nuclei", *Sov. J. Nucl. Phys.* **49** (1989), no. 2, p. 384-385.
[36] S. Cook *et al.*, "Delivering the worlds most intense muon beam", *Phys. Rev. Accel. Beams* **20** (2017), no. 3, article ID 030101.
[37] Y. Kuno *et al.* (PRISM collaboration), J-PARC LOI, (2006), unpublished.
[38] M. Pendlebury *et al.*, "Revised experimental upper limit on the electric dipole moment of the neutron", *Phys. Rev. D* **92** (2015), article ID 092003.
[39] J. Brod, U. Haisch, J. Zupan, "Constraints on CP-violating Higgs couplings to the third generation", *JHEP* **1311** (2013), article ID 180.
[40] J. Brod, E. Stamou, "Electric dipole moment constraints on CP-violating heavy-quark Yukawas at next-to-leading order", 2018, preprint, https://arxiv.org/abs/1810.12303.
[41] J. Brod, D. Skodras, "Electric dipole moment constraints on CP-violating light-quark Yukawas", *JHEP* **1901** (2019), article ID 233.
[42] J. M. Cline, "Is electroweak baryogenesis dead?", *Philos. Trans. R. Soc. Lond. A* **376** (2018), no. 2114, article ID 20170116.
[43] J. H. Smith, E. M. Purcell, N. F. Ramsey, *Phys. Rev.* **108** (1957), p. 120-122.
[44] C. Abel *et al.*, "nEDM experiment at PSI: data-taking strategy and sensitivity of the dataset", *EPJ Web Conf.* **219** (2019), article ID 02001.
[45] www.psi.ch/nedm/edms-world-wide.
[46] M. W. Ahmed *et al.*, "A new cryogenic apparatus to search for the neutron electric dipole moment", *JINST* **14** (2019), no. 11, article ID P11017.
[47] C. Abel *et al.*, "The n2EDM experiment at the Paul Scherrer Institute", *EPJ Web Conf.* **219** (2019), article ID 02002.
[48] T. M. Ito *et al.*, "Performance of the upgraded ultracold neutron source at Los Alamos National Laboratory and its implication for a possible neutron electric dipole moment experiment", *Phys. Rev. C* **97** (2018), article ID 012501.
[49] S. Ahmed *et al.* [TUCAN Collaboration], "First ultracold neutrons produced at TRIUMF", *Phys. Rev. C* **99** (2019), article ID 025503.
[50] A. Serebrov, "Present status and future prospects of n-EDM experiment of PNPI-ILL-PTI collaboration", *PoS* **INPC2016** (2017), p. 179.
[51] E. Chanel *et al.*, "The pulsed neutron beam EDM experiment", *EPJ Web Conf.* **219** (2019), article ID 02004.
[52] D. Wurm *et al.*, "The PanEDM neutron electric dipole moment experiment at the ILL", *EPJ Web Conf.* **219** (2019), article ID 02006.

# *Comptes Rendus*
# *Physique*

**Objet de la revue**
Les *Comptes Rendus Physique* sont une revue électronique évaluée par les pairs de niveau international, qui couvre l'ensemble des domaines de la physique et de l'astrophysique. Ils publient principalement des numéros thématiques, mais également des articles originaux de recherche, des annonces préliminaires, des articles de revue, des mises en perspective historiques, des textes à visée pédagogique ou encore des actes de colloque, sans limite de longueur, en anglais ou en français. Ils proposent également des numéros spéciaux consacrés à certains aspects récents et/ou significatifs de la discipline, dont les auteurs sont choisis parmi les chercheurs les plus actifs sur le sujet et dont la coordination est assurée par des rédacteurs en chef invités.
Les *Comptes Rendus Physique* sont diffusés selon une politique vertueuse de libre accès diamant, gratuit pour les auteurs (pas de frais de publications) comme pour les lecteurs (libre accès immédiat et pérenne).



**À propos de la revue**
Toutes les informations concernant la revue, y compris le texte des articles publiés qui est en accès libre intégral, figurent sur le site https://comptes-rendus.academie-sciences.fr/physique/.

**Informations à l'attention des auteurs**
Pour toute question relative à la soumission des articles, les auteurs peuvent consulter le site https://comptes-rendus.academie-sciences.fr/physique/.

**Contact**
Académie des sciences
23, quai de Conti, 75006 Paris, France
Tél. : (+33) (0)1 44 41 43 72
CR-Physique@academie-sciences.fr

# Comptes Rendus de l'Académie des sciences

## Physique

Volume 21, nº 1, janvier 2020


**Special issue / *Numéro thématique***
A perspective of High Energy Physics from precision measurements / *La physique des Hautes Energies du point de vue des mesures de précision*

**Guest editors / *Rédacteurs en chef invités***
Stéphane Monteil (Clermont Université, CNRS/IN2P3, Clermont-Ferrand)
Marie-Hélène Schune (Université Paris-Saclay, CNRS/IN2P3, Orsay)

**Cover illustration / *Illustration de couverture***
La cueillette des pommes (Apple harvest), Camille Pissaro, 1886.
(Public domain, courtesy Dallas Museum of Art.)




1878-1535 (electronic)

**Académie des sciences — Paris**

Comptes Rendus
de l'Académie des sciences
Physique
Volume 21, nº 1, janvier 2020